Dynamic Simulation of MEA Absorption Process for CO_2 Capture from Power Plants

by

Noorlisa Harun

A thesis
presented to the University of Waterloo
in fulfillment of the
thesis requirement for the degree of
Doctor of Philosophy
in
Chemical Engineering

Waterloo, Ontario, Canada, 2012

I hereby declare that I am the sole author of this thesis. This is a true copy of the thesis, including any required final revisions, as accepted by my examiners.

I understand that my thesis may be made electronically available to the public.

Abstract

The monoethanolamine (MEA) absorption for CO_2 capture process is an inherently dynamic system that is affected by the variations occurring in the power plant due to start-up, shut-down and changes in the flue gas load. The development of the MEA absorption process model has been extensively published in the open literature to study the behaviour of this process at steady-state. Techno-economic studies and process optimization have been widely studied based on steady state models. However, steady state simulations cannot predict the operability of the plant in the presence of continuous and sudden fluctuations in the systems' parameters. To this date, only two studies have been conducted to model the dynamic model of the complete MEA absorption process. However, those studies used a standard software packages such as Aspen Plus Dynamic® to simulate the transient behaviour of the MEA CO_2 capture plant.

In this work, a dynamic MEA absorption process model has been developed to study the operability of this process in a dynamic fashion and to develop a control strategy to maintain the operation of the MEA scrubbing CO_2 capture process in the presence of the external perturbations that may arise from the transient operation of the power plant. The MEA absorption process considered in this study consist of an absorber, a stripper, a cross heat exchanger, and a buffer tank. The novelty in this work is that a mechanistic model based on the conservation laws of momentum, mass and energy have been developed for the complete MEA CO_2 capture process. The model developed in this work was implemented in gPROMS, a general process modeling software. A detailed dynamic model for each of the process units considered in this process was developed and integrated to describe the transient behaviour of the complete MEA plant. The process response of the key output variables to changes in the key input process variables, i.e., the flue gas flow rate and the reboiler heat duty, are presented and discussed in this study. The results from this analysis showed the dynamic response of the percentage of CO_2 absorbed in the absorber column is directly influenced by the dynamic behaviour of lean solvent flow rate. The percentage of CO_2 absorbed takes about 8 hours (4 hours) to reach a new steady state for a 5% ramp up

(5% ramp down) test in flue gas flow rate considered in this study. On the other hand, the reboiler temperature reached a new steady for both ramp tests in approximately 4 hours. The percentage of CO_2 absorbed was increased by 1% (decreased by 2%) from its nominal operating condition for -5% (+5%) changes in the flue gas flow rate. However, the response in the reboiler temperature due to changes in the flue gas flowrate was not significant (~0.1K change). The buffer tank considered in this process reduced the fluctuations in the absorber column due to variations coming from the stripper column. Hence, changes in the reboiler heat duty did not have a significant effect on the transient operation of the absorber unit. In order to represent the actual operation of a power plant, the dynamic response of the MEA absorption process to a sinusoidal change in the flue gas flow rate was also considered in the present analysis. The results of the open loops tests showed that the response of the CO_2 absorbed was mainly affected by the lean solvent flow rate profile. Likewise, the simulation results showed that the reboiler temperature responded very quickly to changes in the reboiler heat duty. A small change in the reboiler temperature was also observed when the amount of heat supplied to the stripper reboiler was reduced.

The mechanistic dynamic model was applied to develop a basic feedback control strategy. Proportional-Integral (PI) feedback controllers were used in this study to control the operation of this process in closed-loop. Internal Model Control (IMC) was applied to obtain the initial settings for the PI controller tuning parameters. The implementation of a control strategy in this work was tested by changing the operating conditions for the flue gas flow rate, which is the main disturbance considered in this controllability analysis. The controlled variables, i.e., the percentage of CO_2 absorbed in the absorber column and the reboiler temperature, were maintained around their nominal set point values by manipulating the valve stem positions, which determine the lean solvent feed flow rate at the top of the absorber column, and the reboiler heat duty, respectively. The PI feedback controller action was able to bring the controlled variable to their set point values during the ramp test whereas for the sinusoidal test, the controlled variables oscillated around their set point values. The amplitude of the oscillations observed for the controlled variables was smaller than those

observed for the open-loop tests. This is because the variability of the controlled variables was transferred to the manipulated variable in the closed loop. The closed loop analysis in the presence of changes in the disturbance shows that the control strategy can be applied to control the key process variables in the CO_2 capture process.

Based on the above, the mechanistic dynamic model developed in this process can be potentially used as a practical and efficient tool that can provide insight regarding the dynamic operation of MEA absorption process. The model developed in this work can also be used as a basis to develop other studies related to the operability, controllability and dynamic flexibility of this process.

Acknowledgements

I would like to thank my supervisors Prof. Eric Croiset, Luis-Ricardez Sandoval and Prof. P.L. Douglas for their invaluable comments, guidance, patience and encouragement throughout my study.

I appreciate the prayers, understanding, encouragement, sacrifice and unconditional love from my mom (Asinah Mohd), my dad (Harun Muda) and my siblings. I am also grateful to fellow researchers Pui, Lena and Thanita for their sharing and help. I also owe my special thank to all my 'families' in Waterloo for the support and courage that I shall not forget, in my mind and my heart. Last but not least, my best ever friend, Mazni for her support, tolerance, courage and help.

Finally, financial supports from Ministry of Higher Education, Malaysia and Prof. P.L. Douglas are also gratefully acknowledged.

Dedicated to my beloved parents…

Table of Contents

List of Figures

List of Tables

Nomenclature

List of English symbols

ΔH_{rxn}	Heat of reaction per mol CO_2 (J/mol)
ΔH_{vap}	Heat of vaporization of H_2O (J/mol)
$a_{g/l}$	Specific gas-liquid interfacial area (m^2/m^3)
a_i	Activity of component *i*
a_p	Total surface area of packing (m^2/m^3)
a_1, a_2, a_3	Constant parameter
A_{shell}	Area of shell (m^2)
A_{tube}	Area of tube (m^2)
a_w	Wetted surface area of packing (m^2/m^3)
$b_1, b_2, \ldots, b_n$	Constant parameter
C^*	Molar concentration at equilibrium (mol/m^3)
$C_{g,i}$	Molar concentration in gas phase (mol/m^3)
$C_{g,total}$	Total gas molar concentration (mol/m^3)
C_i^I	Molar concentration at gas-liquid interfacial (mol/m^3)
$C_{l,CO2}^*$	Molar concentration of free CO_2 at equilibrium (mol/m^3)
$C_{l,i}$	Molar concentration in liquid phase of component *i* (mol/m^3)
$C_{l,MEA}^*$	Molar concentration of free MEA at equilibrium (mol/m^3)
C_p	Specific heat capacity (J/mol/K)
$C_{p,w}$	Heat capacity of the tube material (J/kg/K)
C_{pm}	Mass specific heat capacity (J/kg/K)
C_v	Valve flow coefficient (0.001011828 m^2)
CV	Controlled variable
d_c	Column diameter (m)
$D_{g,avg}$	Average diffusion coefficient in the gas phase (m^2/s)
$D_{g,i}$	Diffusivity in the gas phase of component *i* (m^2/s)
$d_{i,shell}$	Inside shell diameter (m)

$d_{i,tube}$	Inside tube diameter (m)
$D_{l,i}$	Diffusivity of component *i* in the liquid phase (m^2/s)
$D_{l,i}^{H2O}$	Diffusivity of component *i* in water (m^2/s)
$d_{o,tube}$	Outside tube diameter (m)
d_p	Nominal diameter of the packing element (m)
E	Enhancement factor for pseudo-first-order reaction (dimensionless)
E_2	Enhancement factor for irreversible second order reaction (dimensionless)
E^{∞}	Enhancement factor for an instantaneous reaction (dimensionless)
E_{abs}	Enhancement factor for absorber
E_m	Mass specific internal energy (J/kg)
E_{reb}	Energy holdup in the reboiler (J)
E_{shell}	Volumetric specific internal energy of shell (J/m^3)
E_{tube}	Volumetric specific internal energy of tube (J/m^3)
e	Controller error
f	Fugacity
$F_{g,i}$	Molar flow rate in gas phase (mol/s)
F_{hx}	Molar flow rate entering the heat exchanger (mol/s)
F_{in}	Molar flow rate at the inlet (mol/s)
$F_{l,i}$	Molar flow rate in liquid phase (mol/s)
g	Gravitational constant (m/s^2)
Ha	Hatta number (dimensionless)
H^E	Henry's excess quantity ($kPa.m^3/mol$)
he	van Krevelen coefficients for ions
He_i	Henry's Law constant of component *i* in aqueous MEA solution($kPa.m^3/mol$)
He_i^{H2O}	Henry's Law constant of component *i* in water ($Pa.m^3/mol$)
$H_{e,i}^{MEA}$	Henry's Law constant of component *i* in MEA ($Pa.m^3/mol$)
H_v	Vapor enthalpy at the outlet (J/mol)
h_{gl}	Interfacial heat transfer coefficient ($W/m^2/K$)
H_{in}	Liquid enthalpy at the inlet (J/mol)

H_l	Liquid enthalpy at the outlet (J/mol)
H_m	Mass enthalpy (J/kg)
h_{out}	Wall heat transfer coefficient (W/m^2/K)
H_{shell}	Molar enthalpy of shell (J/mol)
H_{tube}	Molar enthalpy of tube (J/mol)
I	Ionic strength
J_H	Heat transfer coefficient Chilton-Colburn factor
J_M	Mass transfer coefficient Chilton-Colburn factor
k_2	Second-order reaction rate constant (m^3/mol/s)
k_{app}	Pseudo-first order reaction rate constant (1/s)
K_c	Proportional controller gain
$K_{eq,i}$	Equilibrium constant of reaction *i*.
K_p	Process gain
k_g	Mass transfer coefficient in gas phase (mol/kPa/m^2/s), (mol/Pa/m^2/s)
k_l	Mass transfer coefficient in liquid phase (m/s)
K_{value}	Vapor liquid equilibrium ratio
L	Superficial liquid mass velocity (kg/m^2/s)
L_B	Liquid level of reboiler drum (m)
L_{hx}	Tube length (m)
M	Dimensionless parameter, Hatta number
$M_{i,reb}$	Molar holdup of component *i* in the reboiler (mol)
MW	Molecular weight (g/mol)
ΔM	Change in the manipulated variable
N_i	Molar flux (mol/m^2/s)
N_{Pr}	Prandtl number
N_{Sc}	Schmidt number
P_g	Gas pressure (kPa)
p_g	Gas partial pressure (kPa)
p_g^I	Gas partial pressure at gas-liquid interfacial (kPa)

P_{hx}	Heat exchanger pressure (kPa)
p_i^*	Gas partial pressure of component *i* at equilibrium (kPa)
P_i^s	Vapour pressure (kPa)
$Q_{f,shell}$	Heat flux of shell ($J/m^2/s$)
$Q_{f,tube}$	Heat flux of tube ($J/m^2/s$)
q_g	Interfacial heat transfer in gas phase ($J/m^3/s$)
q_l	Interfacial heat transfer in liquid phase ($J/m^3/s$)
Q_{reb}	Reboiler heat duty (J/s)
Q_{shell}	Energy flow rate of shell (J/s)
Q_{tube}	Energy flow rate of tube (J/s)
R	Ideal gas constant (8.314 J/mol/K)
R_g	Ideal gas constant ($8.314x10^{-3}$ m^3.kPa/mol/K)
r_{shell}	Radius of shell (m)
r_{tube}	Radius of tube (m)
t	Time (s)
T_{amb}	Ambient temperature (K)
T_g	Gas temperature (K)
T_l	Liquid temperature (K)
T_{shell}	Shell temperature (K)
T_{tube}	Tube temperature (K)
T_{wall}	Wall temperature (K)
u	Velocity (m/s)
U_{shell}	Overall heat transfer coefficients for shell ($W/m^2.K$)
U_{tube}	Overall heat transfer coefficients for tube ($W/m^2.K$)
v_i	Molar volume of pure component *i* (m^3/mol)
v_g	Molar volume of gas (m^3/mol)
v_l	Molar volume of liquid (m^3/mol)
v_m	Molar volume of solution (cm^3/mol)
v^*	Molar volume associated with interaction between H_2O and MEA (cm^3/mol)

V	Volume (m^3)
x_i	Liquid mole fraction
$x_{i,in}$	Liquid mole fraction at the inlet
y_i	Vapor mole fraction
Δy	Changed in the controlled variable
z	Element of height (m)

Subscript

$*$	At the equilibrium
abs	Absorber
g,l	Gas and liquid phase respectively
i	Components
s	Solvent
sp	Set point
str	Stripper
hx	Heat exchanger
v	Vapor
m	Mass
1	CO_2 controller
2	Reboiler temperature controller

Superscript

I	At the gas-liquid interfacial

List of Greek symbols

μ_g	Gas viscosity (kg/m/s)
α	CO_2 loading (mol CO_2/mol MEA)
α_f	Valve stem position
γ	Activity coefficient
γ^*	Henry's laws activity coefficient
λ	Thermal conductivity (W/m/K)
ξ	Molar extent of the reactions (mol/cm^3)
ρ	Density (kg/m^3)
ρ_m	Molar density (mol/m^3)
σ_{ct}	Critical surface tension of packing material
σ_l	Surface tension of liquid
φ	Fugacity coefficient of gas phase
Φ_i	Volume fractions of component *i* in aqueous MEA
τ_c	Closed loop time constant (s)
τ_I	Integral time constant (s)
τ_p	Time constant (s)
χ	Vapor phase fraction

List of abbreviations and acronyms

AMP	Amino methyl propanol
DEA	Diethanolamine
DEA	Diethanolamine
DGA	Diglycolamine
H_2S	Hydrogen Sulfide
MDEA	Methyldiethanolamine
MEA	Monoethanolamine
PDAE	Partial Differential Algebraic Equation
VLE	Vapor-Liquid Equilibrium

Chapter 1
Introduction

1.1 Energy production and CO_2 emissions

The 20th century has experienced a rapid increase in population and explosive growth in energy consumption. As more countries are becoming industrialized, it is expected that more energy will be consumed in the 21st century. The International Energy Agency (IEA) predicts a 57% increase of energy demand from 2004 to 2030 (IEA, 2007). This would contribute to an increase in the energy production, which is required to meet the growing energy demands. Fossil fuels such as coal, petroleum and natural gas have been the major energy sources since 1900 (Song, 2006). Over 85% of the world energy demand is supplied by fossil fuels (Davison and Thambimuthu, 2005). Most of the fossil-fuelled electricity production in the world is from coal (63%) followed by natural gas (29%) and oil (9%) (IEA, 2008a).

Environmental problems due to emissions of pollutants from fossil fuel combustion are becoming major global problems which involve not only pollutants such as NO_x, SO_x, and particulate matter, but also greenhouse gases (GHG). The IPCC (Intergovernmental Panel on Climate Change) has identified six anthropogenic gases with climate change potential: CO_2, CH_4, N_2O, SF_6, CFC'S (chlorofluorocarbons), and HFC'S (hydrofluorocarbons).Through studies over the past five decades, particularly in the past 15 years, increased GHG levels in the atmosphere is believed to cause global warming (Yang, *et al*., 2008). Canada has the long term goal of reducing GHG emissions by 60-70% from 1990's level by 2050 (IEA GHG, 2008). In 2008, Canada's GHG emissions are more than 25% higher than they were in 1990, putting Canada more than 32% above what was initially planned as part of the now defunct Kyoto accord. Without immediate action, Canada's GHG emissions are projected to grow over 24% with respect to 1990's level by 2020 to reach about 940 Mt, which would represent 58% above 1990 levels (IEA GHG, 2008).

Among the GHGs, CO_2 is the largest contributor in regard to its amount present in the atmosphere, contributing to 60% of global warming effects (Yamasaki, 2003). Its annual

emissions have grown by about 80% between 1970 and 2004, from 21 to 38 gigatonnes (Gt), and represented 77% of the total anthropogenic GHG emissions in 2004 (IPCC, 2005). Based on 2006 data shown in Figure 1.1, the world CO_2 emission was 28,003 Mt (IEA, 2008b). In 2007, coal accounted for 76% of the fuels used to generate electricity in Canada (Statistic Canada, 2002).

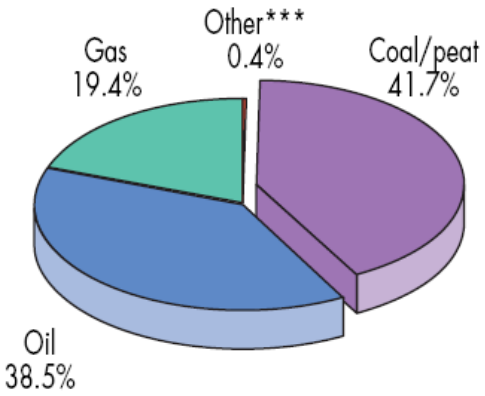

****Other includes geothermal, solar, wind, combustible renewables & waste.**

Figure 1.1: 2006 fuel shares of CO_2 emission (IEA, 2008b)

The largest growth in GHG emissions between 1970 and 2004 has come from energy supply, transport and industry, while residential and commercial buildings, forestry (including deforestation) and agriculture sectors have been growing at a lower rate. Power plants are the largest point sources of diluted CO_2, with CO_2 emissions around 30% of overall emissions (Feron and Hendriks, 2005). A 1,000 MW pulverized coal fired power plant generates between 6 and 8 Mt/year of CO_2 (Abass, 2010). The CO_2 emissions in these sectors are generated by boilers and furnaces burning fossil fuels and are typically emitted from large exhaust stacks. These stacks can be described as large stationary sources (IPCC, 2005). Figure 1.2 illustrates world energy sources used for electricity generation in recent years. As shown in this Figure, thermal power plants are the main electricity generator. It uses lignite, hard coal, natural gas, fuel oil or a combination of gas and fuel oil for producing heat and electricity. In 2006, fossil fuels accounted for more than half of the world's electricity

generation (IEA, 2008b). As shown in Figure 1.3, 41% of the electricity generated in 2006 was based on technologies that required coal. Coal is expected to remain as the leading fuel for power generation in 2020 (about 36%) while natural-gas generation is expected to become the second largest source, surpassing hydro (IPCC, 2005).

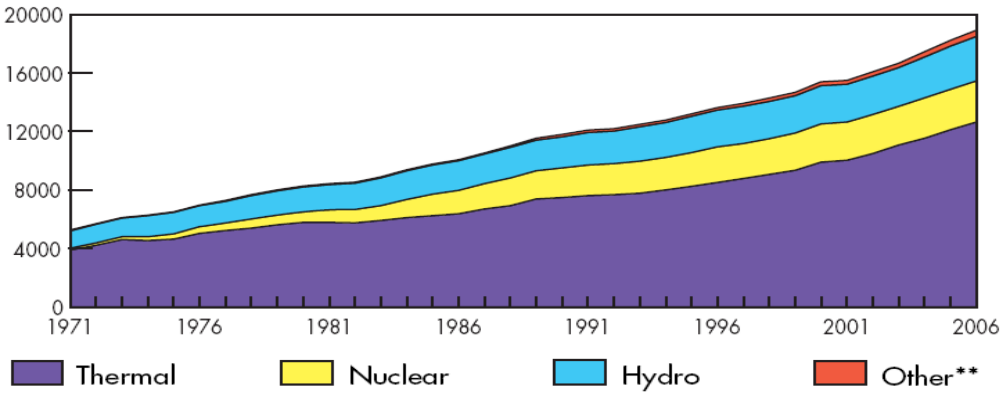

**Other includes geothermal, solar, wind, combustible renewable & waste.

Figure 1.2: Evolution from 1971 to 2006 of world electricity generation by fuel (TWh) (IEA, 2008b)

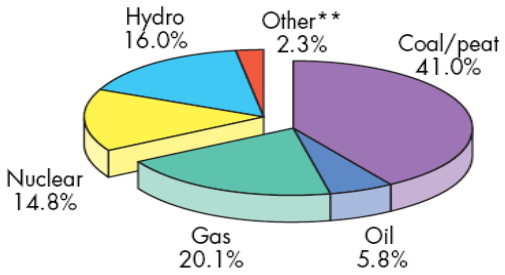

**Other includes geothermal, solar, wind, combustible renewables & waste.

Figure 1.3: 2006 Fuel shares of electricity generation (IEA, 2008b)

Large amounts of economic fossil fuel energy resources such as coal, oils and natural gas will probably continue to be used by humankind for power generation. It is expected that fossil fuels will generate more than 85% of the global increase in energy demand over the coming 25 years (IEA, 2004). As stated by the National Energy Board of Canada, the

domestic energy supplies in Canada will continue to use fossil fuels (Natural Resources Canada, 2006). Although it is expected that there will be a gradual switch to other alternatives like renewable energy resources and nuclear, fossil fuels power plants will remain the major electricity producer. Fossil fuels power plants present several advantages over other sources of energy. To name a few, fossil fuel plants can respond quickly to short term changes in peak demand for power; provide backup when other sources of energy, e.g. wind or solar, are used for electricity production; produce energy in larger quantities, and a lower cost, than those obtained from emerging renewable sources; and provide the flexibility to meet short and long term changes in the demands (OPG, 2009).

Thus, it is important to develop technologies for fossil fuels plants that can assist in the reduction of CO_2 emissions from fossil fuels. Several options for reducing CO_2 emissions from conventional power plants are available:

1. Increase the fuel conversion efficiency using advanced fossil-fuel technologies such as integrated gasification combined cycle (IGCC), supercritical and ultra-supercritical pulverized coal power plants, and natural gas combined cycle (NGCC) to reduce the CO_2 emissions.
2. Fuel switching from carbon-intensive fuels (e.g. coal) to less carbon-intensive fuels (e.g. natural gas) or non-fossil fuel energy alternatives such as nuclear, biomass, solar energy etc.
3. Capturing and storing the CO_2 emitted from the fossil fuel combustion.

It is expected that the implementations of all the options mentioned above will provide longer-term benefits to global warming. Carbon capture technologies have the potential to allow continuous use of fossil fuel while mitigating CO_2 emissions. Since power production is the major source of CO_2 emissions, capturing CO_2 from electricity plants is an attractive alternative for reducing the CO_2 generated from fossil-fuels. A number of technologies have been studied to capture CO_2 from various types of power plants including pre-combustion,

post-combustion and oxy-fuel combustion processes. However, none of these technologies have been applied yet to any existing large commercial power plants.

In Canada, over 104,579 GWhr of electricity is generated from existing coal-based power plants which contribute to 17% of the total electricity generation in (Natural Resources Canada, 2008). Due to this fact, there is vast potential for retrofitting carbon capture technologies to the existing coal fleet. The cost might be cheaper to retrofit CO_2 capture on existing power plants rather than building a new power plant with CO_2 capture. Pre-combustion and oxy-fuel combustion are not tail-end processes which would require a significant capital investment to deploy the technology to the existing power plant. Post-combustion is end-of-pipe treatment which does not affect the upstream part of the original power plant. Additionally, a report on CO_2 capture as a factor in power station investment decisions concluded that, post-combustion capture is viewed as the most promising technology, despite the fact that it has not been fully demonstrated (IEA GHG, 2006a).

Based on the above, the present study focused on the post combustion process technology to remove CO_2 from flue gas that can be retrofitted to existing fossil-fuel power plants. Post-combustion CO_2 capture with amine based solvent systems is currently the most suitable technology for fossil fuel power plants for many reasons. This process has been established for over 60 years in chemical and oil industries for gas purification to remove acid gases, e.g., CO_2 and H_2S, from natural gas streams (Kohl and Nielsen, 1997). The recovery rate of CO_2 is 98% using monoethanolamine solution (Yamasaki, 2003). This technology is the most compatible with existing power generation plant for retrofitting as it only involves adding equipments at the downstream without changing the existing plant. The CO_2 partial pressures in the flue gas after combustion is low, typically 3-15 kPa (IPCC, 2005). Thus, chemical absorption is the most likely used technology because chemical solvents are less dependent on partial pressure.

1.2 Significance of the research

CO_2 removal by amine scrubbing has been extensively studied to optimize the process operating conditions, to improve or test new solvents and to propose new designs that minimize energy consumption and reduces plant efficiency loses. Most of these studies describe the behaviour of this process using steady-state models, i.e., those studies assume that the power plant operates continuously at a given base load. However, power plants are subject to start-up, shut-down and changes in the flue gas load due to fluctuations in electricity demands. In addition, the time-varying conditions of the power plant will directly affect the performance of the CO_2 capture process.

Figure 1.4 shows the typical output from coal power generation plants in Ontario, Canada. As shown in this Figure, the output of the boilers varies from 1900 to 3100 MW over the course of a day. This data shows that the operating conditions of the power plant changes significantly in one day of operation. The flow rate of the flue gas from the boilers, and the corresponding amount of CO_2 released from flue gas, will also change in a similar fashion.

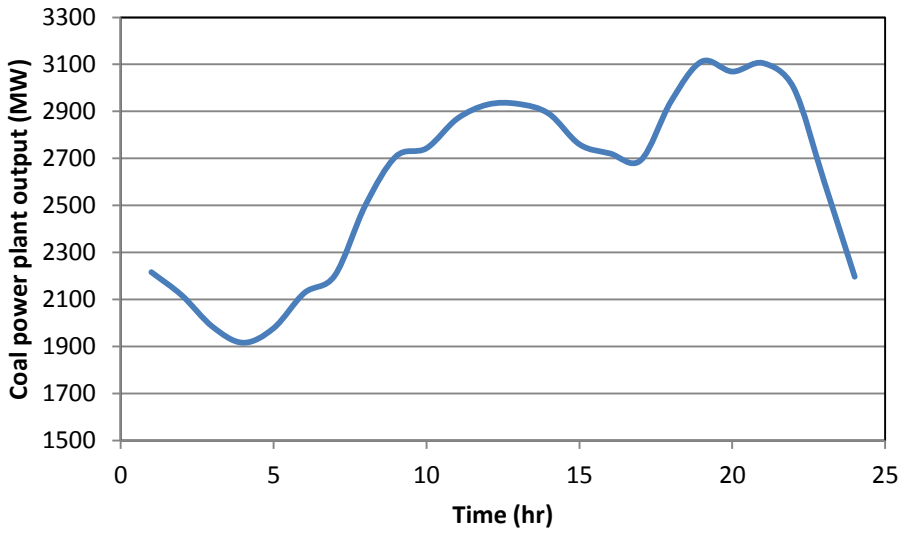

Figure 1.4: A typical output from coal power generation plants in Ontario, Canada (IESO, 2011)

Therefore, the ability of the amine absorption process to operate within limits in the dynamic fashion need to be evaluated. Although studies have been developed to analyze the flexibility[1] of the power plants with CO_2 capture with respect to part load (Chalmers and Gibbins, 2007; Davison, 2007) and variation in CO_2 recovery (Alie *et al*., 2006), those studies were performed under steady-state conditions. That is, the dynamic performance of plant due to changes in time in the part load was not included in those studies. Although valuable insight can be obtained from a steady-state analysis, the steady-state simulation is not sufficient to study the operability[2] of the power plant with CO_2 capture.

A complete understanding of the dynamic operability of the power plant with CO_2 capture using amine scrubbing is fundamental to successfully implement this process in commercial scale power plants. Also, several aspects need to be considered to determine the influence of power plant's dynamic behaviour on the CO_2 capture process using amine scrubbing. For example, the estimation of the residence times for the CO_2 capture process or the determination of the optimal operating conditions of the CO_2 capture process that will meet a given CO_2 removal in the presence of changes in the flue gas flowrate. Furthermore, a dynamic process model is required to develop suitable control strategies that can be implemented in this process for on-line control. These studies cannot be conducted using a steady-state model and thus a dynamic model of the MEA process is necessary.

The implementation of a control strategy for the MEA absorption process will ensure that the process will remain stable and feasible in the presence of external perturbations while meeting the performance specifications outlined for the process.

[1] Flexibility is the ability of the process to operate in an acceptable manner over a range of steady state condition

[2] Operability is the ability of a process to operate satisfactorily under conditions different than the nominal design conditions.

1.3 Research objectives

Based on the above discussion, the two main research objectives of the present study are stated as follows:

1. Develop a comprehensive mechanistic first principle dynamic model for the complete MEA absorption process.
    - A detailed mathematical formulation that describing the transient operation of each of the units involved in this process will be considered first.
    - Integrate the process models of each of the units to generate the complete MEA CO_2 process model. The complete mathematical formulation will be validated using data reported in the literature.
    - Insight regarding the transient behaviour of the MEA absorption plant due to changes in the flue gas flow rate and reboiler heat duty will be provided with this research. Ramp, step and sinusoidal input tests will be implemented in key process variables, i.e., the flue gas flow rate and the reboiler's heat duty, to study the transient response that may occur in a real process plant due to changes in these process variables.

2. Develop a basic control strategy that allows the operation of the MEA process at specific operating conditions in the presence of external disturbances
    - The control strategy will be developed based on the mechanistic process model proposed in this work for the complete MEA process. The development of a control strategy for the CO_2 capture process is relevant to keep the controlled variables at their set points despite any possible disturbance changes while maintaining the process operation within the feasible region. Also, a suitable control strategy needs to guarantee the process meet the desired operating conditions and remain stable in the presence of disturbances.

1.4 Research contribution

The mechanistic process model of the complete CO_2 capture plant proposed in this work is based on the conservation laws of mass, energy and momentum. This represents a unique feature since the current simulations available for this process have made used of standard software packages to describe the transient behaviour of this system. Consequently, the dynamic MEA process model proposed in this work provides insight regarding the key transient characteristics of this process. For example, a sinusoidal test, representing a sustained change in the flue gas flow rate, was used to simulate the entire MEA plant. The insight obtained from that test, which is a typical behaviour for power plant outputs and has not been presented before, will be useful to analyze the plant's process characteristics introduced in the process model to study the oscillatory behaviour of this process.

Moreover, the resulting mechanistic process model can be used as a tool to determine the operability of this process in a dynamic fashion. The insight gained with the mechanistic process model can be used to design new control strategies for this system. For example, a decentralized control strategy based on Proportional-Integral (PI) controllers was developed in this research to study the closed-loop performance of this system under the effect of external perturbations. The present research provides the first control strategy based on a mechanistic process model since the current control strategies proposed for this system have been based on simulations of the plant using standard software packages, e.g., Aspen Plus®.

1.5 Outline of thesis

The thesis is organized in six chapters as follows:

Chapter 1: *INTRODUCTION*

This chapter presents an overview of the research work that was performed. The objectives and research contributions of this work are discussed in this chapter.

Chapter 2: *LITERATURE REVIEW*

This chapter provides a review of the literature on topics relevant to CO_2 capture with particular focus on post-combustion. This chapter also summarizes the published works related to the modelling and simulation of MEA absorption process with special emphasis on the current development of dynamic and control strategies for this process. Some theories related to model development such as chemical kinetics and vapour-liquid equilibrium (VLE) are also presented in this chapter.

Chapter 3: *MATHEMATICAL MODELLING*

This chapter describes in detail the mathematical formulation used to develop each of the unit operations in the MEA absorption process. This chapter also describes some theories related to model development i.e. rate-based vs. equilibrium-based approach, enhancement factor and film theory model and mention the information required to model the process. In addition, the methods used to estimate the physical properties of the system are also presented in this chapter to provide a complete quantitative description of the process. The steps needed to implement the model in the gPROMS software are also mentioned in this chapter.

Chapter 4: *STEADY-STATE AND DYNAMIC SIMULATIONS*

This chapter presents first the steady state simulation results obtained from the dynamic process model described in Chapter 3. The steady state results of the individual units and the complete process model are compared with Aspen Plus® simulations for model validation at different operating conditions. Dynamic simulations of the complete process model are performed to study the open loop performance of the system in the presence of changes in the flue gas flow rate and reboiler duty.

Chapter 5: *PROCESS CONTROL*

This chapter discusses the development of a decentralized control strategy to maintain the CO_2 capture process at its desired nominal operating conditions in the presence of

disturbances. The implementation of a Proportional-Integral (PI) controller in this study to achieve the controller objectives is described in this chapter. Several open loop tests to determine the first order model parameters to design the controller are also presented. Closed-loop simulations of the MEA process in the presence of sustained changes in the flue gas flow rate also are presented and discussed in this chapter.

Chapter 6: *CONCLUSIONS AND RECOMMENDATIONS*

This chapter presents the conclusions obtained from the thesis work and the recommendations for future work.

Chapter 2
Literature Review

This chapter is organized as follows: Section 2.1 briefly describes potential CO_2 capture systems for power plants such as post-combustion, pre-combustion and oxy-fuel combustion. In Section 2.2, the suitable separation technologies that can be used to capture CO_2, which depends on the characteristics of the gas stream from which CO_2 needs to be separated, are presented. Section 2.3 provides the overview of various studies based on modeling and simulation of amine absorption process. This section is divided into steady state simulation and dynamic simulations. Section 2.4 presents details of the chemistry, kinetics and vapour-liquid equilibrium (VLE) that are related for the development of the MEA absorption process model.

2.1 CO_2 capture system for power plant

Nowadays, CO_2 capture technology is mainly used to purify synthesis gas in the chemical industry (ammonia, hydrogen), to remove CO_2 from natural gas, to supply CO_2 for the merchant market (beverage, dry ice, etc.) and has been also recently considered in enhanced oil recovery (EOR). However, there is no commercial market for its use in the power industry for CO_2 capture (IEA GHG, 2006a), i.e., CO_2 capture has only been considered at pilot scale (Suda et al., 1992). Its application to commercial size power plants has only been studied in terms of the power plant performance and economic analysis (e.g. Booras and Smelser, 1991; Desideri and Paolucci, 1999; Singh et al., 2003; Davison, 2007; Rubin et al., 2007; Lucquiaud and Gibbins, 2011). CO_2 capture process technologies for power plant can be divided into three general process routes (see Figure 2.1):

- *Post-combustion processes*
- *Pre-combustion processes*
- *Oxy-combustion processes*

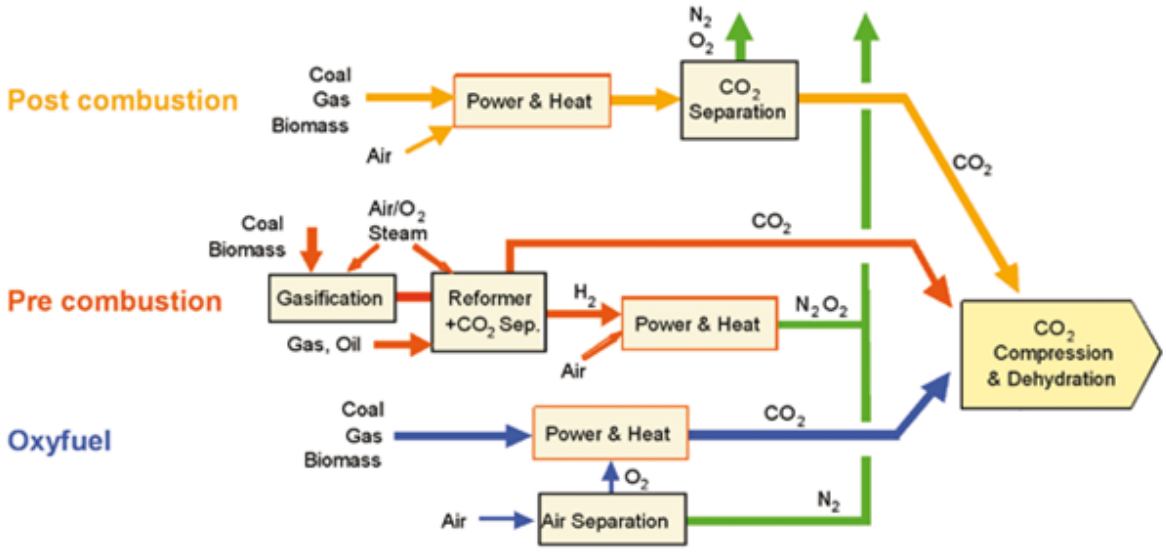

Figure 2.1: CO_2 capture options for power plant (IPCC, 2005)

In the post-combustion process, CO_2 is captured from the exiting flue gas, while in oxy-fuel combustion air is replaced by oxygen in the combustion process producing concentrated CO_2. In the pre-combustion capture process, fossil fuels are reformed into synthesis gas (syngas) comprised mainly of hydrogen and carbon monoxide. The following section briefly discussed these three CO_2 capture system that can be applied for power plant.

2.1.1 Post-combustion

The principle of post-combustion capture is the separation of CO_2 from flue gases produced by the combustion of fossil fuels. Post-combustion processes consist of two main process steps. The first step is an energy conversion, used to generate power, followed by a CO_2 separation process in which a concentrated stream of CO_2 is produced (Feron and Hendriks, 2005). A number of CO_2 separation technologies can be applied for post-combustion capture system such as chemical absorption, membrane separation and adsorption. Despite the fact that post combustion has not been fully considered in large power plants, the leading option for post combustion process is an absorption process using amine based solvents (IPCC, 2005; IEA GHG, 2007). A drawback of the post-combustion capture technology using the amine scrubbing process is that it requires large equipment sizes which leads to high capital

costs due to large volume of gas at low concentration of CO_2 that needs to be handled. A key challenge for this technology is the large amount of energy required for regeneration of the solvents. This heat is normally drawn from the steam cycle and considerably reduces the net efficiency of the power plant (Alie, 2004; Cifre et al., 2009). Based on the above, there is a need to improve the current solvents or develop new solvents which could reduce both the energy penalty and capital cost of post-combustion capture. Other needed technologies for post-combustion systems are integrated pollutant control and waste management processes for both retrofits and new power plants. In addition, controllability of the post combustion process is key because the power plant output, i.e., the flue gas flow rate and its composition, and the steam rate provided by the steam cycle are continuously changing due to changes in the power grid's demands. These aspects will definitively affect the operation of a CO_2 capture plant. The development of a control strategy for this process will be able to maintain the CO_2 removal and minimize the energy consumption for solvent regeneration.

2.1.2 Pre-combustion

In this process, the CO_2 is captured prior to burning the fuel in a combustor. Pre-combustion process involves reforming/conversion of fossil fuel to produce a synthesis gas (syngas), a mixture containing hydrogen (H_2), carbon dioxide (CO_2) and carbon monoxide (CO) (Feron and Hendriks, 2005). The CO then undergoes a shift reaction where the CO reacts with steam to generate more H_2 and CO_2. CO_2 is then separated, usually by a physical or chemical absorption process, resulting in a hydrogen-rich stream which can be used in many applications, such as boilers, furnaces, gas turbines, engines and fuel cells. The CO_2 concentration and pressure are higher in pre-combustion capture than in post-combustion capture, allowing the use of physical solvent for CO_2 removal, which is much less energy intensive than the MEA process (IPCC, 2005). The conversion of fossil fuel to syngas can be done using gasification, partial oxidation or steam reforming technology. Gasification is most often used for solid fuels, partial oxidation for liquids, and steam reforming for gases. Integrated coal gasification combined cycle (IGCC) plant is an example of this technology. The fuel conversion of this process is costly (IPCC, 2005) and would be appropriate for new plant projects (Elwell and Grant, 2006).

2.1.3 Oxy-fuel combustion

The oxy-fuel combustion process uses relatively pure oxygen (95% or higher) for combustion in place of atmospheric air. The use of enriched oxygen significantly improves the combustion of fossil fuel due to higher combustion rates and temperature. The resulting flue gas is primarily CO_2, with trace amounts of oxygen and other gases that can be flashed off during the compression of the CO_2. A major part (70-80%) of the CO_2-rich exhaust gas is recycled back to the boiler to control the combustion temperature (Buhre et al., 2005). The remaining part of the flue gas, (consisting mainly of CO_2 and water vapour and small quantities of Ar, N_2, NO_x, SO_x and other constituents from air leakage and fuel) is cleaned, compressed and transported to storage or another suitable application, such as enhanced oil recovery (EOR). This process is easier to be applied for steam turbine plants rather than gas turbine plants. In the former, relatively straightforward boiler modifications are required. For the latter, much more complex gas turbine design changes will be required.

The greatest challenge faced by oxy-fuel is to lower the energy penalty (and therefore the penalty cost) involved in producing large quantity of oxygen**.** It is expected that this emerging technology will have operating, maintenance and capital costs that would be comparable to that of post-combustion technology. Particularly, the oxygen separation plant would consume about 23% to 37% of the total plant output and costs about the same as a chemical absorber (Yang et al., 2008). Another important challenge is that oxy-fuel combustion process requires major changes in combustion equipment and materials because current design configurations and materials are unable to operate at high temperature values; however, it is expected that through the use of exhaust gas recirculation should be able to control the combustion temperature to prevent damage to the boiler. This technology has been built and operated at pilot plant scale but further development is required before this process is ready for the design and construction of a full-scale system (IPCC, 2005).

2.2 CO_2 separation technologies

CO_2 capture systems may use many of the known technologies available for gas separation such as adsorption, membrane separation, cryogenic separation, physical and chemical absorption. A brief summary of these separation methods is given in the following sections. The choice of a suitable technology depends upon the characteristics of the gas stream from which the CO_2 needs to be separated, the sensitivity of the method to other impurities or trace components, the amount of CO_2 recovery, the capital and operating costs and the environmental impacts (waste or by-product production) (Steeneveldt et al., 2006). Studies that reviews and discuss in detailed the CO_2 capture technologies are currently available (IPCC, 2005; Steeneveldt et al., 2006; Yang et al., 2008; Rackley, 2010; Abass, 2010; Pires et al., 2011).

Adsorption

In this technology, carbon dioxide is removed from the flue gas using solid adsorbents that have a high surface area and desorbed through a regeneration process. Solid adsorbents may include natural or synthetic zeolites, activated carbon, alumina, molecular sieves, and polymers. The adsorption process is typically cycled between two beds of adsorbents; one bed is adsorbing CO_2 while the other is being regenerated. In the regeneration process, CO_2 can be desorbed by either pressure swing adsorption (PSA) (pressure reduction) (Ishibashi et al., 1999; Gomes and Yee, 2002; Yokoyama, 2003), temperature swing adsorption (TSA) (temperature increase) (Drage et al., 2009; Tlili et al., 2009), electrical swing adsorption (ESA) (Grande and Rodrigues, 2008; Grande et al., 2009), which adjusts the electric current passed through the adsorbents, or vacuum swing adsorption (VSA) (Chaffee et al., 2007). PSA is commercially used for gas separation, in hydrogen production and in the removal of CO_2 from natural gas (Diagne et al, 1995; Yong et al., 2002; IPCC 2005). However, the key challenge of CO_2 capture using adsorption technology is low capacity and selectivity for current adsorbents, which limits its application for large scale CO_2 removal.

Membrane separation

The membrane separation process is based on the diffusion rate of individual components from one side of a membrane barrier to the other side. The CO_2 dissolves into the membrane and then diffuses through the membrane as the result of concentration gradient. Membranes with high selectivity and permeability for the component to be separated are more suitable for this technology. Gas separation membranes have been commercially used to remove CO_2 from natural gas streams which have high concentration of CO_2 and are commonly used for H_2 recovery in refineries (Scholes et al., 2010). There are many different types of membrane materials such as polymeric, metallic and ceramic that may find application in CO_2 capture systems. The advantages of a gas membrane separation process include lower capital cost, ease of skid-mounted installation, lower energy consumption, its ability to be installed in remote areas, especially offshore, and flexibility (IPCC, 2005). Membrane separation can be potentially used in CO_2 capture, i.e., separation of CO_2 from hydrogen in pre-combustion process and produce oxygen-enriched stream from air in the oxy-fuel combustion process. Metallic membrane, which is selective for hydrogen, is particularly attractive compared with polymeric membranes because of its high permeability, operating pressures and temperatures. Due to its long period of lifetime, metallic membrane can be potentially be used in integrated gas combined cycle (IGCC) power plant with pre-combustion CO_2 capture (Carapellucci and Milazzo, 2003). The application of membrane gas separation for post-combustion process requires a large membrane areas combined with high energy consumption rates which increases the cost of this capture technology (Pires et al., 2011). The membrane separation technology for CO_2 capture from flue gas can be competitive with respect to chemical absorption if CO_2 flue gas concentration is higher than 10% in moles (Corti et al., 2004). Recent studies have focused on the development of a hybrid membrane technology, where membranes are combined with another separation process such as chemical absorption (IPCC, 2005). Using this method, a liquid solvent is used to carry out the CO_2 molecules that diffuse through the membrane such that no high hydrostatic pressure is required. The membrane serves as an interface between the flue gas and the liquid solvent

which offers high surface-to-volume ratio for mass transfer between the gas and liquid solvent (Rackley, 2010).

Cryogenic separation

Cryogenic distillation is an air separation process that can be applied to separate CO_2 from other components by compression, cooling, condensation, and distillation to produce liquid CO_2. The CO_2 produced in the liquid form is easy to handle for transportation and storage. This technology is widely used in the industry for streams which have high CO_2 concentrations (typically >90%) but not used for dilute CO_2 streams (Abass, 2010). This process is energy intensive because it requires large amount of energy for the refrigeration and would result in large efficiency reductions when applied for CO_2 capture from flue gas (Pires et al., 2011). Cryogenic separation is economic for streams having high concentration of CO_2 such as pre-combustion and oxy-fuel combustion process.

Physical absorption

Physical absorption uses organic or inorganic solvents to physically absorbed the CO_2 rather than chemically react with the solvent. This process is mostly applicable to gas streams which have relatively concentrated streams of CO_2 at high pressures. They are commercially used to remove acid gases, CO_2 and H_2S from natural gas and for removing CO_2 from synthesis gas in ammonia, hydrogen, and methanol production. Some commercially available solvents include dimethyl ether, polyethylene glycol (Selexol) and cold methanol (Rectisol) (Abass, 2010). In physical absorption, the untreated gas is contacted with the solvent in an absorber column and CO_2 is absorbed by the solvent. The CO_2 rich liquid stream exits the bottom of the absorber and then passes through a series of flash drums at varying pressures. Depressurization releases the CO_2 from the solvent. The lean solvent is then recycled back to the absorber column. The process has low energy consumption, as only the energy for pressurizing the solvent (liquid pumping) is required. Physical absorption processes typically operate near 40°C and therefore the flue gas must be cooled accordingly. Physical absorption

processes are the preferred method to remove CO_2 removal that comes from the shift reaction in pre-combustion CO_2 capture processes (IPCC, 2005). The physical absorption is not economically competitive for low partial pressure of CO_2 because the capacity of physical solvents is strongly dependent on partial pressure (Kohl and Nielsen, 1997; Chakravati et al., 2001; IEA, 2004).

Chemical absorption

Chemical absorption processes are currently the preferred option for post-combustion CO_2 capture due low partial pressure of CO_2 in the exhaust gas. In the chemical absorption, the CO_2 is absorbed and chemically react with the solvent. Chemical absorption processes are applicable for removing CO_2 that is present in dilute concentration (low partial pressure). However, the challenge of this technology for CO_2 capture from power plant is due to high energy demand for solvent regeneration and solvent degradation. The solvent such as amine solution, aqueous ammonia and carbonate removes CO_2 from the gas stream by means of chemical reactions in the absorption column. The ideal chemical solvent should have the following characteristics (Davidson, 2007):

- lower energy/cost for solvent regeneration
- higher absorption rate
- higher reactivity for CO_2 capture
- better stability, less degradation and lower corrosivity
- lower solvent cost
- lower environmental impact.

MEA solution is widely investigated solvent for post-combustion capture process due to high capacity for CO_2 capture, fast reaction kinetic, cheap and largely available. On the other hand, MEA solution requires considerable amounts of thermal energy to strip CO_2 from loaded MEA solutions. Also MEA is more corrosive than secondary and tertiary amine and solvent degradation due to reaction with oxygen in flue gas (Resnik et al., 2004). Alternatively, mixed amine solvents have been proposed to maximize the desirable qualities

of the individual amines. MEA has been blended with amines that are less corrosive and require less steam to regenerate such as MEA/2-amino-2-methyl-1-propanal (AMP) (Dey and Aroonwilas, 2009) and MEA/MDEA (Idem et al., 2006). The additive piperazine (PZ) in MEA solutions was able to accelerate CO_2 absorption and allows use of lower MEA concentrations (Dang and Rochelle, 2003; Dugas and Rochelle, 2011). Freeman et al., 2010 proposed new amine solvent, i.e., concentrated aqueous piperazine (PZ), which has an absorption rate that is higher than MEA. Chowdhury et al. (2009) investigated different tertiary amine based absorbents with high absorption rate and low heats of reaction. Inhibitors has also been tested in the process to reduce solvent degradation. Delfort et al. (2011) tested specific oxidation inhibitor to reduce MEA degradation. An alternative to amine based solvents such as chilled ammonia process (CAP) (Darde et al., 2009), ammonia based solution (Pellegrini et al., 2010), and carbonate based solution (Li et al., 2008; Fang et al., 2009) has been identified to be potentially used to improve the CO_2 absorption process.

Summary of CO_2 separation technologies

The previous section presented the three CO_2 capture systems, i.e., post-combustion, pre-combustion and oxy-fuel combustion, for power plant applications. These CO_2 capture systems may use several CO_2 capture technologies which have been discussed in this section. Although these technologies are basically feasible from a technical point of view, their efficiency, reliability, long-term performance and economics are still uncertain. Most technologies are expensive and their costs can only be reduced if the technologies are improved further. Physical/chemical absorption, adsorption and membrane separation are relatively mature CO_2 separation technologies and have been implemented in the industry. For post-combustion process, chemical absorption represents the most promising option for CO_2 capture from power plant and the most cost-effective technology in terms of cost, recovery and purity (Yang et al., 2011). The technology for chemical absorption is available and has been implemented in the industry (IPCC, 2005):

Table 2.1: The application of chemical absorption process in the industry

Process	Description
Kerr-McGee/ABB Lummus Crest Process	15-20 wt% MEA solution. The largest capacity experienced for this process is 800 tCO_2 per day utilizing two parallel trains.
Fluor Daniel ® ECONAMINE™ Process	30 wt% aqueous solution MEA solution with an inhibitor to resist carbon steel corrosion. It has been used in many plants worldwide recovering up to 320 tCO_2 per day in a single train for use in beverage and urea production.
Kansai Electric Power Co., Mitsubishi Heavy Industries, Ltd., KEPCO/MHI Process	Sterically-hindered amines solvents (KS-1, KS-2 and KS-3). Low amine losses and low solvent degradation have been noted without the use of inhibitors or additives. The first commercial plant at 200 tCO_2 per day recovery from a flue gas stream for urea production.

In order to employ CO_2 capture for commercial power plants, more research is needed for the development and identification of optimal solvents for absorption and the minimization of the energy penalty for the capture system

2.3 Modelling and simulation of amine absorption process for CO_2 capture

Absorption of gases in liquids accompanied by chemical reactions (also known as *reactive absorption*) is one of the basic operations in many gas purification processes. It involves a combination of mass transfer and reactions taking place in a two phase system with an interface (Danckwerts, 1970). The gaseous components, which are being absorbed, react with a component of the liquid phase to form a loosely bonded reaction product. The chemical reactions can increase the rate of absorption, the absorption capacity of the solvent and the selectivity to preferentially dissolve only certain compound. Absorption of carbon dioxide into amine solution is classified as a reactive absorption process.

The amine absorption process refers to a process that uses aqueous amine solutions to remove carbon dioxide (CO_2) from gases. It is a common process unit used in refineries, petrochemical plants, natural gas processing plants and other industries. Amines of particular commercial interest for gas purification are monoethanolamine (MEA), diethanolamine (DEA) and methyldiethanolamine (MDEA) (Kohl and Nielsen, 1997). The amine absorption process consists of two basic units: an absorber, which operates at high pressure and moderate temperature, and a stripper, which operates at low pressure and high temperature. A simplified process flow diagram of amine absorption process is shown in Figure 2.2.

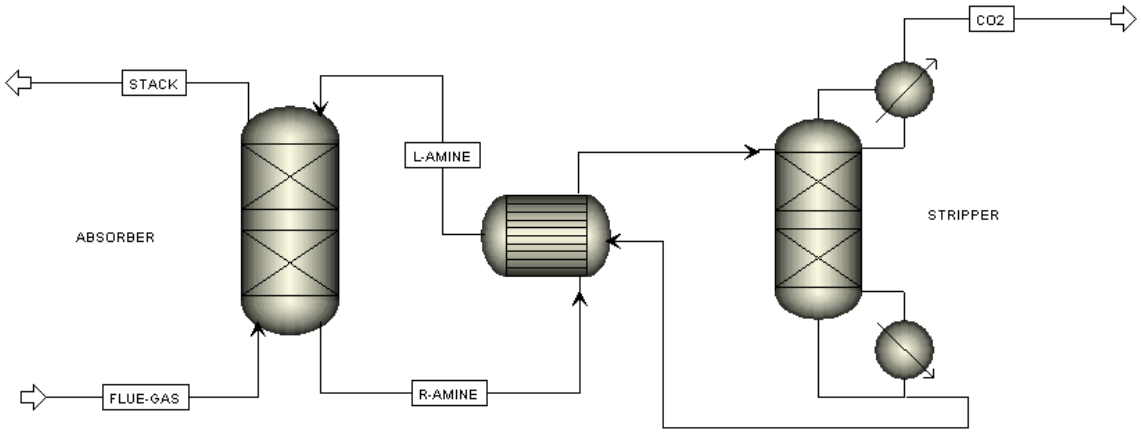

Figure 2.2: Process flow diagram of amine absorption process

The flue gas enters the bottom of the absorber and is contacted counter currently with the amine solution. The CO_2 is absorbed by the amine solution and reacts to form a loosely bound compound. As the CO_2 is absorbed into the amine solution, a cleaner, treated gas leaves the top of the absorption tower. The rich amine solution, which is loaded with CO_2, leaves the absorber unit through the bottom and is heated through a heat exchanger with the hot lean amine solution coming from the bottom of the stripper. Then, the solution is sent to the top of the stripper where it is heated again with steam for the desorption process (reverse of absorption) for CO_2 stripping from the amine solution. The CO_2 is released at the top of the stripper while the lean amine solution is recycled back to the absorber.

Modelling and simulation of amine absorption process have been extensively studied in the industry and the academia. In general, modeling amine absorption process to capture CO_2 can be classified in two main groups: steady state and dynamic simulation. The following sections will briefly describe simulation works published in the literature.

2.3.1 Steady state modeling and simulation

Steady-state simulation is important for the design or process synthesis because most processes operate around a nominal (steady-state) condition. Steady-state studies for the MEA process have usually considered the performance of CO_2 capture process at constant output from the power plant, i.e., constant flue gas flow rate. The area of studies can be further classified as techno-economic studies and process optimizations studies.

Techno-economic studies

Techno-economic studies have reported the incremental cost and performance reduction of various types of power plants with the implementation of CO_2 capture using MEA scrubbing process. Booras and Smelser (1991) showed that addition of CO_2 capture using MEA scrubbing result in increasing the cost of existing pulverised coal-fired power plant by a factor of up to 2.6 and reduce the net power plant output by 35%. According to Desideri and Paolucci (1999), the addition of CO_2 capture process to reduce 90% CO_2 emissions from a conventional power plant is penalized by high capital cost of the removal plant and the cost of electricity more than doubles at optimal absorber and stripper performance parameters. Singh et al. (2003) found that the CO_2 capture cost using MEA scrubbing process is $55/ton of CO_2 avoided, which translates into 3.3 ¢/kWh and represents an increase of 30% in electricity price. Singh et al. (2003) reported that thermal energy requirement to regenerate MEA solvents contribute a major part of the process overall annual cost.

The impacts of CO_2 capture on different types of power plants have also been studied. The plant efficiency reduction with CO_2 capture for a coal-fired power plant (21%) is higher than natural gas-fired power plant (15%) in which more than half of the efficiency reduction is

due to thermal energy requirement for solvent regeneration (Davison, 2007). Kanniche et al. (2010) reported that the efficiency of a pulverized coal (PC) power plant with CO_2 capture using amine absorption process was reduced by 15% from the PC plant without CO_2 capture. The investment cost of implementation of CO_2 capture for PC plant was increased by 78% relative to PC power plant without CO_2 capture. OECD/IEA (2011) has conducted an analysis about the cost and performance of power plant installed with CO_2 capture process, based on several techno-economic studies published in the literature. They found that, an average net efficiency penalty for post combustion capture using amine solvent was 10% relative to the pulverized coal-fired power plant (> 300 MW net power) without CO_2 capture process, which is on average a 25% reduction in efficiency. As discussed above, the implementation of a CO_2 capture process to the power plant will significantly affect the plant efficiency and the cost operation. Thus, reducing the capture cost and power plant efficiency losses is very important in order to implement the CO_2 capture to the power plant in the future.

Process optimization

As mention above, the reboiler heat duty in the regeneration column is the main energy consumer in amine scrubbing process for CO_2 capture (Desideri and Paolucci, 1999; Singh et al., 2003). The overall energy efficiency of CO_2 capture can be substantially improved by reducing this energy demand. Heat required for solvent regeneration in the stripper column can be supplied by either an auxiliary boiler or from power plant steam extraction. Several studies have proposed different approaches to reduce the reboiler heat duty (Aroonwilas and Veawab, 2007; Alie et al., 2004; Romeo et al., 2008). Aroonwilas and Veawab (2007) reported that blended MEA/MDEA returned significant reductions in thermal energy requirements and lowered the power plant efficiency penalty. Alie (2004) proposed a steam extraction system from an intermediate pressure/low pressure (IP/LP) crossover pipe to reduce efficiency losses. Romeo et al. (2008) pointed out that extracting steam from the

steam cycle of a power plant is an attractive (economic) option to reduce the efficiency penalty on the power plant performance.

A number of publications have been aimed to reduce the energy consumption by optimizing the operation of this process using steady-state models. Freguia and Rochelle (2003) modeled CO_2 capture by aqueous MEA using Aspen Plus® software. The RateFrac model was used to model the absorber and stripper columns. The effects of process design and operating variables, i.e., solvent circulating rate, absorber and stripper height, and stripper pressure on energy requirement were studied. The optimization of these variables could not be able to reduce the steam requirements by more than 10%. Alie et al. (2005) modelled an MEA absorption process using Aspen Plus®. Several parameters were varied including flue gas, CO_2 and MEA concentration, lean solvent loading and rich solvent temperature in order to find the lowest reboiler duty settings. This study showed that the lean solvent loading has a major effect on the thermal energy requirement. A minimum reboiler heat duty of the stripper could be achieved at lean solvent loading of 0.25 mol CO_2/mol MEA with 30 wt.% aqueous MEA solution. Abu-Zahra et al. (2007a) investigated the effect of design parameters (i.e. MEA concentration, stripper pressure and lean MEA loading) on the process economics, and concluded that, the optimizations of these process parameters resulted in a reduction in the overall cost of a CO_2 capture process. From that study, the optimum lean loadings were found to be between 0.32 and 0.30 mol CO_2/mol MEA in 30 wt % and 40 wt % MEA cases, respectively, as the major energy saving factors. Cifre et al. (2009) conducted a simulation study that showed that the optimization of the amine scrubbing process parameters (i.e. stripper pressure, lean solvent flow rate and absorber column height) reduced the energy penalty, i.e., the energy requirement that reduces the net efficiency of the power plant due to the steam extraction from power plant to supply heat for CO_2 capture process, by 1-3%. Ziaii et al. (2009) developed a rate-based stripper model using Aspen Custom Modeler to analyze the effect of lean loading and height of packing in order to minimize energy consumptions. The optimum operating conditions were found to be at a lean loading of 0.42 mol CO_2/mol MEA with a packing height of 1.8 m.

2.3.2 Dynamic modeling and simulation

In recent years dynamic simulation has become an increasingly important tool in the process industries for several reasons: operability studies, safety and risk analyses, analysis of start-up and shut-down procedures and systematic process optimization using optimal control techniques. Dynamic simulation is the basis for the design of standard and advanced control strategies and a platform for the preliminary implementation of process control systems.

Several dynamic simulation studies have been carried out to examine the flexibility of the power plant with CO_2 capture with respect to part load and CO_2 recovery rate. Davison (2007) discussed the effect of operating the power plant at lower load factor (65% and 35% load factor) on the cost of coal-fired and natural gas-fired power plant with CO_2 capture. The costs of electricity generation for coal-fired plants are higher than for gas-fired plant at low load factors due to higher fixed cost for coal-fired plants. Chalmers and Gibbins (2007) proposed to store the rich solvent and regenerate it when the electricity price is low in order to take advantage of varying electricity price. Solvent storage may be used at times of high demand (allowing the plant to generate additional revenues as a result of the high electricity prices associated with periods of high demand) by storing solvent and then regenerating additional solvent at times of lower demand when electricity prices are attractive.

To study disturbances in the process operations such as flue gas fluctuations due to load changes or plant start-up and shut-down, knowledge of the dynamic process behaviour is required. Further areas where the dynamic information is crucial are process control and dynamic flexibility analyses for the optimal dynamic operation of the process. Although several steady-state studies have been reported for the MEA process, only a few (recent) studies have focused on the dynamic behaviour of this process.

Kvamsdal et al. (2009) developed a dynamic rate-based model of an absorber column for CO_2 capture using gPROMS. The mass and heat transfer were described by the two-film theory. The overall mass transfer coefficients were used to describe the inter-phase mass

transfer. The enhancement factor of pseudo-first order reaction was used to incorporate the effect of chemical reaction in the liquid film on mass transfer. Constant values of heat of absorption and heat of vaporization were assumed in that study. The model was validated at steady state using data obtained from a pilot plant (Dugas, 2006). Both inlet gas flow rate and column height were adjusted to match the percentage of CO_2 removal and liquid temperature profile with the corresponding pilot plant data. The dynamic simulation results were presented for partial load reduction (reduced the base load from 100% to 50%) and start up. It was found that L/G ratio significantly affects the performance of the absorption process during partial load reduction.

Lawal et al. (2009a) modelled a standalone absorber and used the same pilot plant process to enable a comparison with Kvamsdal's work (Kvamsdal et al., 2009). Both equilibrium and rate-based packed column models were developed using the Radfrac column model in Aspen Plus and the Advanced Model Library for Gas–Liquid Contactors (AML:GLC) in gPROMS software (PSE, 2009), respectively. The inlet flue gas flow rate was adjusted to fit the model prediction with the pilot plant data. The rate-based model developed in gPROMS returned better results than the equilibrium model in terms of the liquid temperature profile in the absorber column, percentage of CO_2 captured and CO_2 loading at steady state. In the rate-based model, the mass transfer through the gas-liquid interface was described using Maxwell-Stefan theory, based on a two film model (Taylor and Krishna, 1993). Liquid phase non-idealities were described with the electrolyte non-random-two-liquid (electrolyte NRTL) model obtained from the Aspen Properties software through CAPE-OPEN Thermo interface. Dynamic analysis of partial load reductions and 10% increased in lean loading were presented. The results showed that a reduction of the plant load while maintaining the L/G ratio (lean MEA solvent to flue gas ratio)does not affect the absorption process while increasing CO_2 loading of the lean MEA solvent by 10% decreased the CO_2 recovery rate by 9%.

Lawal et al. (2009b) developed a standalone dynamic stripper model using rate-based approach with the assumption equilibrium reaction in the liquid phase. The impact of the reboiler duty on the CO_2 loadings in the solvent at the bottom of the stripper was analyzed in this work. The results showed that the reduction in heat duty increased the CO_2 loading in the lean solvent which could reduce the absorption capacity.

Ghaemi et al. (2009) presented a dynamic standalone absorber model for CO_2 capture using partially carbonated ammonia solution. Unsteady state two-film model and enhancement factor approaches were applied to describe the mass transfer between gas and liquid phases. The chemical reactions were assumed to take place in both gas and liquid phases. Pilot plant experimental data were used to validate the model. The comparison between simulation results and experimental data using enhancement factor and film theory showed that the model using film model approach provided more accurate results than those using enhancement factors.

Ziaii et al. (2009) developed a standalone rate-based dynamic stripper column model using Aspen Customer Modeler. In that study, the two-film theory was applied to describe the mass transfer. The packed column model was described by a mixed of ordinary differential equations (ODE) and algebraic equations. Two control strategies during the period of electricity peak load were presented in order to reduce the energy consumptions of the stripper.

The previous dynamic simulation studies were carried out using dynamic standalone absorber/stripper. That is, the integration between absorber and stripper, which represent the complete MEA absorption process, was not considered in those studies. Lawal et al. (2010) extended their previous models (Lawal et al., 2009a; Lawal et al., 2009b) to consider the complete MEA absorption process by integrating both absorber and stripper with the recycle stream. The analysis of the dynamic response with respect to changes in flue gas flow rate and compositions, and reboiler heat duty were discussed. The importance of appropriate

water balance in the absorber column was also highlighted. In that study, a built in gPROMS Advanced Model Library for Gas–Liquid Contactors (AML:GLC) was used for the packed column model and gPROMS Process Model Library was used for other unit operations. As such, a formal mathematical model for the complete process was not provided. Also, the model used for the dynamic simulations in this study neglected the accumulation of mass and energy in the vapour phase because it was assumed that the residence time in the vapour phase is small compared to that in the liquid phase in packed column. Furthermore, the physical properties used in those simulations were obtained from the Multiflash physical property interface and Aspen Properties packages.

2.4 Development of control strategy of amine absorption process for CO_2 capture

Despite the advances that have been made to improve the efficiency of the MEA CO_2 capture technology, only a few process control strategies for this process have been recently published in the literature. Bedelbayev (2008) implemented a Model Predictive Control (MPC) method using MATLAB software to control the concentration of CO_2 at the top of the absorber by manipulating the liquid velocity in the absorber. However, that study only focused on the absorber column in the MEA process.

Using the Aspen Custom Modeller, Ziaii et al. (2009) developed a ratio control strategy for a stripper column that minimizes the energy consumption during the peak load electricity usage. A ratio control strategy was performed to keep the lean loading entering the absorber constant by controlling the ratio between the rich solvent flow rate and the reboiler heat duty. The ratio control strategy implemented in this work was able to keep the lean loading and the reboiler temperature close to their set point values. Nevertheless, the control strategy was tested for the standalone stripper column only.

Kvamsdal et al. (2009) proposed a control strategy during partial load reduction in the power plant output based on the dynamic analysis of a standalone absorber column model. The

control strategy proposed in that study was aimed to maintain the percentage of CO_2 removal rate at a desired set point value while controlling the lean solvent flow. However, it should be mentioned that this control strategies was not tested via dynamic simulations, i.e., the closed-loop performance of the system using that control strategies was not verified in that study.

The process control studies mentioned above have only focused on the individual units (absorber/stripper) included in the CO_2 capture process. There are very few recent publications that discuss the development of a control system for the integrated absorber and stripper columns. Panahi et al. (2010) developed a control structure based on the concept of self optimizing control for this system. A self optimization concept was applied in that study to select the control variable that will minimize a cost function, which is defined as the ratio between the energy consumption and the amount of CO_2 removed. In that control study, a UniSim simulator package was used to simulate the behavior of the MEA absorption process. The control structure proposed in that study considered nine feedback loops that control the percentage of CO_2 removal, the lean solvent temperature, the condenser temperature, the top column pressure, the temperature of the 4^{th} tray in the stripper column and the liquid levels in the recycle surge tank, the reboiler drum, and the condenser and the absorber bottoms. The temperature of fourth tray in the stripper column was selected as a controlled variable by manipulating the reboiler heat duty using the self optimization approach. However, the closed-loop performance of the MEA process proposed in that was not tested and verified.

Lawal et al. (2010) proposed a process control strategy for the complete MEA process, which was simulated using the Advanced Model Library for Gas-Liquid Contactors (AML:GLC) in gPROMS. Five feedback control loops were proposed in that work, i.e., reboiler and condenser temperature of the stripper column, reboiler drum liquid level, CO_2 capture level in absorber and water make up in the absorber. Three case studies that show the closed loop performance of the MEA process due to due to changes in the flue gas flow rate and its composition, and in the reboiler heat duty were presented. The results of that study showed that the amount of lean solvent needs to reduced to maintain the CO_2 capture level at the

desired set point value when the system is subject to a sudden increase in the CO_2 composition in the flue gas flow rate.

Lin et al. (2011) proposed a control strategy for this process using Aspen Plus Dynamics® software. The equilibrium column model was applied in this work but no model validation was conducted. Seven control loops were considered in the control structure with four of them automatically installed by Aspen Plus Dynamics® simulator. That is, two pressure and two level controllers that control the pressure at the top of both columns and the level in the columns were automatically installed by the simulator. The additional controllers were implemented to control the lean solvent temperature, the percentage of CO_2 removal and reboiler temperature. The percentage of CO_2 removal was controlled by manipulating the lean solvent flow rate. The lean solvent flow rate was reduced to maintain 90% CO_2 removal during a 10% step change in flue gas flow rate while keeping the temperature in the reboiler at a constant value. Similar process responses were observed when the CO_2 composition in the flue gas was varied. Furthermore, a case study that shows the set point tracking performance when changing the percentage of CO_2 removal target was also presented in that work. Based on the above, it is clear that a control strategy based on a complete mechanistic process model for the MEA CO_2 capture process have not been developed.

2.5 Review on theory of amine absorption process modeling

2.5.1 Chemistry and chemical kinetics

Aqueous solutions of alkanolamines have been widely employed as solvents in gas treating processes for the removal of the acidic components, H_2S and CO_2. The alkanolamines are characterized by the presence of the hydroxyl group (-OH) and the amino group ($-NH_2$). The presence of the hydroxyl group (-OH) reduces the amine vapour pressure and increases its water solubility, while the amino group provides the necessary reactivity with acid gases to cause the absorption of acidic gases (Kohl and Nielsen, 1997). As shown in Figure 2.3, alkanolamines are classified as primary, secondary, or tertiary according to the number of carbons bonded directly to the nitrogen atom. Primary amines have one carbon bonded to the

nitrogen; secondary amines have two carbons bonded to the nitrogen whereas tertiary amines have three carbons bonded to the nitrogen.

Primary amine

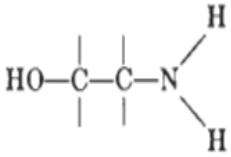

Monoethanolamine (MEA)

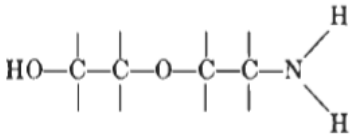

Diglycolamine (DGA)

Secondary amine

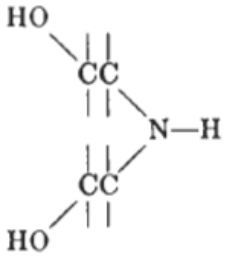

Diethanolamine (DEA)

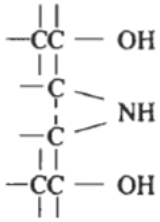

Diisopropanolamine (DIPA)

Tertiary amine

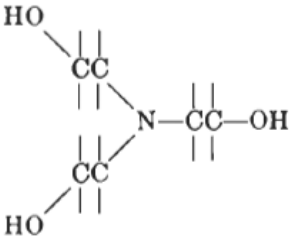

Triethanolamine (TEA)

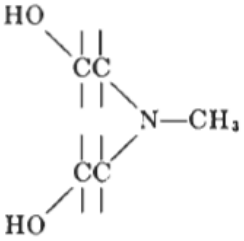

Methyldiethanolamine (MDEA)

Figure 2.3: Molecular structure of alkanolamine used in gas treating processes (Kohl and Nielsen, 1997)

The reaction meachanism and kinetics of the reaction between CO_2 and alkanolamines have been summarized and reviewed by several authors in the literature (Mahajani and Joshi, 1988; Versteeg et al. 1996; Vaidya and Kenig, 2007). Amine-based CO_2 capture relies on the reaction of weak alkanolamine base with weak CO_2 acid gas to produce a water soluble salt.

The reactions between CO_2 and primary and secondary amine solutions have been described as zwitterion and termolecular mechanism. The former mechanism was originally proposed by Caplow (1968) and reintroduced later by Danckwerts (1970) while the later mechanism was introduced by Crooks and Donnellan (1989).

In the zwitterion mechanism, the primary and secondary amines react rapidly with CO_2 to form carbamates. This reaction is reversible and can be represented in simplified form by,

$$CO_2 + 2RNH_2 \overset{K_{eq}}{\leftrightarrow} RNHCOO^- + RNH_3^+ \quad 2.1$$

Tertiary alkanolamines cannot react with CO_2 directly to form carbamate due to the absence of a hydrogen atom attached to the nitrogen atom to be displaced by CO_2. The zwitterion mechanism takes place in two steps. The first step involves the formation of a zwitterion as an intermediate.

$$CO_2 + RNH_2 \underset{k_{-1}}{\overset{k_2}{\leftrightarrow}} RNH_2^+COO^- \quad 2.2$$

The zwitterion then undergoes deprotonation by a base, B, resulting in carbamate formation,

$$RNH_2^+COO^- + B \overset{k_b}{\leftrightarrow} RNHCOO^- + BH^+ \quad 2.3$$

The base *B* can be considered as the water species, OH^- ions and the amine which leads to the following deprotonation reactions (Blauwhoff et al., 1984),

$$RNH_2^+COO^- + H_2O \leftrightarrow RNHCOO^- + H_3O^+ \quad 2.4$$

$$RNH_2^+COO^- + OH^- \leftrightarrow RNHCOO^- + H_2O \quad 2.5$$

$$RNH_2^+COO^- + RNH_2 \leftrightarrow RNHCOO^- + RNH_3^+ \quad 2.6$$

The capacity of the primary and secondary amine solution for CO_2 is limited to approximately 0.5 mol of CO_2 per mol of amine. This limitation is due to formation of highly stable carbamate ions and low rate hydrolysis to bicarbonate. Based on this reaction scheme, Danckwerts (1979) derived the rate of reaction of CO_2 with amine via zwitterion mechanism as follows,

$$r = \frac{k_2 C_{l,CO_2} C_{l,\mathrm{RNH_2}}}{1 + \frac{k_{-1}}{\sum k_B C_{l,\mathrm{RNH_2}}}} \qquad 2.7$$

The term $k_B C_{l,\mathrm{RNH_2}}$ represents the removal of the proton by the base present in the solution. When deprotonation of zwitterions by a base is very fast compared to the reverse reaction in Equation 2.2 ($k_B C_{l,\mathrm{RNH_2}} \gg k_{-1}$) and zwitterions formation is rate limiting, equation 2.7 reduce to (Versteeg et al., 1996),

$$r = k_2 C_{l,CO_2} C_{l,\mathrm{RNH_2}} \qquad 2.8$$

That is, the rate of reaction becomes first order with respect to both CO_2 and amine. On the other hand, when the zwitterion deprotonation is slow compared to its reversibility to amine and becomes rate determining ($k_B C_{l,\mathrm{RNH_2}} \ll k_{-1}$), equation 2.7 results in a more complex kinetic equation (Versteeg et al., 1996),

$$r = \frac{k_2}{k_{-1}} C_{l,CO_2} C_{l,\mathrm{RNH_2}} \sum k_B C_{l,\mathrm{RNH_2}} \qquad 2.9$$

Thus, the overall reaction order may be three, with order of reaction between one and two with respect to amine.

The termolecular mechanism assumes that the reaction between CO_2 and amine takes place in a single step with a loosely–bound encounter complex as shown in Figure 2.4.

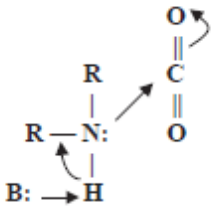

Figure 2.4: Single step, termolecular reaction mechanism for the formation of carbamate (Crooks and Donnellan, 1989)

Most of these complexes break up to form reactant molecule (CO_2) and a few reacts with a second molecule of amine, or a water molecule, to give ionic products. Bond formation and

charge separation only occur in the second step. The forward reaction rate for this mechanism is as follows (Crooks and Donnellan, 1989; Versteeg et al., 1996),

$$r = (k_{\mathrm{RNH_2}} C_{l,\mathrm{RNH_2}} + k_{\mathrm{H_2O}} C_{l,\mathrm{H_2O}})\, C_{l,CO_2} C_{l,\mathrm{RNH_2}} \qquad 2.10$$

The reaction mechanism of tertiary amine with CO_2 is described as base-catalyzed hydration as proposed by Donaldson and Nguyen (1980). This can be represented as follows,

$$\mathrm{RN} + \mathrm{H_2O} + \mathrm{CO_2} \overset{k_3}{\leftrightarrow} \mathrm{RN^+H} + \mathrm{HCO_3^-} \qquad 2.11$$

In this reaction, tertiary amines facilitate the CO_2 hydrolysis reaction to form bicarbonates. The heat of reaction for bicarbonate formation is lower than carbamate formation. Thus tertiary amines like MDEA are often blended with primary or secondary amines to reduce solvent regeneration costs (Vaidya and Kenig, 2007). In addition to this reaction, the following reactions may also occur in the case of aqueous solution,

$$\mathrm{RN} + \mathrm{H_2O} \leftrightarrow \mathrm{RN^+H} + \mathrm{OH^-} \qquad 2.12$$

$$\mathrm{CO_2} + \mathrm{OH^-} \overset{k_{\mathrm{OH^-}}}{\longleftrightarrow} \mathrm{HCO_3^-} \qquad 2.13$$

$$\mathrm{CO_2} + \mathrm{H_2O} \overset{k_{\mathrm{H_2O}}}{\longleftrightarrow} \mathrm{HCO_3^-} + \mathrm{H^+} \qquad 2.14$$

Therefore, the rate of reaction of tertiary amine can be written as follows:

$$r = (k_3 C_{l,\mathrm{RNH_2}} + k_{\mathrm{OH^-}} C_{l,\mathrm{OH^-}} + k_{\mathrm{H_2O}}) C_{l,CO_2} \qquad 2.15$$

2.5.2 Mass transfer model

The rate of interface mass transfer coupled with chemical reaction is essential in a rate-based modeling approach. The mass transfer rate across the interface can be calculated using three different methods; the film model, the penetration model and surface renewal model. The simplest and oldest model, which has been proposed for the description of mass transport processes, is the so-called film theory suggested by Whitman (Whitman, 1923).

The film theory is based on the assumption that when two phases of fluid are in contact with each other, a thin layer of stagnant fluid exists on each side of the phase boundary. Mass transfer by convection within this layer is assumed to be insignificant, and thus the transport is solely achieved by steady state molecular diffusion. The turbulence is sufficient to

eliminate concentration gradient beyond the thin layers. The penetration model proposed by Higbie (1935) assumes that the replacement of each liquid element at the gas-liquid interface, which has been exposed to the gas by liquid of the bulk composition, occurs in period time that is equal to the contact time. Surface renewal model has a similar concept as the penetration model except that the exposure time for all elements at the gas-liquid interface are not the same (Danckwerts, 1970). During the exposure time of a liquid element at the gas-liquid interface, mass transfer for both penetration and surface renewal model, are assumed to occur at unsteady-state molecular diffusion. The predictions based on the film model are usually remarkably similar to those based on more sophisticated models, and in a few cases identical (Danckwerts, 1970). According to Kohl and Nielsen (1997), the film theory seems to be the most convenient approach for packed column design.

There are two different approaches that can be used to model mass transfer using film theory. A simple approach is using enhancement factor to include the effect of chemical reaction on mass transfer (Danckwerts, 1970). On the other hand, a more rigorous approach is to apply a non-linear differential equation of diffusion-reaction for the liquid film (Danckwerts, 1970). In the latter case, concentration profiles of liquid species and solute gas in the film can be estimated.

2.5.3 Vapour-Liquid Equilibrium (VLE)

Numerous vapour-liquid equilibrium experimental studies for acid vapour-alkanolamine systems have been conducted and a large amount of equilibrium data has been published in the literature (Kent and Eisenberg, 1976; Deshmukh and Mather, 1981; Austgen et al., 1989; Liu et al., 1999; Aroua and Mohd Salleh, 2004; Vrachnos et al., 2006). Also, considerable progress has been made in the development of generalized correlations for predicting the equilibrium data for acid vapour-alkanolamine system, which is essential for the accurate representation of these data for process simulation and optimal process design. Several different thermodynamic models that account for the chemical equilibrium reactions as well as liquid phase non-idealities are currently available (Austgen et al., 1989; Liu et al., 1999; Kaewsichan et al., 2001). These models can be used for calculating CO_2 partial pressure and

liquid speciation over a large loading area. In this regard, both simple and rigorous thermodynamic models have been developed to correlate the equilibrium data.

The general equilibrium constant for reaction,

$$A + B \leftrightarrow C \tag{2.16}$$

can be written in terms of activities of the species,

$$K_{eq} = \frac{a_C}{a_A a_B} \tag{2.17}$$

where a_i is the activity of species *i*. The activity of species can be determined by multiplying the activity coefficient with the concentration,

$$K_{eq} = \frac{\gamma_C}{\gamma_A \gamma_B} \frac{C_C}{C_A C_B} \tag{2.18}$$

The true equilibrium constant as shown in Equation 2.18 will be temperature dependent and equal to concentration based equilibrium constant at infinite dilute solution. It is important to mention that most of the equilibrium constant correlations published are temperature dependent.

Early equilibrium models were developed based on "apparent" equilibrium constant in terms of species concentration rather than activities. In fact, the activity coefficients of all species were set to unity. Kent and Eisenberg (1976) used this approach to develop the apparent equilibrium constants for CO_2-H_2S-MEA-H_2O and CO_2-H_2S-DEA-H_2O systems as a function of temperature only. The equilibrium constant of amine protonation and carbamate reversion reaction were adjusted to fit the predicted equilibrium partial pressure of acid gas (CO_2 and H_2S) over monoethanolamine (MEA) and diethanolamine (DEA) aqueous solution with the experimental data. The Kent-Eisenberg correlation has been applied in several studies because it provides good fitting to the experimental data.

Several studies have been performed to improve the Kent and Eisenberg model approach in developing the equilibrium constant correlation to include other factors rather than a function of temperature alone. Jou et al. (1982) adopted a similar approach as Kent and Eisenberg (1976) for the correlation of H_2S and CO_2 partial pressure in aqueous methyldiethanolamine

(MDEA) solutions. In that study, temperature, amine concentration and acid gas (H_2S and CO_2) loading factors were included in the equilibrium constant of amine protonation. Hu and Chakma (1990a) incorporated a dependence of amine concentration and acid gas partial pressure for the equilibrium constant correlation of aqueous diglycolamine (DGA) solutions. Hu and Chakma (1990b) also successfully fitted the VLE data of CO_2 and H_2S in aqueous amino methyl propanol (AMP) using the same method. The equilibrium constant of Kent and Eisenberg for CO_2-H_2S-DEA-H_2O system has been modified by Chakma and Meisen (1990). In the latter, the dependence on the amine concentration and free acid gas concentration in the amine protonation equilibrium constant correlation was considered in the analysis. Li and Shen (1993) have extended the model approach for aqueous mixtures of MEA with MDEA.

Kritpiphata and Tontiwachwuthikul (1996) modified the Kent and Eisenberg model to develop apparent equilibrium constants of amine protonation, dissociation and physical dissolution of CO_2. The sensitivity analysis showed that these three equilibrium constants were the most significant parameters in the CO_2-AMP-H_2O system. Park et al. (2002) developed the correlation of deprotonation and carbamate equilibrium constant for MEA, DEA, and AMP solutions at different temperatures based on the Kent-Eisenberg model. The predicted solubility of CO_2 in amine solutions calculated from equilibrium model was in good agreement with the experimental data. Aroua and Salleh (2004) used the Kent-Eisenberg approach to develop the equilibrium constant for CO_2-H_2O-PZ system. Three of the equilibrium constants were adjusted to fit the solubility of CO_2 in aqueous piperazine (PZ) at various pressures and temperature with experimental data.

The previous equilibrium model approach did not account for the physical interactions among the species in the system. A more rigorous model of equilibrium constants was developed (Deshmukh and Mather, 1981; Austgen et al., 1989; Kaewsichan et al., 2001). That model was expressed in terms of activities rather than concentrations to represent non-ideality of species and the interactions among the species for aqueous solution containing weak electrolytes. Deshmukh and Mather (1981) applied the extended Debye-Huckel

expression to determine the activity coefficient of the solute molecules except water. Both electrostatic interactions and short-range binary interactions were considered in equilibrium model for CO_2-H_2S-MEA-H_2O system. Weiland et al. (1993) applied the Deshmukh and Mather model to predict CO_2 and H_2S equilibrium in aqueous solutions of MEA, DEA, DGA and MDEA.

Austgen et al. (1989) implemented the electrolyte nonrandom-two-liquid (NRTL) theory developed by Chen and Evan to model VLE of CO_2 and H_2S in aqueous MEA and DEA solutions. Non-idealities of solutions were taken into consideration by allowing short- and long-range interaction between the different species. That model is readily extendable to chemical systems containing mixed amines and has received considerable attention in the literature (Hoff et al., 2004). Liu et al. (1999) modified the model by Austgen et al. (1989) in order to give better prediction of VLE for CO_2-MEA-H_2O system at higher temperature. Austgen et al. (1991) extended the proposed thermodynamic model for the calculation of H_2S and CO_2 solubility in aqueous solutions of MDEA and CO_2 solubility in mixtures of MDEA with MEA and DEA. Posey and Rochelle (1997) used similar model structures as Austgen et al. (1989) to develop a VLE model for MDEA-H_2O-H_2S-CO_2 system.

Kaewsichan et al. (2001) modeled the VLE for aqueous solutions of MEA, MDEA, and mixtures of MEA and MDEA using the electrolyte-UNIQUAC (UNIversal-QUAsi-Chemical) method. This model used ion-pair interaction approach instead of individual ions to determine the activity coefficient. As a result, the activity coefficient expression is relatively simple compared to the NRTL electroneutrality model and the number of interaction parameters is reduced. Faramarzi et al. (2009) used the extended UNIQUAC to model the solubility of carbon dioxide absorption in aqueous MEA, MDEA and mixed MEA–MDEA in a wide range of pressure (3–13000 kPa) and temperature (25–200^{o}C).

Based on the thermodynamic models developed for CO_2-alkanolamine system, which has been discussed in the preceding paragraph, rigorous thermodynamic models are more

accurate and mathematically complex when compared to simple model approach. However, the applications of rigorous models are computationally intensive since they need to solve a large number of nonlinear equations simultaneously. Failure to provide a good initial value may cause convergence problems in the calculation (Li and Shen, 1993). On the other hand, a simple model, like that of Kent and Eisenberg, generally yields satisfactory results for aqueous single-amine solutions containing only CO_2 or H_2S. According to Hu and Chakma (1990b), the Deshmukh and Mather approach are no better than those using the model of Kent and Eisenberg. The Kent-Eisenberg model approach has been proved to give good performance for the prediction of CO_2 solubility in alkanolamine solutions while saving computational time.

The general equation of multicomponent vapour-liquid phase equilibrium is,

$$f_{l,i} = f_{g,i} \qquad 2.19$$

where $f_{l,i}$ and $f_{g,i}$ are the fugacity of component *i* in a liquid and a gas mixture, respectively. At equilibrium, the fugacity of each component must be the same in both gas and liquid phases. This is the basic equation for phase equilibrium calculations. In order to apply this equation, the component fugacity in both phases at the temperature and pressure of the mixture must be estimated. For practical applications, Equation 2.19 is transformed into a more commonly used expression in terms of the composition of the vapour phase at equilibrium by introducing pure component fugacity, which is evaluated at the system temperature and pressure. The fugacity of component *i* in gas phase can be written as,

$$f_{g,i} = \varphi_i y_i P \qquad 2.20$$

where y_i is the mole fractions of component *i* in the gas phase; φ_i is the fugacity coefficient of pure component *i*; *P* is the total pressure. The fugacity coefficient depends on temperature, pressure and gas composition. For an ideal gas mixture, the fugacity coefficient of a component *i* is equal to one (φ_i = 1) and the fugacity is assumed to be its partial pressure. This reduce the preceding equation to,

$$f_{g,i} = y_i P \qquad 2.21$$

However, for the case of non-ideal gas mixture, the fugacity coefficient is not unity and it must be evaluated from the equation of state, e.g., Soave-Redlich-Kwong or Peng-Robinson (see Prausnitz et al., 1999).

In the case of the liquid solvents, the fugacity of a component *i* is determined in terms of an activity coefficient (Prausnitz et al., 1999),

$$f_{l,i} = \gamma_i x_i P_i^s \varphi_i^s \exp\left(\frac{v_i^s (P - P_i^s)}{RT}\right) \qquad 2.22$$

where x_i is the mole fraction of component *i* in the liquid phase; φ_i^s is the fugacity coefficient of pure component *i*; γ_i the activity coefficient of component *i*; P_i^s is the vapour pressure of component *i*; v_i^s is the molar volume of pure component *i*. The exponential term in Equation 2.22 is referred to as the Poynting factor for pressure correction if the system pressure is different (by several orders of magnitude) from the reference pressure (i.e. saturation pressure). The Poynting factor differs significantly from unity at high pressure, when the compressibility of liquid is taken into account.

Further simplification of Equation 2.22 can be made with regards to the conditions encountered. Often at low pressure (< 10 bar) the Poynting factor may be considered negligible and assumed equal to one, and the fugacity coefficient in liquid phase is nearly equal to that in the vapour (Winnick, 1997). Therefore, for ideal gases, the fugacity coefficient of pure component *i* (φ_i^s) is set to unity. Therefore, Equation 2.22 simplifies to,

$$f_{l,i} = \gamma_i x_i P_i^s \qquad 2.23$$

In an ideal liquid solution (γ_i= 1), the liquid fugacity of each component in the mixture is directly proportional to the mole fraction of the component,

$$f_{l,i} = x_i P_i^s \qquad 2.24$$

The relationship for vapour-liquid equilibrium is obtained by substituting Equations 2.20 and 2.23 in Equation 2.19,

$$\varphi_i y_i P = \gamma_i x_i P_i^s \qquad 2.25$$

If each liquid and gas phases form an ideal mixtures (γ_i = 1 and φ_i = 1), the preceding equation further reduce to,

$$y_i P = x_i P_i^s \qquad 2.26$$

which is known as Raoult's law. Dissolved gases or solute molecules (such as O_2, N_2 and CO_2) are usually in their supercritical state at the temperature and pressure of the solution, i.e., when the system temperature exceeds its critical temperature. In that case, its vapour pressure is meaningless and therefore its fugacity as a pure liquid at the system temperature cannot be calculated by Equation 2.23. To apply Equation 2.23, the species must exist as a liquid at the temperature and pressure of the mixture. An alternative approach is required to calculate the fugacity for a dissolved gas. The phase equilibrium relationship for dissolved gases is determined in terms of Henry's law constant,

$$f_{l,i} = \gamma_i^* x_i He_i \qquad 2.27$$

where He_i (kPa) is the Henry's constant of component i. Henry's constant is a strong function of temperature, but only weakly dependent on pressure (Smith et al., 1996). Note that the Henry's activity coefficient (γ_i^*) in Equation 2.27 is different than the activity coefficient γ_i in Equation 2.23. The Henry's activity coefficient (γ_i^*) is converted to the infinite dilution reference state through the relationship.

$$\gamma_i^* = \frac{\gamma_i}{\gamma_i^\infty} \qquad 2.28$$

where γ_i^∞ is the infinite dilution activity coefficient of component *i* in the mixture. By this definition, γ_i^∞ approaches unity as x_i approaches zero (infinitely dilute solution). Treating the gas phase as ideal, the phase equilibrium relationship for dissolved gases becomes,

$$\varphi_i y_i P = \gamma_i^* x_i H_{e,i} \qquad 2.29$$

2.6 Chapter summary

This chapter summarizes the technologies available to CO_2 capture for power plant which can be classified as post-combustion, pre-combustion and oxy-fuel combustions. Depending on the characteristics of the gas stream from which CO_2 needs to be separated, several technologies can be applied for CO_2 capture, i.e., adsorption, physical/chemical absorption, membrane separation and cryogenic separation. Modeling and simulation studies on amine

absorption process at steady state has been extensively studied while only a handful of dynamic simulation of this process has been published. The control strategies proposed in the published literature were also discussed in this chapter. The concepts and essential information that is needed to develop a mechanistic model of CO_2 absorption were also presented in this chapter and will be used in the next chapter as a basis to develop the dynamic process model for the MEA CO_2 capture process.

Chapter 3
Mathematical Modelling

A mathematical formulation is an essential tool for the development of a dynamic MEA absorption process model. This chapter presents the dynamic mechanistic model developed in this work to study the transient behaviour of the complete MEA process plant. This chapter is organized as follows: Section 3.1 describes the process and unit operations involved. Sections 3.2 to 3.5 explain the mathematical equations used to model the packed column, reboiler, heat exchanger and tank, respectively. The concepts and essential information for the developments of each unit is emphasized in these sections. Section 3.6 gives an overview of process simulation tools that have been used for modeling the amine absorption process. The chapter summary is provided in the last section.

3.1 Introduction

A typical MEA absorption process consists of an absorber, a stripper and a cross heat exchanger as shown in Figure 2.2. The MEA absorption process considered in this study, as shown in Figure 3.1, has an additional unit operation, a storage (buffer) tank, located before the absorber column. This storage tank was included in the pilot plant (Dugas, 2006) that holds a large amount of liquid solvent to minimize any disruption from the stripper column. The storage tank allows any fluctuations in the composition coming from the stripper column to be attenuated so that the lean loading entering the absorber column remains at a desired value. The absorber packed column provides intimate contact of the flue gas with the amine solvent so that the CO_2 molecules can be transferred from the gas phase to the solvent liquid phase. The stripper packed column acts as a regenerator to strip the CO_2 from the solvent, so that the solvent can be recycled back to the absorber.

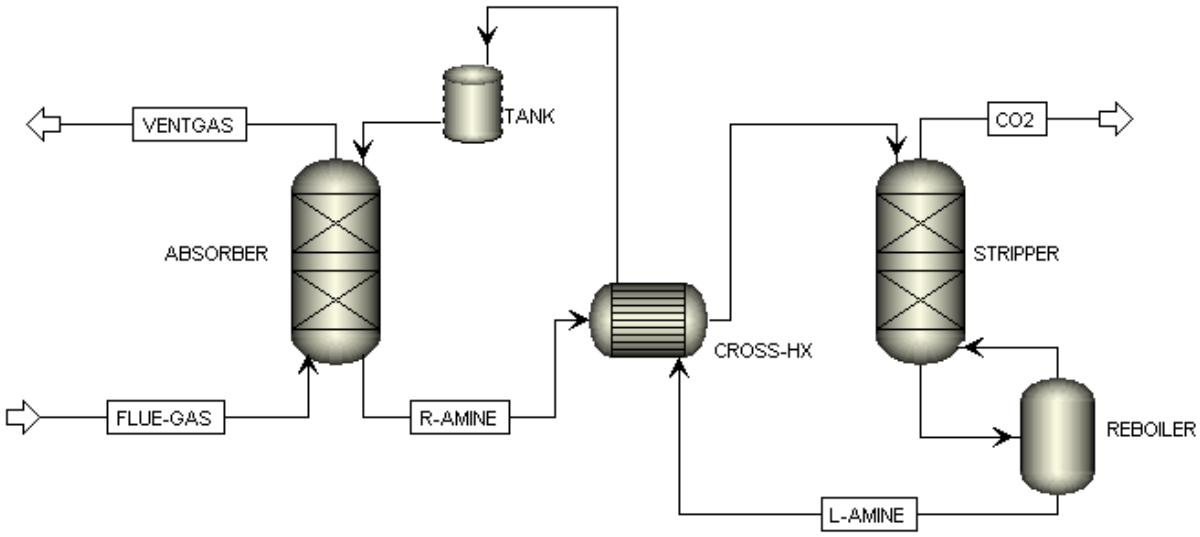

Figure 3.1: Process flow diagram of an amine absorption process

The reboiler drum provides the heat to the stripper by boiling water and this steam flows through the stripper tower for solvent regeneration. The reboiler temperature range is 110-120°C to reverse the chemical reactions and decrease the solubility of the CO_2 in the solution. However, the temperature of the liquid in the in the tower should not be greater than 120^{o}C to minimize solvent degradation (Alie, 2004). Following Figure 3.1, the cross heat exchanger uses the hot lean amine from the stripper column to heat up the rich amine from the absorber. The lean amine solution enters the absorber at 40°C.

To develop a dynamic model for the complete process, dynamic models of each of the units involved in this process were developed first. The resulting mechanistic process models for each unit were then integrated to form the comprehensive dynamic model for the complete MEA process. The mathematical models of the unit operations involved in this process are based on conservation laws for mass and energy. The mathematical models of the packed column and heat exchanger are formulated as partial differential algebraic equations (PDAEs), i.e., the proposed model takes into account the spatial and temporal variations of

the state variables in these systems. Likewise, the reboiler and buffer tank models are described as ordinary differential equations (ODE), i.e., the state variables for these systems only consider changes in the time domain. In addition, the model parameters for these process units, e.g. heat fluxes, mass fluxes, physical properties, are estimated from non-linear algebraic correlations, which are described in detail in this chapter. The modeling details of each of the process units considered in this process and the development of the integrated dynamic model are discussed next.

3.2 Packed Column Model

The MEA absorption process consists mainly of two basic equipments; absorber and stripper columns. The mathematical descriptions of the absorber and the stripper are basically similar except for a few points. At absorber temperatures typically between 40 and 60^{o}C, CO_2 diffuses from the flue gas into the liquid solution to react with MEA to form bound CO_2. The mass transfer of CO_2 occurs thus from the gas to the liquid phase in the absorber. On the other hand, the solvent regeneration that occurs in the stripper column at higher temperature causes the CO_2 to be stripped from the liquid solution to the gas phase. The reaction rate constants for the reactions occurring in the absorber are based on a second order reaction while in the stripper column the reactions are assumed instantaneous due to the high temperature. The different approaches applied to calculate the mass transfer and reaction rate constants for both absorber and stripper columns will be discussed in detail in the following sections.

There are two design approaches normally used for modelling an absorption/stripping column: the equilibrium model and the rate-based model. The equilibrium stage model assumes theoretical stages in which the liquid and gas streams leaving any particular stage are in equilibrium with each other. The performance of this theoretical stage is then adjusted by incorporating tray efficiency correction factors. However, with reactive absorption which involved chemical reactions, the correlation of tray efficiency is much more complex because the reactions affect both the equilibrium relationships and the rate of absorption (Kohl and

Nielsen, 1997). On the other hand, equilibrium is rarely attained as mass and heat transfer processes are driven by gradients of chemical potential and temperature.

On the other hand, the rate-based model analyzes the heat and mass transfer on actual tray rather than theoretical tray. Mass and energy balances are modeled using rate-based equations. Stage efficiency calculations are then avoided in this approach. The first rate-based model was developed by Krishnamurthy and Taylor (1985) for the simulation of counter-current, multicomponent separation process. Based on rate-based process models, unit operations are characterized by coupled phase equilibrium, mass and heat transfer and chemical reaction phenomena. A rate-based model requires information about the column configuration for calculation of parameters such as mass and heat transfer coefficients and interfacial area.

For reactive absorption processes such as absorption of carbon dioxide (CO_2) in a monoethanolamine (MEA) solution, unrealistic assumptions need to be made when using the equilibrium stage model. The assumption of phase equilibrium for the contacting liquid and gas phases is inadequate to describe the static and dynamic behaviour of reactive absorption units. A study by Lawal et al. (2009a) has shown that the rate-based model provides more accurate descriptions for these process units. Thus, the rate-based approach is more suitable for the present application and was the method applied in this work.

Several studies have employed steady state model of reactive absorption process at different level of complexity. Kenig et al. (2001) described different levels of complexity in developing a reactive absorption process using rate-based approach. As shown in Figure 3.2, the simplest rate based approach model is to assume that the chemical reaction is at equilibrium. A more rigorous approach is to consider the chemical kinetics in the liquid bulk phase. The reaction in the liquid film can be determined either through the differential equations governing the simultaneous diffusional mass transfer and chemical reactions or using a simplified method, i.e., an enhancement factor that takes into account the effect of

chemical reaction on mass transfer. The complexity of the rate-based model increases substantially if one considers kinetically controlled in which the chemical reactions take place in the liquid film and liquid bulk phase. Additional effects like the electrolyte influence on mass transfer are considered within the analysis. Modeling a rigorous reactive absorption process leads to a large set of systems of equations which solution is tedious and time consuming.

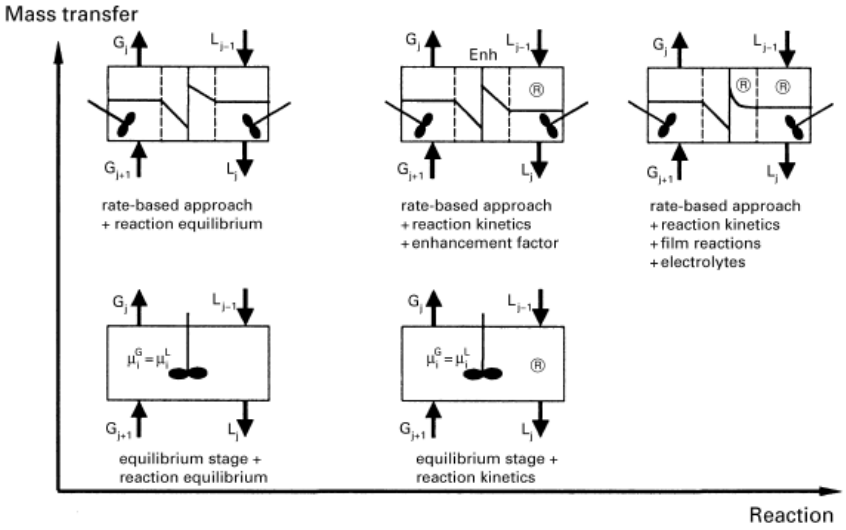

Figure 3.2: Model complexity with regard to the description of mass transfer and chemical reactions (Kenig et al., 2001)

In this study, a dynamic rate-based model using the two-film theory with the assumption of chemical equilibrium was selected. The mathematical model describes the dynamic behaviour of the column, in which the dependent variables vary with the axial position and time. The resulting partial differential equations are combined with algebraic equations that describe equilibrium relationships, physical properties and rate equations. The mathematical model of the packed column model (absorber and stripper) involves the following equations:

1. Material balance equations.
2. Energy balance equations.
3. Rate equations.

4. Equilibrium relations.
5. Chemical Kinetics.

The partial differential equations for the material and energy balances integrate the dynamic model for the column. These equations are derived over a volume element which represents a small part of the column. The integration of these equations with the appropriate boundary conditions gives the temperature and concentration profiles inside the column. In order to complete the column model, the following information is required:

1. Heat and mass transfer coefficients in both gas and liquid phases.
2. Vapour-liquid equilibrium relationship such as the Henry's constant, chemical equilibrium constant and activity coefficient.
3. The reaction rate constant for the chemical reactions taking place in the liquid film.
4. The hydrodynamic of packing columns such as the pressure drop of the column and mass transfer area in the column.

Most of these quantities often depend on the temperature and concentration of particular components; therefore, they vary along the height of the tower. In addition to these equations, physical properties such as solubility, density, diffusivity and viscosity must be included to provide a complete quantitative description of the process.

A detailed mathematical model of packed column model was presented by Kvamsdal et al. (2009). Therefore, the model presented in that study was used as a basis to develop the dynamic model for the packed columns proposed in this work. The following assumptions were made in the present work for the packed column model (Kvamsdal et al., 2009):

1. The fluid is in turbulent flow.
2. Linear pressure drop (fixed outlet pressure).
3. Ideal gas phase due to low pressure.
4. No accumulation in gas and liquid films.

5. Fluxes of CO_2, H_2O and MEA between the two phases are allowed in both directions.

3.2.1 Molar component balance for the gas and liquid phase

Material and energy balance equations are written in a derivative form in order to account for the spatial and temporal behaviour of the column. The packed column is divided into elements of height, Δz. The axial position z is chosen to be positive in the direction of the gas flow, i.e., from the bottom to the top. The present model was obtained from the development of a differential volume element approach around an element in the packed column of height Δz. The resulting differential mass balances of component i in gas and liquid phases over a volume element as shown in Figure 3.3 and are as follows:

$$\frac{dC_{g,i}}{dt} = -u_g \frac{\partial C_{g,i}}{\partial z} - C_{g,i} \frac{\partial u_g}{\partial z} - a_{gl} N_i \qquad 3.1$$

$$\frac{dC_{l,i}}{dt} = u_l \frac{\partial C_{l,i}}{\partial z} + a_{gl} N_i \qquad 3.2$$

where $C_{g,i}$(mol/m^3) and $C_{l,i}$ (mol/m^3) are the molar concentrations of component i in the gas and liquid phase, respectively; u_g(m/s) and u_l(m/s) are the gas and liquid velocities, respectively; a_{gl} (m^2/m^3) is the specific gas-liquid interfacial area, N_i (mol/m^2/s) is the molar flux of component i. As shown in Equations (3.1) and (3.2), the concentration of component i in the gas and liquid phase changes with time (t) and distance (z) along the height of the column. For the absorption column, the molar flux, N_i in Equations (3.1) and (3.2) are defined as the net loss of component i in the gas phase and the net gain of the same component in the liquid phase, respectively. On the other hand, the interfacial mass transfer in the stripping column will occur in the opposite direction, i.e., the net loss and gain of component i occur in the liquid and gas phase, respectively. The component i in the column can be monoethanolamine (MEA), nitrogen (N_2), carbon dioxide (CO_2) or water (H_2O). However, nitrogen is not involved in the reaction and was not considered to be transferred between the two phases.

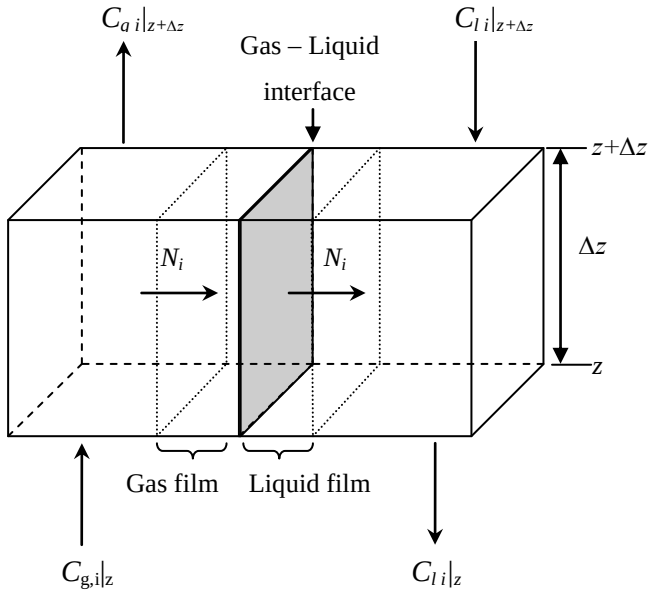

Figure 3.3: Generalized mass balance over a volume element

The liquid velocity through the column is assumed constant while the gas velocity, u_g is estimated from the following expression (Hoff et al., 2004),

$$\frac{du_g}{dz} = \frac{u_g}{P_g}\frac{\partial P_g}{\partial z} + \frac{u_g}{T_g}\frac{\partial T_g}{\partial z} - \frac{a_{gl}}{C_{g,total}}\sum N_i \qquad 3.3$$

where P_g (kPa) is the gas pressure, T_g(K) is the gas temperature, and $C_{g,total}$(mol/m^3) is total gas molar concentration. The present column model assumed a high gas velocity and constant pressure drop.

3.2.2 Energy balance for the gas and liquid phases

The energy balance for the gas phase and the liquid phase can be obtained from the application of the differential volume element approach for a section inside the packed column. Accordingly, the resulting energy balance equations for the liquid phase and the gas phase are as follows:

$$\frac{\partial T_g}{\partial t} = -u_g\frac{\partial T_g}{\partial z} - T_g\frac{\partial u_g}{\partial z} + \frac{q_g a_{gl}}{\sum C_{g,i}C_{p,i}} \qquad 3.4$$

$$\frac{\partial T_l}{\partial t} = -u_l \frac{\partial T_l}{\partial z} - \frac{q_l a_{gl}}{\sum C_{l,i} C_{p,i}} \quad 3.5$$

where T_l(K) is the liquid temperature, q_g(J/m^3/s) and q_l(J/m^3/s) represent the interfacial heat transfer in the gas and the liquid phase, respectively; a_{gl} (m^2/m^3) is the specific gas-liquid interfacial area and C_p(J/mol/K) is the specific heat capacity. The interfacial heat transfer is made up of a conductive heat flux due to temperature gradients in the fluid and a convective contribution due to transport enthalpy by interface transport (Bird et al., 2002). In this work, conductive heat flux due to a temperature difference between the two phases is estimated as follows,

$$q_g = h_{gl}(T_l - T_g) \quad 3.6$$

where h_{gl}(W/m^2/K) is the interfacial heat transfer coefficient. The liquid heat transfer due to the temperature difference between the two phases, heat of reaction (exothermic reaction of CO_2 and MEA), heat of vaporization of water and heat loss to the surroundings are calculated in the present model as follows,

$$q_l = h_{gl}(T_l - T_g) + \Delta H_{rxn} N_{CO_2} + \Delta H_{vap} N_{H_2O} + h_{out}(T_l - T_{amb}) \quad 3.7$$

where ΔH_{rxn} (J/mol) is the heat of reaction per mol CO_2, h_{out} (W/m^2/K) is the wall heat transfer coefficient and T_{amb} (K) is the ambient temperature. The heat of reaction (ΔH_{rxn}) and wall heat transfer coefficient (h_{out}) are obtained from Kvamsdal and Rochelle (2008). The sign in the last term of Equation (3.7) was changed from the model proposed by Kvamsdal et al.(2009) because the heat losses from the column to the surroundings need to be subtracted from the liquid heat transfer equation, i.e., the heat loss term in (3.7) need to have a negative sign. Likewise, the present model assumes that the chemical reaction of CO_2 takes place in the liquid phase, i.e., the heat of reaction is only considered in the energy balance for the liquid bulk (see Equation (3.7). The heat losses to the surroundings are explicitly considered in the liquid phase. Therefore, these terms have not been included in vapor energy balance.

The heat transfer coefficient of the liquid phase is larger than that observed for the gas phase due to the very high thermal conductivity of the aqueous solution. Therefore, the heat transfer between liquid and gas phases is controlled by the resistance to heat transfer in the gas phase. The interfacial heat transfer coefficient in the gas phase was calculated using the Chilton-Colburn analogy that can be deduced from the mass-transfer coefficient (Geankoplis, 2003). Based on the Chilton-Colburn analogy, the dimensionless heat transfer coefficient Chilton-Colburn factor (J_H), is equal to the dimensionless mass transfer coefficient Chilton-Colburn factor (J_M). The Chilton-Colburn factors are functions of the Prandtl and Schmidt number (Geankoplis, 2003):

$$J_H = \frac{h_{gl}}{C_{pm}\rho_g u_g}(N_{Pr})^{2/3} \quad 3.8$$

$$J_M = \frac{k_g R T_g}{u_g}(N_{Sc})^{2/3} \quad 3.9$$

where J_H and J_M are the Chilton-Colburn factor for heat and mass transfer, respectively; C_{pm} (J/kg/K) is the mass specific heat capacity of the gas phase; ρ_g (kg/m^3) is the gas density; u_g (m/s) is the gas velocity; R is the ideal gas constant; N_{Pr} is the Prandtl number; k_g (mol/kPa/m^2/s) is the mass transfer coefficient in gas phase and $N_{Sc}$is the Schmidt number. Prandtl and Schmidt numbers are defined as follows:

$$N_{Pr} = \frac{C_p \mu}{\lambda} \quad 3.10$$

$$N_{Sc} = \frac{\mu}{\rho D_{avg}} \quad 3.11$$

Substituting the Equations (3.10) and (3.11) into the Equations (3.8) and (3.9) yields:

$$J_H = \frac{h_{gl}}{C_{pm}\rho_g u_g}(N_{Pr})^{2/3} = J_M = \frac{k_g R T_g}{u_g}(N_{Sc})^{2/3} \quad 3.12$$

$$\frac{h_{gl}}{C_{pm}\rho_g u_g}\left(\frac{C_{pm}\mu_g}{\lambda_g}\right)^{2/3} = \frac{k_g R T_g}{u_g}\left(\frac{\mu_g}{\rho_g D_{g,avg}}\right)^{2/3} \quad 3.13$$

The latter can be solved for the heat transfer coefficient , i.e.,

$$h_{gl} = k_g R T_g \left(C_{pm}\rho_g\right)^{1/3}\left(\frac{\lambda_g}{D_{g,avg}}\right)^{2/3} \quad 3.14$$

where μ_g (kg/m/s) is the gas viscosity, λ_g (W/m/K) is the gas thermal conductivity and $D_{g,avg}$ (m^2/s) is the average diffusion coefficient in gas phase.

3.2.3 Rate equations

Absorption/desorption processes involve mass and energy transfer in both gas and liquid phases through the gas-liquid interfacial. Interfacial mass transport involves a transfer of a soluble component in the gas/liquid phase that takes place across the gas-liquid interface which separates the two phases. The depiction of mass transfer rates across the interfacial range varies from the simple two-film theory to a more complex penetration model (Danckwerts, 1970).

Following previous works on packed column design, the two-film theory was applied to describe the heat and mass transfer in this process (Pacheco, 1998; Kenig *et al*., 1999; Schneider *et al*., 1999; Al-Baghli *et al*., 2001; Schneider *et al*., 2003; Kucka *et al*., 2003; Lawal *et al*., 2008; Kvamsdal *et al*., 2009). The two-film theory model offers several advantages; simpler mathematical formulation (algebraic equations instead of differential equations) that allows for a fast calculation of multicomponent mass transfer; also, many correlations for mass transfer coefficients on the basis of the two-film model have been developed. The film model is the oldest and simplest model of mass transfer proposed by Whitman (Whitman, 1923). It is assumed that the gas and liquid are in equilibrium at the interface and that the thin films separate the interface from the main bodies of the two phases (Lewis and Whitman, 1924).

Mass transfer through the gas-liquid interface can occur due to convection and component diffusion. In the film theory model, the convection in the interface layer is insignificant when compared to that in the bulk phase of gas and liquid where the level of turbulence is such that all composition gradients are eliminated. Consequently any transfer of solute through these films must be affected by the relatively slow process of diffusion at steady state in the direction normal to the interface. For steady state mass transfer, the rate at which component

i reaches the interface from the gas must equal the rate at which it diffuses to the bulk liquid, so that no accumulation or depletion of component *i* occurs at the interface. Thus, the accumulation takes place only in the bulk phases and all resistance to mass transfer is located in the thin films.

The interfacial mass transfer rate is affected by the diffusion rate of reactants and products and chemical reaction rates. The rate of mass transfer is driven by the chemical potential gradient. In practice, mole fraction or partial pressure difference are the preferred methods to define the driving force (Pacheco, 1998). A model of mass transfer using two-film theory is shown in Figure 3.4. The solute of a gas phase passes through the gas film from the bulk gas phase to the gas-liquid interface due to difference of partial pressure in the bulk gas and partial pressure at the interface. The solute reacts with the solvent once this have crossed the gas-liquid interface and diffused into the bulk liquid phase. Beyond the liquid film, the turbulence is sufficient to eliminate concentration gradients.

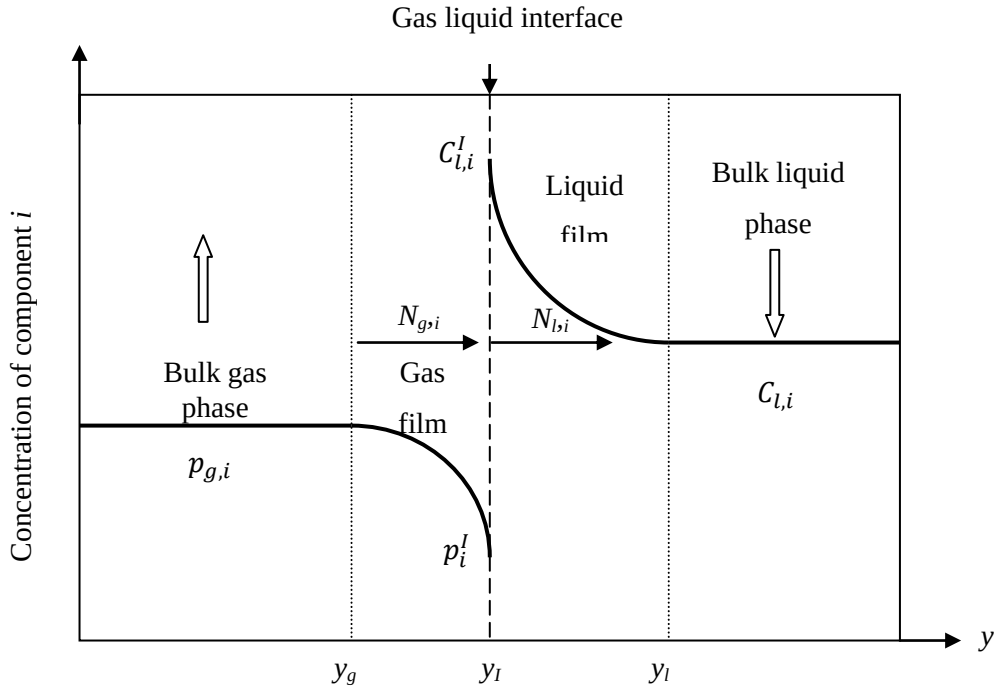

Figure 3.4: Two-film model for mass transfer between gas and liquid (adapted from Froment and Bischoff, 1990)

Other factors such as temperature, physical properties of liquid and gas, system geometry and column hydrodynamics also affect the mass transfer rate significantly. All these effects are considered when calculating the mass transfer coefficients. The component molar fluxes in the gas and liquid film are based on one-dimensional steady-state diffusion. The direction from the gas to the liquid phase was taken as the positive direction for mass transfer. Using the generalized Fick's law, the rate of mass transfer of component *i* through the gas-liquid interfacial in gas and liquid phases are,

$$N_{g,i} = k_{g,i}\left(p_{g,i} - p_i^I\right) \quad 3.15$$

$$N_{l,i} = k_{l,i}\left(C_{l,i}^I - C_{l,i}\right) \quad 3.16$$

where $k_{g,i}$ (mol/Pa/m^2/s) and $k_{l,i}$ (m/s) are the mass transfer coefficients in gas and liquid phases, respectively; $p_{g,i}$(kPa) and p_i^I(kPa) are the partial pressure of absorbing gas in the gas phase and at gas-liquid interfacial, respectively; $C_{l,i}$(mol/m^3) and $C_{l,i}^I$(mol/m^3) are the concentrations in liquid phase and at gas-liquid interfacial, respectively. The mass transfer rate through the interface should be continuous, which leads to the following equation,

$$N_i = N_{g,i} = N_{l,i} \quad 3.17$$

$$N_i = k_{g,i}\left(p_{g,i} - p_i^I\right) = k_{l,i}\left(C_{l,i}^I - C_{l,i}\right) \quad 3.18$$

Chemical reactions occurring in the liquid film increase the solubility of solute in the gas phase, thus accelerating the rate of absorption in the liquid phase. For example, once CO_2 gas reaches the gas-liquid interface, it is rapidly absorbed in the MEA aqueous solution and reacts with MEA. The effect of chemical reaction on rate on mass transfer can be expressed in terms of an enhancement factor, E. Considering this factor, a dimensionless enhancement factor, *E* is incorporated in the mass transfer equation,

$$N_i = Ek_{g,i}\left(p_{g,i} - p_i^I\right) = Ek_{l,i}\left(C_{l,i}^I - C_{l,i}\right) \quad 3.19$$

Due to this condition, concentration gradients in the liquid film build up while the gas concentrations remain low. Thus, the rate of diffusion in the gas film will mostly determine the absorption rate though the effect of liquid film cannot be neglected. The driving force as shown in Equation (3.19), is defined as the difference between the component concentration in the bulk phase and at the interface. In order to eliminate the interfacial compositions (p_i^I

and $C_{l,i}^{I}$) and use bulk driving force instead, the overall mass transfer coefficients is used in the mass transfer equation. Assuming that Henry's law for the physical equilibrium between gas and liquid interfacial concentrations holds,

$$p_i^I = He_i C_{l,i}^I \tag{3.20}$$

the gas partial pressure (p_i^*) in equilibrium with the liquid phase concentration is expressed as follows:

$$p_i^* = He_i C_{l,i}^* \tag{3.21}$$

The liquid concentration ($C_{l,i}^*$) in equilibrium with the bulk gas partial pressure is given by,

$$C_{l,i}^* = \frac{p_i^*}{He_i} \tag{3.22}$$

The rate of mass transfer of component i, N_i in terms of the overall mass transfer coefficients becomes,

$$N_i = K_{g,i}(p_i - p_i^*) = K_{l,i}(C_i^* - C_i) \tag{3.23}$$

where,

$$\frac{1}{K_{g,i}} = \frac{1}{k_{g,i}} + \frac{He_i}{k_{l,i}E}$$
$$\frac{1}{K_{l,i}} = \frac{1}{He_i k_{g,i}} + \frac{1}{k_{l,i}E} \tag{3.24}$$

where $K_{g,i}$ (mol/m^2/Pa/s) and $K_{l,i}$ (m/s) are the corresponding overall mass transfer coefficients in gas and liquid phases, respectively; p_i^* (kPa) is the partial pressure and C_i^* (mol/m^3) is the molar concentration at equilibrium. The overall mass transfer coefficient is composed of the contributions of two individual mass transfer coefficients in gas and liquid phases. The detailed derivation of mass transfer using overall mass transfer coefficient is described in Appendix A.

Following equation (3.24), the terms, ($1/\ k_{g,i}$) and ($1/He_i k_{g,i}$) represent the resistance in the gas phase whereas the terms, ($He_i/k_{l,i}E$) and ($1/k_{l,i}E$) denotes the resistance in the

liquid phase. The present model assumes that the resistance to mass transfer for both H_2O and MEA in the liquid phase is negligible. This is because, for the components that have higher solubility such as H_2O and MEA, the major resistance for mass transfer occurs in the gas phase. However, the mass transfer resistance for CO_2 is considered to occur in both gas and liquid films. Thus, the molar flux for each component involved in mass transfer is as follows:

$$N_{MEA} = k_{g,MEA}(p_{MEA} - p^*_{MEA})$$
$$N_{H_2O} = k_{g,H_2O}(p_{H_2O} - p^*_{H_2O})$$
$$N_{CO_2} = \frac{(p_{CO_2} - p^*_{CO_2})}{\frac{1}{k_{g,CO_2}} + \frac{He_{CO_2}}{k_{l,CO_2}E}} \qquad 3.25$$

Mass transfer coefficients

The mass transfer coefficients in the gas and liquid phases depend on the flow velocity of both phases, the physical properties of gas and liquid phases such as density, viscosity, diffusion coefficients, and the type and size of packing. Heat and mass transfer coefficients are required to determine the interfacial heat and mass transfer rates. Wang et al. (2005) reviewed several mass transfer coefficients for packed column that are available in the literature. One of the most widely used mass transfer coefficients is that proposed by Onda et al. (1968) and validated by Bravo and Fair (1982). Several studies on MEA absorption process have used this correlation (Pacheco, 1998; Liu et al., 2006; Kvamsdal et al., 2009; Ghaemi et al., 2009). The gas and liquid film mass transfer coefficients, k_g and k_l are determined from the generalized correlations proposed by Onda et al. (1968),

$$k_g = 5.23\left(\frac{\rho_g u_g}{a_p \mu_g}\right)^{0.7}\left(\frac{\mu_g}{\rho_g D_g}\right)^{1/3}\left(\frac{D_g}{R_g T_g a_p d_p^2}\right) \qquad 3.26$$

$$k_l = 0.0051\left(\frac{\mu_l g}{\rho_l}\right)^{1/3}\left(\frac{\rho_l u_l}{a_w \mu_l}\right)^{\frac{2}{3}}\left(\frac{\mu_l}{\rho_l D_l}\right)^{-1/2}(a_p d_p)^{0.4} \qquad 3.27$$

where a_p(m^2/m^3) is the total surface of packing, a_w(m^2/m^3) is the wetted surface area of packing, μ_g(kg/m/s) and μ_l (kg/m/s) are the gas phase and liquid phase viscosities,

respectively; D_g (m^2/s) and D_l (m^2/s) are the molecular diffusivities in the gas and liquid phases, respectively; d_p(m) is the nominal diameter of the packing element and R_g (m^3.kPa/mol/K) is the ideal gas constant. These correlations cover commonly used packings such as Raschig rings, Berl saddles and Pall rings.

Wetted surface area

Since mass transfer in packed columns takes place on the surface of the liquid flowing over the surface of the packing, the wetted area of the packing is usually taken as the effective interfacial area, which is usually smaller than the total dry surface area of the packing due to imperfect wetting. Kvamsdal et al. (2009) used the packing material specific area as the effective contact area between the gas and liquid phases. However, the present model estimates the wetted surface area of packing using the correlation proposed by Onda et al. (1968) as the effective surface. The latter approach provides better prediction for mass transfer than that used by Kvamsdal because it takes into account the effect of various factors, such as the liquid flow rate and the shape, size, and constituent material of the packing. Furthermore, the wetted area, which is usually smaller than the total dry surface area of the packing due to imperfect wetting of the packing, is usually taken as the effective interfacial area. Onda *et al*. (1968) proposed the following correlation for the wetted area of packings commonly used in gas absorption,

$$\frac{a_w}{a_p} = 1 - \exp\left\{-1.45\left(\frac{L}{\mu_l a_p}\right)^{0.1}\left(\frac{a_p L^2}{g\rho_l^2}\right)^{-0.05}\left(\frac{L^2}{\rho_l a_p \sigma_l}\right)^{0.2}\left(\frac{\sigma_{ct}}{\sigma_l}\right)^{0.75}\right\} \qquad 3.28$$

where L ($kg/m^2/s$) is the superficial mass velocity of the liquid, μ_l (kg/m/s) is the liquid viscosity, g (m/s^2) is the gravitational constant, σ_l (N/m) is the surface tension of the liquid and σ_{ct} (N/m) is the critical surface tension of the packing material. The value of the σ_l and σ_{ct} is 0.04 and 0.075, respectively (Oyenekan and Rochelle, 2009). To simplify the analysis, the heat-transfer area was set equal to the effective mass-transfer area.

Enhancement factor

The chemical reactions that occur in the MEA absorption process increase the rate of CO_2 absorption in the liquid phase. This effect is taken into account in the liquid phase mass

transfer through an enhancement factor (*E*). This factor is an approximate analytical solution of the differential equations governing the simultaneous diffusional mass transfer and chemical reactions in the liquid film. It is defined as the ratio of the rate of absorption with chemical reaction to the rate of absorption without chemical reaction (Danckwerts, 1970). This definition reduces to ratio of mass transfer coefficient in the liquid phase with chemical reaction to without chemical reaction provided that the bulk liquid phase is in a state of chemical equilibrium and with the same driving force. The enhancement factor equation varies depending on the type of reaction. The CO_2-MEA reaction is second-order (Astarita, 1967; Danckwerts, 1970) and the approximate solutions to the computation of the enhancement factor have been proposed for this type of reactions (van Kravelen and Hoftijzer, 1948),

$$E_2 = \frac{\sqrt{\left(M\frac{E_i - E_2}{E_i - 1}\right)}}{\tanh\sqrt{\left(M\frac{E_i - E_2}{E_i - 1}\right)}} \qquad 3.29$$

where E_2 and E_i are the enhancement factor for second order and instantaneous reaction, respectively; $\sqrt{M}$ is the dimensionless parameter and sometimes referred to as the Hatta number (*Ha*) (DeCoursey, 1982; Froment and Bischoff, 1990). As shown in Figure 3.5, E_2 as a function of $\sqrt{M}$ with E_i as a parameter.

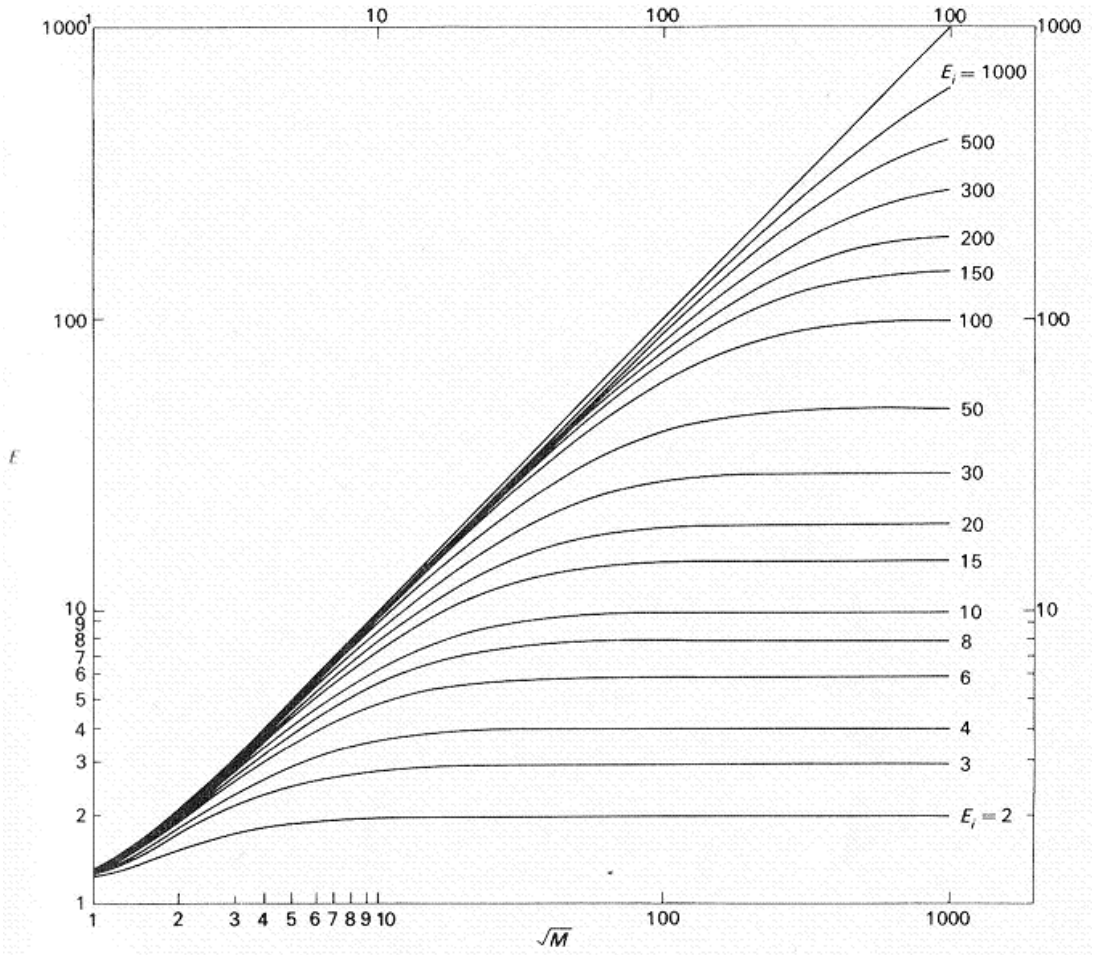

Figure 3.5: Enhancement factor for second order reaction (E_2) as a function of $\sqrt{M}$ (Danckwerts, 1970)

The relationship between enhancement factor for the irreversible second order reaction (E_2) with $\sqrt{M}$ represents three different regimes of absorption process:

1. For a very slow reaction compared to diffusion of dissolved gas in which $\sqrt{M} \leq 1$, the physical absorption predominates and the reaction has negligible effect. As a consequence, there is no enhancement due to the reaction and $E_2 \approx 1$.
2. For moderately rapid reaction in which $1 \leq \sqrt{M} \leq E_i$, E_2 lies on a straight line and the reaction can occur in both the liquid film and bulk liquid phases. If the reaction is fast enough, a substantial amount of the dissolved gas react in the film instead of transferring unreacted gas into the bulk liquid. This results in a higher

concentration gradient and a higher mass transfer rate of dissolved gas. Under these conditions, the mass-transfer rate is dependent on the reaction kinetics. The mass transfer is enhanced and the enhancement factor is approximately, $E_2 = \sqrt{M}$. The amine concentration at the gas-liquid interface is not significantly different from that in the bulk solution.

3. For fast reactions, when $\sqrt{M} \geq E_i$, E_2 approaches a plateau at each value of E_i. The limiting rate of absorption is the diffusion of liquid solvent, so no further increase of enhancement can be obtained with increasing reaction kinetics. The enhancement in this regime is only dependent on the concentrations and diffusivities of the reaction partners, $E_2 = E_\infty$. The reaction in this regime is called instantaneous. Mass transfer phenomena predominantly determine the absorption rate.

The study of mass transfer enhancement due to chemical reaction in the gas-liquid reactions has been the focus of a number of studies. Van Kravelen and Hoftijzer (1948) first developed a correlation for the enhancement factor based on film theory model for irreversible second order reaction. Danckwerts (1970) provided several correlations of enhancement factor for various kinds of chemical reactions. DeCoursey (1974) developed a relation for irreversible second order reaction based on Danckwerts's penetration theory model. Wellek *et al*. (1978) discussed a number of mathematical expressions and proposed an explicit correlation to calculate the enhancement factor for irreversible second order reaction. Astarita and Savage (1980a) proposed correlations considering an instantaneous reversible chemical reaction. In that sudy, the model was applied for absorption and desorption of hydrogen sulfide from aqueous diisopropanolamine solution. DeCoursey (1992) presented the enhancement factor for gas absorption with reversible second order reaction.

The enhancement factor has been used in studies for the development of absorber and stripper column models. Escobillana et al. (1991), Freguia and Rochelle (2003) and Kvamsdal et al. (2009) applied the enhancement factor of pseudo-first order reaction with respect to the concentration of CO_2 in modeling a packed absorption column.

Tontiwachwuthikul et al. (1992) and Pintola et al. (1993) adopted an explicit equation of enhancement factor for irreversible second order reaction developed by Wellek et al. (1978) in their absorption column model. Alatiqi et al. (1994) applied enhancement factor with the assumption of instantaneous irreversible reaction proposed by DeCoursey and Thring (1989) and Astarita and Savage (1980a) for absorber and stripper, respectively. Faramarzi et al. (2009) used an implicit equation of enhancement factor for irreversible second order reaction proposed by van Kravelen and Hoftijzer (1948) in their absorber model. Weiland et al. (1982) and Tobiesen et al. (2008) modeled a packed stripper column using the enhancement factor of instantaneous reversible reaction.

The enhancement factor of pseudo-first order reaction with respect to the concentration of CO_2 was used in the modeling of the packed absorption column. It is assumed that the reaction occurs at a rate that enhances the mass transfer but not so fast that it depletes the amine concentration in the liquid film significantly. The amine concentration is considered to be constant throughout the liquid film and equal to the liquid concentration in the bulk phase. The influence of the reaction rate on mass-transfer using the enhancement factor for absorber (E_{abs}) is approximated by the following equation,

$$E_{abs} = \sqrt{M} = \frac{\sqrt{k_2 C^*_{l,MEA} D_{l,CO_2}}}{k_{l,CO_2}} \qquad 3.30$$

where $\sqrt{M}$ is a dimensionless parameter and sometimes referred to as the Hatta number (Ha) (DeCoursey, 1982; Froment and Bischoff, 1990), k_2(m^3/mol/s) is the second-order reaction rate constant, $C^*_{l,MEA}$ (mol/m^3) is the liquid molar concentration of free MEA, D_{l,CO_2}(m^2/s) is the diffusivity of CO_2 in the aqueous MEA solution and k_{l,CO_2} is the liquid mass transfer coefficient of CO_2. Equation (3.30) shows that the second order reaction rate constant, k_2 is important in determining the mass transfer rate.

On the other hand, mass transfer with a reversible instantaneous reaction is assumed in the stripper column due to high temperatures in the column where chemical equilibrium prevails

in the liquid phase. Accordingly, the enhancement factor in the stripper model (E_{str}) is calculated as follows (Tobiesen et al., 2008),

$$E_{str} = 1 + \frac{\frac{D_{l,MEACOO^-}}{D_{l,CO_2}}\sqrt{K_{eq}}C^*_{l,MEA}}{\left(1 + 2\frac{D_{l,MEACOO^-}}{D_{l,MEA}}\sqrt{K_{eq}C^I_{l,CO_2}}\right)\left(\sqrt{C^I_{l,CO_2}} + \sqrt{C^*_{l,CO_2}}\right)} \qquad 3.31$$

where $C^*_{l,MEA}$ (mol/m^3) and C^*_{l,CO_2} (mol/m^3) are the concentration of free MEA and CO_2 in bulk liquid phase, respectively; C^I_{l,CO_2} (mol/m^3) is the concentration of CO_2 at the interface, K_{eq} (m^3/mol)is the equilibrium constant for the overall reaction, $D_{l,MEACOO^-}$, $D_{l,MEA}$ and D_{l,CO_2} are the diffusion of carbamate ion, MEA and CO_2 in the aqueous MEA solution, respectively. Under these conditions, the reactions are so fast that the mass transfer becomes independent of the reaction rate and is limited by the diffusion of the liquid reactant to the interface. The concentration of reactant in the liquid at the interface can be calculated by solving the chemical equilibrium model.

3.2.4 Chemical kinetics

A large number of experimental studies on the reaction kinetics between CO_2 and aqueous MEA have been established since the early 1960's. A review of various reaction kinetics of this process is available in published literature (Blauwhoff et al., 1984; Versteeg et al., 1996; Aboudheir et al., 2003;Vaidya and Kenig, 2007). Zwitterion mechanism which describes the reaction between CO_2 and MEA via the formation of a zwitterions, $R_1N^+H_2COO^-$ (a locally ionic, net neutral molecule) followed by deprotonation is the most accepted kinetic model for absorption of CO_2 in aqueous MEA (Astarita, 1961; Clarke, 1964; Hikita et al., 1977; Danckwerts, 1979; Penny and Ritter, 1983; Alper, 1990). The zwitterions mechanism takes place in two steps. The first step is rate controlling which involves the formation of a zwitterion. The second step is deprotonization by the base *B*. In this study, R_1 is defined as – CH_2CH_2OH, which is the ethanol component of MEA. The reactions between CO_2 and MEA in aqueous solutions may be presented as,

Zwitterion formation

$$CO_2 + MEA \underset{k_{-1}}{\overset{k_2}{\longleftrightarrow}} MEACOO^- \quad 3.32$$

Zwitterion deprotonation

$$MEACOO^- + MEA \overset{k_{MEA}}{\longleftrightarrow} MEACOO^- + MEAH^+ \quad 3.33$$

which leads to the overall reaction,

$$CO_2 + 2MEA \overset{K_{eq,1}}{\longleftrightarrow} MEACOO^- + MEAH^+ \quad 3.34$$

Based on this mechanism, the capacity of the solution for CO_2 is limited to approximately 0.5 mole of CO_2 per mole of MEA, even at relatively high partial pressures of CO_2 in the gas to be treated. The reason for this limitation is the high stability of the carbamate ($MEACOO^-$) and its low rate of hydrolysis to bicarbonate (HCO_3^-). The stoichiometry of this overall reaction explained why the CO_2 loading of MEA-solutions is limited to around 0.5 mol/mol.

The overall forward reaction at quasi-steady state for this reaction can be expressed as the following (Danckwerts, 1979),

$$r_{CO_2} = \frac{k_2 C_{l,CO_2} C_{l,MEA}}{1 + \frac{k_{-1}}{\sum k_{MEA} C_{l,MEA}}} \quad 3.35$$

where k_{-1}(s^{-1}) is the backward first order reaction rate constant, k_{MEA}(m^3/mol/s) is the second order reaction rate constant for MEA (see Equation 3.33), $C_{l,MEA}$(mol/m^3) is the molar concentration of MEA solution. The second term in the denominator of Equation (3.35),$\sum k_{MEA} C_{l,MEA}$, indicates the contribution to the proton removal step by base in the solution. For the reaction of CO_2 with aqueous MEA, the formation of the zwitterion is the rate limiting step and the zwitterion deprotonation is very fast as compared to the reverse reaction to CO_2 and MEA (Blauwhoff et al., 1984). Due to this reason, the second term in the denominator is very small ($\frac{k_{-1}}{\sum k_{MEA} C_{l,MEA}} \ll 1$) and therefore can be neglected. The reaction rate can be simplified as a first order one with respect to both CO_2 and amine (Danckwerts, 1979),

$$r_{CO_2} = k_2 C_{l,CO_2} C_{l,MEA} \quad 3.36$$

Most of the absorption experimental works assumed that the amine concentration did not change appreciably and the forward reaction dominated (Sada et al., 1976; Penny and Ritter, 1983; Alper, 1990). As a consequence, Equation 3.36 can be simplified further and results the following pseudo-first order reaction,

$$r_{CO_2} = k_{app} C_{l,CO_2} \quad 3.37$$

where $k_{app} = k_2 C_{MEA}$ is a pseudo-first order reaction rate constant.

Kinetic data of the reaction between CO_2 and aqueous MEA at different temperature has been published in the open literature (Versteeg et al., 1996). In this study, the empirical correlation for the second-order reaction rate constant k_2 (m^3/mol/s) proposed by Hikita et al. (1977) is used,

$$k_2 = 9.77 \times 10^7 \exp\left(\frac{-4955}{T_l}\right) \quad 3.38$$

3.2.5 Equilibrium relations

The rate based model explicitly accounts for the mass transfer rate. This requires an equilibrium model to determine the equilibrium partial pressures and the liquid speciation in the MEA aqueous solution in order to identify the driving force for mass transfer rate. The equilibrium model considered in this study is based on the coupling between vapour-liquid phase equilibrium and chemical equilibrium as shown in Figure 3.6. Phase equilibrium which exists at the vapour-liquid interface governs the distribution of the molecular species between the vapour and liquid phases while chemical equilibrium describes the distribution of the molecular and ionic species in the liquid phase.

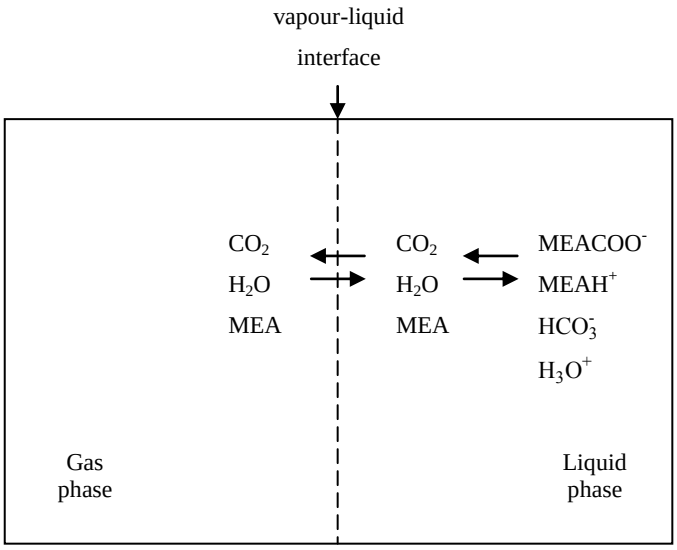

Figure 3.6: Phase and chemical equilibrium in the CO_2-H_2O-MEA system

Both CO_2 and MEA are considered as weak acid gas and base in aqueous solutions, respectively. Thus, carbon dioxide partially dissociates to form weak electrolytes in the aqueous solution due to chemical reactions as well as MEA. A weak electrolyte is partially dissociated into its constituent ions. The existence of ionic species leads to non-ideality of the liquid solutions resulting from interaction energy between species in solution. Therefore, the non-ideality of the liquid phase cannot be neglected. Deviations from ideality can be described by the use of activity coefficient which describes the physical interaction between solute species in the liquid phase.

Equilibrium in electrolyte solutions is usually referred to as ionic equilibrium. The general properties and laws of phase equilibrium for non-polar systems also hold in the case of equilibrium in which ions are present (Zarzycki and Chacuk, 1993). Therefore, the phase equilibrium model (see section 2.4.3) was applied in this work. To apply these equations, information about activity coefficients for CO_2, H_2O and MEA as well as the Henry's constant are required. The estimation of these variables will be discussed in the following subsections.

Equilibrium partial pressure

The distribution of species between at the vapour-liquid interface is dominated by phase equilibrium (see Figure 3.6). In this study, it is assumed that the vapour phase behaves as an ideal gas while liquid phase is assumed to be a non-ideal solution. Therefore, the fugacity of solvent (H_2O and MEA) and solute molecules (CO_2) is assumed to be unity. The partial pressures of H_2O and MEA were determined using the following equation,

$$p_i^* = \gamma_i x_i P_i^S \qquad 3.39$$

where p_i^*(kPa) is the equilibrium partial pressure, x_i is the mole fraction, γ_i is the activity coefficient and P_i^S(kPa) is the vapour pressure. The activity coefficients of H_2O and MEA were calculated using Wilson correlation (Smith et al., 1996). The Wilson model is well accepted and is used on a regular basis to model highly non-ideal systems at low pressures.

In the case of CO_2, the temperature of the system exceeds its supercritical temperature, i.e.,CO_2 does not exist as a liquid at that temperature, i.e., Equation (3.39) cannot be applied for this system. The equilibrium partial pressure of CO_2 which is related to the free CO_2 concentration in the solution through Henry's law is expressed as follows,

$$p_{CO_2}^* = \gamma_{CO_2} C_{l,CO_2}^* He_{CO_2} \qquad 3.40$$

where C_{l,CO_2}^* is the molar concentration of free CO_2 in solution and He_{CO_2} (Pa.m^3/mol) is the Henry's law constant of CO_2 in aqueous MEA solution. The Henry's law constant (He) has to be determined from experimental solubility data. Generally, the measurement of the physical solubility is based on determining the concentration of gas absorbed in a solution at equilibrium. If the absorbed gas reacts with the solvent, then the physical equilibrium cannot be directly measured. Due to the chemical reaction that occurs in the solution, the physical solubility of carbon dioxide in alkanolamine solutions cannot be measured using conventional methods (Browning and Weiland, 1994).Therefore, it must be estimated from experimental data reported to systems that are similar, i.e., non-reacting gases. In view of the similarities with regard to configuration, molecular volume, and electronic structure, N_2O is often used as a non-reacting gas to estimate the properties of CO_2 (Sada *et al*., 1978;

Haimour and Sandall, 1984; Versteeg and van Swaaij, 1988; Al-Ghawas *et al*., 1989; Littel *et al*, 1992). Therefore, the Henry's constant of CO_2 is expressed as the following form,

$$\frac{He_{Co_2}}{He_{N_2O}} = \frac{He_{CO_2}^{H_2O}}{He_{N_2O}^{H_2O}} \qquad 3.41$$

where $He_{CO_2}^{H_2O}$(Pa.m^3/mol) and $He_{N_2O}^{H_2O}$ (Pa.m^3/mol) are the Henry's law constants of carbon dioxide (CO_2) and nitrous oxide (N_2O) in water, respectively; He_{Co_2}(Pa.m^3/mol) and He_{N_2O}(Pa.m^3/mol) are Henry's law constants of CO_2 and N_2O in aqueous MEA solution, respectively. Haimour and Sandall (1984) confirmed the N_2O analogy in their study to measure the solubility of CO_2 in MDEA solution.

Chemical equilibrium

Reactions between the dissolved gas and liquid reactants are assumed to be completed within the liquid film. As a result, the bulk liquid is in a state of chemical equilibrium. The chemical equilibrium model is required to provide the concentration of liquid phase compositions, molecular and ionic species. The following chemical equilibrium describing the species distribution are established for the present system (Austgen *et al*., 1989),

Carbamate reversion to bicarbonate:

$$MEACOO^- + H_2O \overset{K_{eq,2}}{\longleftrightarrow} MEA + HCO_3^- \qquad 3.42$$

MEA deprotonation:

$$MEAH^+ + H_2O \overset{K_{eq,3}}{\longleftrightarrow} MEA + H_3O^+ \qquad 3.43$$

Bicarbonate formation:

$$CO_2 + 2H_2O \overset{K_{eq,4}}{\longleftrightarrow} HCO_3^- + H_3O^+ \qquad 3.44$$

Carbonate formation:

$$HCO_3^- + H_2O \overset{K_{eq,5}}{\longleftrightarrow} CO_3^{2-} + H_3O^+ \qquad 3.45$$

Dissociation of water:

$$2H_2O \overset{K_{eq,6}}{\longleftrightarrow} OH^- + H_3O^+ \quad (3.46)$$

The chemical reactions described above result in a complex mixture of nonvolatile or moderately volatile molecular species and nonvolatile ionic species. The corresponding apparent (concentration-based) equilibrium constants ($K_{eq,i}$) are given by,

$$K_{eq,2} = \frac{C^*_{l,MEA} C_{l,HCO_3^-}}{C_{l,MEACOO^-} C_{l,H_2O}} \quad (3.47)$$

$$K_{eq,3} = \frac{C^*_{l,MEA} C_{l,H_3O^+}}{C_{l,MEAH^+} C_{l,H_2O}} \quad (3.48)$$

$$K_{eq,4} = \frac{C_{l,HCO_3^-} C_{l,H_3O^+}}{C^*_{l,CO_2} C_{l,H_2O}{}^2} \quad (3.49)$$

$$K_{eq,5} = \frac{C_{l,CO_3^{2-}} C_{l,H_3O^+}}{C_{l,HCO_3^-} C_{l,H_2O}} \quad (3.50)$$

$$K_{eq,6} = \frac{C_{l,OH^-} C_{l,H_3O^+}}{C_{l,H_2O}{}^2} \quad (3.51)$$

Based on the reactions above, the overall material balances of MEA and CO_2 are formulated as follows,

$$C_{l,MEA} = C_{l,MEACOO^-} + C_{l,MEAH^+} + C^*_{l,MEA} \quad (3.52)$$

$$C_{l,CO_2} = C_{l,MEACOO^-} + C_{l,HCO_3^-} + C_{l,CO_3^{2-}} + C^*_{l,CO_2} \quad (3.53)$$

Thus, the electroneutrality balance equation is as follows,

$$C_{l,MEAH^+} + C_{l,H_3O^+} = C_{l,MEACOO^-} + C_{l,HCO_3^-} + 2C_{l,CO_3^{2-}} \quad (3.54)$$

There are eight species of components and ions that must be solved by eight independent equations. Initial estimates of the concentrations have to be provided to solve this system of nonlinear algebraic equations. The equilibrium constants are also necessary to solve these equations. Once the equilibrium constants are known, the concentrations of unreacted CO_2 and MEA concentrations in the liquid phase can be calculated.

The set of non-linear equations, 3.47 to 3.54, can be solved using numerical methods such as the Newton method. The reliability of these methods depends on the initial values of the concentration of each individual species provided to the solution which has to be very close to the actual solution. An iteration on solute concentration proceeds until convergence is achieved. Failure to provide good estimates of initial values may cause convergence problems. As for the packed column model, the chemical equilibrium has to be determined at every discretization point. This iterative procedure may become computationally intensive.

Hoff et al. (2004) developed a non-iterative procedure to solve this chemical equilibrium model for the speciation in the liquid phase. The Hoff speciation equilibrium model was developed using Kent and Eisenberg approach which is based on apparent equilibrium constant. Based on this model, it is assumed that CO_2 is initially in the form of bicarbonate and react with MEA until reach equilibrium state as follows,

$$MEA + HCO_3^- \overset{K_{eq,7}}{\longleftrightarrow} MEAH^+ + CO_3^{2-} \qquad 3.55$$

$$MEA + HCO_3^- \overset{K_{eq,8}}{\longleftrightarrow} MEACOO^- + H_2O \qquad 3.56$$

The equilibrium in reaction 3.55 results from a combination of the equilibrium of the protonation of amine and carbonate formation.

$$\begin{array}{l} MEA + H_3O^+ \overset{1/K_{eq,3}}{\longleftrightarrow} MEAH^+ + H_2O \\ \underline{HCO_3^- + H_2O \overset{K_{eq,5}}{\longleftrightarrow} CO_3^{2-} + H_3O^+} \\ MEA + HCO_3^- \overset{K_{eq,7}}{\longleftrightarrow} MEAH^+ + CO_3^{2-} \end{array} \qquad 3.57$$

Therefore, the equilibrium constant of reaction 3.55 ($K_{eq,7}$)is determined as follows,

$$K_{eq,7} = \frac{K_{eq,5}}{K_{eq,3}} \qquad 3.58$$

The equilibrium in reaction 3.56 results from reverting bicarbonate to carbamate. Therefore, the equilibrium constant of reaction 3.56 ($K_{eq,8}$) is estimated as follows:

$$K_{eq,8} = \frac{1}{K_{eq,2}} \tag{3.59}$$

The concentration of free MEA molecule and ionic species, protonated MEA ($MEAH^+$) carbamate ($MEACOO^-$), bicarbonate (HCO_3^-) and carbonate (CO_3^{2-}) ,described in terms of the molar extents of reaction ξ_1 and ξ_2, are defined as follows,

$$\begin{aligned} C^*_{l,MEA} &= C_{l,MEA}(1-\alpha) - \xi_1 - \xi_2 \\ C_{l,MEAH^+} &= C_{l,MEA}\alpha + \xi_1 \\ C_{l,MEACOO^-} &= \xi_2 \\ C_{l,HCO_3^-} &= C_{l,MEA}\alpha - \xi_1 - \xi_2 \\ C_{l,CO_3^{2-}} &= \xi_1 \end{aligned} \tag{3.60}$$

The molar extent of reaction, ξ_1 is calculated as the roots of a fourth order polynomial equation (Hoff et al., 2004), i.e.,

$$\xi_1 = \text{roots of } (A\kappa^4 + B\kappa^3 + C\kappa^2 + D\kappa + E) \tag{3.61}$$

where,

$$\begin{aligned} A &= K^2_{K_{eq,8}} \\ B &= 2K^2_{K_{eq,8}} C_{MEA}\alpha + 2K_{K_{eq,7}}K_{K_{eq,8}} \\ C &= K^2_{K_{eq,7}} - K_{K_{eq,7}} + 2K_{K_{eq,7}}K_{K_{eq,8}}C_{MEA}\alpha + K^2_{K_{eq,8}}C^2_{MEA}\alpha^2 \\ &\quad - K_{K_{eq,7}}K_{K_{eq,8}}C_{MEA} \\ D &= -K^2_{K_{eq,7}}C_{MEA} - K_{K_{eq,7}}C_{MEA}\alpha - K_{K_{eq,7}}K_{K_{eq,8}}C^2_{MEA}\alpha \\ E &= K^2_{K_{eq,7}}C^2_{MEA}\alpha - K^2_{K_{eq,7}}C^2_{MEA}\alpha^2 \end{aligned} \tag{3.62}$$

The roots must satisfy the following constraints to return a feasible (physical) solution,

$$\begin{gathered} \xi_1 \geq 0 \\ \xi_2 \geq 0 \\ \xi_1 + \xi_2 \leq C_{l,MEA}\alpha \\ \xi_1 + \xi_2 \leq C_{l,MEA}(1\text{-}\alpha) \end{gathered} \qquad 3.63$$

where α is the CO_2 laoding (mol CO_2/mol MEA). Meanwhile, the molar extent of reaction ξ_2 is determined by the following equation (Hoff et al., 2004),

$$\xi_2 = \frac{K_{eq,8}\xi_1\left(\xi_1 + C_{l,MEA}\alpha\right)}{K_{eq,7}} \qquad 3.64$$

The molar extent of reactions ξ_1 and ξ_2, obtained from equation 3.61 and 3.64, are incorporated in equation 3.60 to determine the concentration of the free MEA and other ionic species. Then, the concentration of free CO_2 can be calculated as follows:

$$C^*_{l,CO_2} = \frac{C_{l,MEAH^+}C_{l,MEACOO^-}}{K_{eq,1}{C^*_{l,MEA}}^2} \qquad 3.65$$

This free CO_2 concentration is in equilibrium with the chemically bound CO_2 and MEA as represented by reaction 3.34. The equilibrium constant of this reaction is evaluated as a combination of three other equilibrium constants, i.e.,

$$K_{eq,1} = \frac{K_{eq,4}}{K_{eq,2}K_{eq,3}} \qquad 3.66$$

The temperature dependence of equilibrium constants ($K_{eq,i}$) for reactions 3.47 to 3.51 are determined as follows (Austgen *et al*., 1989):

$$\ln K_{eq,i} = C_1 + \frac{C_2}{T} + C_3 \ln T + C_4 T \qquad 3.67$$

where T (K) is the temperature and $C_1 - C_4$ are constant parameters (see Table 3.1).

Table 3.1: Parameters for equilibrium constant (Austgen et al., 1989)

Reaction	C_1	C_2	C_3	C_4
Carbamate reversion to bicarbonate	2.8898	-3635.09	0	0
MEA deprotonation	2.1211	-8189.38	0	-0.007484
Bicarbonate formation	231.465	-12092.10	-36.7816	0
Carbonate formation	216.049	-12431.70	-35.4819	0
Ionization of water	132.899	-13445.9	-22.4773	0

3.3 Reboiler model

The reboiler unit is used to provide heat to the bottom of the stripper column. The regeneration of a CO_2-rich amine solution requires a high amount of energy (IPCC, 2005). The related energy demand can be divided into three different categories:

1. to break chemical bonds between the CO_2 and the amine.
2. to heat up the temperature of rich amine solution to the boiling point.
3. to evaporate water as CO_2 stripping steam.

As shown in Figure 3.7, the liquid stream, heated using steam, is separated into a liquid and a vapour product. The vapour product is returned to the column for the regeneration of the MEA while the stripped MEA solution (Lean MEA) is recycled back to absorber. The reboiler temperature should not exceed 120^{o}C to avoid MEA thermal solvent degradation (Alie, 2004).

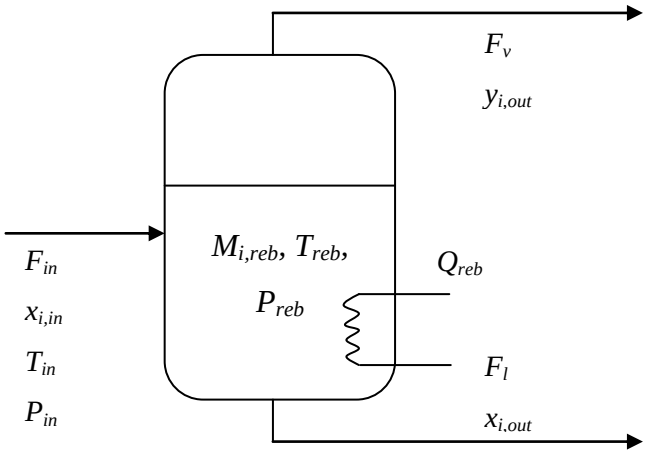

Figure 3.7: Reboiler drum diagram

The present study represents the reboiler as a single equilibrium stage. Isothermal Pressure (P), Temperature (T)-flash calculation is applied to determine the compositions of vapour and liquid phases at a given pressure, temperature and overall compositions (Smith et al., 1996). The P,T-flash calculations is a simple method that can be used for this process because the temperature and pressure are specified to determine the equilibrium ratio (K_{value}) which depends on these variables. The mathematical model of the reboiler requires the following equations:

1. Material balance equations.
2. Energy balance equations.
3. Equilibrium relations

3.3.1 Molar component balance

The material balance for each component in the liquid phase with negligible vapour hold-up is shown in Equation 3.68. This material balance equation considers an accumulation term and the flow rate entering and leaving the reboiler drum for each component, i.e., CO_2, H_2O and MEA.

$$\frac{dM_{i,reb}}{dt} = F_{in}x_{i,in} - F_v y_{i,out} - F_l x_{i,out} \qquad 3.68$$

Following Equation 3.68, the state variable $M_{i,reb}$ (mol) represents the moles for each component *i* accumulated in the reboiler, F_{in} (mol/s), F_v (mol/s), F_l (mol/s) are the inlet, vapour and liquid flow rates, respectively; x_i and y_i are the liquid and vapour mole fractions of each component *i*, respectively. The mole fraction of the liquid phase is calculated as follows:

$$x_i = \frac{x_{i,in}}{1 + \chi\left(K_{value,i} - 1\right)} \tag{3.69}$$

where $K_{value,i}$ is the vapour-liquid equilibrium ratio of each component *i* and χ is the vapour fraction. The vapour-liquid equilibrium ratio is a function of the vapour and liquid composition, the temperature and the pressure in the reboiler. The $K_{value,i}$ was estimated as follows:

$$K_{value,i} = \frac{y_i}{x_i} = \frac{\gamma_i P_i^v}{P_{reb}} \tag{3.70}$$

where $\gamma_i$is the activity coefficient of component *i*, P_i^v(kPa) is the vapour pressure of component *i*, P_{reb}(kPa) is the reboiler pressure. This thermodynamic equilibrium relation is used to calculate the vapour phase mole fraction which was determined using the Rachford-Rice equation (Smith et al., 1996),

$$\sum \frac{x_{i,in}\left(K_{value,i} - 1\right)}{1 + \chi\left(K_{value,i} - 1\right)} = 0 \tag{3.71}$$

3.3.2 Energy balance

The temperature in the reboiler can be estimated from the energy balance for this unit. Thus, the energy balance for the reboiler can be written as follows:

$$\frac{dE_{reb}}{dt} = F_{in}H_{in} - F_vH_v - F_lH_l + Q_{reb} \tag{3.72}$$

where the state variable E_{reb} (J) is represents the energy accumulated inside the reboiler, H_{in} (J/mol) and H_l (J/mol) are liquid enthalpy entering and leaving the reboiler, respectively; H_v (J/mol) is the vapour enthalpy leaving the reboiler and Q_{reb} (J/s) is the reboiler heat duty. The reboiler heat duty in this model is considered to be an input of the model. Thus, Q_{reb} can

be adjusted to supply the heat for solvent regeneration in the stripper column, i.e., it can be potentially used as manipulated variable to control this process due to changes in the flue gas flowrate. The definitions for $M_{i,reb}$ and E_{reb} are as follows:

$$M_{i,reb} = \frac{\pi}{4} d_c^2 L_B \rho_m x_i \qquad E_{reb} = \frac{\pi}{4} d_c^2 L_B H_l \rho_m \tag{3.73}$$

where, d_c(m) is the diameter of the column, L_B (m) is the liquid level of reboiler drum, ρ_m (mol/m^3) is the molar density, H_l (J/mol) is the liquid enthalpy.

3.4 Heat exchanger model

The cross heat exchanger considered in the process is assumed to be a counter-current shell and tube heat exchanger. In practice, changes in the inlet temperature or mass flow rate may occur, which will affect the behaviour of the entire system. A change in any of these variables creates an unsteady-state behaviour in the system. The heat exchanger model used in the present study considers the fluctuations in heat between the hot lean amine solution (flowing inside the tube) and the cold rich amine solution (flowing counter-currently through the shell) coming from the stripper and the absorber columns, respectively. The proposed heat exchanger model estimates the conditions of the outlet streams given the inlet stream conditions. The standard gPROMS Process Model Library (PML) was used in the present study to model the transient behaviour of this heat exchanger unit. The heat exchanger model considers the following assumptions (PSE, 2009):

1. The fluid is in turbulent flow.
2. The fluid streams do not change phase.
3. The tube metal is modeled as an axially distributed system.
4. Thermal conduction in the tube metal is negligible in the axial direction and infinitely fast in the radial direction.
5. The pressure is assumed to be constant.
6. Heat loss to surroundings is negligible.

The cross heat exchanger model used in this work explicitly describes the dynamics of this unit when the inlet flow rates to this unit are changing in time. For incompressible fluids, the outlet flow rate will change instantaneously if the inlet flow is changed, i.e., the mass inside the shell and tube counter-current heat exchanger is assumed constant. Therefore, the dynamic behaviour of the heat exchanger was modeled using only an energy conservation balance.

3.4.1 Energy balance for tube/shell heat exchanger

A tube and shell energy balance was used in the present analysis to calculate the change in fluid temperature for both streams. As shown in Figure 3.8, the heat exchanger was subdivided into individual volumes of length *dz* that are in counter current flow. Each element considered in Figure 3.8 includes the tube side, the shell side and the tube wall, respectively.

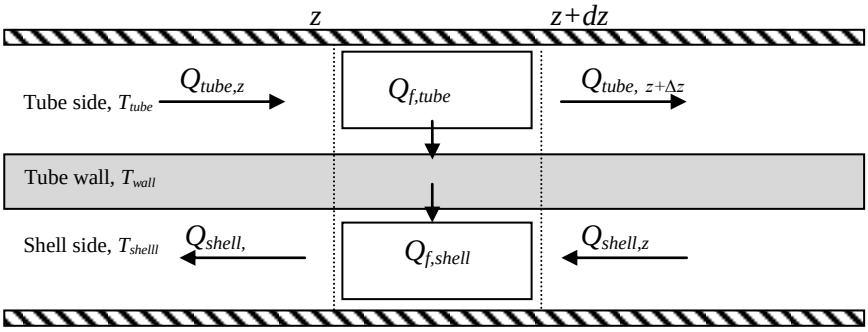

Figure 3.8: Elementary energy balance taking into account convective heat transfer and counter-current flow

The energy balance for the fluids around *dz* in Figure 3.8 consists of the rate of accumulation of energy, rate of energy entering and leaving the balance space by convective flow, and the heat flux transferred through the tube wall. Therefore, the energy balances applied to a differential volume of tube and shell sides yields (PSE, 2009):

$$\frac{dE_{tube}}{dt} = -\frac{1}{A_{tube}L_{hx}}\frac{\partial Q_{tube}}{\partial z} + Q_{f,tube}\frac{2}{r_{tube}} \quad 3.74$$

$$\frac{dE_{shell}}{dt} = -\frac{1}{A_{shell}L_{hx}}\frac{\partial Q_{shell}}{\partial z} + Q_{f,shell}\frac{2}{r_{shell}} \quad 3.75$$

where E_{tube} (J/m^3) and E_{shell} (J/m^3) are the volumetric specific internal energy of tube and shell, respectively; Q_{tube} (J/s) and Q_{shell} (J/s) are the energy flowrate of tube and shell, respectively;$Q_{f,tube}$ (J/m^2/s) and $Q_{f,shell}$ (J/m^2/s) are the heat flux of tube and shell, respectively; A_{tube} (m^2) and A_{shell} (m^2) are the area of tube and shell, respectively; r_{tube} (m) are r_{shell} (m) the radius of tube and shell, respectively; and L_{hx} (m) is the tube length. The derivation of this equation was provided in Appendix B. The volumetric specific internal energy is correlated to mass specific internal energy as follows,

$$E_{tube/shell} = E_{m,tube/shell}\rho, \quad E_{m,tube/shell} = H_m - \frac{P_{hx}}{\rho} \quad 3.76$$

where E_m (J/kg) is the mass specific internal energy, ρ (kg/m^3) is the fluid density, H_m (J/kg) is the mass enthalpy and P_{hx} (kPa) is the pressure. The energy flow rates for a single tube and shell is estimated as follows,

$$Q_{tube} = \frac{F_{hx}}{n_{Tube}}H_{tube} \qquad Q_{shell} = F_{hx}H_{shell} \quad 3.77$$

where F_{hx} (mol/s) is the total molar flowrate entering the heat exchanger, H_{tube} (J/mol) and H_{shell} (J/mol) are the molar enthalpy of the fluid in the tube and shell, respectively.

The heat flux for tube and shell sides are estimated using overall heat transfer coefficients. The tube side heat flux for a single tube per unit area ($Q_{f,tube}$) and the shell side heat flux per unit area, ($Q_{f,Shell}$), were calculated using Equations 3.78 and 3.79, respectively. The term $Q_{f,tube}$ is the energy transferred to the wall from the tube side (hot lean amine) whereas $Q_{f,shell}$ is the energy transferred to shell side (cold rich amine) from the wall.

$$Q_{f,tube} = -U_{tube}(T_{wall} - T_{tube}) \quad 3.78$$

$$Q_{f,shell} = n_{tube}U_{shell}(T_{wall} - T_{Shell}) \quad 3.79$$

The overall heat transfer coefficients for the tube (U_{tube}, W/m^2/K) and the shell (U_{shell}, W/m^2/K) were assumed constant. The areas of the tube (A_{tube}, m^2) and the shell (A_{shell}, m^2) were estimated from the following expressions:

$$A_{tube} = \frac{\pi}{4} d_{i,tube}^2 \qquad 3.80$$

$$A_{shell} = \frac{\pi}{4}\left(d_{i,shell}^2 - d_{o,tube}^2 n_{tube}\right)$$

where $d_{i,tube}$ (m) and $d_{o,tube}$ (m) are the inside and outside tube diameters, respectively; $d_{i,shell}$ (m) is the shell's diameter.

3.4.2 Energy balance for the wall

As shown in Equation 3.81, the model assumes that the wall temperature (T_{wall}) is time-dependent. The terms within the parentheses in Equation 3.81 represent the energy change between shell and tube and the wall.

$$m_{wall} C_{p,wall} \frac{dT_{wall}}{dt} = L_{hx}\left(Q_{f,tube} - \frac{Q_{f,shell}}{n_{tube}}\right) \qquad 3.81$$

where $$m_{wall} = L_{hx}\rho_{wall}\frac{\pi}{4}\left(d_{o,Tube}^2 - d_{i,Tube}^2\right)$$

where ρ_{wall} (kg/m^3) is the wall density, $C_{p,wall}$ (J/kg/K) is the specific heat capacity of the tube material, $d_{i,Tube}$ (m) and $d_{o,Tube}$ (m) are the inner and outer tube diameters, respectively. The present heat exchanger model considers that the tubes are made of stainless steel (Dugas, 2006).

3.5 Tank model

A buffer tank model is used in the present study to damp-out any fluctuations in the lean amine stream's flow rate coming from the stripper column. The material balance of the tank is as follows:

$$\rho_m \frac{dV_{tank}}{dt} = F_{in} - F_{out} \qquad 3.82$$

where ρ_m (mol/m^3) is the molar density of liquid mixture, V_{tank} (m^3) is the volume of the liquid in the tank, F_{in}(mol/s) and F_{out}(mol/s) is the inlet and outlet molar flow rate,

respectively. The liquid outlet flow rate is determined using following equation (Thomas, 1999),

$$F_{out} = C_v \alpha_f \sqrt{|\Delta P| \rho} \qquad 3.83$$

where α_f is valve stem position, C_v is the flow coefficient (m^2), ΔP (Pa or $kg/m/s^2$) is the pressure drop across the valve, ρ (kg/m^3) is the liquid density. The fluctuations in the stripper column's flow rates will be reflected in the tank's liquid level.

3.6 Physical properties

Physical properties of gas and liquid phases are the additional information required to complete the model development. Correlations for physical property data are necessary with computer-based calculations. The physical properties used in this study are presented in the following subsections.

3.6.1 Liquid phase

Density

The density of amine solution loaded with CO_2 is given by its average molecular weight divided by its total molar volume, i.e.,

$$\rho_l = \frac{\sum x_i (MW)_i}{v_m} \qquad 3.84$$

where ρ_l (g/cm^3) is the solution density, v_m (cm^3/mol) is the molar volume of the solution, x_i is the mole fraction, MW_i is the molecular weights and subscript i refers to components MEA, CO_2 and water. The molar volume of the solution, v_m can be determined using the following equation which includes the interaction term for MEA+water, v^* (Weiland *et al*., 1998),

$$v_m = \sum x_i v_i + x_{MEA} x_{h_2o} v^* \qquad 3.85$$

where v_i (cm^3/mol) is the molar volume of pure components and v^* (cm^3/mol) is the molar volume associated with the interaction between MEA and water (given at a constant value of -1.8218). The molar volume of pure CO_2 is equal to 0.04747 (cm^3/mol) while the molar

volumes of pure MEA and water were calculated using the pure component density data of Hsu and Li (1997).

$$v_i = \frac{(MW)_i}{\rho_i} \qquad 3.86$$

where

$$\rho_i = b_1 + b_2 T_l + b_3 {T_l}^2$$

The values of the parameters used in Equation 3.86 are given in Table 3.2.

Table 3.2: Parameters for density equation for pure MEA and H_2O

	MEA	H_20
b_1	1.19093	0.863559
b_2	-4.2999 x 10^{-4}	1.21494 x 10^{-3}
b_3	-5.66040 x 10^{-7}	-2.57080 x 10^{-7}

Viscosity

The liquid viscosity of for each component is calculated using Andrade's equation (Aspen, 2006),

$$\ln \mu_{l,i} = b_1 + \frac{b_2}{T_l} + b_3 ln T_l \qquad 3.87$$

where $\mu_{l,i}$ (Pa.s) is the liquid viscosity; and b_1, b_2 and b_3 are the parameters given in Table 3.3.

Table 3.3: Parameters for liquid viscosity equation

	CO_2	H_2O	MEA
b_1	-14.09345	-12.260477	-19.355128
b_2	1331.0784	1515.6766	4568.5591
b_3	0	0	0

The viscosity of the MEA solution was determined by multiplying the viscosity of pure component by its mole fraction, i.e.,

$$\ln \mu_l = \sum x_i \, \mu_{l,i} \tag{3.88}$$

Henry's constant

The Henry constant of CO_2 and N_2O in water can be obtained from the following correlations proposed by Versteeg and van Swaaij (1988):

$$He_{CO_2}^{H_2O} = 2.82 \times 10^6 exp \frac{-2044}{T_l} \tag{3.89}$$

$$He_{N_2O}^{H_2O} = 8.55 \times 10^6 exp \frac{-2284}{T_l} \tag{3.90}$$

where $He_{CO_2}^{H_2O}$ (Pa.m^3/mol) and $He_{N_2O}^{H_2O}$ (Pa.m^3/mol) are the Henry's constant of CO_2 and N_2O in water, respectively. The Henry's constant of N_2O in aqueous MEA solution (He_{N_2O}) is determined from a semi empirical model of the excess Henry's quantity, H^E(Pa.m^3/mol), developed by Wang et al. (1992),

$$\ln He_{N_2O} = \Phi_{\text{MEA}} \ln He_{N_2O}^{MEA} + \Phi_{H_2O} \ln He_{N_2O}^{H_2O} + H^E \tag{3.91}$$

where Φ_{MEA} and Φ_{H_2O} denote the volume fractions of MEA and water in aqueous MEA, respectively; and $H_{N_2O}^{MEA}$ denote the Henry's constants of N_2O in pure MEA. The excess Henry's quantity can be calculated using correlation proposed by Tsai et al. (2000),

$$H^E = \Phi_{\text{MEA}} \Phi_{H_2O} \left(4.793 - 0.007446 T_l - 2.201 \Phi_{H_2O}\right) \tag{3.92}$$

The Henry's constant of N_2O in pure MEA, ($He_{N_2O}^{MEA}$) is calculated using following equation (Wang et al., 1992),

$$He_{N_2O}^{MEA} = 1.207 \times 10^5 \exp\left(\frac{-1136}{T_l}\right) \tag{3.93}$$

The volume fraction of MEA, Φ_{MEA} and water, Φ_{H_2O} were calculated as follows,

$$\Phi_{\text{MEA}} = \frac{x_{MEA} v_{MEA}}{x_{MEA} v_{MEA} + x_{H_2O} v_{H_2O}} \tag{3.94}$$

$$\Phi_{H_2O} = \frac{x_{H_2O} v_{H_2O}}{x_{MEA} v_{MEA} + x_{H_2O} v_{H_2O}} \tag{3.95}$$

Diffusivity

Due to the chemical reaction of CO_2 with MEA, the diffusivity of CO_2 in the MEA aqueous solution is also determined from the nitrous oxide (N_2O) analogy,

$$\frac{D_{l,CO_2}}{D_{l,N_20}} = \frac{D_{l,CO_2}^{H_2O}}{D_{l,N_20}^{H_2O}} \tag{3.96}$$

where $D_{l,CO_2}^{H_2O}$(m^2/s) and $D_{l,N_20}^{H_2O}$(m^2/s) are diffusivities of CO_2 and N_2O in water, respectively; and D_{l,CO_2}(m^2/s) and D_{l,N_20}(m^2/s) are diffusivities of CO_2 and N_2O in aqueous MEA solution, respectively. The diffusivities of CO_2 and N_2O in water are calculated from the correlations of Versteeg and van Swaaij (1988),

$$D_{l,CO_2}^{H_2O} = 2.35 \times 10^{-6}\exp\left(\frac{-2119}{T_l}\right) \tag{3.97}$$

$$D_{l,N_20}^{H_2O} = 5.07 \times 10^{-6}\exp\left(\frac{-2371}{T_l}\right) \tag{3.98}$$

The diffusivity of N_2O in aqueous MEA can be estimated using following equation (Ko et al., 2001),

$$D_{l,N_20} = \left(5.07 + 0.865C_{l,MEA} + 0.278C_{l,MEA}^2\right)\exp\left(\frac{-2371 - 93.4C_{l,MEA}}{T_l}\right) \times 10^{-6} \tag{3.99}$$

The diffusivity of MEA molecule in aqueous MEA is calculated by using the correlation developed by Snijder et al. (1993),

$$D_{l,MEA} = \exp\left(-13.275 - \frac{2198.3}{T_l} - 0.078142C_{l,MEA}\right) \tag{3.100}$$

The diffusivity of carbamate ion was determined using the correlation developed by Hoff et al. (2004):

$$D_{carbamate} = \exp\left(-22.64 - \frac{1000}{T_l} - 0.7ln\mu_{l,MEA}\right) \tag{3.101}$$

where $D_{carbamate}$ (m^2/s) is the diffusivity of the carbamate ion, μ_{MEA}(Pa.s) the viscosity of liquid MEA.

Vapour pressure

The extended Antoine vapour pressure for pure components is based on the following expression (Aspen, 2006):

$$\ln\left(P_i^s\right) = b_1 + \frac{b_2}{T_l + b_3} + b_4 T_l + b_5 \ln T_l + b_6 {T_l}^{C_7} \qquad 3.102$$

where the values for the constant parameters, b_1, b_2,…, are listed in Table 3.4.

Table 3.4: Parameters for vapour pressure equation

	CO_2	H_2O	MEA
b_1	72.829119	72.55	172.78
b_2	-3403.28	-7206.7	-13492
b_3	0	0	0
b_4	0.0094907	0	0
b_5	-8.560337	-7.1385	-21.914
b_6	$2.91\text{x}10^{-16}$	$4.05\text{x}10^{-6}$	$1.38\text{x}10^{-5}$
b_7	6	2	2

Heat capacity

The liquid heat capacity is determined using the following relation (Hilliard, 2008):

$$C_{p,l} = b_1 T_l + b_2 T_l + b_3 {T_l}^2 + b_4 {T_l}^3 + b_5 {T_l}^4 \qquad 3.103$$

where $C_{p,l}$ (kJ/kg/^{o}C) is the liquid heat capacity and T_l (^{o}C) is the liquid temperature. The constants used in this equation are given in Table 3.5.

Table 3.5: Parameters for liquid heat capacity equation

	b_1	b_2	b_3	b_4	b_5
H_2O	4.2107	$-1.696\text{x}10^{-5}$	$2.568\text{x}10^{-5}$	$-1.095\text{x}10^{-7}$	$3.038\text{x}10^{-10}$
MEA	2.6161	$3.706\text{x}10^{-3}$	$3.787\text{x}10^{-6}$	0	0

Heat of vaporization

The heat of vaporization is determined using the Watson equation (Aspen, 2006):

$$\Delta H_{vap} = \Delta H^0_{vap}(T_o)\left(\frac{1-\frac{T_l}{T_c}}{1-\frac{T_o}{T_c}}\right)^{a+b\left(1-\frac{T_l}{T_c}\right)} \quad 3.104$$

where ΔH_{vap}(J/mol) is the heat of vaporization, ΔH^0_{vap}(J/mol) is heat of vaporization at reference temperature, T_o (K), T_c (K) is the critical temperature. The values for the constant parameters are given in Table 3.6.

Table 3.6: Parameters for heat of vaporization equation

	CO_2	H_2O	MEA
T_c (K)	304.2	647.3	614.45
ΔH^0_{vap}(J/mol)	17165.880	40683.136	54835.8
T_o(K)	194.7	373.2	399.82
a	0.3576292	0.31064607	0.3287809
b	0	0	-0.0856624

3.6.2 Gas phase

Density

The density of ideal gas phase is determined using the ideal gas equation, i.e.,

$$v_g = \frac{RT_g}{P} \quad 3.105$$

$$\rho_i = \frac{\sum y_i (MW)_i}{v_g} \quad 3.106$$

where v_g (m^3/mol) is the total gas molar volume, P (kPa) is the pressure, R is the ideal gas constant (8.314x10^{-3} m^3.kPa/mol/K).

Viscosity

The equation for the vapour viscosity is calculated using the following equation:

$$\mu_{v,i} = \frac{b_1 T_g^{\,b_2}}{1 + \frac{b_3}{T_g}} \qquad 3.107$$

where μ_v (Pa.s) is the vapour viscosity of component i; and b_1, b_2 and b_3 are parameters which values are given in Table 3.7.

Table 3.7: Parameters for vapour viscosity equation (Aspen, 2006)

	CO_2	H_2O	MEA	N_2
b_1	2.148x10^{-6}	1.7851x10^{-7}	2.1602x10^{-7}	6.56x10^{-7}
b_2	0.46	0.813	0.7105	0.6081
b_3	290	304.72	229.78	54.714

The viscosity of gas mixtures is calculated using the Wilke equation (Reid *et al*., 1987),

$$\mu_v = \sum_{i=1}^{n} \frac{y_i \mu_{v,i}}{\sum_{j=1}^{n} y_j A_{ij}} \qquad 3.108$$

where μ_v(Pa.s) is the viscosity of gas mixture. The correlations for A_{ij} and A_{ji} are estimated as follows (Reid *et al*., 1987):

$$A_{ij} = \frac{\left[1 + \left(\mu_{v,i}/\mu_{v,j}\right)^{1/2}\left(MW_j/MW_i\right)^{1/4}\right]^2}{\left[8\left(1 + MW_i/MW_j\right)\right]^{1/2}} \qquad 3.109$$

$$A_{ji} = \frac{\mu_{v,j}}{\mu_{v,i}}\frac{M_i}{M_j}A_{ij} \qquad 3.110$$

Diffusivity

The binary molecular diffusivity for gas phase was calculated using Fuller's equation, which is an empirical approximation to the Chapman-Enskog theory. The Fuller expression for the diffusion coefficient for components *i* and *j* is calculated using following equation (Reid et al., 1987):

$$D_{ij} = \frac{0.00143 T_g^{\,1.75}}{P_{bar}(MW)_{ij}^{1/2}\left[(\sum_v)_i^{1/3} + (\sum_v)_j^{1/3}\right]^2} \quad 3.111$$

where D_{ij} (cm^2/s) is the binary diffusion coefficient, P_{bar} (bar) is the pressure, T_g (K) is the gas temperature, MW_{ij} (g/mol) is the average molecular weights of components *i* and *j*, $(\sum_v)_i$ and $(\sum_v)_i$ are the summation of molecular diffusion volumes for each components *i* and *j*, respectively. The atomic diffusion volume values are shown in Table 3.8.

Table 3.8: Atomic diffusion volumes (Reid et al., 1987)

Atomic diffusion volumes	
C	15.9
H	2.31
O	6.11
N	4.54
Simple molecules diffusion volumes	
CO_2	26.9
H_2O	13.1
N_2	18.5

The average molecular weight of binary gas components is determined using the following equation:

$$MW_{ij} = \frac{2(MW)_i(MW)_j}{(MW)_i + (MW)_j} \quad 3.112$$

The diffusivity in the gas mixtures (D_g) is obtained using Blanc's law (Veldsink et al., 1995):

$$D_g = \frac{1}{(1 - x_i)} \sum_{j=1, i \neq j}^{n} x_j D_{ij} \qquad 3.113$$

Thermal conductivity

The vapour thermal conductivity of each component *i* is determined using the following equation (Aspen, 2006):

$$\lambda_{v,i} = \frac{b_1 {T_g}^{b_2}}{1 + \frac{b_3}{T_g} + \frac{b_4}{{T_g}^2}} \qquad 3.114$$

where $\lambda_{v,i}$ (W/m/K) is vapour thermal conductivity of component *i*. The constants in 3.113 are defined as follows:

Table 3.9: Parameters for vapour thermal conductivity equation

	CO_2	H_2O	MEA	N_2
b_1	3.69	6.93×10^{-5}	-0.0011442	0.00033143
b_2	-0.3838	1.1254	0.6373	0.7722
b_3	964	847.68	-2418.1	16.323
b_4	1860000	-150000	0	373.72

The thermal conductivity of a gas mixture is not usually a linear function of mole fraction. At low pressure, the thermal conductivity of a gas mixture is calculated using the Wassiljewa-Maxon-Saxena mixing rule equation (Reid et al., 1987):

$$\lambda_v = \sum_{i=1}^{n} \frac{y_i \lambda_{v,i}}{\sum_{j=1}^{n} y_j A_{ij}} \qquad 3.115$$

where λ_v (W/m/K) is the thermal conductivity of a gas mixture and the correlation for A_{ij} and A_{ji} are determined using following equations:

$$A_{ij} = \frac{\left[1 + \left(\lambda_i/\lambda_j\right)^{1/2}\left(MW_j/MW_i\right)^{1/4}\right]^2}{\left[8\left(1 + MW_i/MW_j\right)\right]^{1/2}} \quad 3.116$$

$$A_{ji} = \frac{\lambda_j}{\lambda_i}\frac{MW_i}{MW_j}A_{ij} \quad 3.117$$

Heat capacity

The ideal gas heat capacity is determined using following equation (Aspen, 2006):

$$C_{p,g} = b_1 + b_2T_g + b_3{T_g}^2 + b_4{T_g}^3 + b_5{T_g}^4 + b_6{T_g}^5 \quad 3.118$$

where $C_{p,g}$ (J/kmol/K) is gas heat capacity. The constants used in this equation are given in Table 3.10.

Table 3.10: Parameters for gas heat capacity equation

	CO_2	H_2O	MEA	N_2
b_1	19795.19	33738.112	13207.4	31149.792
b_2	73.436472	-7.0175634	281.577	-13.565232
b_3	-0.056019	0.0272961	-0.1513066	0.02679552
b_4	$1.72\text{x}10^{-5}$	$-1.67\ \text{x}10^{-5}$	$3.13\ \text{x}10^{-5}$	$-1.17\ \text{x}10^{-5}$
b_5	0	$4.30\text{x}10^{-9}$	0	0
b_6	0	$-4.17\text{x}10^{-13}$	0	0

3.7 Model implementation

The complete MEA absorption process model contains unit operations with variables that show temporal and spatial distributions. Thus, the complete process model is a combination of partial differential equations, ordinary differential equations, and algebraic equations (PDAEs). Several commercial dynamic simulators such as Aspen Plus Dynamics® and Aspen Custom Modeler® have been used to study this process (Ziaii et al., 2009; Lin et al., 2011). However, the Aspen Plus Dynamics® process simulator only supports equilibrium calculations for the packed column model which is not suitable for this particular process. The Aspen Custom Modeler® software is only applicable to solve a system of ordinary differential equations (ODEs) whereas the model proposed in this work involves partial differential equations (PDE). Kvamsdal and Rochelle (2008) used gPROMS software to develop a dynamic standalone absorber. Similarly, Lawal et al. (2010) also used gPROMS in developing the complete CO_2 capture process. Since the system developed in this work involved PDAEs and previous works have successfully developed the same process using gPROMS(Kvamsdal and Rochelle, 2008; Kvamsdal et al., 2009; Lawal et al. 2010), the dynamic model developed in this work was also implemented in gPROMS. Also, gPROMS is also a suitable tool to conduct controllability studies.

In gPROMS, the system of PDAE was numerically solved using the method of lines (MOL) (Schiesser, 1991). This involves the discretization of the distributed equations with respect to spatial domain, which resulted in a mixed set of time-dependent differential and non-linear algebraic equations (DAEs). This set of discretized equations was coupled with the ordinary differential equations from the lumped parameter models of other units to form one large set of differential algebraic equations (DAEs). The resulting system of DAE was integrated over time by employing a differential algebraic equation solver (DASOLV) integration code (Jarvis and Pantelides, 1992). DASOLV, based on backward differentiation, automatically adjusts the time step size as well as the integration order to maintain the error of integration within the users' specified tolerance.

In this study, standard third-order orthogonal collocation finite element method (OCFEM) with 30 number of discretization intervals was used to discretize the spatial domain of packed column and second order backward finite difference method (BFDM) with 10 discretization points was used to discretize the spatial domain of the cross heat exchanger model.

The implementation of the dynamic simulation of the MEA absorption process involves the following steps:

1. The proposed model was developed and simulated in gPROMS project which consists of group of entities i.e. VARIABLE TYPES, MODELS, PROCESSES, SAVED VARIABLE SETS and MISCELLANEOUS FILES. The mathematical equations describing the system are declared in the MODELS entity which contains parameters and variables that characterize the system. Variables which are declared need to be specified in the VARIABLE TYPES entity in order to provide upper and lower bounds as well as initial guesses which are used for initialization. These values can be over written by using data from SAVED VARIABLE SETS. The simulation activities are specified in the PROCESSES entity. The values of the various model parameters, the input stream specifications and the discretization method are specified in this entity. The PROCESS entity might have several process descriptions, each defining different simulation activities such as start-up, shut-down, etc. The input file from Multiflash™ property package, which is used to calculate the liquid activity coefficient, was imported in MISCELLANEOUS FILES.
2. The individual unit process models were developed first. During the execution of a PROCESS entity, at first gPROMS determines whether the model is well posed by checking the information regarding the mathematical model and its initial and boundary conditions. Boundaries and initial conditions are specified for partial differential equations (PDE) which describe the absorber, stripper and heat exchanger. In the buffer tank and reboiler models, there is no spatial dependence. Thus, the dynamic model led to ordinary differential equations (ODE), i.e., only initial conditions are required. The calculation for packed columns and cross heat exchanger involved two-point boundary values since the inlet conditions are given at

two opposite ends. Boundary and initial conditions required for each unit operations are summarized in Table 3.11.

Table 3.11: Boundary and initial conditions

Unit operation	Initial Condition, IC	Boundary Condition, BC
Packed column	For $0 \leq z \leq L, t = 0$ Gas phase: $C_g(z,0) = C_{g,o}(z)$ $T_g(z,0) = T_{g,o}(z)$ $u_g(z,0) = u_{g,o}(z)$	For $t \geq 0$ Gas phase: $C_g(0,t) = C_{g,initial}(t)$ $z = 0$ $T_g(0,t) = T_{g,initial}(t)$ $z = 0$ $u_g(0,t) = u_{g,initial}(t)$ $z = 0$
Packed column	Liquid phase: $C_l(z,0) = C_{l,o}(z)$ $T_l(z,0) = T_{l,o}(z)$	Liquid phase: $C_l(0,t) = C_{l,initial}(t)$ $z = L$ $T_l(0,t) = T_{l,initial}(t)$ $z = L$
Reboiler	For $t = 0$ $F(0) = F_{inlet}$, $T(0) = T_{inlet}$	
Heat exchanger	For $0 \leq x \leq L, t = 0$ $T_h(x,0) = T_{h,o}(x)$ $T_c(x,0) = T_{c,o}(x)$	For $t \geq 0$ $T_h(0,t) = T_{h,initial}(t)$ $x = 0$ $T_c(0,t) = T_{c,initial}(t)$ $x = L$
Tank	For $t = 0$ $F(0) = C_{inlet}$, $T(0) = T_{inlet}$	

3. The process operating conditions and equipment specifications for the unit operations involved need to be specified. In this study, the data reported by Dugas (2006) presented in Table 3.12 and Table 3.13 and were used for flue gas conditions and packed column specifications, respectively.

Table 3.12: Flue gas conditions (Dugas, 2006)

Temperature (K)	319.71
Molar flowrate (mol/s)	4.013
Mole fraction	
CO_2	0.175
H_2O	0.025
MEA	0
N_2	0.8

Table 3.13: Packing parameters for the absorber and stripper column (Dugas, 2006)

Packed column characteristic:	
Column internal diameter (m)	0.43
Packing height (m)	6.1
Packing type	IMTP #40
Nominal packing size (m)	0.038
Specific area (m^2/m^3)	143.9

4. At the start of each simulation, gPROMS first solves all algebraic equations simultaneously. Thus, initial values of all variables declared in the model must be given. There are two methods for providing initial values to the model (Moe et al., 1995):
    - The simple method is to select heuristic initial values for the dependent state variables and solve for the algebraic equations. The DAE's are then simulated until steady state is reached.
    - Another method for providing the initial values is to set the derivative equations equal to zero (assume steady state initial condition) and solve for the algebraic equations. In order to achieve the solution of algebraic equations

at steady state, the initial values for variables in algebraic equations must be closed to the steady state value.

In this work both approaches were applied. The individual process model was first simulated by specifying the state variables using pilot plant data (Dugas, 2006) until steady state was reached. The steady state results obtained from each unit were used as initial value to start the simulation at steady state using the second approach. Then, the steady state results from these units were used as initial value for the complete process model. By using the steady state data from individual process model as initial value, the initialization of the complete model successfully led to convergence.

5. Once the simulation program was able to produce steady state data, then the developed complete process model is ready to be used for dynamic simulation. The initial conditions for each of the state variables must be specified either by setting the derivative equations equal to zero (steady state initial condition) or specifying the state variable with certain value.

3.8 Chapter summary

This chapter has presented the mechanistic mathematical equations used to develop the complete MEA absorption process model. The mathematical models of the packed columns (absorber and stripper columns) were formulated as PDAEs. This model is characterized by highly non-linear equations which required educated initial guesses for the initialization procedure in gPROMS. The model implementation at steady state and dynamic conditions has also been discussed. The results obtained from this model will be discussed in the next chapter.

Chapter 4
Steady-state and dynamic simulations

The process model described in Chapter 3 can be simulated at steady state and in the time domain (dynamic simulations). This chapter presents the steady-state and the dynamic simulation results of the MEA process model presented in the previous Chapter. This chapter is organized as follows: Section 4.1 describes the model validation approach used in the present analysis. Section 4.2 describes the model development in Aspen Plus® software for model validation. The steady state results of standalone absorber and stripper models for model validation with Aspen Plus® simulation are presented in Sections 4.3 and 4.4, respectively. Section 4.5 presents the results of the heat exchanger model at steady state while Section 4.6 presents the dynamic results of the tank model. The analysis of dynamic behaviour of the complete process model is presented in Section 4.7. A summary of this chapter is provided in last section.

4.1 Introduction

Because plant data for dynamic operation of a MEA process was not readily available, it was only possible to validate the steady-state results of the dynamic model presented in this thesis. The dynamic model implemented in this study was validated at steady-state through comparison to results of an Aspen Plus® model and to steady-state data reported by Dugas (2006) for a MEA absorption pilot plant. Aspen Plus® software has been widely used for modelling the MEA absorption process at steady state (Desideri and Paolucci, 1999; Freguia and Rochelle, 2003; Alie et al., 2005). This software includes a property method that is based on electrolyte-non-random two-liquid (eNRTL) equilibrium model for the CO_2-H_2O-MEA system that calculates the key chemistry and thermodynamic properties of this system. A rigorous rate-based column model is also available in Aspen Plus®. Therefore, Aspen Plus® was selected for model validation at steady-state conditions.

The base case process operating conditions obtained from the pilot plant process data (Dugas, 2006) was used as the input data for the models implemented in gPROMS and Aspen Plus®.

Data that describes the transient behaviour of the pilot plant is not currently available in the open literature. Therefore, it is not possible to validate the present process model in a dynamic fashion. Several authors have used the steady-state data available from this pilot plant to validate their dynamics models. Kvamsdal et al. (2009) validated a standalone dynamic absorber model in terms of the liquid temperature profile and the percentage of CO_2 removal using the steady-state data from this pilot plant. Likewise, Lawal et al. (2010) also used the same approach to validate their gPROMS dynamic model, i.e., the model proposed by Lawal et al. (2010) was validated against the steady-state liquid temperature profile provided by Dugas (2006).

To study the effect of the power plants operating conditions on the CO_2 capture process, the proposed dynamic model was used to simulate the transient behaviour of the MEA absorption plant in response to changes in the flue gas flow rate and reboiler heat duty. Ramp, step and sinusoidal input tests were implemented in key process variables, i.e., the flue gas flow rate and the reboiler's heat duty, to study the transient response that may occur in a real process plant due to changes in these process variables.

4.2 Model development in Aspen Plus®

The absorber and stripper columns were modeled using RadFrac column model in Aspen Plus®. The Aspen Plus® provides the options to model the columns either using equilibrium or rate-based approached. For the absorber and stripper columns the RadFrac model with rate-based calculation was used. RadFrac allows the user to discretize the liquid and gas films and incorporate kinetic reactions within the segments of each film. The options for film resistance are *NoFilm*, *Film*, *Filmrxn* and *Disrxn*. The *Nofilm* method assumes no liquid film. The *Film* method considers diffusion resistance but no reactions in the film while *Filmrxn* considers both the film resistance and reactions. In order to consider film discretization with reactions, the *Discrxn* method can be chosen. In this study, *Film* and *Filmrxn* were selected for gas and liquid phase, respectively. The diffusion resistance was considered on both phases but the reaction occurred only in the liquid phase. This is because

in the gPROMS model, the reaction is assumed to occur in the liquid film using the enhancement factor approach.

There are several electrolyte-based physical property models provided by Aspen Plus® such as *emea, kemea, mea* and *kmea* that specify the property method and solution chemistry for processes containing CO_2, H_2O and MEA. These property packages inserts use electrolyte-NRTL method to calculate the fluid transport and thermodynamic properties. Electrolyte-NRTL is an activity coefficient model-based property method that uses electrolyte NRTL model for the liquid phase and Redlich-Kwong EOS for the vapour phase. In this work, *emea* property insert was selected in modeling the MEA absorption process in Aspen Plus®. *Emea* property insert is applicable for the systems containing CO_2-H_2S-H_2O-MEA with temperature up to 120^oC and MEA concentrations up to 50%. It assumes that the reaction is at equilibrium.

Following is a description of each Aspen Plus® Unit Operation Block in the simulation

Absorber: RadFrac Block, no condenser or reboiler, 6 stages, Stage 1 pressure 101.325 kPa, Column pressure drop 2.5 kPa.

Stripper: RadFrac Block, no condenser or reboiler, 5 stages, Stage 1 pressure 170 kPa, Column pressure drop 0.25 kPa.

Reboiler: Flash2 Block, Heat duty 155kW, Pressure 160 kPa

The following sections describe in detail the Aspen results and compare them to those obtained from the model developed in gPROMS.

4.3 Absorber column model analysis

The flue gas and lean MEA information for the standalone absorber model (see Figure 4.1) obtained from Dugas (2006) were defined as boundary conditions for this system (see Table 4.1). These operating conditions were selected as the base case in this study.

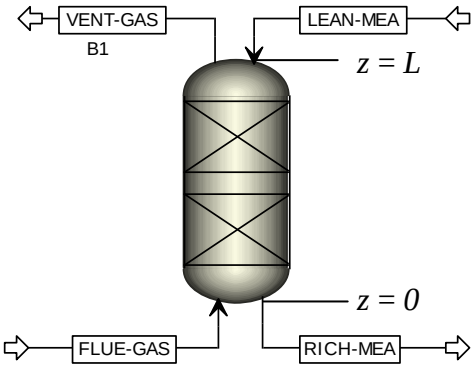

Figure 4.1: Absorber standalone model

Table 4.1: Boundary conditions for absorber (absorber base case conditions)

Boundary condition For $t \geq 0$		
	Flue gas ($z = 0$)	Lean MEA ($z = L$)
Molar flow rate (mol/sec)		
CO_2	0.70	0.92
H_2O	0.10	26.97
MEA	0	3.31
N_2	3.21	0
Mole fraction		
CO_2	0.175	0.029
H_2O	0.025	0.86
MEA	0	0.11
N_2	0.8	0
Total molar flow rate (mol/sec)	4.013	31.19
Temperature (K)	319.7	314

At the start of the simulation, gPROMS performs an initialisation procedure to obtain the solution of the algebraic equations for the unknown dependent variables using initial guesses. Specifying arbitrary initial guesses for these unknown variables might work well for systems in which there is not a high degree of non-linearity. However, the column model developed

in this work is described by highly non-linear equations, as presented in Chapter 3. Nonlinearity arises from equations describing equilibrium relations and physical properties. Consequently, setting arbitrary initial guesses for the unknown variables will cause a failure at the start of simulation. Therefore, educated initial guesses must be provided to assist in the initialisation step. In this work, the initial solution was achieved by implementing the following steps:

1. Simplify the column model equation by setting the mass transfer term in material balance equations as a constant value and assume constant temperature. The mass transfer term was assumed constant because it involved many non-linear algebraic equations, i.e. equilibrium model and physical properties.
2. The state variables, i.e., the initial value of the component's concentrations and temperature were obtained from the pilot plant data (Dugas, 2006) and the column model was simulated dynamically until it reached steady-state. This allows the determination of feasible initial conditions for the components material balance, physical properties and equilibrium equations.
3. Next, the mass transfer term is incorporated in the material balance equations that provide another initial solution for the components material balance but at constant temperature. Once the process model converged, then the energy balance equations were incorporated in the process model to give the final initial solutions to the process model.

The packed column model was simulated using steady-state initial conditions by setting the derivative equations equal to zero, as shown in Table 4.2. The results from the steady state simulation were compared with the results from the Aspen Plus® simulation. For the dynamic simulations, the process model was initialized using these steady-state results as a base case operating conditions.

Table 4.2: Initial conditions for absorber

Initial conditions For $0 \leq z \leq L, t = 0$	
Gas phase: $\frac{dC_{g,i}}{dt} = 0$ $\frac{dT_g}{dt} = 0$ $\frac{du_g}{dt} = 0$	Liquid phase: $\frac{dC_{l,i}}{dt} = 0$ $\frac{dT_l}{dt} = 0$

Table 4.3 displays the comparison between plant data and simulation results for CO_2 loading in liquid stream at the bottom of the absorber column and the percentage of CO_2 absorbed in the column. The amount of CO_2 transferred from the gas to the liquid phase obtained from the gPROMS model was higher than that of the pilot plant data, resulting in higher simulated CO_2 loading in the liquid stream coming from the absorber. This is because the flue gas flow rate entering the absorber column in the gPROMS model was chosen to be slightly lower than that for the pilot plant data, in order to minimize the differences between the simulated and pilot plant data temperature profiles, as shown in Figure 4.2. As can be seen from this Figure, the adjusted flue gas flow rate gave a better liquid temperature profile (see solid line) than when using the actual flow rate from pilot plant (see dotted line). It also shows that the simulation results slightly under predicted the pilot plant data at the top of the column.

Table 4.3: Comparison with pilot plant data (Dugas, 2006)

	Pilot plant	gPROMS model
Flue gas flow rate (mol/s)	4.25	4.013
Rich loading (mol CO_2/mol MEA)	0.43	0.49
CO_2 absorbed (%)	95	97

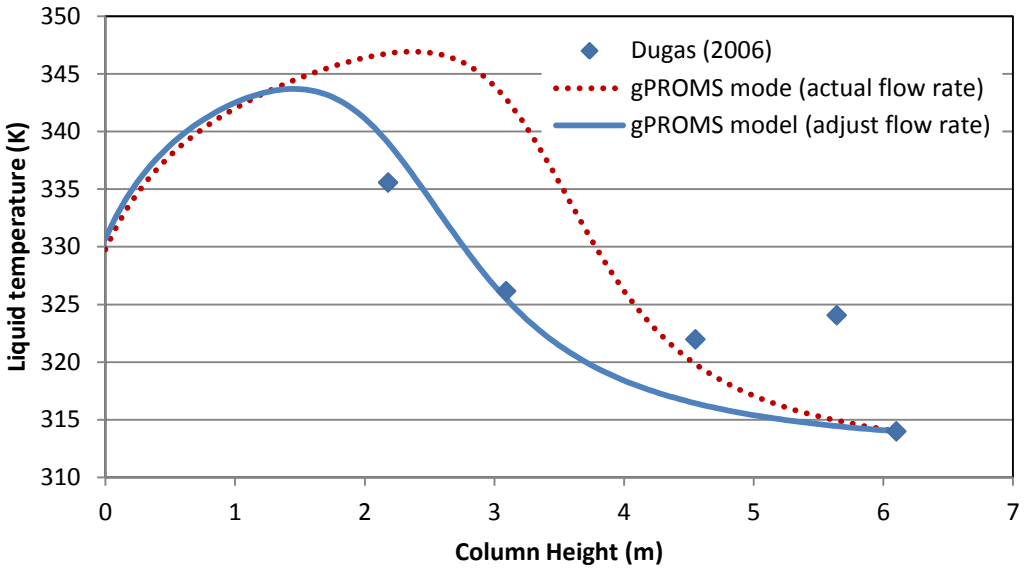

Figure 4.2: A comparison liquid temperature profile with pilot plant data

The standalone absorber was further validated using an Aspen Plus® model. Table 4.4 shows a comparison between the results obtained with the present dynamic model implemented in gPROMS, referred to as the gPROMS model, and the Aspen Plus® simulation for the standalone absorber at base case operating conditions. As shown in Table 4.4, the results obtained with the gPROMS model are in reasonable agreement with those obtained from the Aspen Plus® steady-state simulation. The vent gas contains all N_2 gas in the flue gas and a small amount of CO_2 and H_2O. N_2 is considered as inert and not being transferred to the liquid phase. 97% of CO_2 was absorbed in the absorber column. Note that the amount of water released at the top of absorber using the gPROMS model is less than that reported by the Aspen Plus® model. This is because heat losses were taken into account in the gPROMS model, which lowers the gas temperature at the top of the absorber. In the Aspen Plus® model, the clean gas exits at a higher temperature at the top of the absorber, which produces a water flow rate higher than that obtained in the gPROMS model. Overall, the percent difference between gPROMS and Aspen Plus® was less than 10% for the gas phase (except for water) and 2% for the liquid phase. The N_2 mole fraction was determined from the

knowledge of all other component mole fractions. The N_2 mole fraction difference between the gPROMS model and Aspen Plus® arises thus from the mole fraction difference in water.

Table 4.4: Comparison between gPROMS and Aspen Plus® result at base case condition for absorber

	Vent gas ($z = L$)		Rich MEA ($z = 0$)	
	gPROMS	Aspen Plus®	gPROMS	Aspen Plus®
Molar flow rate (mol/sec)				
CO_2	0.021	0.020	1.601	1.602
H_2O	0.224	0.624	26.844	26.443
MEA	0	0	3.295	3.305
N_2	3.210	3.202	0	0
Mole Frac				
CO_2	0.006	0.005	0.050	0.051
H_2O	0.065	0.162	0.846	0.843
MEA	0	0	0.104	0.105
N_2	0.929	0.833	0	0
Total molar flow rate (mol/sec)	3.455	3.846	31.739	31.359
Temperature (K)	314.1	332.8	328.7	327.1

In order to validate the model at different operating conditions, two steady-state analyses were conducted by increasing and decreasing the flue gas flow rate by 5%. The new steady-state results obtained from gPROMS were compared with Aspen Plus® simulation and (see Table 4.5). The results obtained from gPROMS at the new steady state condition were similar to those obtained from the Aspen Plus® simulation. As in the previous simulation results, the main difference observed here is the molar flow rate of water in the vent gas, which is due to the fact that the heat loss is taken into account in the gPROMS model, but not in the Aspen Plus® model. Overall, the percent differences between the gPROMS model and Aspen Plus® were similar at the base case operating conditions.

Table 4.5: Result comparison between gPROMS and Aspen Plus® at steady state for absorber

	+5% in flue gas flow rate				-5% in flue gas flow rate			
	Vent gas		Rich MEA		Vent gas		Rich MEA	
	gPROMS	Aspen Plus®	gPROMS	Aspen Plus®	gPROMS	Aspen Plus®	gPROMS	Aspen Plus®
Molar flow rate (mol/sec)								
CO_2	0.045	0.045	1.612	1.612	0.013	0.013	1.574	1.585
H_2O	0.240	0.706	26.832	26.366	0.211	0.486	26.851	26.576
MEA	0	0	3.287	3.305	0	0	3.298	3.305
N_2	3.371	3.362	0	0.008	3.050	3.042	0	0.008
Mole fraction								
CO_2	0.012	0.011	0.051	0.052	0.004	0.004	0.050	0.050
H_2O	0.066	0.172	0.846	0.843	0.064	0.138	0.846	0.844
MEA	0	0	0.104	0.106	0	0	0.104	0.105
N_2	0.922	0.817	0	0	0.932	0.861	0	0
Total molar flow rate (mol/sec)	3.655	4.114	31.732	31.292	3.273	3.531	31.724	31.473
Temperature (K)	314.4	333.8	327.8	325.9	313.9	330	328.6	328.9

4.4 Stripper column model analysis

In the stripper unit, CO_2 is stripped from the aqueous MEA solution. The stripper model is comprised of a packed column model and a flash model for the reboiler. The packed column of the stripper model has been developed using the same principles as for the absorber model. Thus, it required similar input conditions to those considered for the absorber. The initial conditions for the packed column of the stripper (see Figure 4.3) is similar to those of the absorber, as shown in Table 4.2. Table 4.6 shows the boundary conditions for the standalone stripper column. The rich stream conditions from the absorber provide the boundary conditions for the stripping column at the top. However, the temperature from the absorber was increased to 350 K as shown in Table 4.6 to facilitate the CO_2 transfer from the liquid to

the gas phase, hence reducing the reboiler heat duty. On the other hand, the reboiler vapour output provides the boundary conditions for the stripping column at the bottom.

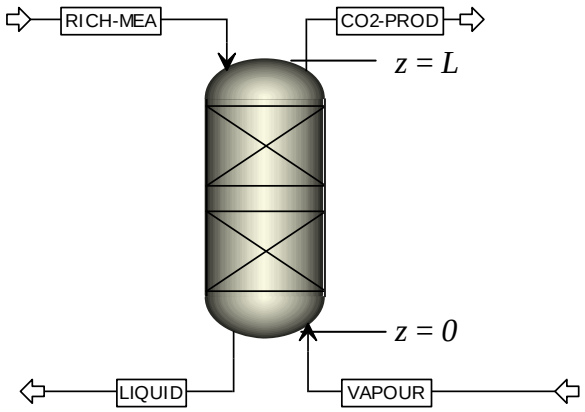

Figure 4.3: Stripper standalone model

Table 4.6: Boundary condition for stripper (stripper base case conditions)

Boundary condition For $t \geq 0$		
	Vapour at the bottom ($z = 0$)	Rich MEA ($z = L$)
Molar flow rate (mol/sec)		
CO_2	0.195	1.601
H_2O	3.230	26.844
MEA	0.008	3.295
Mole fraction		
CO_2	0.057	0.050
H_2O	0.941	0.846
MEA	0.002	0.104
Total molar flow rate (mol/sec)	3.433	31.739
Temperature (K)	389.0	350.6

Table 4.7 shows a comparison between the results obtained with the gPROMS model to those obtained with the Aspen Plus® simulation for the standalone stripper at the base case conditions. The results obtained using the gPROMS model closely matches the steady-state simulation results computed from the Aspen Plus® simulation. The stripper column overhead mainly contains CO_2 product that have to be treated further for the final purification before being sent for storage. This gas stream can be concentrated more when most of the water is condensed. The overall percent difference between gPROMS and Aspen Plus® was less than 10% for the gas phase and 3% for the liquid phase.

Table 4.7: Comparison between gPROMS and Aspen Plus® result at base case condition for stripper

	CO_2 product ($z = L$)		Liquid at the bottom($z = 0$)	
	gPROMS	Aspen Plus®	gPROMS	Aspen Plus®
Molar flow rate (mol/sec)				
CO_2	0.693	0.673	1.103	1.122
H_2O	0.222	0.239	29.852	29.835
MEA	0.001	0	3.302	3.303
Mole fraction				
CO_2	0.757	0.738	0.032	0.033
H_2O	0.243	0.262	0.871	0.871
MEA	0.001	0	0.096	0.096
Total molar flow rate (mol/sec)	0.915	0.912	34.257	34.260
Temperature (K)	352.1	352.6	379.6	383.4

Steady state simulations at different operating conditions were performed by making a 10% change in the vapour flow rate entering the bottom of stripper column to represent the effect of reboiler heat duty changes. On average, the relative error in predicting the component composition, total molar flow rate and temperature between gPROMS and Aspen Plus® simulations was less than 10%.

Table 4.8: Results comparison between gPROMS and Aspen Plus® at steady-state for stripper

	+10% in vapour flow rate at the bottom				-10% in vapour flow rate at the bottom			
	CO_2 product		Liquid at the bottom		CO_2 product		Liquid at the bottom	
	gPROMS	Aspen Plus®	gPROMS	Aspen Plus®	gPROMS	Aspen Plus®	gPROMS	Aspen Plus®
Molar flow rate (mol/sec)								
CO_2	0.783	0.785	1.032	1.030	0.607	0.571	1.169	1.205
H_2O	0.250	0.280	30.147	30.117	0.195	0.201	29.556	29.550
MEA	0.001	0.000	3.303	3.304	0.001	0.000	3.302	3.302
Mole fraction								
CO_2	0.757	0.737	0.030	0.030	0.756	0.739	0.034	0.035
H_2O	0.242	0.263	0.874	0.874	0.243	0.261	0.869	0.868
MEA	0.001	0.000	0.096	0.096	0.001	0.000	0.097	0.097
Total molar flow rate (mol/sec)	1.034	1.065	34.482	34.451	0.803	0.772	34.026	34.057
Temperature (K)	352.1	351.2	381.6	384.7	352.0	351.8	377.4	381.7

The inlet information for the reboiler model (Figure 4.4) was obtained from the liquid outlet stream at the bottom of the stripper. The vapour output from the reboiler provides the inlet boundary conditions for the stripping column at the bottom while the liquid stream is passed through the heat exchanger.

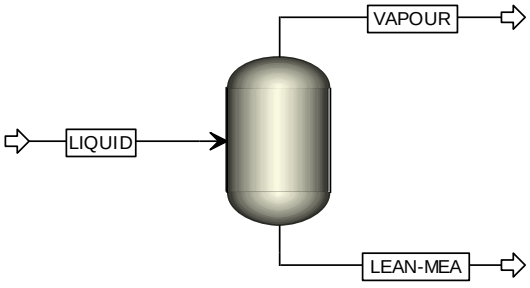

Figure 4.4: Reboiler standalone model

The steady-state initial conditions for this unit were obtained by setting the derivative equations, i.e. material and energy balance equations, equal to zero. These steady-state values are used as initial guess and verified against the Aspen Plus® simulation. The dynamic simulation was initialized using these values. As shown in Table 4.9, the amount of water vaporized was much higher than that of MEA because MEA has a lower vapour pressure. This relation can be seen from the vapour-liquid equilibrium equation (K_{value}) mentioned in Chapter 3. The K_{value} has a strong correlation with the reboiler temperature and component compositions in the inlet stream. The accuracy of the results obtained in this study compared to Aspen Plus® simulation rely on the K_{value}. Two case studies were conducted to study in detail the effect of K_{value} on the results obtained using the gPROMS model. In this analysis, the K_{value} reported from Aspen Plus® was used a constant parameter in gPROMS model. The reboiler heat duty and pressure similar to gPROMS model was specified in the Aspen Plus® simulation. As shown in Table 4.9, the mole fraction and molar flow rate obtained from gPROMS and Aspen Plus models are the same, except the temperature that was slightly different (3% change). The temperature difference might be due to the different approaches used in Aspen Plus and in the gPROMS model to estimate the enthalpy. As shown in Table 4.10, similar results were obtained at different heat duty and inlet conditions.

Table 4.9: Result comparison between gPROMS and Aspen Plus® at steady state for reboiler model

	Inlet stream	Outlet stream			
		Vapor		Lean MEA	
		gPROMS	Aspen Plus®	gPROMS	Aspen Plus®
Molar flow rate (mol/sec)					
CO_2	1.468	0.267	0.267	1.20	1.20
H_2O	27.03	1.096	1.096	25.934	25.934
MEA	3.416	0.002	0.002	3.414	3.414
Mole fraction					
CO_2	0.046	0.196	0.196	0.039	0.039

Table 4.9: Result comparison between gPROMS and Aspen Plus® at steady state for reboiler model (continues)

	Inlet stream	Outlet stream			
		Vapor		Lean MEA	
		gPROMS	Aspen Plus®	gPROMS	Aspen Plus®
H_2O	0.847	0.803	0.803	0.849	0.849
MEA	0.107	0.001	0.001	0.112	0.112
Total molar flow rate (mol/sec)	31.914	1.365	1.365	30.548	30.548
Temperature (K)	368.68	392.18	384.24	392.18	384.24

Table 4.10: Result comparison between gPROMS and Aspen Plus® at steady state for reboiler model at different inlet conditions

	Inlet stream	Outlet stream			
	Liquid	gPROMS	Aspen Plus®	gPROMS	Aspen Plus®
Molar flow rate (mol/sec)					
CO_2	1.263	0.280	0.280	0.983	0.983
H_2O	27.696	2.806	2.806	24.89	24.89
MEA	3.436	0.007	0.007	3.429	3.429
Mole fraction					
CO_2	0.039	0.091	0.091	0.034	0.034
H_2O	0.855	0.907	0.907	0.849	0.849
MEA	0.106	0.002	0.002	0.117	0.117
Total molar flow rate (mol/sec)	32.395	3.093	3.093	29.302	29.302
Temperature (K)	381.6	398.3	388.1	398.3	388.1
Heat duty (W)	155000				

The equation used to determine the K_{value}, (see section 3.3.1 in Chapter 3), gives different results than in the Aspen Plus® simulation. The molar flow rate and component compositions in the vapour and liquid phase obtained from gPROMS model have large deviations compared to Aspen Plus® simulation due to K_{value} difference. As mention above, the results obtained from the gPROMS model were similar to Aspen Plus® when using the same K_{value} as in Aspen Plus®. Therefore, multiple linear regression models were developed to correlate the K_{value} of CO_2, H_2O and MEA as a function of temperature and mole fractions using SPSS software. Several steady state simulations at different inlet conditions i.e. flow rate, component compositions and reboiler heat duty were conducted using the flash model in Aspen Plus® to obtain a suitable range of temperatures and compositions for this correlation. Based on this analysis, the K_{value} correlation was developed for temperature range from 385 to 390 K. The mole fraction of CO_2, H_2O and MEA were varied from 0.03 to 0.05 mol/mol, 0.83 to 0.89 mol/mol and 0.08 to 0.12 mol/mol, respectively. The K_{value} data at various temperatures and component compositions were generated using the flash model in Aspen Plus®. Two third of these data were used for regression analysis while the rest was used for validation. The K_{value} of each component was set as dependent variable while the temperature and mole fraction of each component were set as independent variables. The interaction terms between the independent variables were also included in the multiple linear regression analysis. The K_{value} regression models for each component are summarized in Table 4.11.

Table 4.11: K_{value} regression model

Component	Temperature range	K_{value} correlation
CO_2	385≤T≤ 387 K	$ln\,K_{CO_2} = 385.738 - 64.494lnT - 5.026x_{CO_2} - 0.006Tx_{mea} + 0.129Tx_{CO_2}x_{mea}$
	387 <T≤ 388 K	$ln\,K_{CO_2} = 490.131 - 82.103lnT + 2.562x_{CO_2} + 1.597x_{mea} + 0.022Tx_{CO_2}x_{mea}$
	388 <T≤ 389 K	$ln\,K_{CO_2} = 531.525 - 89.121lnT + 10.441x_{CO_2} + 4.158x_{mea} - 0.062Tx_{CO_2}x_{mea}$

Table 4.11: K_{value} regression model (continues)

Component	Temperature range	K_{value} correlation
CO_2	389 <T≤ 390 K	$ln\ K_{CO_2} = 505.895 - 84.832lnT + 12.072x_{CO_2} + 0.006Tx_{mea} + 0.046Tx_{CO_2}x_{mea}$
H_2O	385≤T≤ 390 K	$K_{H_2O} = -71.927 + 0.34x_{CO_2} + 0.265x_{H_2O} + 12.203lnT$
MEA	385≤T≤ 387 K	$ln\ K_{MEA} = -315.592 + 52.289lnT - 3.471x_{CO_2} - 0.003Tx_{mea} + 0.112Tx_{CO_2}x_{mea}$
	387 <T≤ 389 K	$ln\ K_{MEA} = -341.477 + 56.65lnT - 4.008x_{CO_2} - 1.762x_{mea} + 0.098Tx_{CO_2}x_{mea}$
	389 <T≤ 390 K	$ln\ K_{MEA} = -339.542 + 56.331lnT - 3.901x_{CO_2} - 0.003Tx_{mea} + 0.026Tx_{CO_2}x_{mea}$

The K_{value} correlation for CO_2 at temperatures between 385 and 387 K was obtained using 318 data for temperatures every 0.2 K because K_{value} is strongly dependent on temperature. The statistical analysis for this particular regression model is presented in Table 4.12. The regression analyses for other correlations are presented in Appendix C. The significance of the regression model developed in this study can be determined from the p-value of the F-test. As shown in Table 4.12, the p-values are zero to three decimal places which indicate that the regression model used in the present analysis is statistically significant. The R^2 obtained from the regression analysis shows 99% of the variability of K_{value} for CO_2 is accounted for by the independent variables in the regression model. The standardized coefficient shows the relative importance of each independent variable in predicting the dependent variable. For this correlation model, lnT has the largest standardized coefficient. Thus, lnT was the most significant variable that will affect the K_{value} compared to mole fraction of CO_2 and interaction between temperature and mole fraction. The K_{value} correlation model was validated using the validation data extracted from the set of data generated from

the Aspen Plus® model, as shown in Appendix C. As shown in Table C.8 – C.10, the percent differences between the predicted and actual value were less than 5%.

Table 4.12: SPSS output for the K_{value} correlation of CO_2 for temperature 385≤T≤ 387 K

Model summary

R	R^2	Adjusted R^2	Std. Error of the Estimate
.991[a]	.982	.982	.0144755

Analysis of Variance (ANOVA)

	Sum of Squares	df	Mean Square	F	Sig. (p-value)
Regression	1.660	4	.415	1.981E3	.000
Residual	.030	143	.000		
Total	1.690	147			

Coefficient analysis

	Unstandardized Coefficients		Standardized Coefficients	F test	p-value
	B	Std. Error	Beta		
Constant	385.738	4.348		88.717	.000
lnT	-64.494	.731	-.988	-88.225	.000
x_{CO_2}	-5.026	1.663	-.316	-3.023	.003
Tx_{mea}	-.006	.002	-.237	-3.057	.003
$Tx_{CO_2}x_{mea}$	.129	.046	.418	2.787	.006

These correlations were implemented in the reboiler model to determine the K_{value} to calculate the component composition in the liquid and vapour phases. The inlet operating conditions applied in the reboiler model are shown in Table 4.10. Table 4.13 shows the results obtained using the K_{value} calculated from regression model. As shown in Table 4.13, the composition in the vapour phase was different from the Aspen Plus® simulation, while the liquid compositions are within 3% of those calculated from the Aspen Plus® simulation. The difference in the vapour composition obtained from gPROMS model was due to temperature difference obtained from these two simulations. Because K_{value} is strongly

dependent on temperature, a small difference in temperature will result in a different estimate for K_{value}. To confirm the accuracy of the regression model, the K_{value} was calculated using regression model at Aspen Plus® temperature. As depicted in Table 4.14, the K_{value} calculated at the same temperature gave close results (less than 0.8% difference) to those from the Aspen Plus® simulation. Therefore, similar results in component compositions were obtained, as shown in Table 4.9 and Table 4.10. Thus, the vapour composition obtained from the reboiler model in this study will give different estimates from Aspen Plus® simulation i.e. 20% in CO_2 and 2% in H_2O (the amount of MEA was very small, so the difference is negligible in this study).

Table 4.13: Result comparison between gPROMS and Aspen Plus® at steady state for reboiler using regression model for K_{value}

	Inlet stream	Outlet stream			
	Liquid	gPROMS	Aspen Plus®	gPROMS	Aspen Plus®
Molar flow rate (mol/sec)					
CO_2	1.263	0.267	0.280	0.997	0.983
H_2O	27.696	3.391	2.805	24.307	24.891
MEA	3.436	0.010	0.007	3.424	3.429
Mole fraction					
CO_2	0.039	0.073	0.091	0.035	0.034
H_2O	0.855	0.925	0.907	0.846	0.849
MEA	0.106	0.003	0.002	0.119	0.117
Total molar flow rate (mol/sec)	32.395	3.667	3.092	28.728	29.303
Temperature (K)	381.59	389.20	388.13	389.20	388.13
Heat duty (W)	155000				

Table 4.14: K_{value} comparison between Aspen Plus® and gPROMS

	Aspen Plus®	gPROMS	
Component	T=388.13 K	T=389.20 K	T=388.13 K
CO_2	2.701	2.097	2.702
H_2O	1.068	1.093	1.059
MEA	0.019	0.022	0.019

As shown in Figure 4.5, the packed column and reboiler models were integrated to complete the stripper column model. As shown in Table 4.15, the gPROMS steady-state results at the outlet stream of the stripper column were compared with the results from Aspen Plus®. The results presented in Table 4.15 shows that the gPROMS model reported results are less than 10% difference of those obtained with Aspen Plus®. The amount of CO_2 released at the top of the stripper was slightly higher than in Aspen Plus® because the reboiler temperature calculated using gPROMS model, which is 389.0 K, was higher than in Aspen Plus® (387.6 K). This modest temperature difference in the reboiler model (1.4 K) is still sufficient to cause the vapour compositions entering the bottom of column stripper to be different from those obtained with Aspen Plus®. This is particularly notable for CO_2 because of its K_{value} is strongly dependent on temperature. A higher temperature in the reboiler will cause more CO_2 released at the top of stripper (here ~10% more in gPROMS than in Aspen Plus).

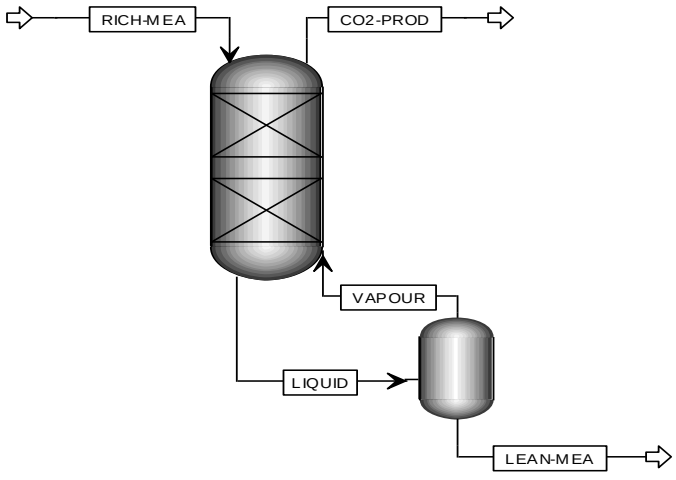

Figure 4.5: Complete stripper model

Table 4.15: Result comparison between gPROMS and Aspen Plus® at steady state for complete stripper

	Rich-MEA	CO_2-PROD		Lean-MEA	
		gPROMS	Aspen Plus®	gPROMS	Aspen Plus®
Molar flow rate (mol/sec)					
CO_2	1.601	0.693	0.626	0.908	0.961
H_2O	26.844	0.222	0.227	26.622	26.624
MEA	3.295	0.001	0	3.294	3.301
Mole fraction					
CO_2	0.050	0.757	0.734	0.029	0.031
H_2O	0.846	0.243	0.266	0.864	0.862
MEA	0.104	0.001	0	0.107	0.107
Total molar flow rate (mol/sec)	31.739	0.915	0.853	30.824	30.886
Temperature (K)	350.6	352.1	352.4	389.0	387.6

4.5 Heat exchanger model analysis

A one dimensional dynamic heat exchanger model with heat exchange between hot and cold streams was developed. Initial conditions at steady state are given by specifying derivatives of all states variables, i.e. energy balance for each stream and wall, equal to zero. The rich stream coming from the bottom of the absorber is preheated before entering the stripper while the lean loading stream exiting the reboiler must be cooled before entering the absorber. The boundary condition on the shell side is provided by the liquid stream temperature from the absorber while the condition on the tube side is provided by the hot liquid stream temperature from the reboiler unit. The inlet conditions entering the heat exchanger for the tube and shell side are shown in Table 4.16.

Table 4.16: Inlet conditions for heat exchanger

	Tube side ($z = 0$)	Shell side ($z = L$)
Total molar flow rate (mol/s)	30.824	31.740
Temperature (K)	389.0	328.7
Pressure (kPa)	160	103

The length and number of tubes were determined such that the temperature of liquid stream entering the stripper was about 80^{o}C (Lawal et al., 2010). The shell diameter was calculated using the preferred tube length to shell diameter ratio which is in the range 5 to 10 (Edwards, 2008). The overall heat transfer coefficient was approximated by considering water/water in tube and outside tube of heat exchanger with no phase change (Carl, 2005). The heat exchangers are assumed to be made of stainless steel on the tube side (Dugas, 2006). The metal density and specific heat capacity of 304 stainless steel was obtained from Geankoplis (2003). The common size of ¾ inch outside diameter was applied in this study (Edwards, 2008). The wall thickness was defined by the Birmingham Wire Gage (BWG) number 14 which is given in Geankoplis (2003). The geometrical and physical parameters of the heat exchanger are summarized in Table 4.17.

Table 4.17: Geometrical and physical parameters of the heat exchanger

Properties		Source
Heat Exchanger:		
Tube metal density, ρ_{wall}	7817 kg/m^3	Geankoplis (2003)
Tube metal specific heat capacity, $C_{p,wall}$	461 J/kg/K	Geankoplis(2003)
Tube inner diameter, $d_{i,Tube}$	0.01483 m	Geankoplis(2003)
Tube outer diameter, $d_{o,Tube}$	0.01905 m	Geankoplis(2003)
Tube heat transfer coefficient, U_{Tube}	850 W/m^2/K	Carl (2005)
Shell heat transfer coefficient, U_{Shell}	850 W/m^2/K	Carl (2005)
Number of tubes, n_{Tube}	12	
Tube length, L_{hx}	1 m	

Figure 4.6 displays the temperature profile of both liquid solutions in shell and tube sides at steady-state. As a rich loading solution (shell side) passes through the heat exchanger, the temperature increased to 350.6 K due to heat transfer from the hot solution in tubes.

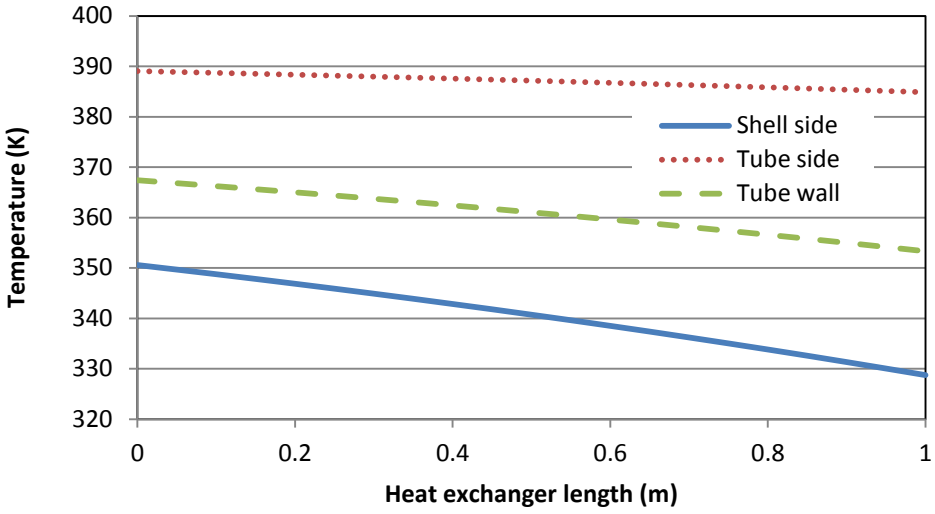

Figure 4.6: Liquid temperature profile in shell and tube side of heat exchanger

The energy flux per unit length shown in Figure 4.7 represents the energy transferred from the fluid in shell and tube to the metal wall of the tube. The amount of heat transferred was slightly increased as the hot fluid flows toward the exit of heat exchanger due to the large temperature difference between both fluids.

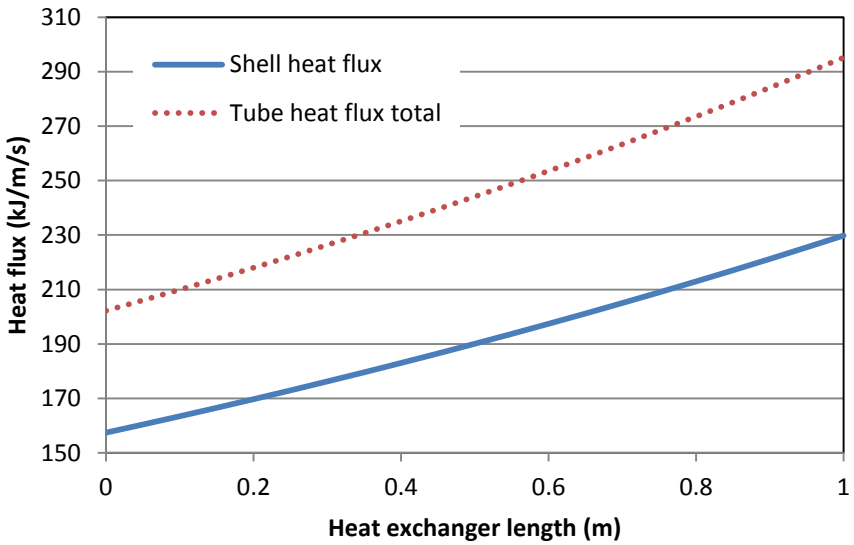

Figure 4.7: Energy flux for shell and tube side of heat exchanger

4.6 Tank model analysis

The buffer tank model developed in this study consists of a single stream inlet coming from the heat exchanger and one outlet stream sent to the top of absorber. This lean solvent storage tank holds the majority of the liquid inventory. Thus, this will minimize any unsteady-state disruption from the stripper. The present analysis assumes that the tank operates at isothermal conditions. A step test in the liquid flow rate entering the tank was introduced to the process model to ensure that the model was able to reach new steady state conditions. Figure 4.8 and Figure 4.9 show the response of outlet liquid molar flow rate and liquid volume to a sudden change in the inlet flow rate. As shown in the Figures, the process response follows the behaviour of a first order process. The outlet flow rate was able to reach new steady-state conditions after 7 minutes.

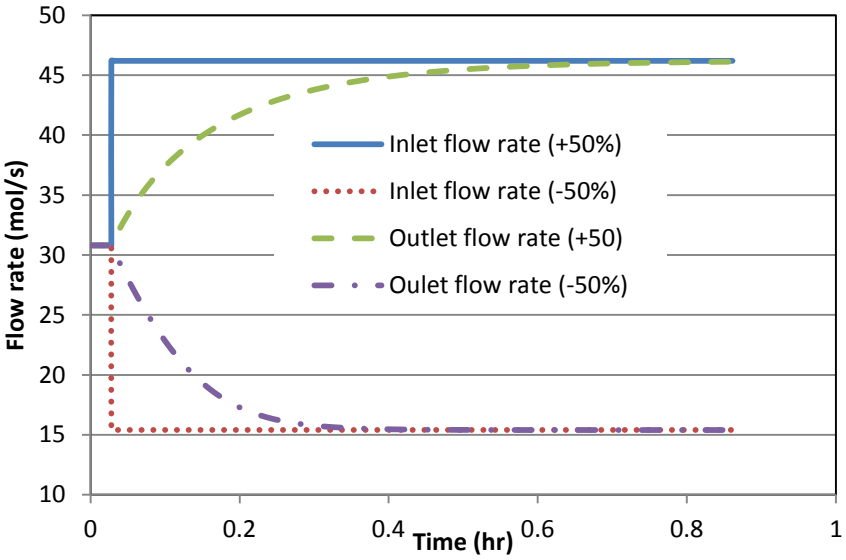

Figure 4.8: Process response to the step change for tank model

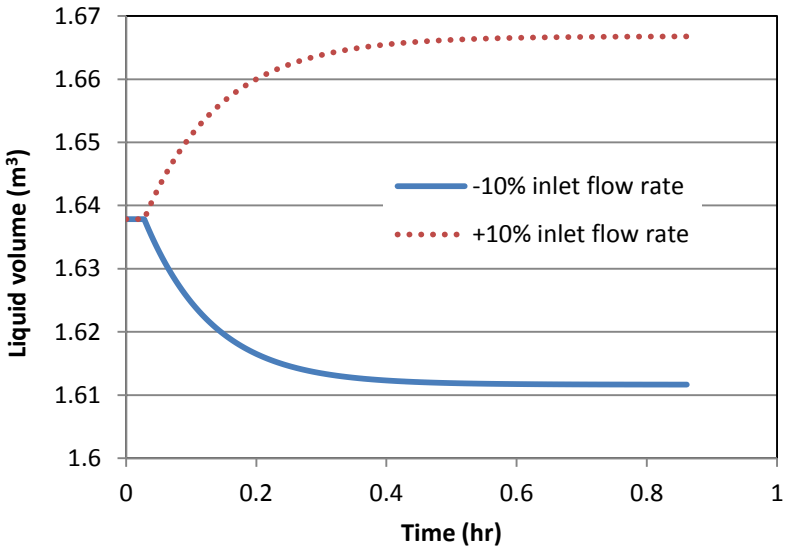

Figure 4.9: Liquid volume profile during step test

4.7 Complete process model analysis

The flow sheet of the complete process model was obtained by connecting all the individual process units described in the previous sections, as per Figure 3.1. Circulation of regenerated MEA solvent between stripper and absorber constitutes the recycle of the system. The following information was provided as the input to the complete process model.

Table 4.18: Inlet operating condition for the complete plant at base case

Flue gas condition:	
Mole fraction	
CO_2	0.175
H_2O	0.025
MEA	0
N_2	0.8
Total molar flow rate (mol/sec)	4.013
Temperature (K)	319.71
Pressure (kPa)	103.5
Reboiler heat duty (kW)	155

Steady-state simulations were carried out and the results obtained were compared with those from the Aspen Plus® simulation. As shown in Table 4.19, the results obtained with the gPROMS model are in reasonable agreement (i.e. less than 10% difference in flow rate and temperature) with those obtained from the Aspen Plus® steady-state simulation, except for the amount of water released at the top of absorber, which has been discussed in the previous section for standalone absorber. The percentage of CO_2 removal from the top of the absorber was 97%, which is similar to the results with the Aspen Plus® model.

Table 4.19: Results comparison between gPROMS and Aspen Plus® simulation at base case conditions for the complete process

	Lean MEA (L-MEA) stream		Vent gas stream		Rich MEA (R-MEA) stream		CO_2-prod	
	gPROMS	Aspen Plus®	gPROMS	Aspen Plus®	gPROMS	Aspen Plus®	gPROMS	Aspen Plus®
Mole Frac								
CO_2	0.0295	0.0307	0.0062	0.0055	0.0504	0.0529	0.7372	0.7292
H_2O	0.8645	0.8605	0.0647	0.1652	0.8458	0.8377	0.2621	0.2622
MEA	0.1060	0.1098	0	0.0001	0.1038	0.1092	0.0007	0.0001
N_2	0	0	0.9291	0.8292	0	0.0002	0	0.0085
Total molar flow rate (mol/sec)	31.19	30.36	3.46	3.86	31.74	30.51	0.9150	0.9140
Temperature (K)	314	314	314.1	333.3	328.7	327.1	352.0	352.6

Two case studies were considered to compare the results at different operating conditions. The flue gas flow rate was changed by $\pm$5% from the base case operating conditions. The results at steady-state are compared in Table 4.20 and Table 4.21. The percentage different between the results from gPROMS model and Aspen Plus® was less than 10%, except for the water flow rate and composition in vent gas.

Table 4.20: Results comparison between gPROMS and Aspen Plus® simulations for the complete process with 5% increase in flue gas flow rate

	Lean MEA (L-MEA) stream		Vent gas stream		Rich MEA (R-MEA) stream		CO_2-prod	
	gPROMS	Aspen Plus®	gPROMS	Aspen Plus®	gPROMS	Aspen Plus®	gPROMS	Aspen Plus®
Mole Frac								
CO_2	0.0295	0.0307	0.0122	0.0117	0.0508	0.0533	0.7647	0.7314
H_2O	0.8645	0.8595	0.0656	0.1725	0.8456	0.8371	0.2347	0.2599
MEA	0.1060	0.1098	0	0	0.1036	0.1094	0.0006	0
N_2	0	0	0.9221	0.8158	0	0.0003	0	0.0086

Table 4.20: Results comparison between gPROMS and Aspen Plus® simulations for the complete process with 5% increase in flue gas flow rate (continues)

	Lean MEA (L-MEA) stream		Vent gas stream		Rich MEA (R-MEA) stream		CO_2-prod	
	gPROMS	Aspen Plus®	gPROMS	Aspen Plus®	gPROMS	Aspen Plus®	gPROMS	Aspen Plus®
Total molar flow rate (mol/sec)	31.19	30.36	3.66	4.12	31.73	30.45	0.92	0.92
Temperature (K)	314	314	314.4	334	327.9	326.1	351.4	352.4

Table 4.21: Results comparison between gPROMS and Aspen Plus® simulations for the complete process with 5% decrease in flue gas flow rate

	Lean MEA (L-MEA) stream		Vent gas stream		Rich MEA (R-MEA) stream		CO_2-prod	
	gPROMS	Aspen Plus®	gPROMS	Aspen Plus®	gPROMS	Aspen Plus®	gPROMS	Aspen Plus®
Mole Frac								
CO_2	0.0295	0.0310	0.0039	0.0040	0.0496	0.0522	0.7505	0.7268
H_2O	0.8645	0.8592	0.0644	0.1526	0.8464	0.8385	0.2489	0.2648
MEA	0.1060	0.1098	0	0.0001	0.1040	0.1090	0.0007	0.0001
N_2	0	0	0.9316	0.8434	0	0.0002	0	0.0083
Total molar flow rate (mol/sec)	31.19	30.35	3.27	3.60	31.72	30.56	0.93	0.91
Temperature K	314	314	313.98	331.79	328.61	328.14	352.39	352.86

The dynamic model of the complete MEA absorption for CO_2 capture process proposed in this work was tested using four case studies:

1. Ramp change in the flue gas flow rate
2. Partial load reduction in flue gas flow rate
3. Step change in the reboiler heat duty
4. Sinusoidal change in the flue gas flow rate

To run the dynamic simulations, the process model was initialized using the base case operating conditions shown in Table 4.22.

Table 4.22: Input conditions at base case operating conditions

Temperature (K)	319.7
Molar flowrate (mol/s)	4.013
Mole fraction	
CO_2	0.175
H_2O	0.025
MEA	0
N_2	0.8
Reboiler heat duty (W)	155000

4.7.1 Ramp changes in the flue gas flow rate

The effect of changes in the flue gas flow rate conditions, which usually occurs due to changes in the output of the power plants, was analysed to determine its influence on the performance of the CO_2 capture process. As shown in Figure 4.10, two independent ramp tests were conducted. In these tests, the flue gas flow rate was linearly increased (decreased) for a period of three hours, which resulted in a change of the flue gas flow rate of approximately +5% (-5%). The ramp tests were performed for a total period of 13 hours.

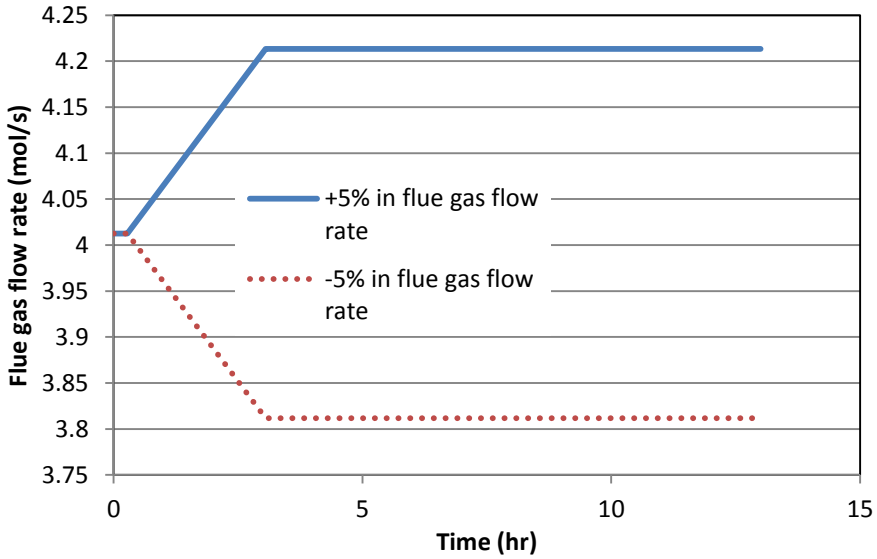

Figure 4.10: Flue gas flow rate during ramp test for absorber

Figure 4.11 illustrates that the liquid to gas ratio (the ratio of lean solvent flow entering the top of absorber to the flue gas flow entering the bottom of absorber) was decreased when the flue gas flow rate was increased, and vice versa, during the ramp tests. The liquid to gas (L/G) ratio immediately responds to the ramp change in the flue gas flow rate because the lean solvent has only small changes during the tests (see Figure 4.12). Thus, the L/G response is mostly influenced by the changes in the flue gas flow rate. As shown in Figure 4.13 and Figure 4.14, the percentage of CO_2 absorbed takes about 8 hours to reach a new steady for a +5% ramp and 4 hours for a -5% ramp from the nominal operating condition of the flue gas flow rate, respectively. Note that the actual ramp tests lasted for a period of three hours. This behaviour occurs because of the lean solvent flow rate response (see Figure 4.15 and Figure 4.16). These Figures show that the percentage of the CO_2 absorbed is significantly influenced by the changes in the lean solvent flow rate. Therefore, the lean solvent flow rate can potentially be used as a manipulated variable to control the amount of CO_2 absorbed.

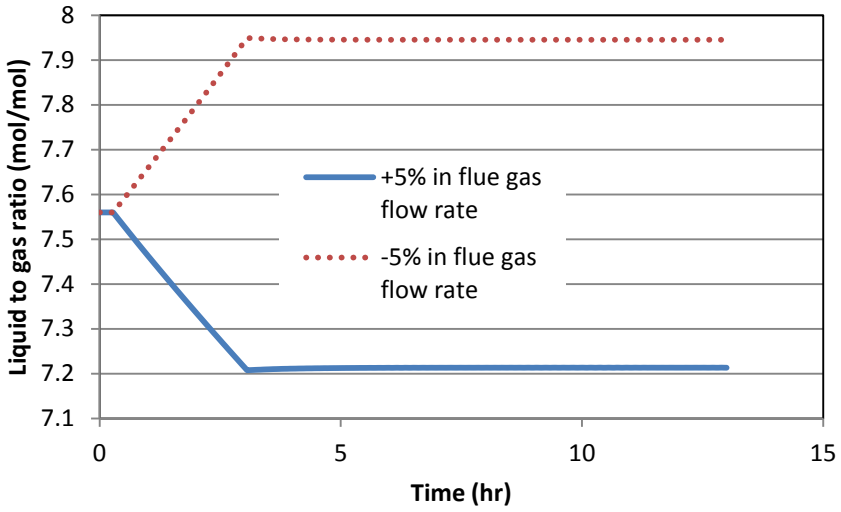

Figure 4.11: Liquid to gas ratio during ramp test for absorber

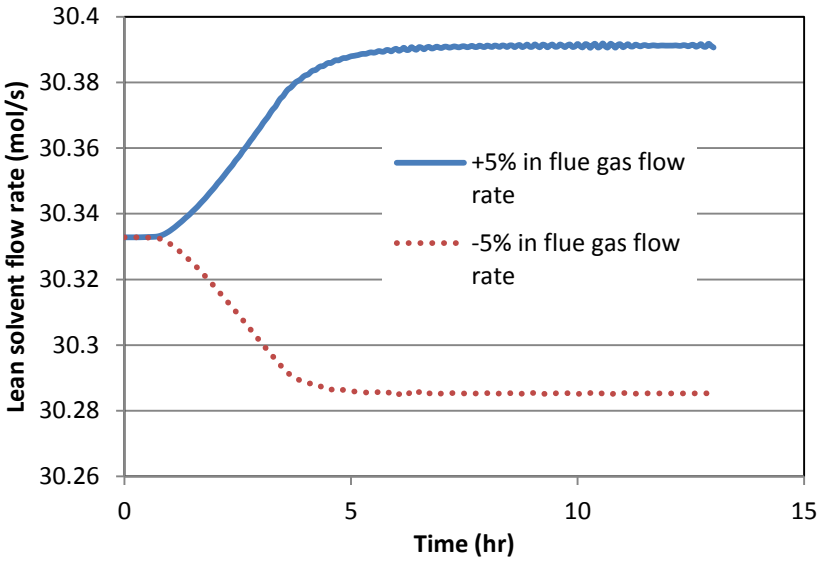

Figure 4.12: Lean solvent flow rate during ramp test

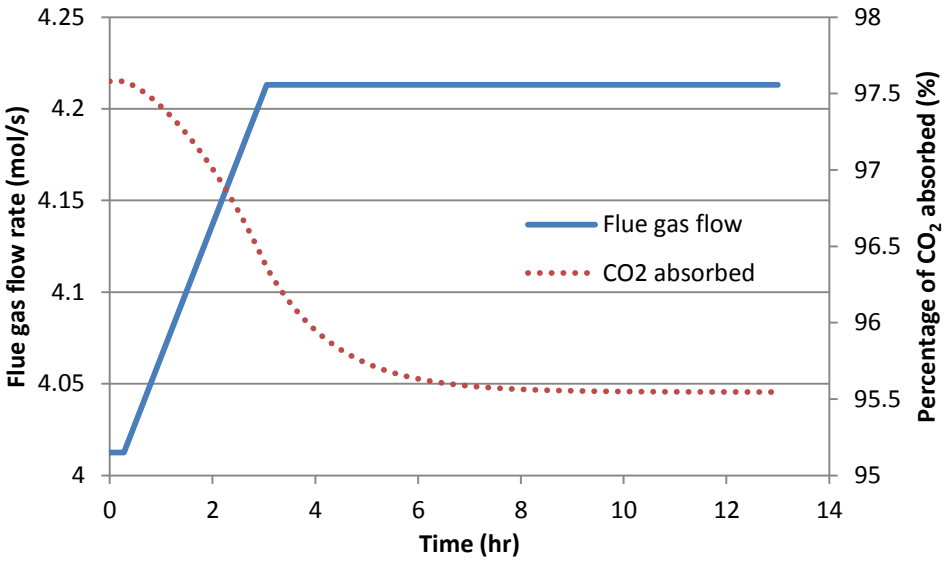

Figure 4.13: Flue gas flow rate and percentage of CO_2 absorbed profile for ramp increased test

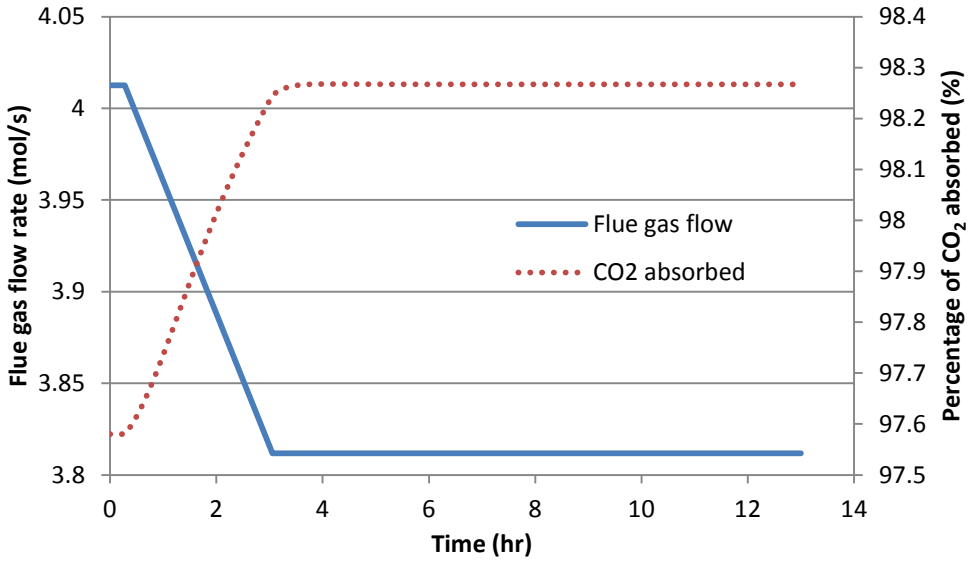

Figure 4.14: Flue gas flow rate and percentage of CO_2 absorbed profile for ramp decreased test

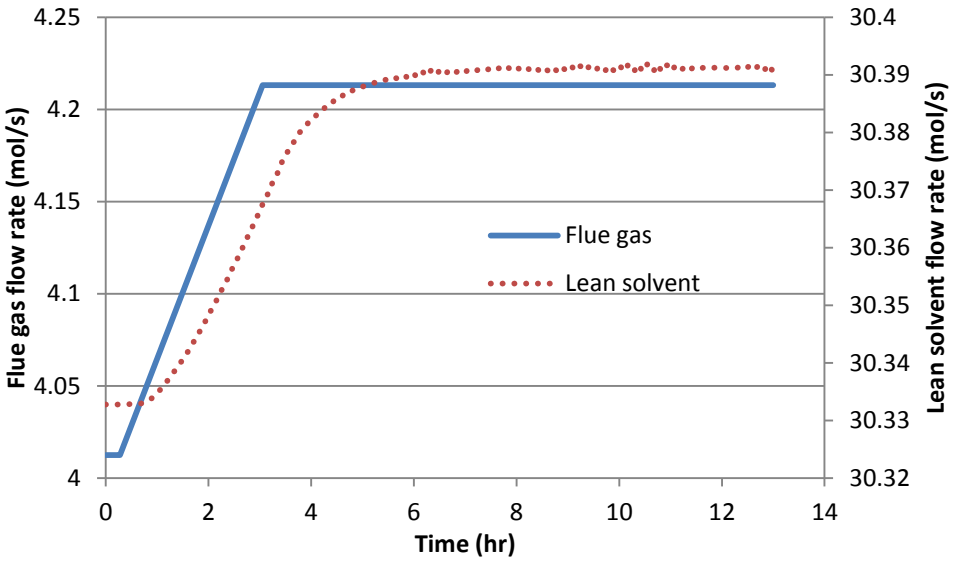

Figure 4.15: Flue gas and lean solvent flow rate profile for ramp increased test

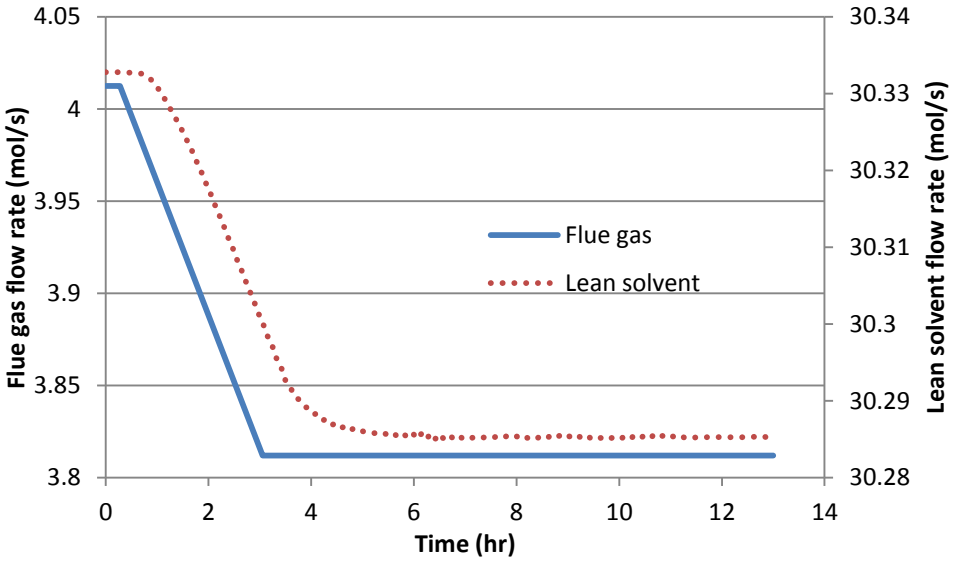

Figure 4.16: Flue gas and lean solvent flow rate profile for ramp decreased test

As shown in Figure 4.17, the rich loading, which is defined as the number of moles of CO_2 per mole of MEA entering the stripper column, was slightly increased (decreased) when liquid-to-gas ratio was decreased (increased). This occurs because more CO_2 is transferred to the liquid solution when the flue gas flow rate is increased. Figure 4.17 also shows the degree

of nonlinearity in the process. While a 1% change in the rich loading flow rate's gain was observed for the ramp test that linearly increased the flue gas flow rate by 5%, a 2% change in the same process variable's gain was observed when the flue gas flow rate was linearly decreased by 5%.

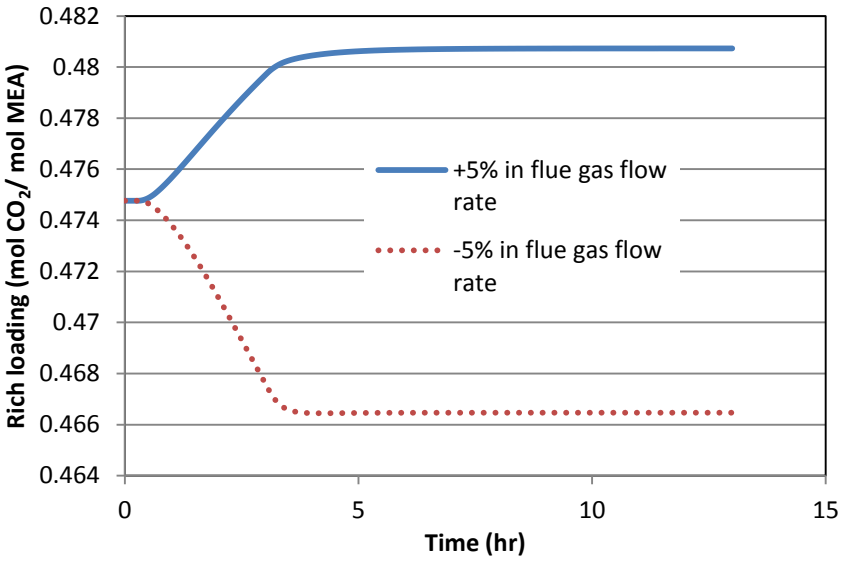

Figure 4.17: Rich loading profile during ramp test for absorber

Figure 4.18 shows the dynamic response of the percentage of CO_2 absorbed in the absorber column which represents the CO_2 not vented to the atmosphere). This Figure shows that the percentage of CO_2 absorbed was increased (decreased) to 98.3% (95.5%) for the flue gas flow rate conditions tested on this study. Figure 4.18 also shows the degree of nonlinearity in the process. While a 1% change in the percentage of CO_2 absorbed's gain was observed for the ramp test that linearly decreased the flue gas flow rate by 5%, a 2% change in the same process variable's gain was observed when the flue gas flow rate was linearly increased by 5%.

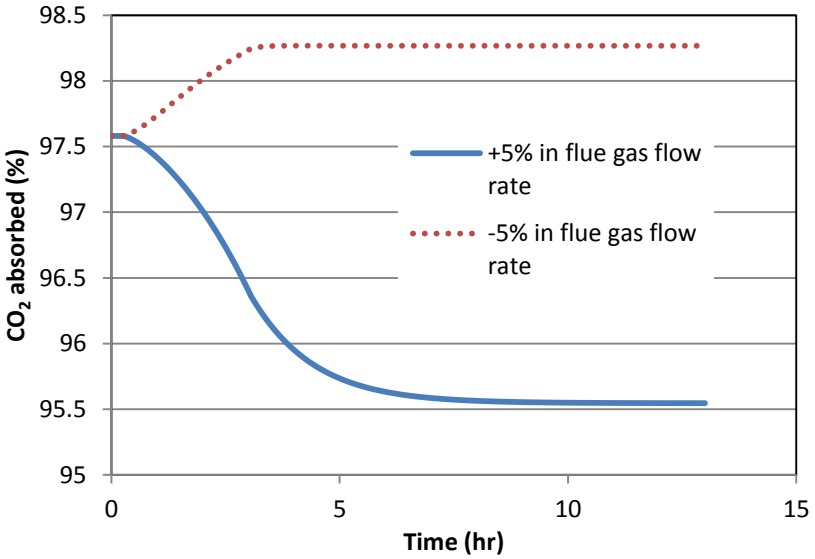

Figure 4.18: The percentage of CO_2 absorbed in the absorber during ramp test

Figure 4.19 and Figure 4.20 show the liquid temperature profiles in the absorber obtained for each of the ramp test at different time intervals. The solid line (t = 0 hr) represents the liquid temperature profile at the base case operating conditions. The magnitude and location of the liquid temperature bulge in the absorber was moved towards the top (resp. bottom) of the column as the flue gas flow rate was increased (resp. decreased). This behaviour was also reported by Kvamsdal and Rochelle (2008) for this process. The temperature bulge that occurred near the bottom of the absorber column for both case studies can be explained as follows: As the liquid flow downward the column, the CO_2 is transferred from the gas to the liquid phase. The absorption of CO_2 into the liquid phase is accompanied by the reaction between CO_2 and MEA which releases heat (due to exothermic reaction) and causes the liquid temperature to increase. The maximum temperature occurs near the bottom of the column due to more CO_2 available to react with MEA. Therefore, more heat is released to the liquid phase near the bottom. The liquid temperature drops as it reaches the bottom of the column because of the heat transferred from the liquid to the gas phase due to low flue gas temperature entering the column. During the ramp test, the magnitude and location of the liquid temperature bulge in the absorber moves towards the top (resp. bottom) of the column

as the flue gas flow rate was increased (resp. decreased), which corresponds to the decrease (resp. increase) in the liquid-to-gas ratio. As the liquid-to-gas ratio decreases (e.g. when increasing the flue gas flow rate), more CO_2 is available to react with MEA and the reaction can occur at higher level in the column. This leads the temperature bulge to move toward the top of the column, as it is shown in Figure 4.19. The opposite behaviour was observed when decreasing the flue gas flow rate (see Figure 4.20).

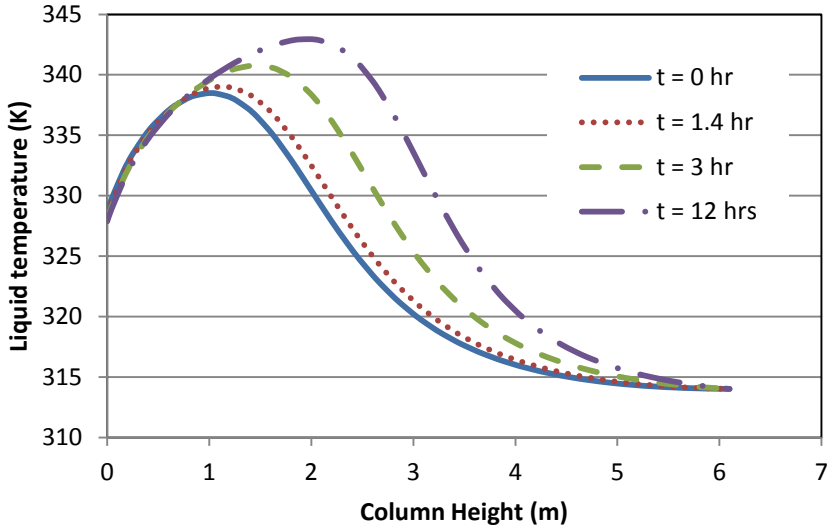

Figure 4.19: Liquid temperature profile in the absorber during ramp test (+5% in the flue gas flow rate)

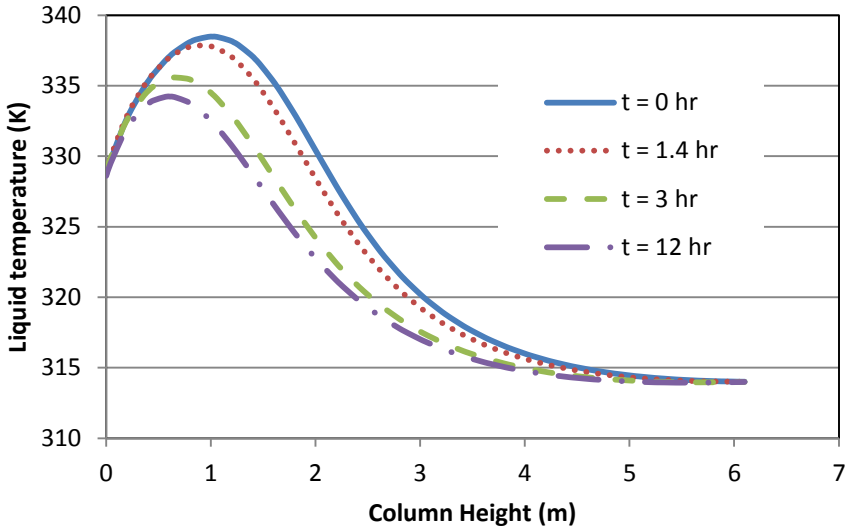

Figure 4.20: Liquid temperature profile in the absorber during ramp test (-5% in the flue gas flow rate)

Figure 4.21 and Figure 4.22 show the concentration profiles of CO_2 and MEA along the absorber column for a 5% increased in the flue gas flow rate, respectively. As shown in those Figures, the concentration of both CO_2 and MEA decreases rapidly near the bottom of the column. This indicates that most of the CO_2 transferred from the gas to the liquid takes place near the bottom of the column. The concentration of CO_2 further reduces towards the top of the column while the concentration of MEA slightly decreases as it moves towards the bottom of the column. Meanwhile, the reduction in the concentration of CO_2 and MEA occurred in the opposite direction (i.e. moves toward the bottom of the column) when the flue gas was reduced with magnitude of 5% as shown in Figure 4.23 and Figure 4.24, respectively.

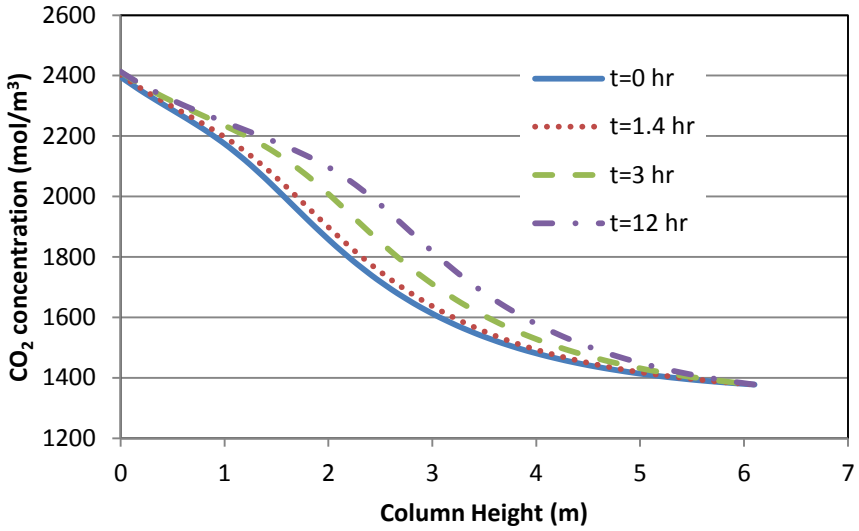

Figure 4.21: CO_2 concentration profile in the absorber during ramp test (+5% in the flue gas flow rate)

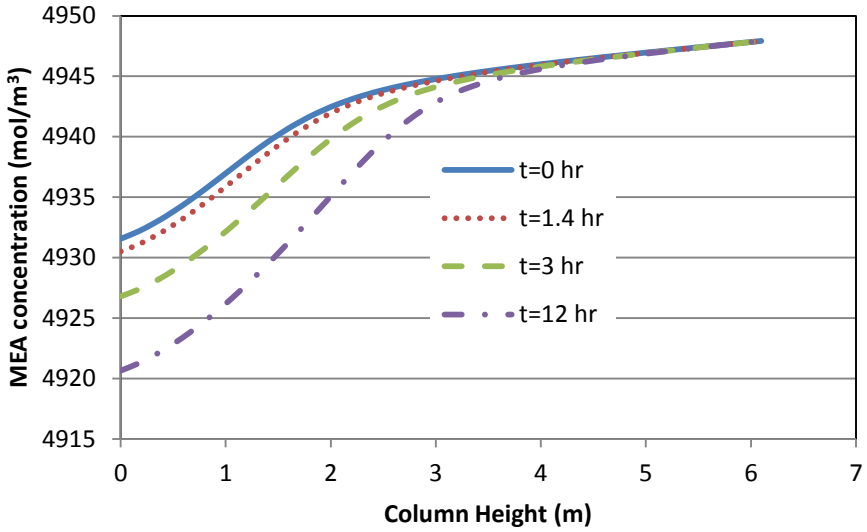

Figure 4.22: MEA concentration profile in the absorber during ramp test (+5% in the flue gas flow rate)

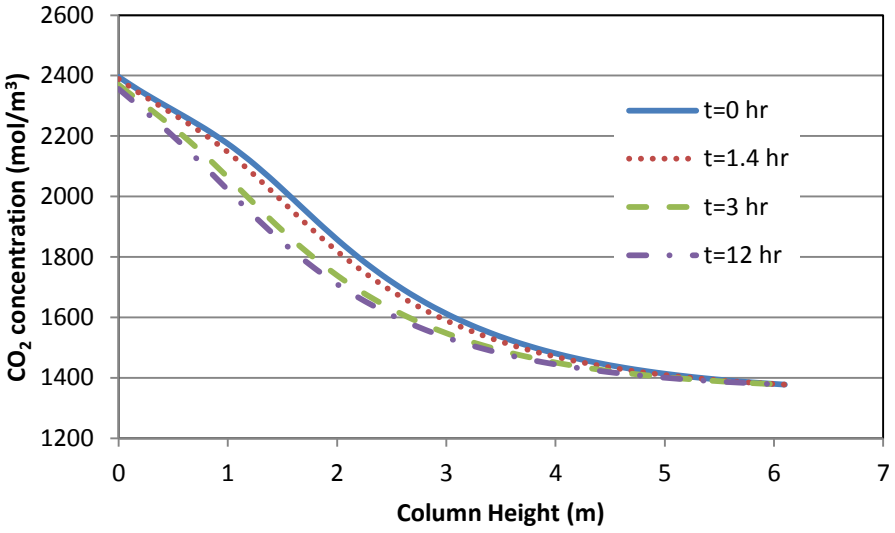

Figure 4.23: CO_2 concentration profile in the absorber during ramp test (-5% in the flue gas flow rate)

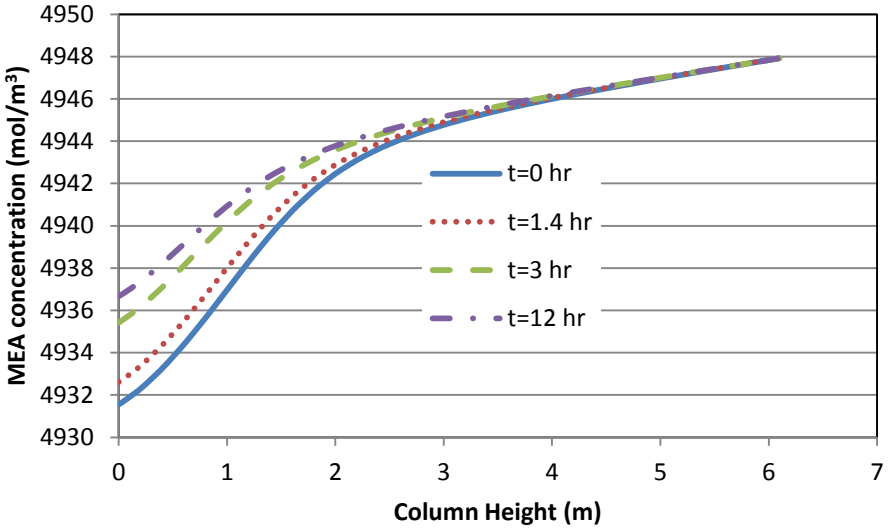

Figure 4.24: MEA concentration profile in the absorber during ramp test (-5% in the flue gas flow rate)

As shown in Figure 4.25 and Figure 4.26, the reboiler temperature takes about 5 hours to reach a new steady for a +5% ramp and 4 hours for a -5% ramp from the nominal operating

condition of the flue gas flow rate, respectively. Thus, both tests showed a similar reboiler temperature response. As shown in Figure 4.27, the composition of CO_2 in the gas product at the top of the stripper column slightly increases (resp. decreases) during the raise (resp. reduction) in flue gas flow rate. This is because the CO_2 loading in the liquid stream entering the stripper column was increased (resp. decreased) as well during the ramp test. As shown in Figure 4.28, the reboiler temperature very slightly changes (~ 0.1 K) because the temperature at the bottom of stripper has changed. Due to the reduction in reboiler temperature, the vapour flow rate also slightly decreases as shown in Figure 4.29. The amount of CO_2 in the liquid stream that recycles back to the absorber slightly decreases (resp. increases) when the reboiler temperature increases (resp. decreases), as shown in Figure 4.30.

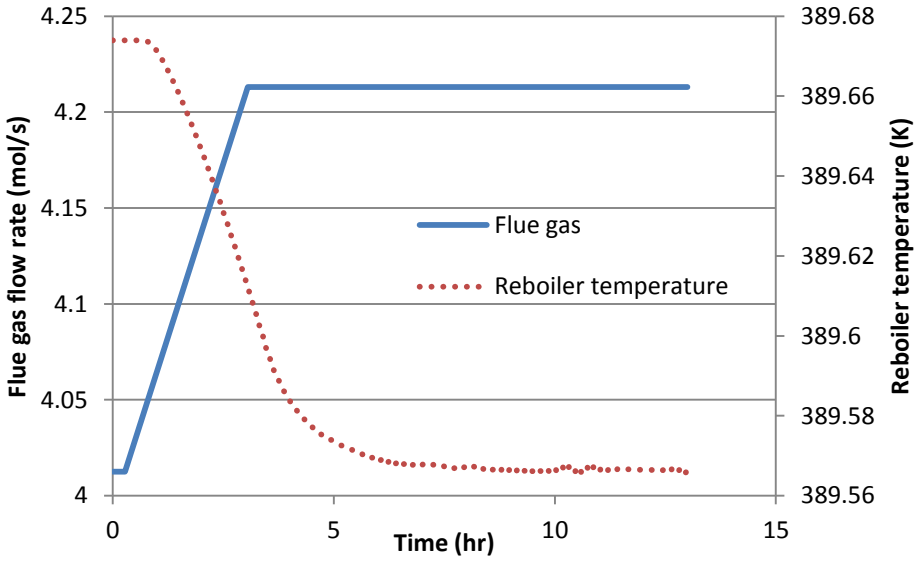

Figure 4.25: Flue gas flow rate and reboiler temperature profile for ramp increased test

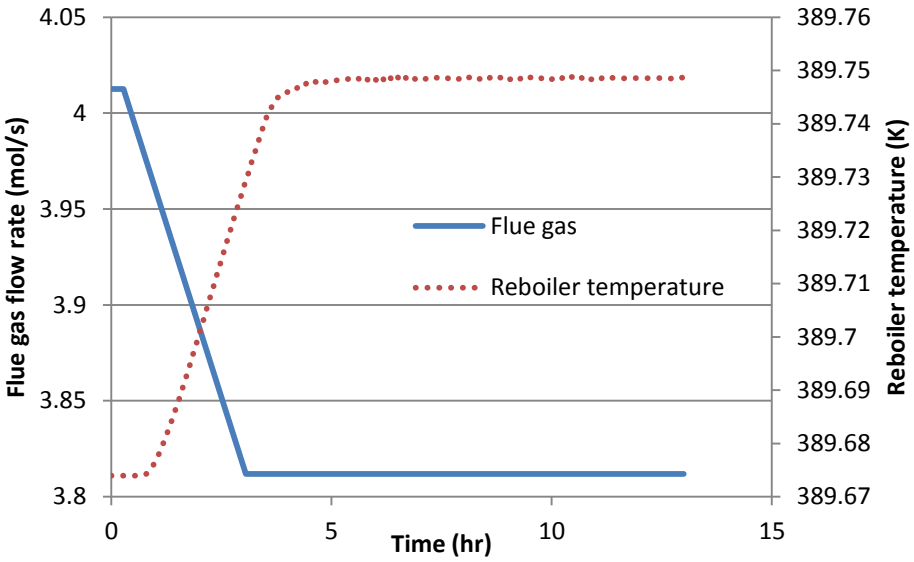

Figure 4.26: Flue gas flow rate and reboiler temperature profile for ramp decreased test

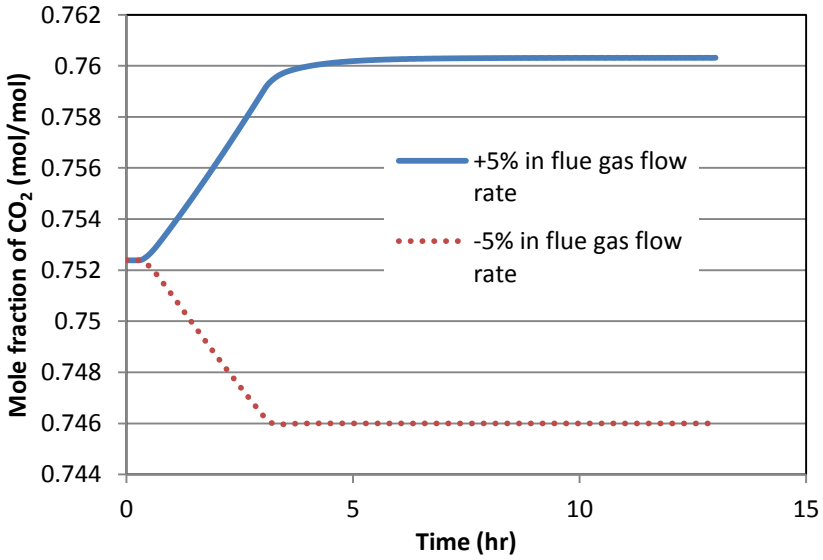

Figure 4.27: CO_2 Mole fraction at the top of stripper column

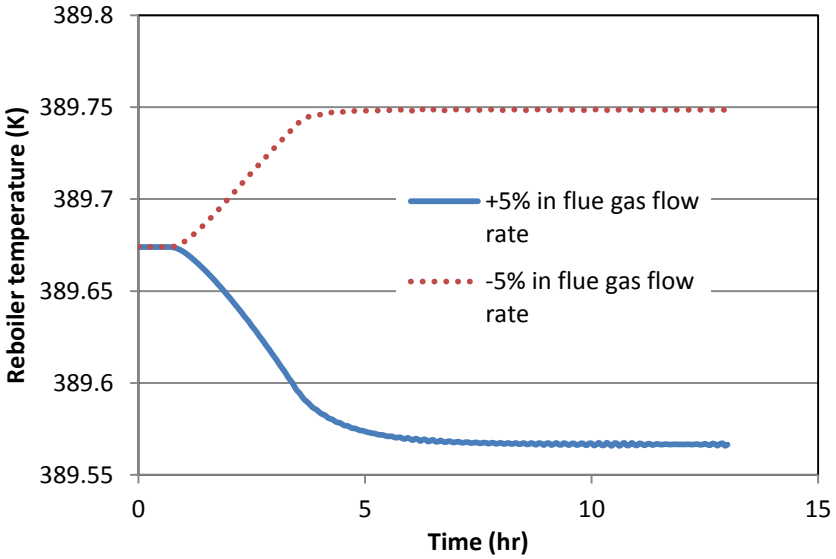

Figure 4.28: Reboiler temperature during the step test

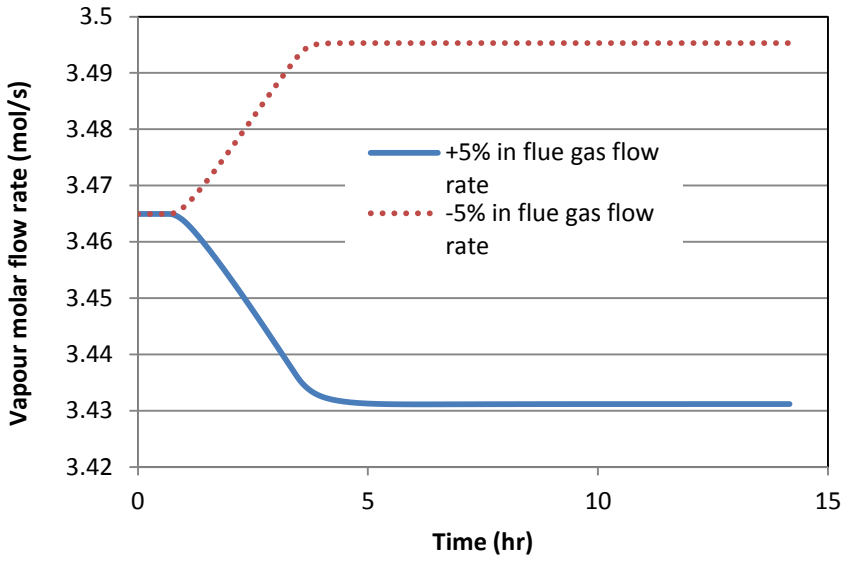

Figure 4.29: Vapour flow rate from the reboiler

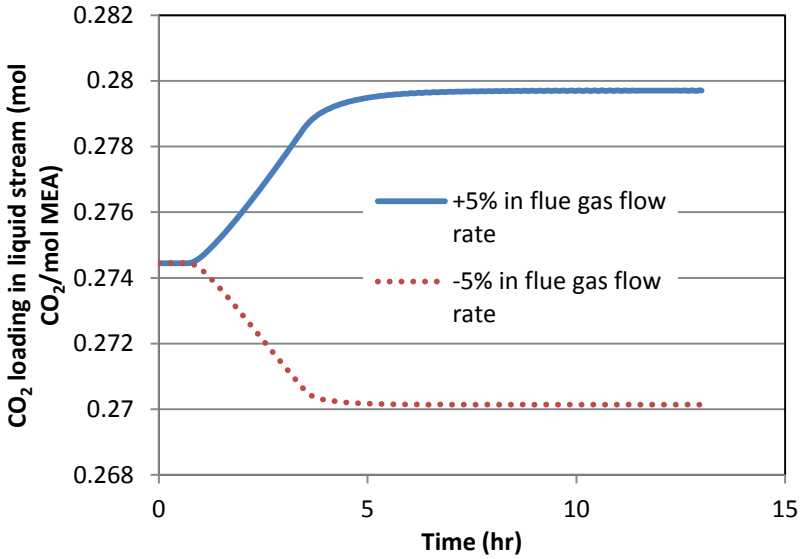

Figure 4.30: CO_2 loading in liquid stream from reboiler

This case study shows that the flue gas flow rate affects significantly the percentage of CO_2 absorbed in the absorber column. The amount of CO_2 absorbed can be maintained if the solvent flow rate were to increase to absorb more CO_2. The effect of flue gas flow changes did not significantly affect the performance of the stripper column, i.e. the changes in the reboiler temperature (0.02%) and CO_2 composition at the top of stripper (1%) were small. This might be due to small changes in flue gas flow rate introduced in the process.

4.7.2 Partial reduction in flue gas flow rate

This case study is to determine the effect of partial reduction in flue gas flow rate (considering partial load reduction in power plant) on the performance of the absorber and stripper. The previous case studies considered small changes ($\pm$5%) in the flue gas flow rate which resulted in much smaller changes in the stripper column performance. A ramp test with 50% reduction in flue gas flow rate was investigated, as shown in Figure 4.31. A small change (~1.4%) in lean solvent flow rate was observed in the same Figure (see dotted line). Due to this small change in lean solvent flow rate, the liquid-to-gas ratio increased by 50% corresponding to the 50% reduction in the flue gas flow rate as depicted in Figure 4.32. The CO_2 loading in the rich stream coming from the bottom of the absorber decreased by 20%, as

displayed in Figure 4.33. Due to the 50% reduction in the flue gas flow rate, more MEA is available to react with CO_2, thus less CO_2 is vented (0.2%). This contributed to large amounts of CO_2 being absorbed in the absorber column. As shown in Figure 4.34, 99.8% of CO_2 was removed from the flue gas in the absorber column. The partial reduction in flue gas flow significantly reduced the composition of CO_2 released from the top of the stripper by 8% (see Figure 4.35). The reboiler temperature as depicted in Figure 4.36 was slightly increased (~0.1%) during the flue gas flow rate reduction due to an increase in inlet temperature (see dotted line in the same Figure). However, the percent decreased for partial reduction was higher than 5% reductions in flue gas flow rate (~0.02%). This shows that the changes in flue gas flow rate does not significantly affect the reboiler temperature. Due to the increased in the reboiler temperature, the vapour flow rate was increased by about 7%, as displayed in Figure 4.37. The CO_2 loading in the liquid stream was decreased by 14%, as shown in Figure 4.38.

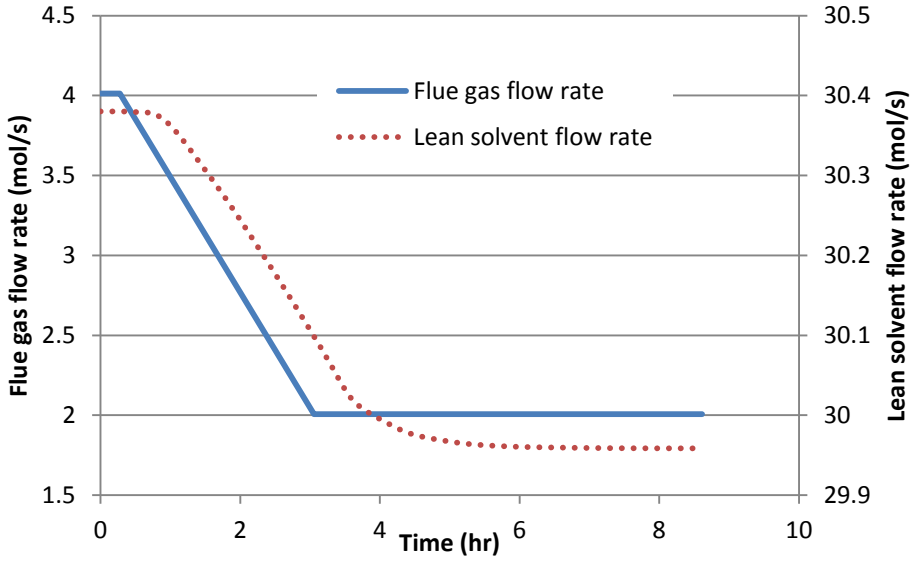

Figure 4.31: Flue gas flow rate and lean solvent flow rate during partial reduction

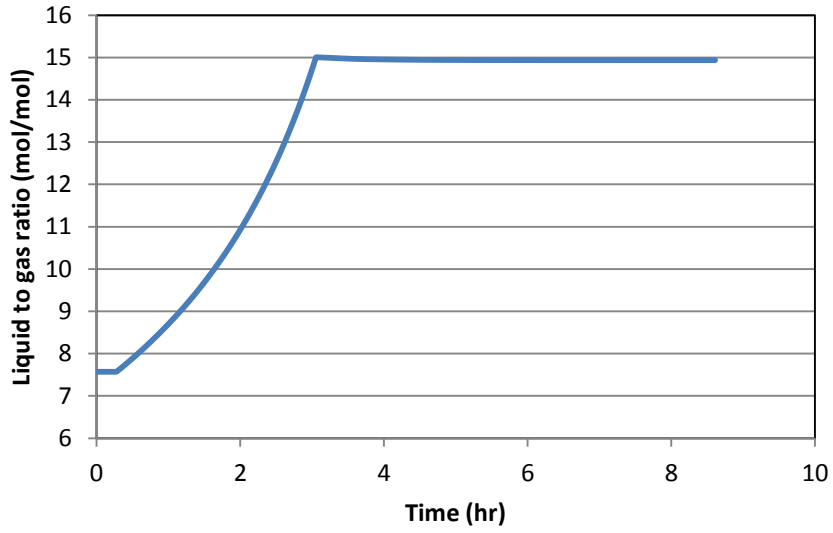

Figure 4.32: Liquid to gas ratio during partial reduction

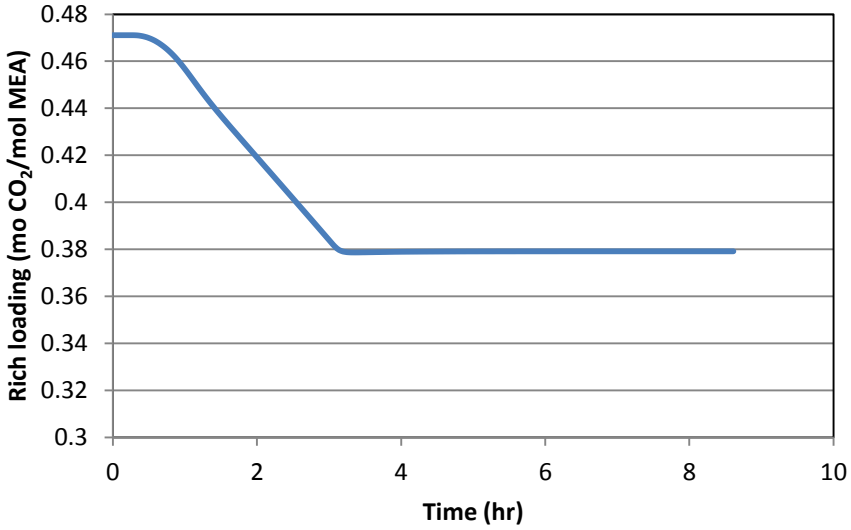

Figure 4.33: Rich loading during partial reduction

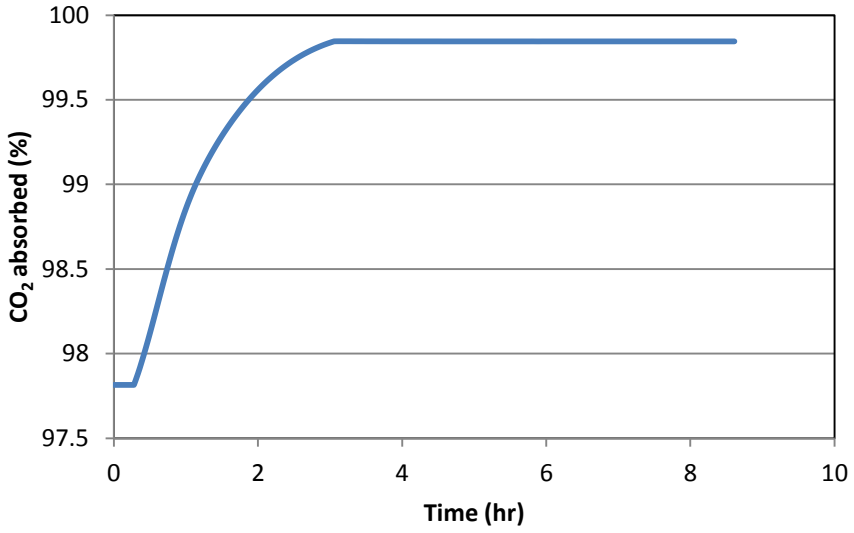

Figure 4.34: The percentage of CO_2 absorbed during partial reduction

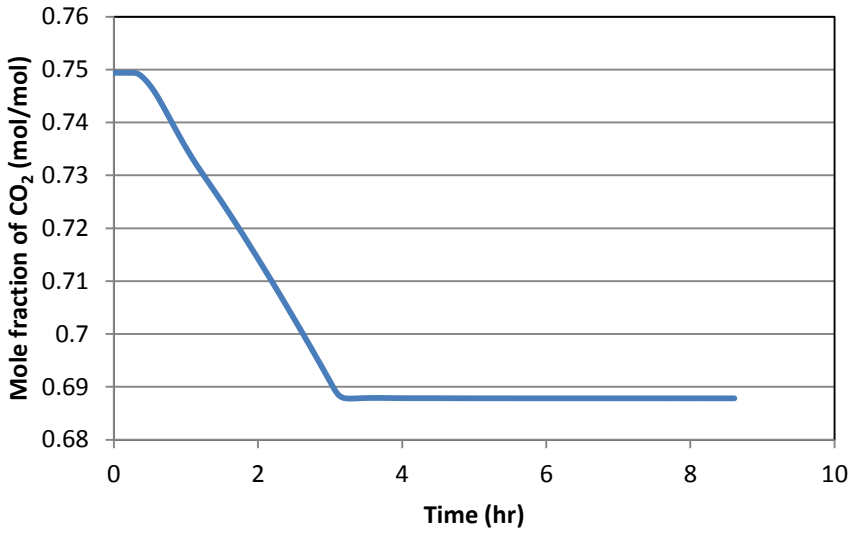

Figure 4.35: CO_2 mole fraction at the top of stripper column during partial reduction

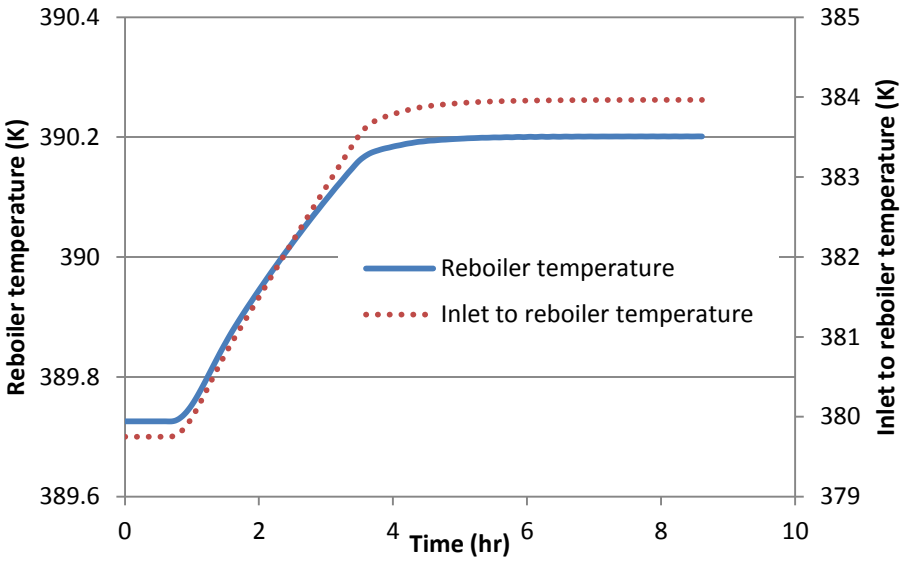

Figure 4.36: Reboiler temperature and inlet temperature during partial reduction

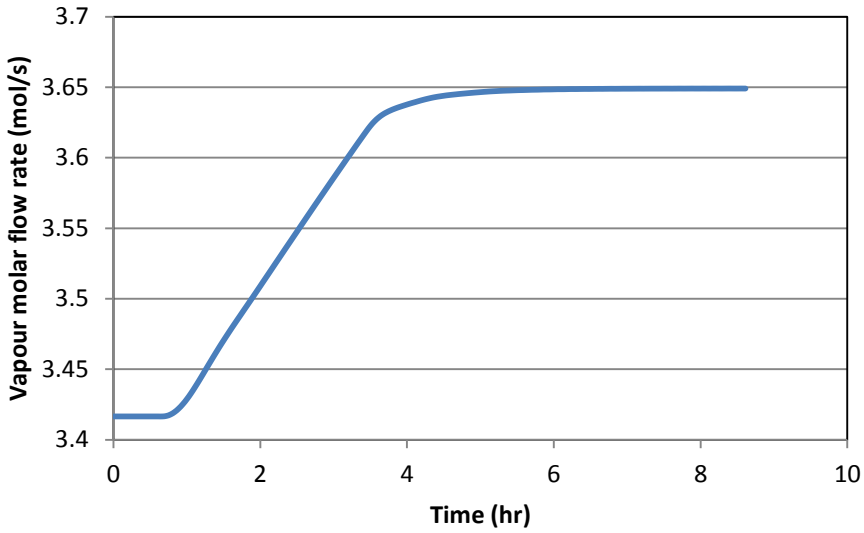

Figure 4.37: Vapour molar flow rate from reboiler during partial reduction

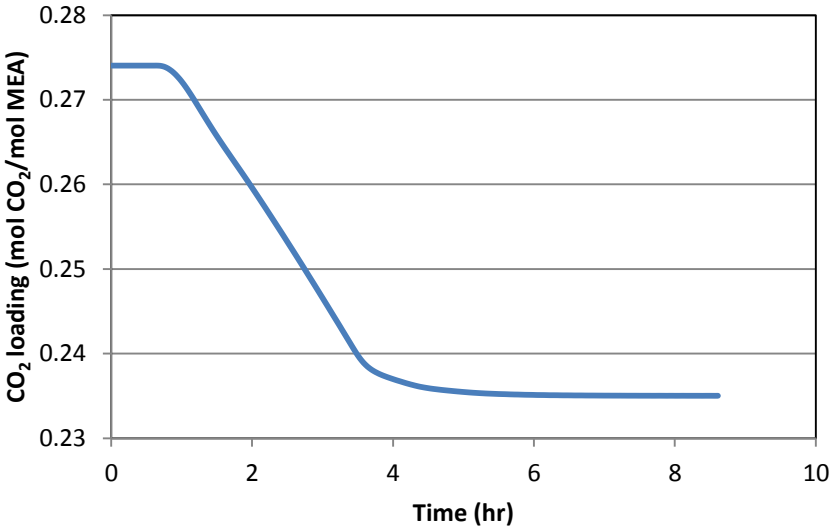

Figure 4.38: CO_2 loading in liquid stream from reboiler during partial reduction

4.7.3 Reducing the reboiler heat duty

The heat duty in the reboiler is a key process variable that can be potentially adjusted to control the operation of this CO_2 capture process, i.e., this variable can be used to control the reboiler temperature, which in turn will affect the performance of the stripper column. Thus, the present scenario analyses the effect of a reduction in the heat duty on the performance of the MEA CO_2 capture process. A reduction in the reboiler heat duty represents a decrease in heat supply from the power plant or external auxiliary systems. As shown in Figure 4.39, a reduction of 10% in the reboiler heat duty, relative to the base case, was considered here. The reboiler temperature (dashed line in Figure 4.39) slightly reduces as the heat duty supplied to the process decreases, which is to be expected. As can be seen from this Figure, the reboiler temperature initially decreases rapidly (immediate response to the step decrease in reboiler heat duty), but then for the last 4^oC change, it takes much longer to get to the final steady state value.

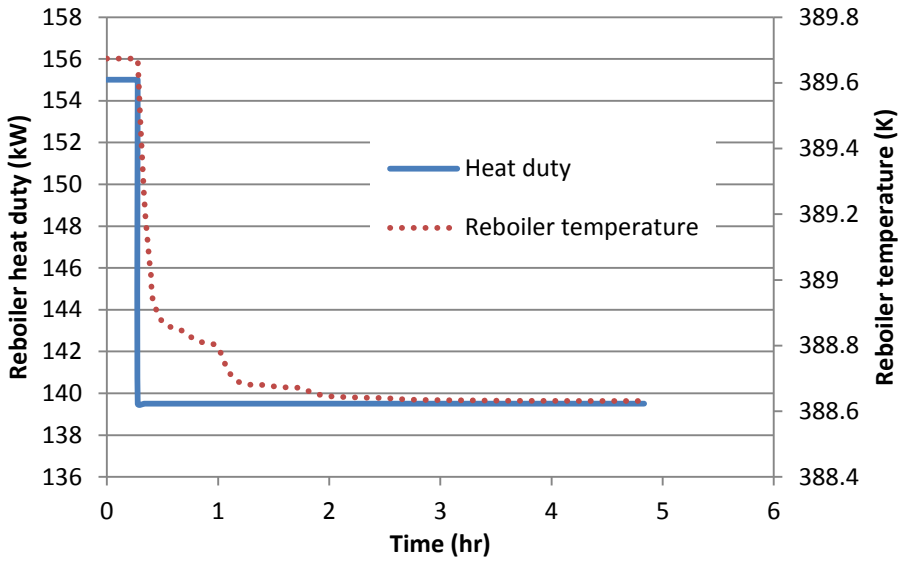

Figure 4.39: Reboiler heat duty and temperature profile during the step test

In response to a step decrease in the reboiler duty, the CO_2 loading in the liquid stream from the reboiler was increased by 12.5% as shown in Figure 4.40 due to reduction in reboiler temperature. This shows that a lower heat duty is required if the remaining CO_2 loading in the liquid stream coming out from the reboiler is high. This result in more CO_2 sent back to the absorber column. Higher CO_2 loading in the lean solution entering the absorber column may leads to poorer absorption performance in the absorber, i.e. reduces the rate of absorption. However, the liquid stream from the reboiler is passed through the heat exchanger and mixed with large liquid inventory (1.5 m^3) in the tank. As shown in Figure 4.41, the increase in liquid volume resulting from the heat duty decrease was only 0.1 m^3. A large amount of liquid solution in the tank leads to a constant lean loading entering the absorber column. Thus, for a tank large enough, the changes in lean loading from the reboiler does not affect the concentration of liquid inventory in the tank. The percentage of CO_2 absorbed slightly increases (0.2%) as shown in Figure 4.42, due to the increased lean solution flow rate entering the absorber (see dotted line in Figure 4.42). Small change (~0.5%) in rich loading coming from the bottom of absorber column was observed as displayed in Figure

4.43. This corresponds to the small percentage of CO_2 being absorbed in the absorber column.

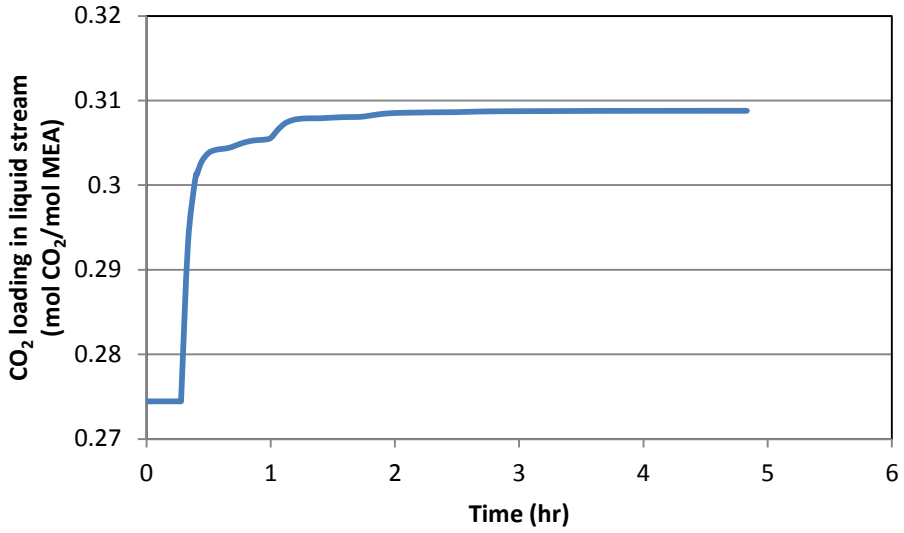

Figure 4.40: CO_2 loading in liquid stream from reboiler

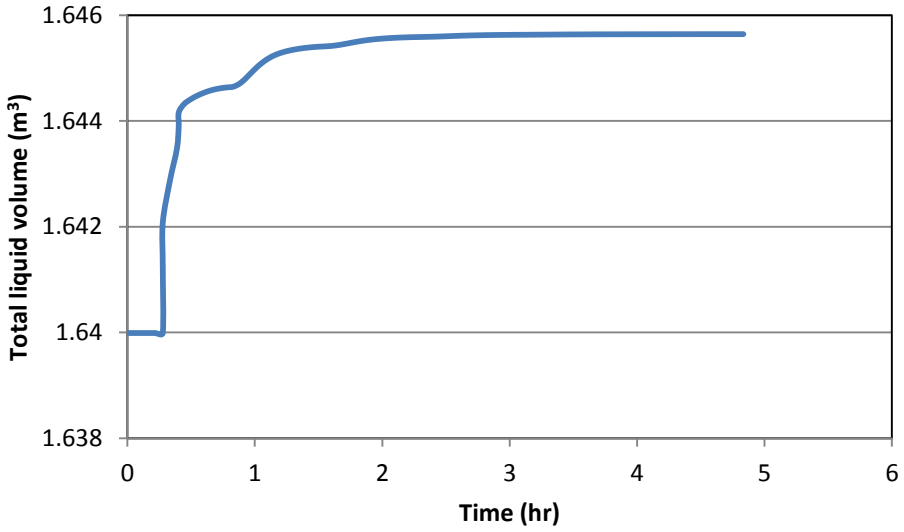

Figure 4.41: Total liquid volume in storage tank

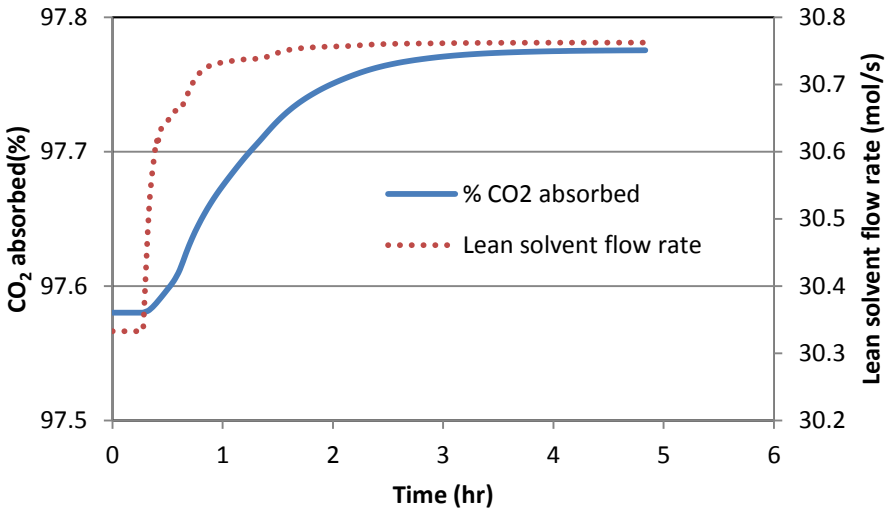

Figure 4.42: Percentage of CO_2 absorbed and lean solvent flow rate at top of absorber

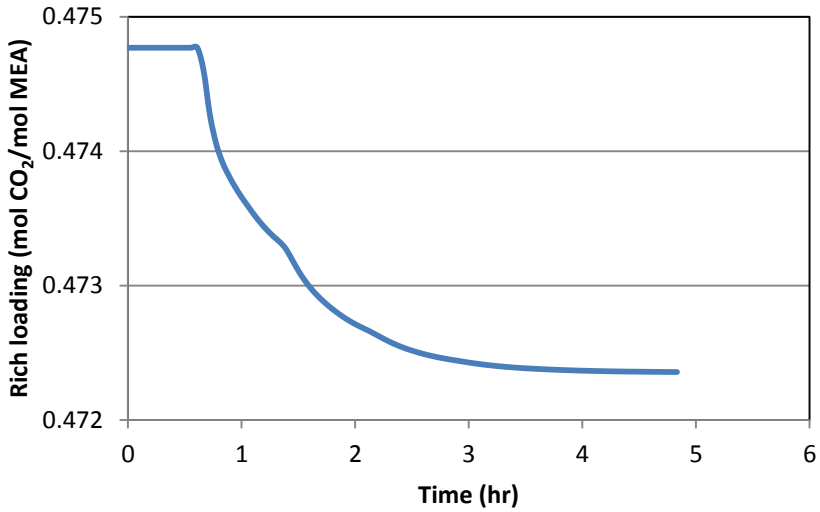

Figure 4.43: Rich loading profile

From this case study, it was found that the reduction in reboiler heat duty significantly affects the reboiler temperature. The decrease in reboiler temperature causes more CO_2 loading in the lean stream that is sent back to the absorber. The change in percentage of CO_2 absorbed in the absorber column is very small (0.2%) due to the small increase in lean solvent flow rate.

4.7.4 Sinusoidal changes in the flue gas flow rate

The dynamic response of the MEA process due to a sinusoidal change in the flue gas flow rate is considered here. This case study was performed to approach the dynamic behaviour of this process when oscillatory conditions, like those typically observed on a daily basis in the power plant outputs (see Figure 4.44), are present in the flue gas flow rate. As illustrated in Figure 4.44, the power plant output exhibit day-to-night-to-day fluctuations. This cyclic process was approximated in the present study using a sinusoidal function.

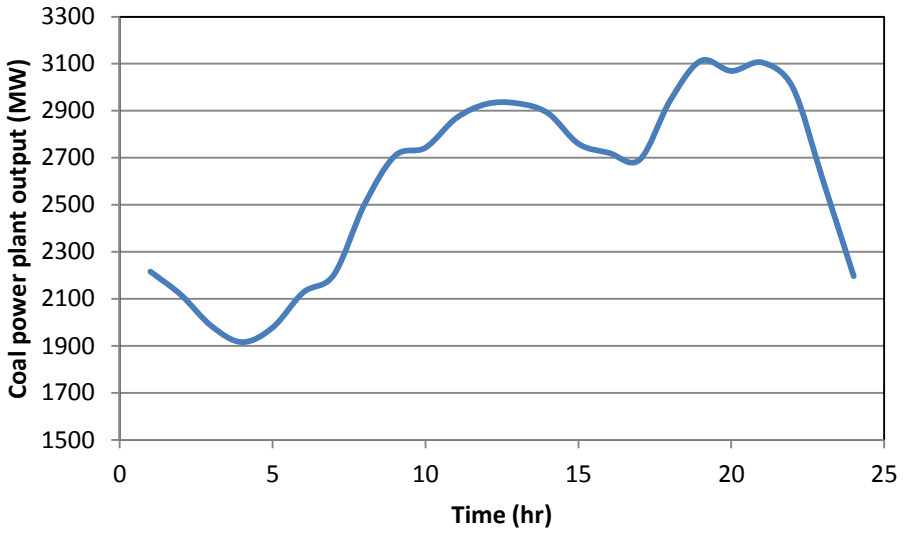

Figure 4.44: A typical output from coal power generation plants in Ontario, Canada (IESO, 2011)

In this case study the amplitude of the sinusoidal function was assumed to be 15% of the base case flue gas and the sinusoidal input was set to complete one cycle within a day. As shown in Figure 4.45, the simulation was performed for three days. The liquid-to-gas ratio reached a maximum value of 9.7 at the minimum flue gas flow rate and minimum value of 7.2 at the maximum flue gas flow rate (dotted line in Figure 4.45). This dynamic behaviour in the liquid-to-gas ratio is due to small changes ($\pm$0.2%) in the lean solvent flow rate, as shown in Figure 4.46. Thus, an increase (resp. decrease) in the flue gas flow rate reduces (resp.

increases) the liquid-to-gas ratio in the absorber. The rich loading shows a similar oscillatory behaviour to that imposed for the flue gas flow rate (see Figure 4.47). The rich loading values varied between 0.48 and 0.43 during the test. Figure 4.48 shows the response of CO_2 absorbed as the flue gas exhibit cyclic process change. As illustrated in Figure 4.48, the percentage of CO_2 absorbed reached a minimum value (95%) when the flue gas flow rate was at its maximum rate. Figure 4.48 also shows that the maximum CO_2 absorbed is 98.8% when the flue gas flow rate is at its minimum value. It shows the minimum and maximum CO_2 absorbed that can be obtained due to a sinusoidal behaviour in the flue gas flow rate. The present results also show that the dynamic behaviour of the CO_2 absorbed does not follow exactly the sinusoidal input embedded in the process model. However, the percentage of CO_2 absorbed profile follow the behaviour of lean solvent as shown in Figure 4.49. This similar behaviour was also observed for the ramp test. The reboiler temperature response behaviour due to sinusoidal changes in flue gas flow rate can be seen in Figure 4.50. The reboiler temperature reached the highest value at 389.2 K and the lowest value at 388.5 K during the flue gas changes. This is due to the changes in the inlet temperature to the reboiler, as depicted in Figure 4.51. The dynamic behaviour of the reboiler temperature follows the inlet temperature profile coming from the bottom of the stripper column. Due to the changes in the flue gas flow rate, the composition of CO_2 at the top of the stripper column also changes with a maximum value of 0.77 and a minimum value of 0.74, as displayed in Figure 4.52.

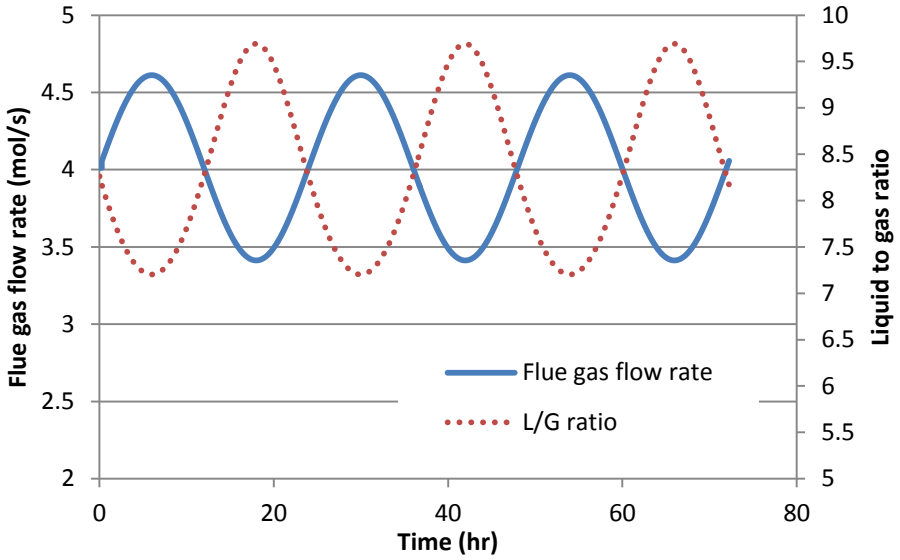

Figure 4.45: Flue gas flow rate and liquid to gas ratio profile during sinusoidal change

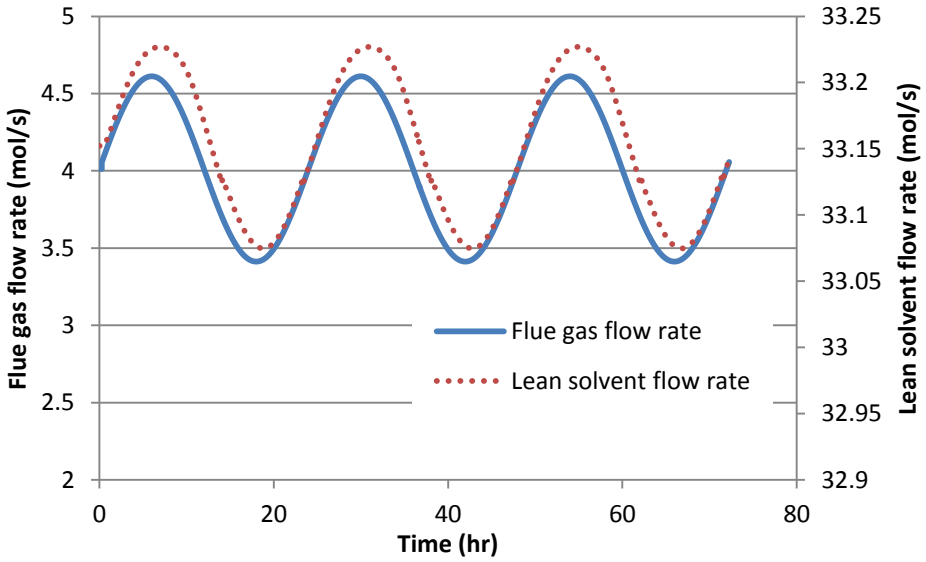

Figure 4.46: Flue gas flow rate and lean solvent flow rate during sinusoidal change

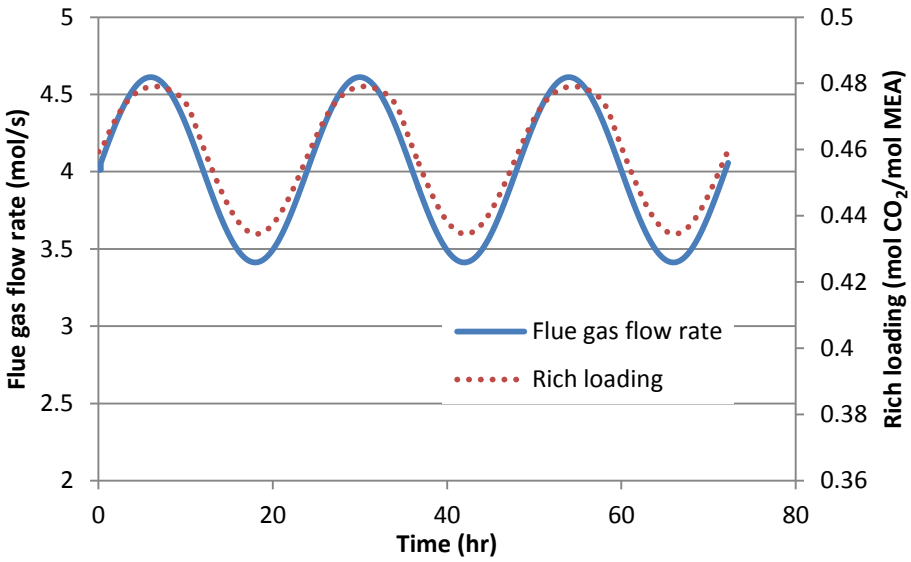

Figure 4.47: Flue gas flow rate profile and rich loading during sinusoidal change

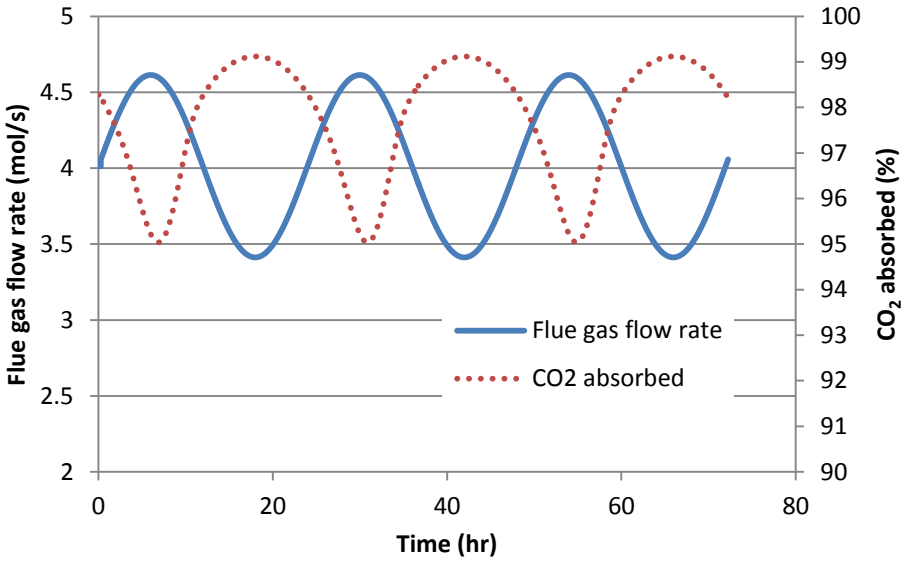

Figure 4.48: Flue gas flow rate and percentage of CO_2 absorbed during sinusoidal test

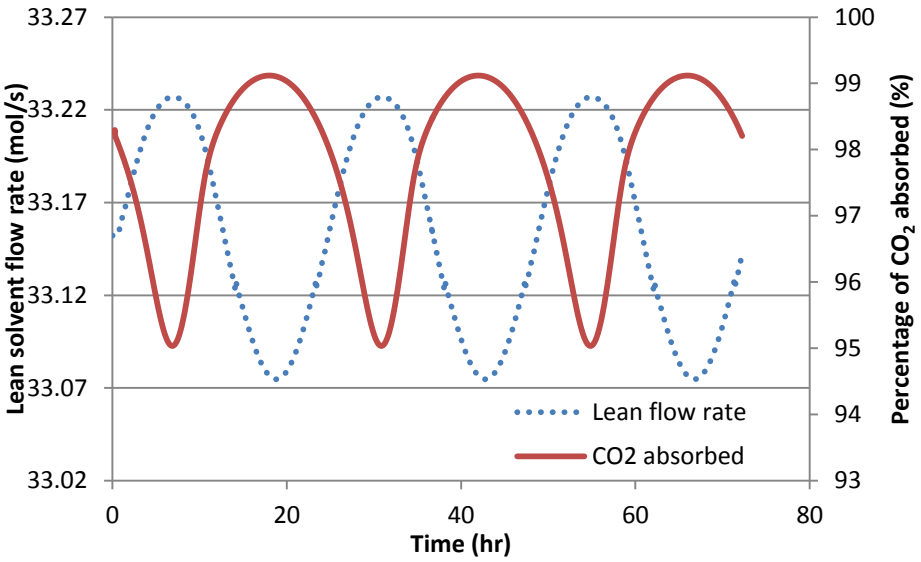

Figure 4.49: Lean solvent flow rate and percentage of CO_2 absorbed during sinusoidal test

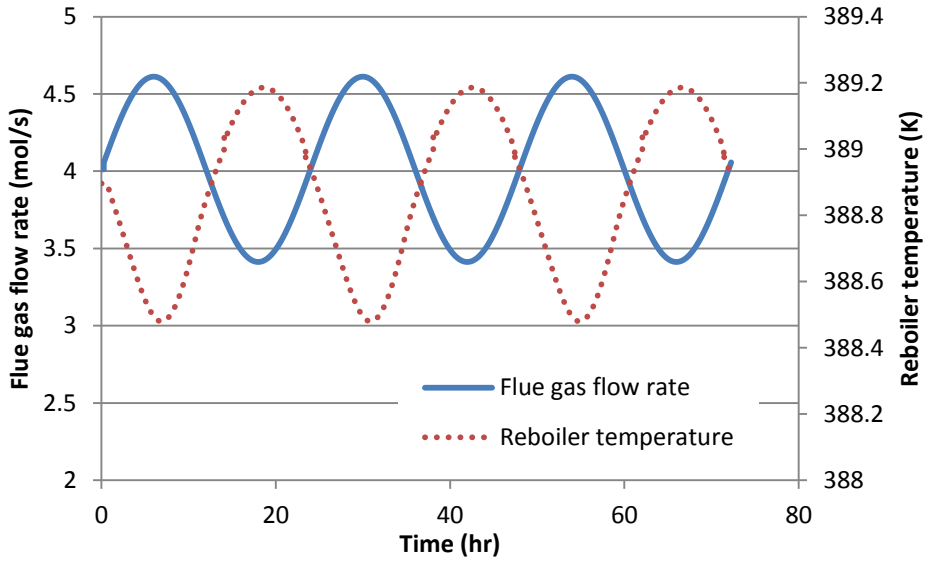

Figure 4.50: Flue gas flow rate and reboiler temperature during sinusoidal test

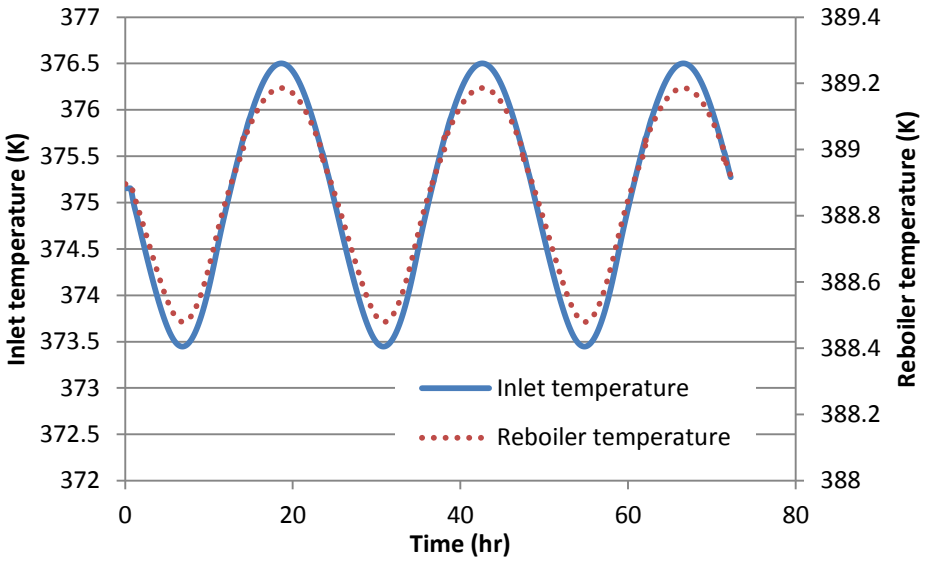

Figure 4.51: Reboiler and inlet reboiler temperature during sinusoidal test

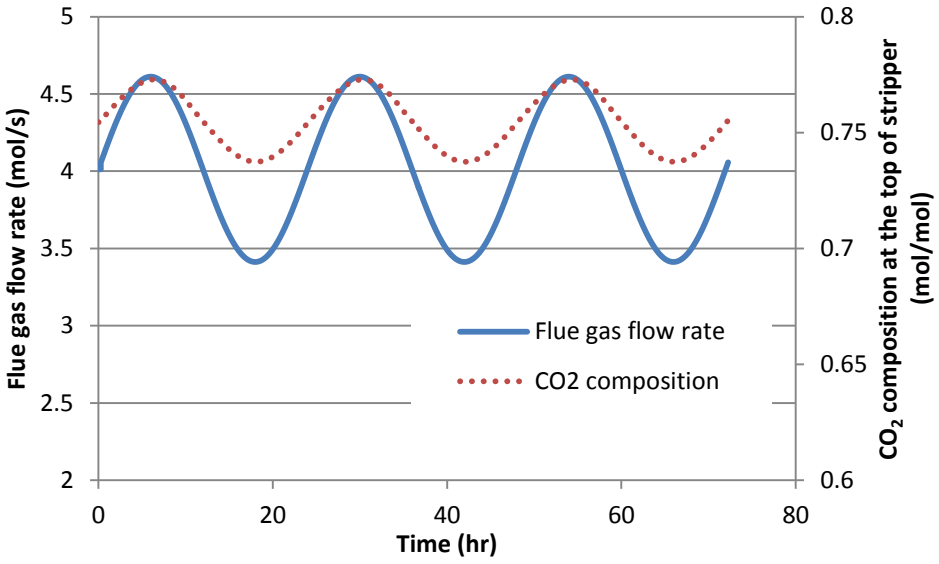

Figure 4.52: Flue gas flow rate and CO_2 composition at the top of stripper during sinusoidal test

4.8 Chapter summary

In this chapter, the mechanistic dynamic MEA absorption process model developed in this study was validated using an Aspen Plus® steady-state simulation and data reported for a CO_2 capture pilot plant (Dugas, 2006). The validation of standalone absorber and stripper and complete plant model has proven to be in reasonable agreement with Aspen Plus® simulation at different operating conditions. The dynamic behaviour of the CO_2 capture process during the course of the dynamic operation of a power plant was studied by incorporating the input changes in the flue gas flow rate and reboiler heat duty. The effect of disturbance changes on key process variables such as liquid-to-gas ratio, lean loading, lean solvent flow rate, percentage of CO_2 absorbed, and reboiler temperature were discussed. The changes in the flue gas flow rate significantly affect the performance of the absorber i.e. the amount of CO_2 absorbed in the column. The reboiler temperature and CO_2 loading in the liquid solution was affected by changing the reboiler heat duty.

Chapter 5
Process Control

This chapter presents the development and implementation of a basic control strategy to maintain the operation of the MEA scrubbing CO_2 capture process in the presence of the external perturbations that may arise from the transient operation of the power plant. The key idea in this work is to develop a relative simple decentralized control configuration that maintains the CO_2 absorbed and the reboiler temperature within their desired set point values when changes in the flue gas flow rate, which is the disturbance selected for this controllability study, enter the CO_2 capture process. Proportional-Integral (PI) feedback controllers were used in this study to control the operation of this process in closed-loop. The PI controllers tuning parameters were initially obtained using the Internal Model Control (IMC) method. The closed-loop performance of the process was improved by manually tuning the PI controllers using process knowledge and heuristics. The closed-loop performance of the MEA CO_2 capture plant was tested for disturbance rejection. The results of those closed-loop tests and the discussion of the results obtained with the decentralized control structure developed in this work are discussed in this chapter.

This chapter is organized as follows: section 5.1 highlights the importance of a control strategy for the CO_2 capture process. Section 5.2 presents the control strategy developed in this work. The effects of disturbance changes on the performance of the CO_2 capture process with control system are discussed in Section 5.3. A summary of the results obtained with the control strategy developed for the present CO_2 capture process is presented at the end of this chapter (section 5.4).

5.1 Introduction

The post-combustion CO_2 capture process is an inherent dynamic system that is affected by the variations occurring in the operating conditions of the power plant. The implementation of a control strategy for the MEA absorption process is needed to ensure the stable operation

of the system and to meet the systems' performance specifications, i.e., maintain the amount of CO_2 absorbed in the presence of external perturbations while meeting the safety operational constraints for this process. The main disturbances expected from the dynamic operation of power plant that will affect the performance of CO_2 capture process are changes in the flue gas conditions and disruption of steam supply for the reboiler unit located at the bottom of the stripper. The steam required for the operation of the reboiler unit is extracted from the power plant's steam cycle.

As discussed in Chapter 2, section 2.4, most of the current control strategies proposed for this process are limited since they have been developed to control the operation of the individual units considered in this process, i.e., absorber column or stripper column. Similarly, simulations of the entire MEA CO_2 process using standard chemical processes simulation packages, e.g., Aspen Plus®, have been used to propose control structures for this process. The key idea in this work is to make use of the mechanistic dynamic process model presented in this work to design a basic control structure for this process. The main advantage in the present analysis is that the process insight obtained from the mechanistic process model can be used to design the controllers that will be included in the control structure configuration, i.e., a model-based control strategy can be used to estimate the controller tuning parameters. Also, the use of a mechanistic process model allows for the implementation of advanced controllability techniques, i.e., Model Predictive Control (MPC), that can in principle improved the closed-loop performance of this process.

The main objective of a CO_2 capture process plant is to reduce the CO_2 emissions from the fossil fuel combustion power plant to meet the environmental specification. The percentage of CO_2 absorbed, which determines the amount of CO_2 in the vent gas that is released to the atmosphere, can be considered as a key variable that needs to be controlled for this process. Moreover, the temperature in the reboiler unit needs to be below 120^oC to avoid thermal solvent degradation but at the same time it is desired to operate the reboiler at a high temperature to provide enough heat for the solvent regeneration in the stripper column. This

operating condition (reboiler's temperature) will also determined the CO_2 loading in the lean solvent that will affect the CO_2 absorption in the absorber column. Thus, the temperature in the reboiler is a key operational constraint that needs to be in closed-loop, i.e., it needs to be controlled at desired set point value.

One variable that can be adjusted to control the operation of this process is the reboiler heat duty. This variable is set as an input for this process model and can be used by a controller to make changes in the system. This process variable can be potentially used as the manipulated variable to control the changes in the reboiler temperature. Thus, the present analysis considered that the reboiler temperature is controlled by changing the heat duty in the reboiler unit since the heat duty in the reboiler has a direct effect on the reboiler temperature. Also, the reboiler heat duty has also been proposed by previous control studies to control the reboiler temperature, e.g., Lawal et al. (2010) and Lin et al. (2011). The other input variable that can be considered as manipulated variable is the valve stem position that regulates the amount of lean liquid solvent flow rate that enters at the top absorber column. This variable is also considered as an input into the present process model. The absorption of CO_2 in the MEA solution relies on the reaction between the CO_2 and the MEA in the absorber unit. As lean solvent flow rate is increased, more MEA is available to react with the absorbed CO_2. A high lean solvent flow rate will increase the absorption of CO_2 in the liquid phase of the absorber column thus reducing the concentration of the CO_2 in the vent gas. Accordingly, the lean solvent flow rate directly affects the CO_2 absorbed in this process can be potentially used to control the percentage of CO_2 absorbed. The previous control studies of the MEA absorption process published in the literature also manipulate the lean solvent flow rate to control the percentage of CO_2 absorbed in the absorber column (Lawal et al., 2010; Lin et al., 2011).

In order to achieve the main objective of CO_2 capture process and to satisfy the temperature constraint in the reboiler unit, the percentage of CO_2 absorbed in the absorber column and reboiler temperature were selected as the controlled variables in the present control strategy.

The percentage of CO_2 absorbed at the nominal operating condition (97.8%) which is obtained from the steady state simulation for this case study, can be maintained by manipulating the valve stem position that will determine the flow rate of lean solvent. Similarly, the reboiler temperature was controlled at base case operating condition (389.7 K) by manipulating the reboiler heat duty. Proportional-Integral (PI) feedback controllers were used in the present analysis to control the closed-loop performance of this system. The development of the control structure and the implementation of control strategies will be discussed in the following sections.

5.2 Controller structure design

Figure 5.1 shows the proposed control structure for CO_2 capture process in this study. As shown in Figure 5.1, the dotted line represents the transmission lines that carry the measurement signals from measuring devices to the controllers, i.e., ratio controller and temperature controller. The percentage of CO_2 absorbed is determined by simultaneously measuring the CO_2 flow rate in the flue gas and in the vent gas. The ratio of CO_2 flow rate between these two streams was calculated and transmitted to the ratio controller as controller input. The CO_2 ratio was calculated using following equation:

$$\text{Ratio} = \frac{CO_2 \text{ flow rate in vent gas}}{CO_2 \text{ flow rate in flue gas}} \qquad 5.1$$

The ratio controller output's signal is transmitted to the process so that the lean solvent flow rate is changed by manipulating the valve stem position so that the percentage of CO_2 absorbed is maintained near its set point (desired) value. On the other hand, the temperature controller will receive the signal from the temperature measurement device and send the output to adjust the reboiler heat duty supplied to the process.

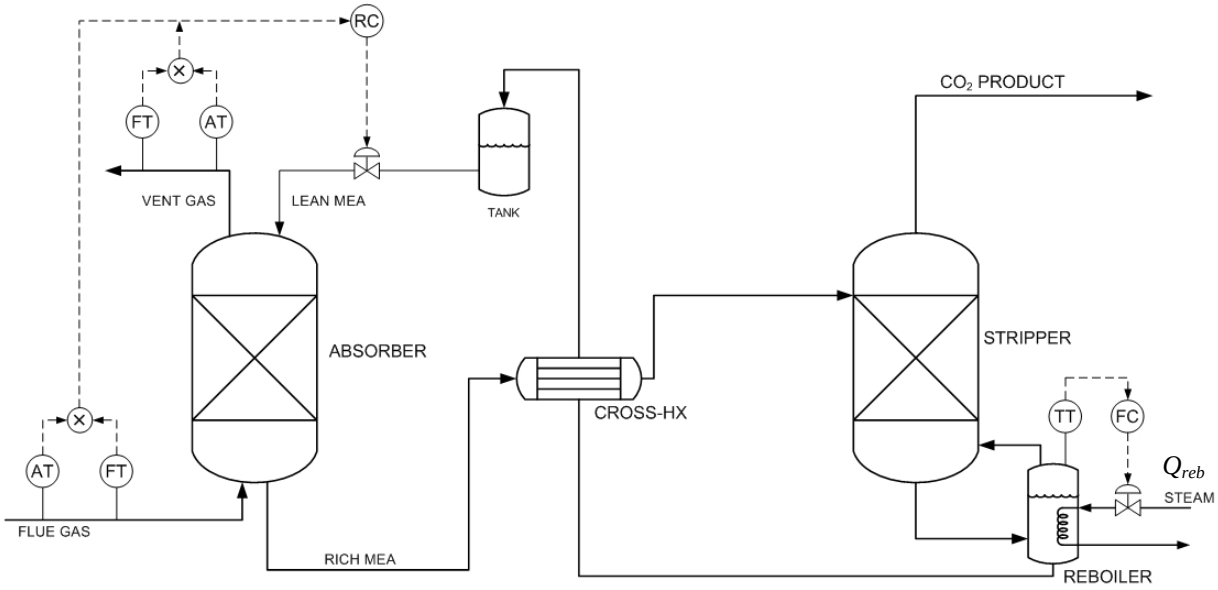

AT: Composition transmitter, FT: Flow transmitter,TT: Temperature transmitter, RC: Ratio controller FC: Flow controller

Figure 5.1: The proposed control structure for CO_2 capture process

Based on the pairings between the manipulated and controlled variables selected for this process, a sensitivity analysis between these variables was conducted to determine meaningful tuning parameters for each of the PI controllers considered in the closed-loop system shown in Figure 5.1. The sensitivity analysis was performed around the nominal operating conditions considered for this system. Step changes in the manipulated variables were enforced and the response of the controlled variables to these changes was recorded. The magnitude of the step changes ranged from 5 to 20% with respect to the manipulated variables' nominal operating condition. The controlled variables' response to those in the manipulated variables was approximated to a first-order linear model so that the process gain (K_p) and the time constant (τ_p) of the process can be determined. As it is shown below, this model was suitable because no overshoots or time delays were observed in the process response of the controlled variables to changes in the manipulated variables. The first order process response in the time domain, Δy to a step change in a manipulated variable of magnitude ΔM is represented as follows (Seborg et al., 2003),

$$\Delta y(t) = K_p \Delta M \left(1 - e^{-\frac{t}{\tau_p}}\right) \quad 5.2$$

where Δy is the response of the controlled variable to a step change of magnitude ΔM in the manipulated variable. The process gain is determined by calculating the ratio of the steady-state change in the controlled variable (Δy) to the size of the input step change (ΔM) as shown in the following equation:

$$K_p = \frac{\Delta y}{\Delta M} = \frac{y_{new,ss} - y_{t=0}}{M_{new,ss} - M_{t=0}} \quad 5.3$$

where $y_{new,ss}$ and $M_{new,ss}$ are the controlled and manipulated variables' new steady state whereas $y_{t=0}$ and $M_{t=0}$ are the controlled and manipulated variables' initial steady-state. The time constant (τ_p) in (5.1) can be estimated from the step response of the controlled variable plot using the value of time at which the response is 63.2 % complete (Seborg et al., 2003).

Step changes of magnitude $\pm$5% from the initial steady state in the valve stem position, which determined the lean solvent flow rate, were introduced in the dynamic process model. The process response of the CO_2 absorbed to these changes was recorded and used to determine the first-order process model parameters that capture the key process characteristics between these input-output variables. Small step changes were introduced in the open loop process in order to design a controller around the nominal operating conditions. The process response plot of the controlled variable (% CO_2 absorbed in the absorber column) to these step changes is depicted in Figure 5.2. As shown in this Figure, a 0.5% change in the percentage of CO_2 absorbed was observed for the +5% step test while a 2% change in the same process variable was observed when the flue gas flow rate was reduced by 5%. This result shows the degree of nonlinearity in the process. The process response data from Figure 5.2 was used to fit the first-order model for this input-output process data using the least-squares method. Figure 5.3 and Figure 5.4 (see dotted line) show the fitting of the first-order linear model to the actual process data when a positive and a negative change in the magnitude of the valve stem position was induced in the system, respectively. As shown in Figure 5.3, the model slightly over predicted the process response

at time less than 2 hrs for step change with magnitude +5%. On the other hand, the model slightly under predicted the process response at time less than 4 hrs for a step change with magnitude -5% (see Figure 5.4). Overall, both models were able to give reasonable predictions for the changes in the valve stem position considered in this analysis. Figure 5.3 and Figure 5.4 also shows the degree of nonlinearity of this process, i.e., the modeling fitting shows that the process model is nonlinear and not follow exactly first-order linear model.

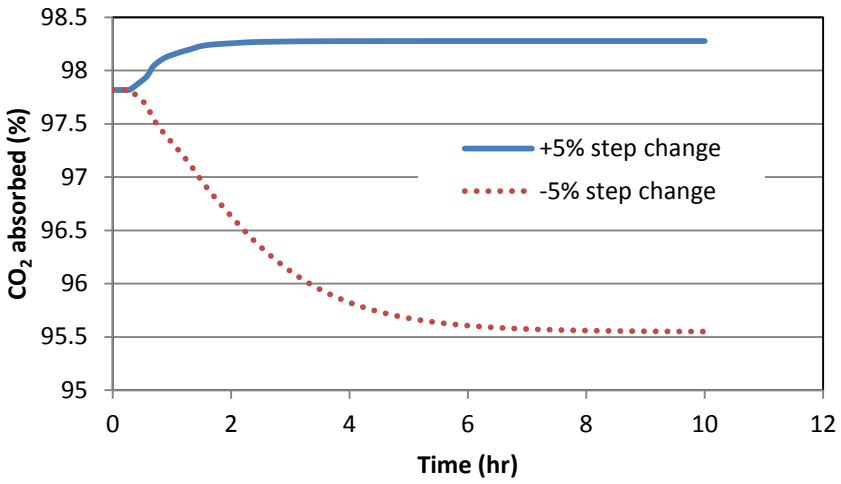

Figure 5.2: The percentage of CO_2 absorbed during step change

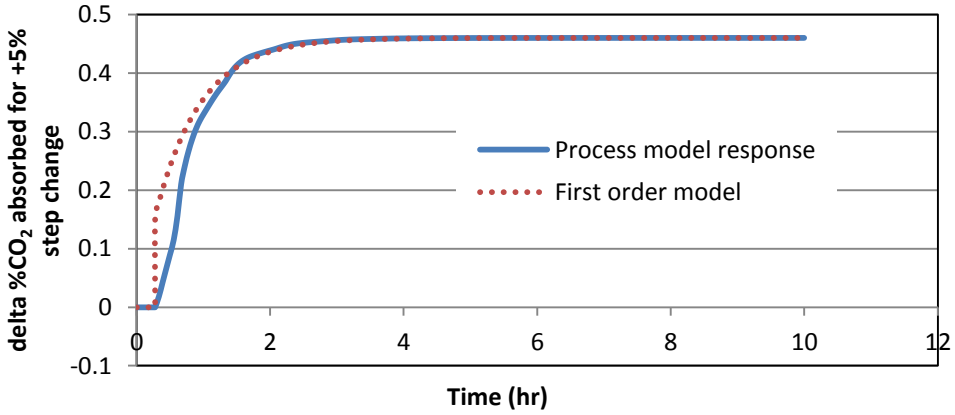

Figure 5.3: First order model approximation for Δ%CO_2 absorbed during +5% step change

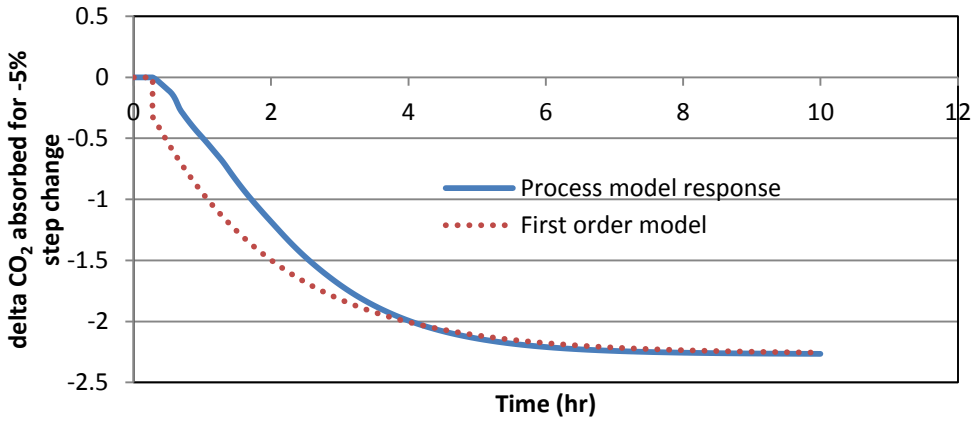

Figure 5.4: First order model approximation for $\Delta\%CO_2$ absorbed during -5% step change

Table 5.1 shows the process gain and the time constant obtained for the first-order linear model. As shown in this Table, the process response for a -5% step change has larger process gain and time constant when compared to the +5% step. The process model parameters shown in Table 5.1were averaged to obtain a representative description of the CO_2 absorbed due to changes in the valve stem position. The averaged process model parameters were used to determine the initial PI controller tuning parameters using the IMC method.

Table 5.1: Process gain (K_{p1}) and time constant (τ_{p1}) for the CO_2 controller

Changes in valve stem position	Process gain, K_{p1} (K)	Time constant, τ_{p1} (hr)
+5%	22.324	0.68
-5%	109.953	1.85
Average value	66.138	1.26

Four step changes with magnitude $\pm$10% and $\pm$20% from the nominal operating conditions in the reboiler heat duty were imbedded in the process model to determine the first-order model parameters to design the reboiler temperature controller. Figure 5.5- Figure 5.8 shows

the temperature to the changes made in the reboiler heat duty. As for the CO_2 absorbed controller, first order process models were used to represent the transient behavior between the reboiler heat duty and reboiler temperature. The fitting of the first order process models gives good prediction to the actual process data in shown in Figure 5.5-Figure 5.8 (dotted line).

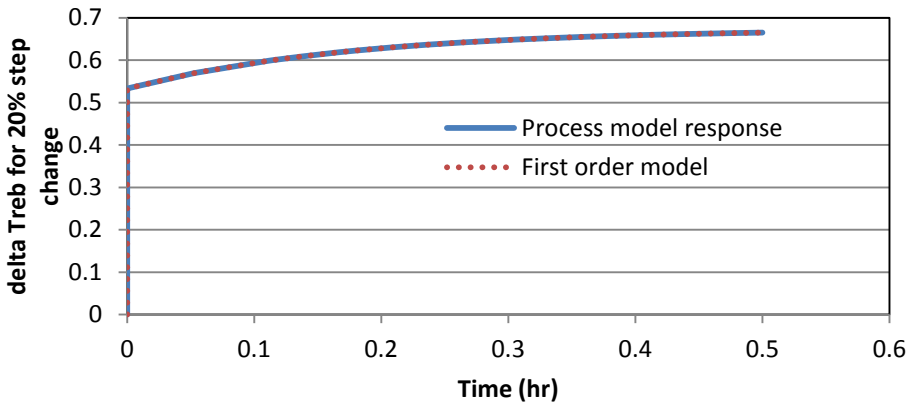

Figure 5.5: Process response and first order model for ΔT_{reb} during +20% heat duty step reduction

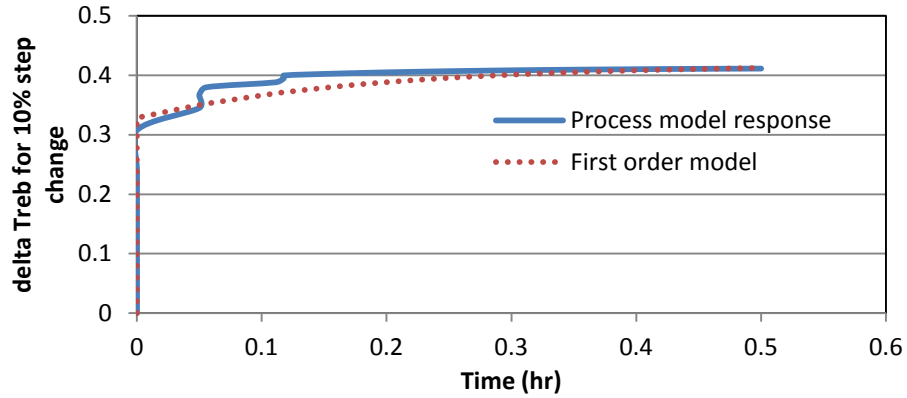

Figure 5.6: Process response and first order model for ΔT_{reb} during +10% heat duty step reduction

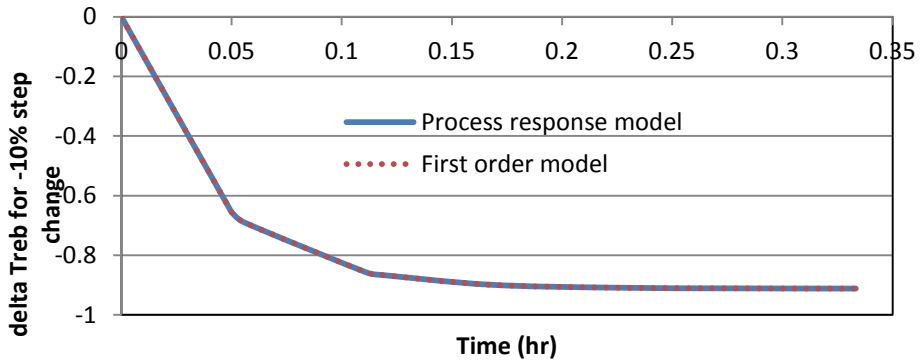

Figure 5.7: Process response and first order model for ΔT_{reb} during -10% heat duty step reduction

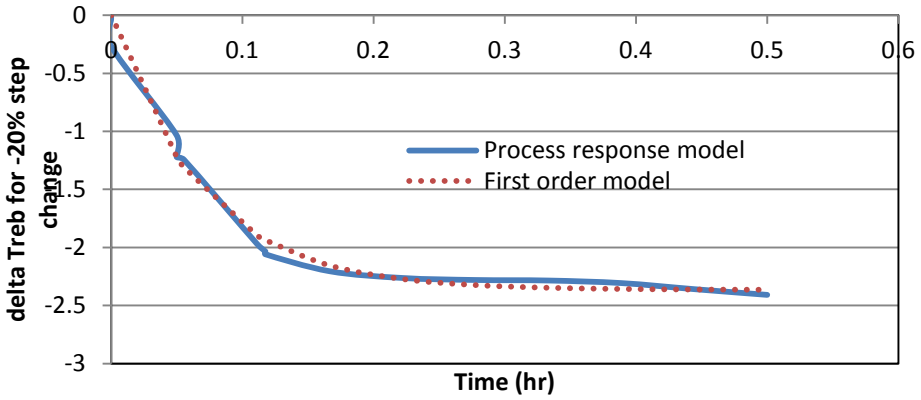

Figure 5.8: Process response and first order model for ΔT_{reb} during -20% heat duty step reduction

Table 5.2 shows the process model parameters, i.e., the process gains and the time constants, obtained for reboiler temperature's response due to the step changes in the reboiler heat duty. As shown in Table 5.2, the process gains estimated for the reboiler temperature due to changes in the reboiler heat duty are significantly small. In order to confirm this behaviour, steady simulations using standalone flash model in Aspen Plus® simulation were conducted. The process operating conditions, i.e., molar flow rate, temperature, molar composition and reboiler heat duty used in the gPROMS process model were used as the process inputs to the flash model in the Aspen Plus®. The reboiler temperature, and the resulting process gains, from the Aspen Plus® simulation are shown in Table 5.3. As shown in this Table 5.3, the

process gains obtained from Aspen Plus® are of the same order of magnitude to those obtained with the gPROMS model. Also, the difference between the temperature estimated using the gPROMS model and Aspen Plus® was less than 0.4%. This result confirms the process gains obtained with the gPROMS model developed in this work. In addition, the time constant observed for the different step changes increased was higher than step decreased as shown in Table 5.2. The process gains and the time constants shown in Table 5.2 were averaged to obtain a representative description of the reboiler temperature due to changes in the reboiler heat duty.

Table 5.2: Process gain (K_{p2}) and time constant (τ_{p2}) for reboiler temperature controller

Reboiler heat duty (W)	Process gain, K_{p2} (K/W)	Time constant, τ_{p2} (hr)
186000 (+20%)	2.172×10^{-5}	0.18
170500 (+10%)	2.696×10^{-5}	0.18
139500 (-10%)	2.940×10^{-5}	0.07
124000 (-20%)	7.636×10^{-5}	0.04
Average value	3.861×10^{-5}	0.12

Table 5.3: Reboiler temperature and process gain for heat duty step changed obtained from Aspen Plus® simulation

Reboiler heat duty (W)	Reboiler temperature (K)		Process gain, K_{p2} (K/W) from Aspen Plus® simulation
	gPROMS	Aspen Plus®	
186000	389.7	389.6	4.415×10^{-5}
170500	389.5	389	5.235×10^{-5}
139500	388.1	387	7.786×10^{-5}
124000	386.6	385	9.918×10^{-5}
Average value			6.838×10^{-5}

For the controller structure proposed in this work (see Figure 5.1), the manipulated variables, i.e. the valve stem position (α_f) and reboiler duty (Q_{reb}) value, are adjusted with the PI controller equations:

$$\alpha_f = \overline{\alpha_f} + K_{c1}e_1 + \frac{K_{c1}}{\tau_{I1}}\int e_1 \ \mathrm{dt} \tag{5.4}$$

$$Q_{reb} = \overline{Q_{reb}} + K_{c2}e_2 + \frac{K_{c2}}{\tau_{I2}}\int e_2 \ \mathrm{dt} \tag{5.5}$$

where $\overline{\alpha_f}$ and $\overline{Q_{reb}}$(J/s) are the valve stem position and the reboiler heat duty at nominal operating conditions, respectively; K_{c1} and K_{c2} are the proportional controller gains for CO_2 ratio controller and reboiler temperature controller, respectively; e_1 and e_2 is the controller errors for CO_2 ratio controller and reboiler temperature controller, respectively; τ_{I1}(s) and τ_{I2}(s) are the integral time constants for the CO_2 ratio controller and the reboiler temperature controller, respectively. The valve stem position and reboiler heat duty will be adjusted to compensate for the deviations in the CO_2 absorbed and reboiler temperature due to changes in the disturbance (flue gas flow rate). The controller errors are calculated as follows:

$$e_1 = CV_{1,sp} - CV_1 \tag{5.6}$$

$$e_2 = CV_{2,sp} - CV_2 \tag{5.7}$$

where $CV_1$and CV_2 are the measured controlled variable for CO_2 ratio controller and reboiler temperature controller, respectively; $CV_{1,sp}$ and $CV_{2,sp}$ are the controller variable set point for CO_2 ratio controller and reboiler temperature controller, respectively. The PI feedback controllers will adjust the manipulated variables such that the controller error is minimized or close to zero.

The averaged model parameters, i.e. process gain (K_p) and time constant (τ_p), obtained from the first order model fitting were used to determine the PI feedback controller tuning parameters using Internal Model Control (IMC). The IMC-based PI feedback controller settings were calculated as follows (Seborg et al., 2003):

$$K_pK_c = \frac{\tau_p}{\tau_c} \qquad \tau_I = \tau_p \tag{5.8}$$

where K_c is the proportional controller gain, τ_c (s) is the closed loop time constant. The closed-loop time constant for the system (τ_c) is assume to be equal to process time constant (τ_p). The resulting controller tuning parameters are shown in Table 5.4.

Table 5.4: PI feedback controller parameters

Controller	Controller gain, K_c	Time integral, τ_I (hr)
CO_2 ratio	0.0151	1.26
Reboiler temperature	25900	0.12

The controller setting obtained from this method can be considered as educated initial controller settings that can be further adjusted to improve the closed-loop performance of the MEA process.

5.3 Control strategy implementations

Using the control configuration shown in Figure 5.1, a series of closed loop dynamic simulations were performed in the system to study the performance of the control system in response to changes in the disturbance. The disturbance investigated in this work was the flue gas flow rate. The following sections discuss the response of process variables in the closed loop system for the regulatory problem (disturbance changes).

5.3.1 Ramp change in the flue gas flow rate

The performance of the control structure proposed in the previous section, aimed to maintain the percentage of CO_2 absorbed and reboiler temperature near their desired operating conditions, was tested by changing the flue gas flow rate in a ramp fashion. As shown in Figure 5.9, the flue gas flow rate was increased (decreased) linearly by 10% within 2.8 hrs of operation and remained at that condition for about 8 hrs. During the simulation of 10% reduction in the magnitude of the flue gas flowrate with respect to its initial steady state value, the process response for the CO_2 ratio controller using the controller settings shown in Table 5.4 was very slow such that the controlled variable was not able to reach its set point

value after 10 hours (See solid line in Figure 5.10). As shown in Equation 5.4 and 5.5, increasing the integral control action, i.e., decreasing the τ_I, makes the response of closed loop system more sensitive which reduces the settling time (faster response) but it may also produce oscillations into the system. Also, a small integral time (τ_I) or a large controller gain (K_c) may eventually lead to process instability. Therefore, in order to obtain a faster closed loop response, the process gain and time integral for the PI controller that controls the CO_2 absorbed were manually tuned so that the controlled variable returned to its set point value in a smooth fashion and within a reasonable closed-loop settling time. Accordingly, the PI CO_2 ratio controller's gain and time constant were set to 0.1 and 0.8 hr, respectively. The dotted line in Figure 5.10 shows the CO_2 absorbed's response using the new tuning controller parameters for this control loop. As shown in this Figure, the process response returned to the set point value with no oscillations after 6 hours of simulation.

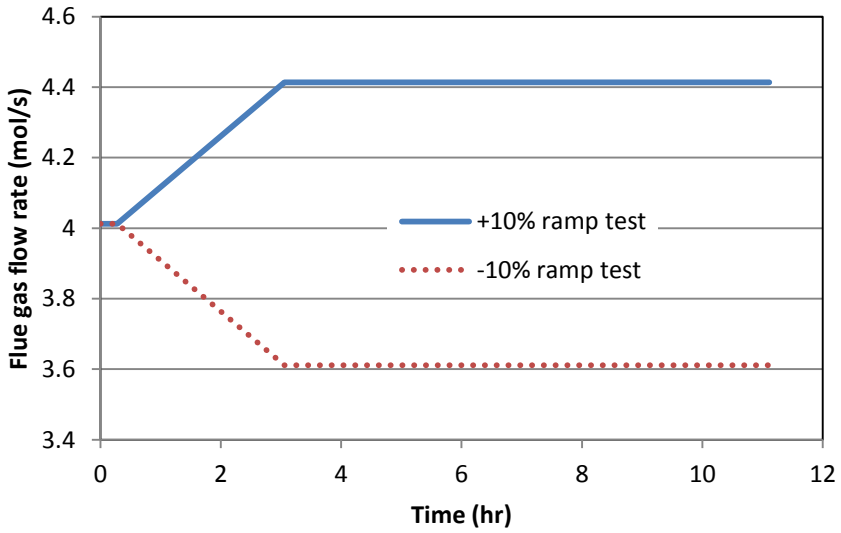

Figure 5.9: Flue gas flow rate for disturbance rejection test

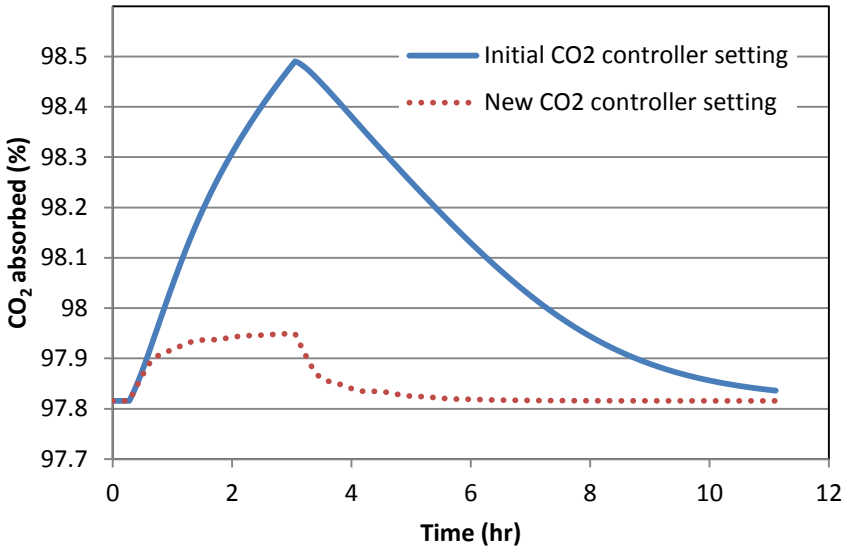

Figure 5.10: Controlled variable response using different controller setting

Figure 5.11 shows the percentage of CO_2 absorbed in the absorber column when a $\pm$10% ramp change in the flue gas flow rate was considered in the analysis. As shown in this Figure, the percentage of CO_2 absorbed was slightly decreased (increased) at the onset of the disturbances. The integral term in the PI feedback controller continues to change as long as there is a non-zero error (see Figure 5.12). Due to the PI feedback controller action, the lean solvent flow rate linearly increased (decreased) as depicted in Figure 5.13. The lean solvent flow rate was increased by 16% and decreased by 13% from its initial steady state condition due to the changes in valve stem position, respectively. As the flue gas flow rate was increased, more lean solvent was required to react with CO_2, so that the amount of CO_2 absorbed can be maintained. The opposite behaviour was observed when the flue gas flow rate was reduced using a change of type ramp.

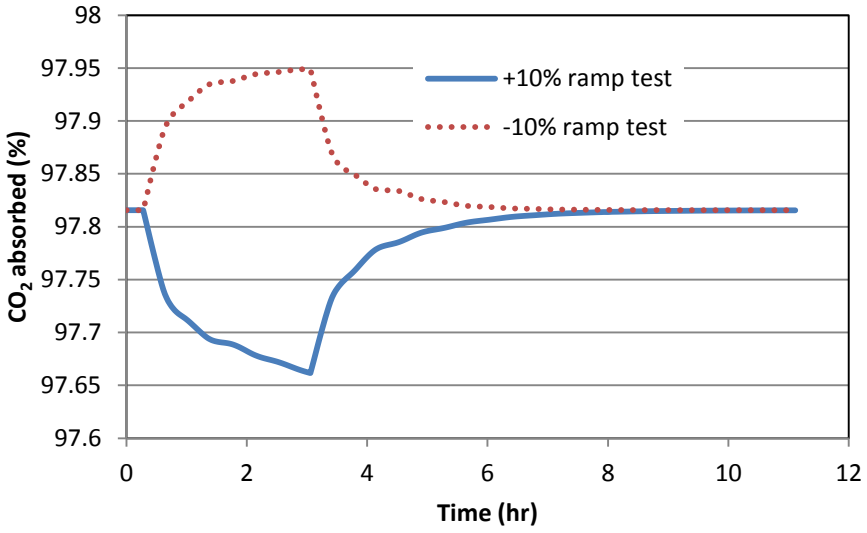

Figure 5.11: The percentage of CO_2 absorbed during disturbance rejection test

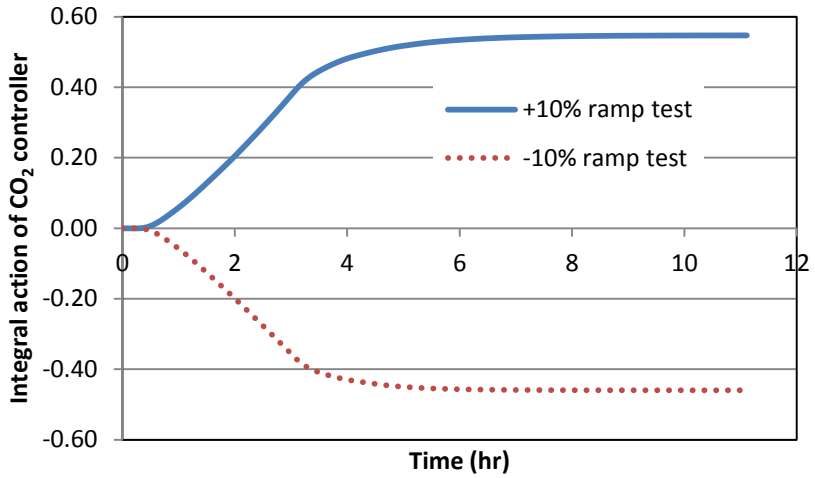

Figure 5.12: Integral action of CO_2 controller during disturbance rejection test

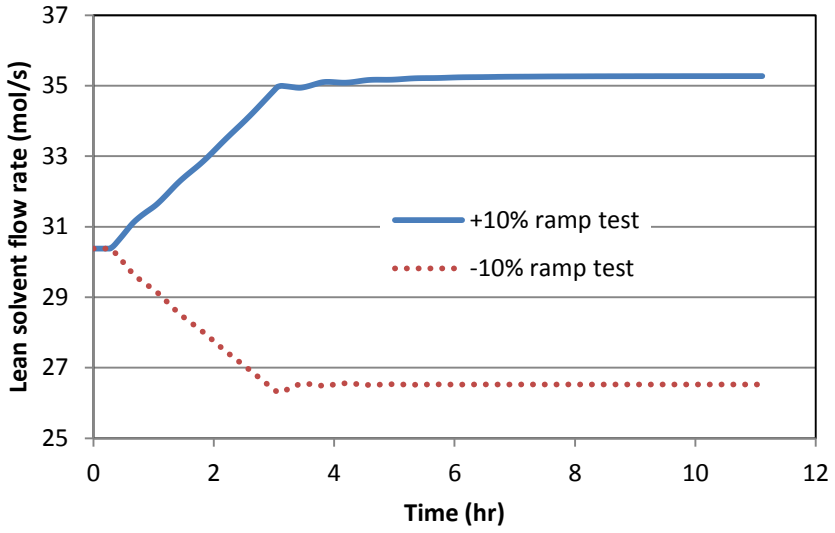

Figure 5.13: Lean solvent flow rate during disturbance rejection test

The responses shown in Figure 5.14 illustrate the behaviour of the reboiler temperature when ramp changes in flue gas flow rate were induced. As shown in this Figure, the reboiler temperature was slightly decreased (increased) at the start of disturbance tests because the inlet temperature of the reboiler was decreased (increased). As a result, the manipulated variable, which is the reboiler heat duty, was slightly increased by a magnitude of 20% (decreased with magnitude of 16%) from the nominal operating conditions to compensate for this error until the reboiler temperature reaches the set point value after 6 hours of operation (See Figure 5.15). As shown in Figure 5.16, the changes in the reboiler heat duty also affected the liquid temperature at the bottom of the stripper column. The liquid temperature at the bottom of the stripper column slightly decreased (increased) due to less (more) heat supplied from the reboiler during the course of the disturbance tests. The PI feedback controller output as shown in Figure 5.17 was changing until it reached a new steady state to minimize the error between the measured reboiler temperature and its set point value.

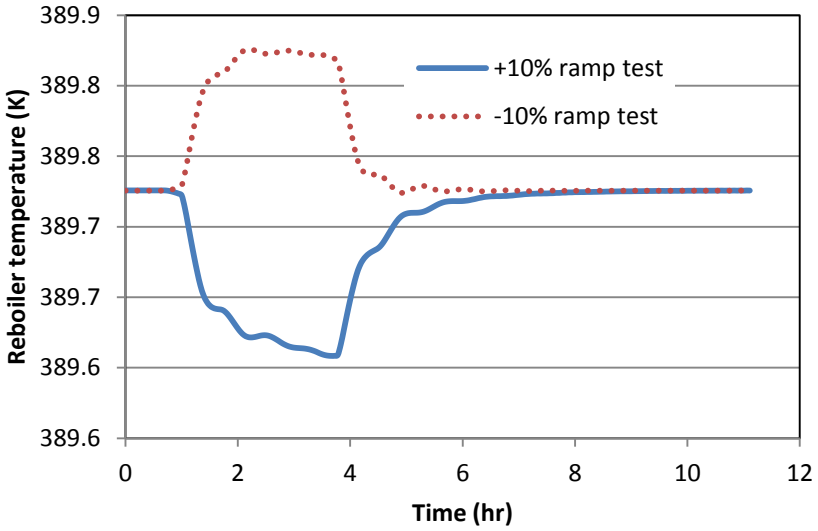

Figure 5.14: Reboiler temperature during disturbance rejection test

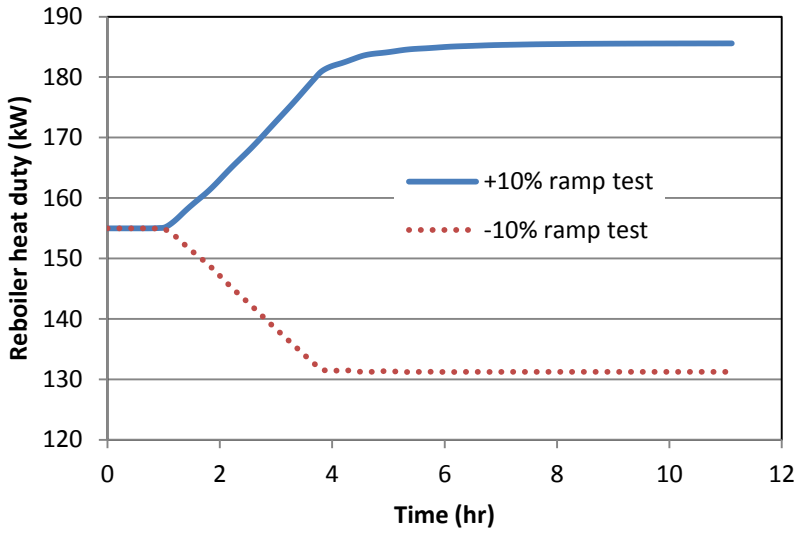

Figure 5.15: Reboiler heat duty during disturbance rejection test

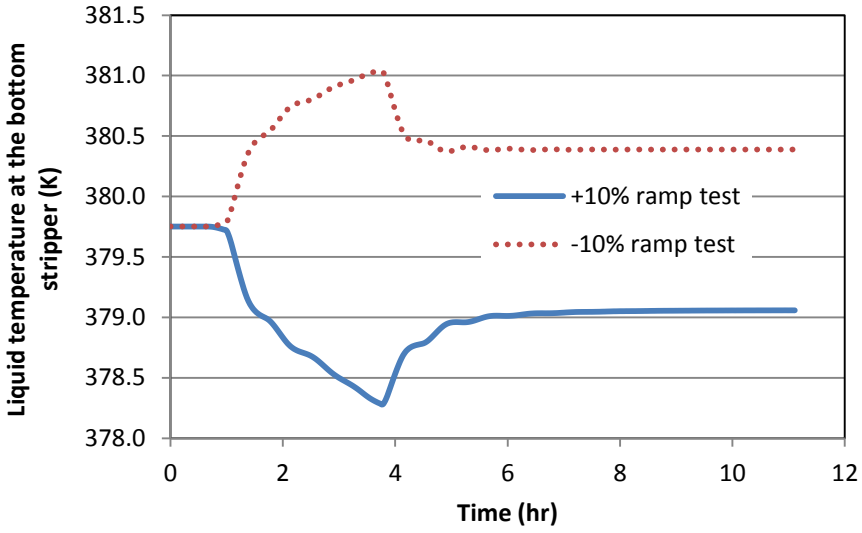

Figure 5.16: Liquid temperature profile at the bottom of stripper during disturbance rejection test

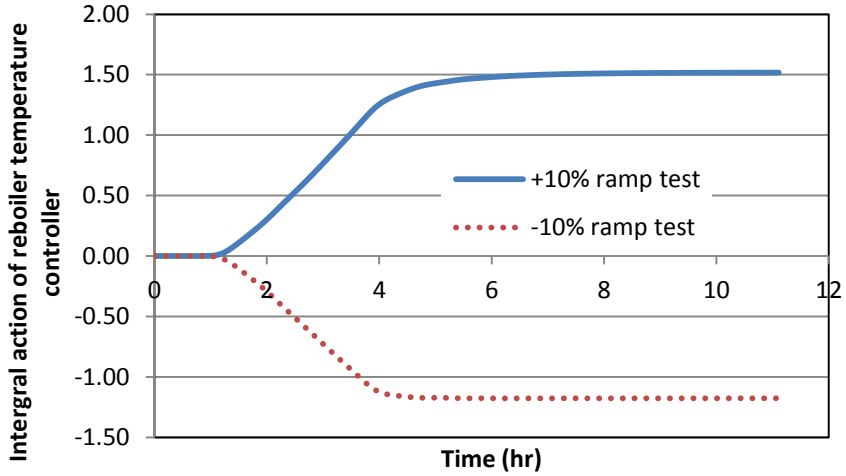

Figure 5.17: Integral action reboiler temperature controller during disturbance rejection test

5.3.2 Sinusoidal changes in the flue gas flow rate

The dynamic behaviour of the process variables in response to the sinusoidal changes in the flue gas flow rate for a system that is controlled using two PI feedback controllers is discussed in this section. The flue gas flow rate was varied in sinusoidal fashion with a

constant amplitude, 10% change with respect to its nominal steady state value, a with a period of 1 day. The complete MEA plant was simulated under the effect of this sinusoidal behaviour in the flue gas flow rate for a period of three days (see Figure 5.18). The sinusoidal change in the flue gas flow rate is used to represent the actual fluctuations in a real power plant output (see Figure 4.44). For comparison purposes, an open loop test using the same sinusoidal function in the flue gas flow rate was conducted and compared to that obtained under closed-loop. The open loop test refers to the case when the controllers are not acting on the system (controllers deactivated) while the closed loop tests takes into account the controller actions to maintain the process controlled variables, i.e., the CO_2 absorbed and the reboiler temperature, at its set point values. The dynamic behaviour of the open loop system has been discussed in Section 4.7.4. The response of the process variables for the open and the closed loop system were plotted on the same graph to study the effect of controller action during the sinusoidal disturbance rejection. As shown in Figure 5.19, the percentage of CO_2 absorbed reached a minimum value of 93.6% at the maximum flue gas flow rate and a maximum of 98.7% at a minimum flue gas flow rate when the system was simulated in open loop. On the other hand, the controlled variable (see dotted line in Figure 5.19) fluctuated around its set point value (varied between 97.76% to 97.86%) due to the controller action in the case of the closed-loop test. This result shows the benefit of implementing a control strategy for the MEA process. Nevertheless, in order for the control system to maintain the CO_2 absorbed at its set point value, large changes in the manipulated variable, i.e., the valve stem position that regulates the lean solvent flow rate entering the absorber, needs to be made. That is, the variability of the CO_2 absorbed observed in the open loop test was transferred to the manipulated variable, i.e. valve stem position, in the closed-loop test; this lead to the adjustment of the lean solvent flow rate as shown in Figure 5.20 (see dotted line). The PI feedback controller adjusted the manipulated variable to minimize the controller error. The integral action of the PI feedback controller keeps changing as long as non-zero errors exist in the process (see Figure 5.21). The controller output cause the valve stem position to increase (decrease) when the flue gas flow rate is increased (decreased) so that more (less) lean solvent is supplied to the absorber to absorb the CO_2. For the open loop test,

the minimum (maximum) CO_2 is absorbed at maximum (minimum) flue gas flow rate due to the small changes in lean solvent flow rate as shown in Figure 5.22. On the other hand, the lean solvent flow rate fluctuates at higher value for the closed loop system compared to the open loop system (see Figure 5.23). The lean solvent flow rate for the closed loop system is increased with a magnitude of 16% from its initial steady state value and decreased by a magnitude of 13% from its initial steady state value in order to maintain the percentage of CO_2 absorbed around its set point value. The fluctuation in the lean solvent flow rate follows the flue gas flow rate profile for both the open and the closed loop tests, respectively.

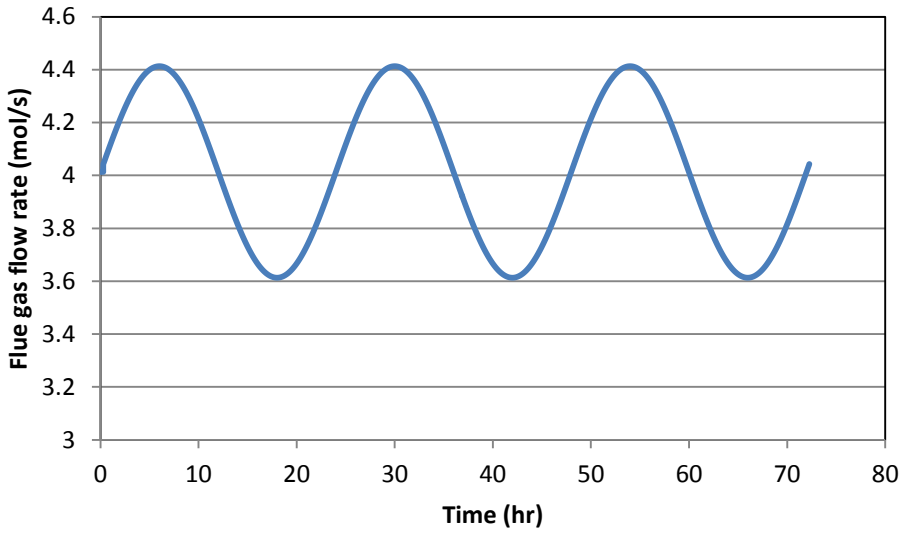

Figure 5.18: Sinusoidal flue gas flow rate

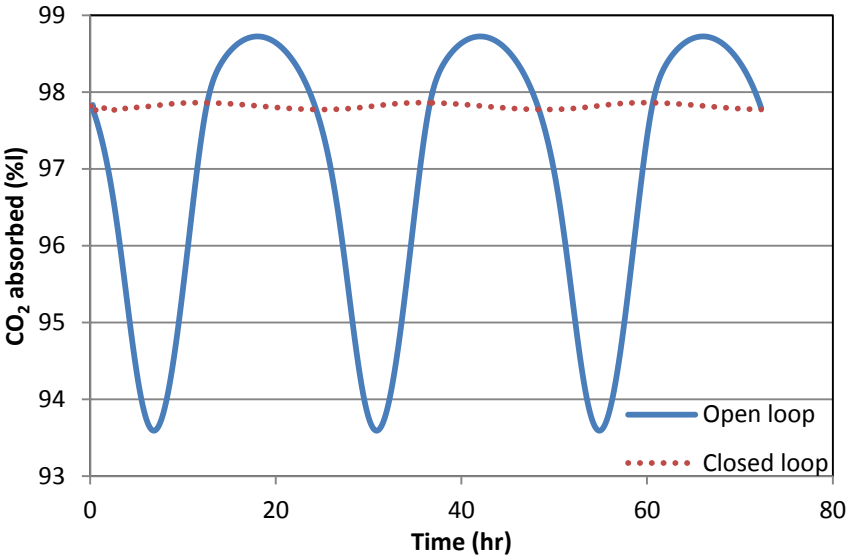

Figure 5.19: Controlled variable profile during sinusoidal disturbance rejection

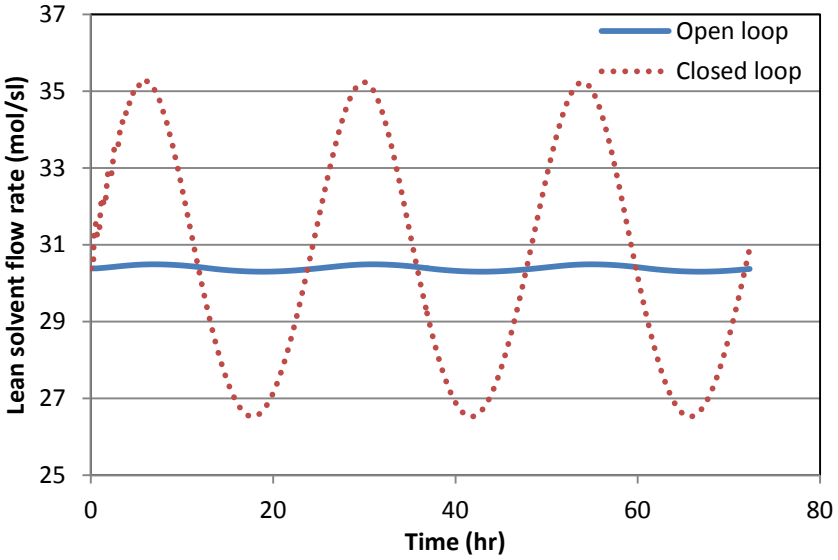

Figure 5.20: Lean solvent flow rate during sinusoidal disturbance rejection

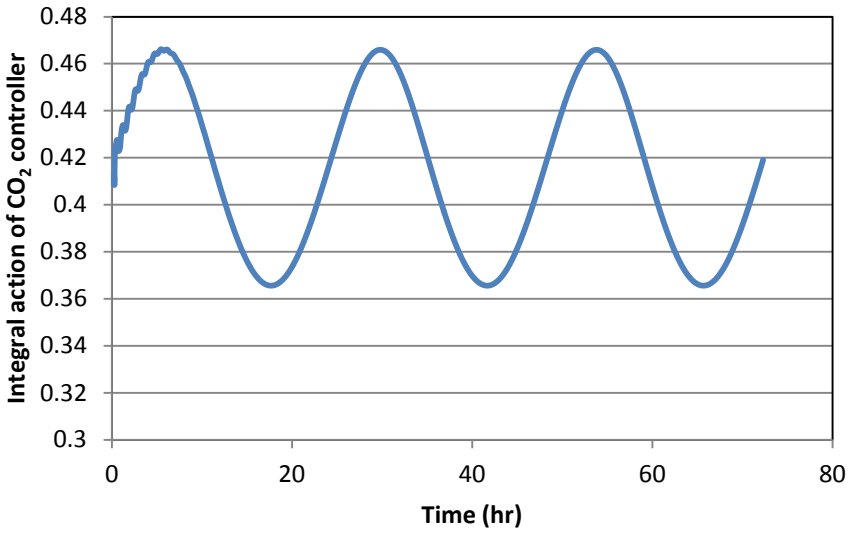

Figure 5.21: Integral action of CO_2 controller during sinusoidal disturbance rejection

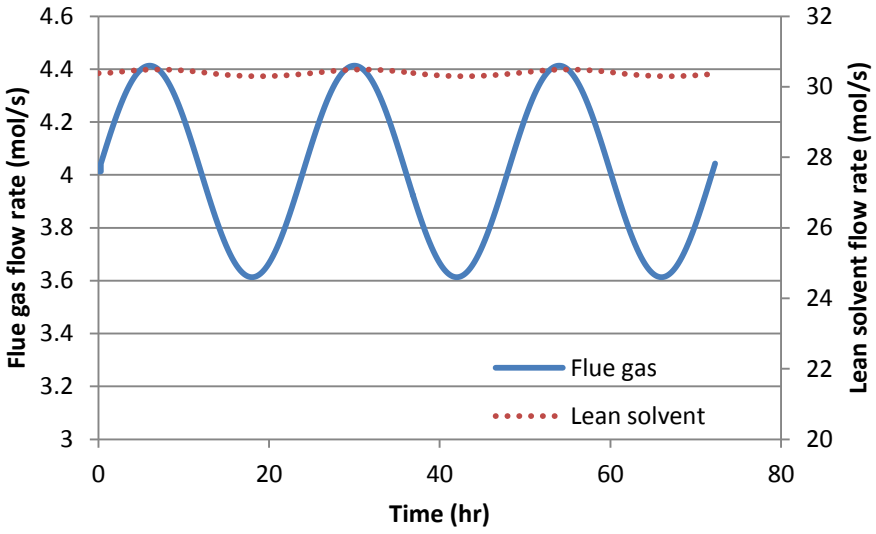

Figure 5.22: Flue gas and lean solvent flow rate for open loop system

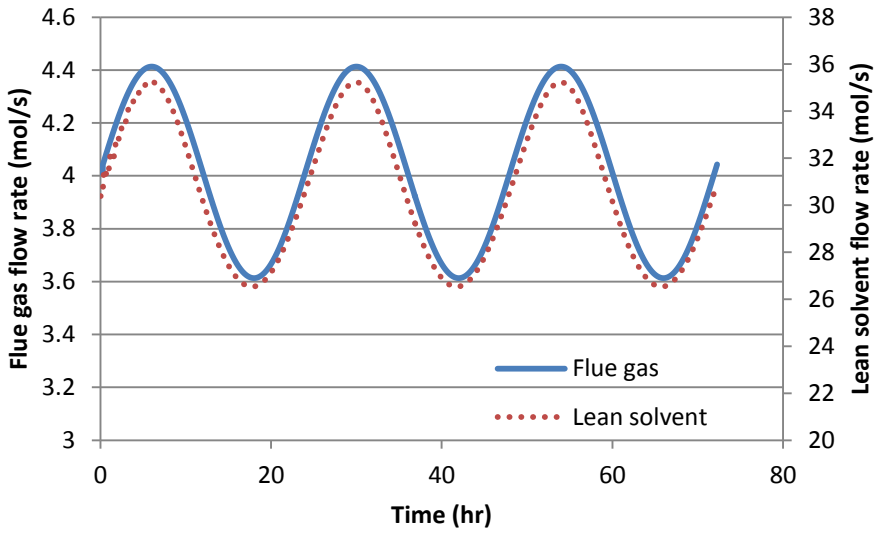

Figure 5.23: Flue gas and lean solvent flow rate for closed loop system

Figure 5.24 shows the response of the reboiler temperature to a sinusoidal change in the flue gas flow rate. As shown in this Figure, the reboiler temperature profile for the closed loop system oscillated around it set point value. However, the amplitude of the oscillations is smaller to those observed to the open-loop test for this variable. The reboiler temperature response for the open loop system also shows a lag behind the closed loop system. For the closed loop system, as the PI feedback controller output changed in response to a change in the reboiler temperature, the reboiler heat duty was adjusted to minimize the controller error. As shown in Figure 5.25, the heat duty increased (decreased) when the reboiler temperature decreased (increased) to keep the controlled variable near its set point value. The reboiler heat duty reached the maximum value of 185 kW and minimum value of 130 kW to minimize the controller error which represent +20% and -16% from the initial steady state value, respectively. The integral action of PI controller changes over time to integrate the non-zero error (see Figure 5.26).

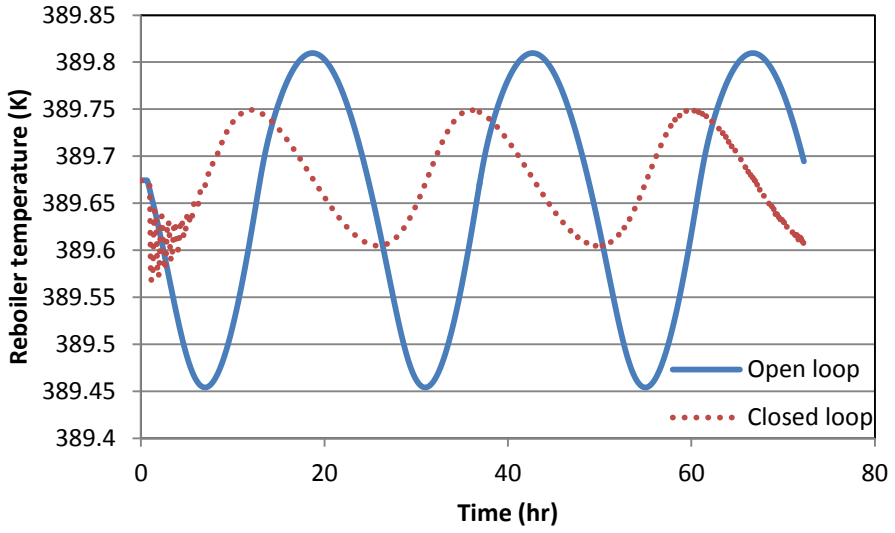

Figure 5.24: Reboiler temperature profile during sinusoidal disturbance rejection

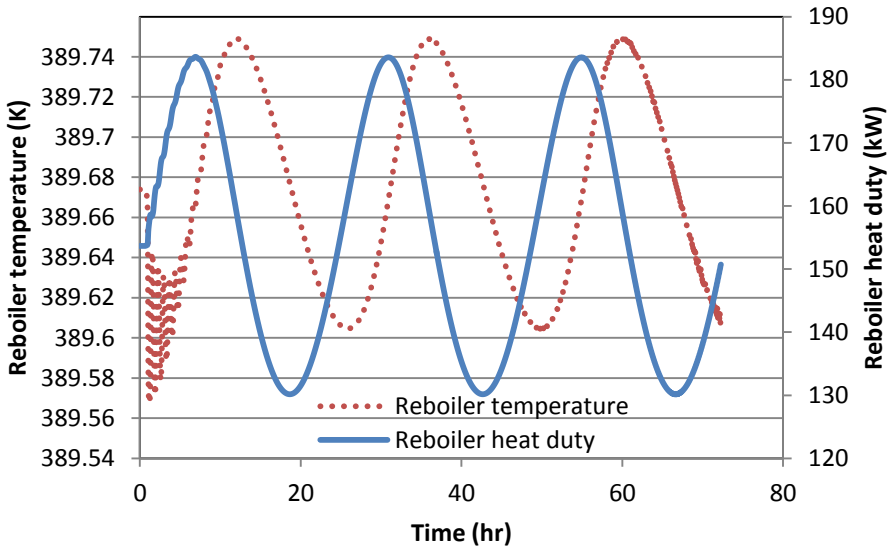

Figure 5.25: Reboiler heat duty and temperature profile during sinusoidal disturbance rejection

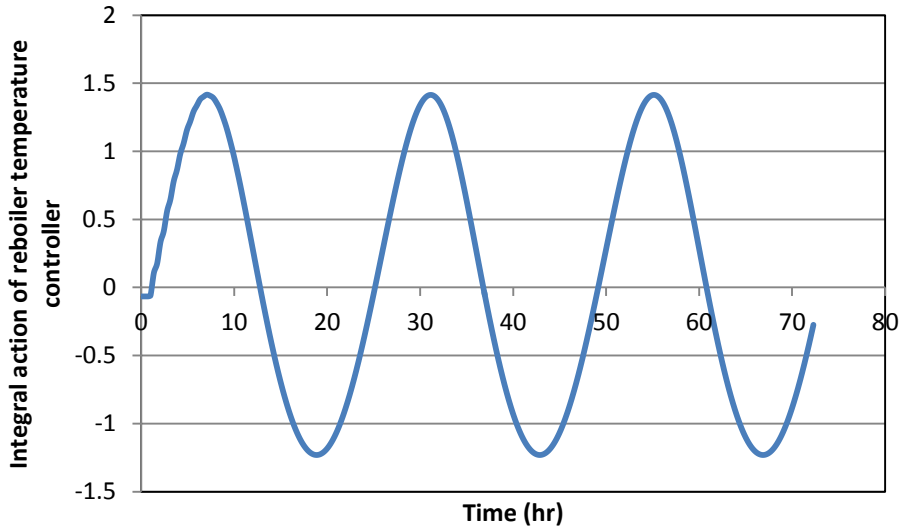

Figure 5.26: Integral action of reboiler temperature controller during sinusoidal disturbance rejection

5.4 Chapter summary

This chapter has presented a basic feedback control system for the CO_2 capture process so that the percentage of CO_2 absorbed and the reboiler temperature are maintained around its nominal set points while manipulating valve stem position that determines the lean solvent feed flow rate to the top of the absorber column and the reboiler heat duty. Open loop step tests were performed by changing the manipulated variables' magnitudes to determine a process model for these input-output data sets. The resulting response of the controlled variables obtained from the step tests were recorded and approximated to a first order process model. The first order process model parameters, i.e., process gain (K_p) and time constant (τ_p), were used to design PI feedback controller using IMC tuning method. The controllers implemented in the process model were tested for disturbance rejection by imposing a ramp and a sinusoidal change in the flue gas flow rate. For the ramp test, the PI feedback controllers maintained the controlled variables near their target values with no oscillations. The valve stem position was adjusted such that the lean solvent flow rate was increased (decreased) by 16% (13%) from the nominal operating conditions during the increased

(decreased) of flue gas flow rate. The reboiler heat duty was increased by magnitude of 20% (decreased by magnitude of 20%) from its nominal operating condition to keep the reboiler temperature near to its set point value during the course of disturbances. For the sinusoidal tests, the controllers were able to keep the controlled variables varies at their set point values by reducing its variability. The variability of the controlled variables was transferred to the manipulated variable due to the controller action which caused a large deviation in the magnitude of the manipulated variables. The lean solvent flow rate was increased by 16% from its initial steady state condition for 10% increased in flue gas flow rate to maintain the percentage of CO_2 absorbed. Likewise, the heat duty was changed between 130 to 185 MW which represent a change between -16% and +20% with respect to its initial steady state value to maintain the reboiler temperature at the desired set point value. The results obtained from the present analysis showed that the control strategy developed in this work is a promising control structure that can be used to control the key process variables in the MEA CO_2 capture process.

Chapter 6
Conclusions and Recommendations

6.1 Conclusions

- In this study, a mechanistic dynamic MEA absorption process model for CO_2 capture from a fossil fuel power plant was developed using gPROMS. This mechanistic dynamic model provides the basic modelling tools to study the transient behaviour of this process in the presence of external perturbations to the system, e.g., changes in the flue gas flow-rate. The model developed in this research can be used as a practical tool to develop operational policies for this process, i.e., shut down or start-up policies, to determine the optimal operating conditions while considering the transient behaviour of the system, to estimate the optimal design of the process units and to propose control structures that can meet the performance specifications in the presence of external perturbations or uncertainties in the process model parameters.
    - The complete MEA absorption process model considered in this study consists of an absorber, a stripper, a cross heat exchanger and a storage tank. Mathematical models for each unit involved in this process were developed based on conservation laws of mass and energy. The storage tank was used in the present system to attenuate the potential variations coming from the stripper column. A counter-current shell and tube heat exchanger was used to develop the cross heat exchanger model in this work.
    - MEA capture process model was implemented in gPROMS. Providing arbitrary initial guesses for the unknown variables will cause failure at the start of simulation. Thus, a simulation strategy was developed in this work to obtain educated initial guesses for the dynamic simulation of the integrated MEA process. Educated initial guesses for the complete process were determined from the steady state solution of the simulation of the individual units.

- The validation of the complete MEA absorption process model in the dynamic fashion could not be done because relevant dynamic data from an existing pilot plant were not available. However, the performance of the absorption column was validated at steady-state because data available (Dugas, 2006). The model comparison for the complete plant model in terms of flow rate, component composition and temperature in the stream outlet have proven to be in reasonable agreement with Aspen Plus® simulation at different operating conditions. Overall, the percentage differences between the gPROMS model and Aspen Plus® was less than 10%.
- The estimation of some of the process model parameters, namely the vapour liquid equilibrium constant (K_{value}), has been challenging since analytical methods available in the open literature yielded large deviations (>10%) in terms of component compositions in the vapour and liquid phases when compared to Aspen Plus® simulation results due to the difference in the K_{value}. Thus, linear regression correlations, based on Aspen Plus® values of the K_{value} parameter were developed to obtain accurate estimates of the component composition in the reboiler model. A similar approach was applied for MEA and H_2O component to ensure a consistency in calculating the K_{value} in this study. The resulting model used to estimate the equilibrium constant was validated against Aspen Plus® simulation results.
- The dynamic simulation of the complete process model requires lengthy computational times (in the order of days) because the process model involves the simultaneous solution (in the time and spatial domain) of partial differential equations combined with algebraic and ordinary differential equations. Note that the model was simulated using a computer with the following specifications: Intel® Core™2 processor, 2.67 GHz, 1.99 GB of RAM.

- Ramp, step and sinusoidal input tests were imposed on the process disturbances to study the dynamic behaviour of the CO_2 capture process. The two main disturbances

affecting the operation of the CO_2 capture process are changes in flue gas flow rate and changes in reboiler heat duty. Both of them were investigated in this work. The response of key process variables, i.e., percentage of CO_2 absorbed, liquid to gas ratio (L/G ratio), rich loading, and reboiler temperature, due to changes in the flue gas flow rate and reboiler heat duty were analyzed and presented in this work.

  - The changes in flue gas flow rate did not significantly affect the reboiler temperature, which increased only by 0.1% (while keeping the heat duty constant). The transient response observed for CO_2 absorbed followed the behaviour of the lean solvent flow rate. The results obtained in this case study shows that the lean solvent flow rate has a direct and significant effect on the percenatge of CO_2 absorbed. The reboiler temperature response followed a similar behaviour of that of the flue gas flow rate.
  - The reboiler heat duty step test (reduction in the heat duty magnitude by 10%) caused a slight reduction of 0.3% in the reboiler temperature. This small change in reboiler temperature to the reboiler heat duty changes was confirmed with the results obtained from Aspen Plus® simulation. Similarly, the results of this test showed a significant increase in the CO_2 loading (~12.5%) in the liquid stream from the reboiler, which was caused by the reduction in the reboiler temperature.
  - Sinusoidal tests in the flue gas flow rate were used to approximate a typical behaviour for power plant outputs in Ontario. The simulation of this case study required lengthy computational times (~6 days) to complete three days cycles. The present results also showed that the dynamic behaviour of the CO_2 absorbed does not follow exactly the sinusoidal input of flue gas flow rate embedded in the process model. However, it follows the dynamic response of lean solvent flow rate.

- The comprehensive dynamic model developed in this work was used to develop a basic feedback control strategy for this process. Proportional-Integral (PI) feedback controllers were included in the MEA process to maintain the operation of this

process around its nominal (desired) conditions in the presence of external perturbations. The tuning parameters of the PI controllers were obtained using a model-based control strategy, i.e., Internal Model Control (IMC).

- The objectives of control structure implemented for this process are: keep the percentage of CO_2 absorbed in the absorber column at 97%, and maintain the reboiler temperature at 389.75 K. The valve stem position that regulates the lean solvent flow rate entering the absorber and reboiler heat duty were chosen as the manipulated variables.
- The flue gas flow rate was considered as the main source of disturbance for this process and thus it was used to test the control strategy developed in this work. Accordingly, ramp and sinusoidal changes in the flue gas flow rate were incorporated in the process layout to study the performance of the closed loop MEA process.
- The closed-loop tests conducted in this study showed that the MEA process remained stable in the presence of changes in the flue gas flow-rate and comply with the controllability goals specified for this process. Also, the results showed that the variability observed in the controlled variables in the open loop tests was significantly reduced when the control strategy was included in the MEA plant. However, large and sustained changes in the manipulated variables are needed to maintain the controlled variables around their nominal set points. Thus, the variability observed in the controlled variables was transferred to the manipulated variables when the PI controllers were added to the MEA process.

6.2 Recommendations

- Integrate the steam power cycle to the complete MEA absorption process to study the interaction of steam power cycle with CO_2 capture process during transient operation, in particular if the heat to the reboiler is to be provided by extracting a fraction of steam from the steam cycle. The location of the steam cycle from the power plant, i.e., high pressure/immediate pressure/low pressure steam, which affects the quality of the steam used in the reboiler unit, need to be identified so that the steam cycle process can be integrated to the MEA-based CO_2 capture process. A dynamic steam cycle model will need to be developed to integrate it with the dynamic model of the CO_2 capture process.
- The control structure developed in this work was developed using a basic feedback control strategy. However, there are several controllability aspects that can also be considered for the MEA process in the future. For example, a new control strategy can be developed that can take into account the saturation limits on the amount of heat that can be supplied to the reboiler unit and the addition of new control objectives within the analysis such as the quality of the CO_2 leaving the stripper column. Also, a switchability analysis can be conducted to study the ability of the closed-loop process to move between different operating points in the presence of external perturbations and uncertainty in the physical parameters of the plant. Moreover, a centralized control strategy based on Model Predictive Control (MPC) can be proposed and compared to those based on traditional feedback controllers (decentralized strategies) to determine the most suitable control strategy for this process. Furthermore, the design of the plant can be redone using integration of design and control, i.e., the optimal design of the plant, and the optimal operation conditions for the system including the controller tuning parameters, are determined from a steady-state analysis combined with a dynamic feasibility analysis of the process. It is expected that the resulting new process design will be more economically attractive than the current plant's design since it will take into account the process dynamics and the process operability constraints that can efficiently reject the disturbances that may affect the system during its normal operation.

- The dynamic model developed in this research can be embedded within a dynamic optimization formulation to determine optimal operating policies that minimizes the operating costs of this process while meeting the process constraints in the presence of fluctuations in the flue gas flow rate. The outcome from this study is essential to develop new operability policies that will enable the safe and optimum dynamic operation of the MEA absorption process.

Bibliography

Abass A., O. (2010). CO_2 capture and separation technologies for end-of-pipe applications – A review. *Energy, 35*(6), 2610-2628.

Aboudheir, A., Tontiwachwuthikul, P., Chakma, A., & Idem, R. (2003). Kinetics of the reactive absorption of carbon dioxide in high CO2-loaded, concentrated aqueous monoethanolamine solutions. *Chemical Engineering Science, 58*(23-24), 5195-5210.

Abu-Zahra, M. R. M., Schneiders, L. H. J., Niederer, J. P. M., Feron, P. H. M., & Versteeg, G. F. (2007a). CO_2 capture from power plants: Part I. A parametric study of the technical performance based on monoethanolamine. *International Journal of Greenhouse Gas Control, 1*(1), 37-46.

Abu-Zahra, M. R. M., Niederer J. P.M., Feron, P. H. M. and Versteeg, G. F. (2007b). CO_2 capture from power plants: Part II. A parametric study of the economical performance based on mono-ethanolamine. *International journal of greenhouse gas control*, 1, 135–142.

Alatiqi, I., Sabri, M. F., Bouhamra, W., & Alper, E. (1994). Steady-state rate-based modelling for CO_2/amine absorption—desorption systems. *Gas Separation & Purification, 8*(1), 3-11.

Al-Baghli, N. A., Pruess, S. A., Yesavage, V. F., & Selim, M. S. (2001). A rate-based model for the design of gas absorbers for the removal of CO2 and H2S using aqueous solutions of MEA and DEA. *Fluid Phase Equilibria, 185*(1-2), 31-43.

Al-Ghawas, H.A., Hagewiesche, D.P., Ruiz-Ibanez, G., and Sandall, O.C. (1989). Physicochemical properties important for carbon dioxide absorption in aqueous methyldiethanolamine. *J. Chem. Eng. Data*, 34 (4), 385-391.

Alie, C. (2004). Simulation and optimization of a coal-fired power plant with integrated CO_2 capture using MEA scrubbing. Master Thesis, University of Waterloo.

Alie, C., Backham, L., Croiset, E., & Douglas, P. L. (2005). Simulation of CO2 capture using MEA scrubbing: A flowsheet decomposition method. *Energy Conversion and Management, 46*(3), 475-487.

Alie, C., Douglas, P., and Croiset, E. (2006). A generalized framework for evaluating the performance of CO2 capture processes. In 8th International Conference on Greenhouse Gas Control Technologies, Trondheim, Norway, June 2006. Elsevier, Ltd.

Alper, E. (1990). Reaction mechanism and kinetics of aqueous solutions of 2-amino-2-methyl-1-propanol and carbon dioxide. *Industrial and Engineering Chemistry Research*, 29, 1725–1728.

Aroua, M. K., & Salleh, R. M. (2004). Solubility of CO_2 in aqueous piperazine and its modeling using the kent-eisenberg approach. *Chem. Eng. Technol., 27*(1), 65-70.

Aroonwilas, A., Veawab, A. and Tontiwachuwuthikul, P. (1999). Behaviour of the mass-transfer coefficient of structured packings in CO2 absorbers with chemical reactions. *Journal of Industrial Engineering Chemical Research*, 38:2044–2050.

Aroonwilas, A., Veawab, A. (2007). Integration of CO_2 capture unit using single- and blended-amines into supercritical coal-fired power plants: Implications for emission and energy management. *International Journal of Greenhouse Gas Control*, 1(2), 143–150.

Aspen (2006). Aspen plus user guide. Cambridge, USA.

Astarita, G. (1961). Carbon dioxide absorption in aqueous monoethanolamine solutions. *Chemical Engineering Science, 16*(3-4), 202-207.

Astarita, G. (1967). Mass transfer with chemical reaction. Amsterdam, London, Elsevier.

Astarita, G., & Savage, D. W. (1980a). Gas absorption and desorption with reversible instantaneous chemical reaction. *Chemical Engineering Science, 35*(8), 1755-1764.

Astarita, G., & Savage, D. W. (1980b). Theory of chemical desorption. *Chemical Engineering Science, 35*(3), 649-656.

Austgen, D. M., Rochelle, G. T., Peng, X., & Chen, C. C. (1989). Model of vapor-liquid equilibria for aqueous acid gas-alkanolamine systems using the electrolyte-NRTL equation. *Industrial & Engineering Chemistry Research, 28*(7), 1060-1073.

Austgen, D. M., Rochelle, G. T., & Chen, C. C. (1991). Model of vapor-liquid equilibria for aqueous acid gas-alkanolamine systems. 2. representation of H_2S and CO_2 solubility in aqueous MDEA and CO_2 solubility in aqueous mixtures of MDEA with MEA or DEA. *Ind. Eng. Chem. Res., 30*(3), 543-555.

Barchas, R. and Davis, R. (1992). The Kerr-McGee/ABB Lummus Crest technology for the recovery of CO2 from stack gases. Energy Conversion and Management, 33(5–8):333–340.

Bedelbayev, A. (2008), "Model based control of absorption column for CO_2 capturing", Master's thesis, Telemark University College, Faculty of Technology.

Bird, R. B., Stewart, W. E., & and Lightfoot, E. N. (2002). In Stewart, Warren E., Jt. Author, Lightfoot E. N.,Jt.Author (Eds.), *Transport phenomena* (Second Edition ed.). New York, Wiley.

Blauwhoff, P.M.M, Versteeg, G.F., Van Swaaij, W.P.M. (1984). A Study on the Reaction between CO_2 and Alkanolamines in Aqueous Solutions. *Chemical Engineering Science*, 39, 207–225.

Booras, G. S. & Smelser, S. C. (1991). An engineering and economic evaluation of CO2 removal from fossil-fuel-fired power plants. *Energy, 16*(11-12), 1295-1305.

Bravo, J. L., & Fair, J. R. (1982). Generalized correlation for mass transfer in packed distillation columns. *Industrial & Engineering Chemistry, Process Design and Development, 21*(1), 162-170.

Browning, G. J., and Weiland, R. H. (1994). Physical Solubility of Carbon Dioxide in Aqueous Alkanolamines via Nitrous Oxide Analogy. *J. Chem. Eng. Data*, 1994, 39 (4), 817-822

Buhre, B. J. P., Elliott, L. K., Sheng, C. D., Gupta, R. P., & Wall, T. F. (2005). Oxy-fuel combustion technology for coal-fired power generation. *Progress in Energy and Combustion Science, 31*(4), 283-307.

Caplow, M. (1968). Kinetics of carbamate formation and breakdown. *Journal of the American Chemical Society, 90*(24), 6795.

Carapellucci, R. and Milazzo, A. (2003). Membrane systems for CO_2 capture and their integration with gas turbine plants. *Proceedings of the Institution of Mechanical Engineers Part A: Journal of Power and Energy*, 217, 505–517.

Carl, B. (2005). *Rules of thumb for chemical engineers a manual of quick, accurate solutions to everyday process engineering problems*. 4th Edition. Boston: Elsevier.

Chaffee, A. L., Knowles, G. P., Liang, Z., Zhang, J., Xiao, P., & Webley, P. A. (2007). CO_2 capture by adsorption: Materials and process development. *International Journal of Greenhouse Gas Control, 1*(1), 11-18.

Chakma, A., & Meisen, A. (1990). Improved kent-eisenberg model for predicting CO2 solubilities in aqueous diethanolamine (DEA) solutions. *Gas Separation & Purification, 4*(1), 37-40.

Chakma,A. Mehrotra, A. K. and Nielsen, B. (1995). Comparison of chemical solvents for mitigating CO2 emissions from coal-fired power plants. *Heat Recovery Systems and CHP*, 15(2):231–240.

Chakravati, S., Gupta, A. and Hunek, B. (2001). Advanced technology for the capture of carbon dioxide from flue gases *1st National Conference on Carbon Sequestration* Washington, DC .

Chalmers, H., & Gibbins, J. (2007). Initial evaluation of the impact of post-combustion capture of carbon dioxide on supercritical pulverised coal power plant part load performance.

Cheng, S., Meisen, A., & Chakma, A. (1996). *Hydrocarbon Process, 75*(2), 81-84.

Chowdhury, F. A., Okabe, H., Shimizu, S., Onoda, M., & Fujioka, Y. (2009). Development of novel tertiary amine absorbents for CO2 capture. *Energy Procedia, 1*(1), 1241-1248.

Cifre, P. G., Brechtel, K., Hoch, S., García, H., Asprion, N., Hasse, H., et al. (2009). Integration of a chemical process model in a power plant modelling tool for the simulation of an amine based CO2 scrubber. *Fuel, 88*(12), 2481-2488.

Clarke, J. K. A. (1964). Kinetic of absorption of carbon dioxide in monoethanolamine solutions at short contact times. *Industrial and Chemical Engineering Fundamentals*, 3 (3), 239–245.

Corti, A., Fiaschi, D., & Lombardi, L. (2004). Carbon dioxide removal in power generation using membrane technology. *Energy, 29*(12-15), 2025-2043.

Crooks, J. E., & Donnellan, J. P. (1989). Kinetics and mechanism of the reaction between carbon dioxide and amines in aqueous solution . *J. Chem. Soc., Perkin Trans. 2,* , 331-333.

Danckwerts, P. V. (1970). *Gas-liquid reactions*. New York: McGraw-Hill.

Danckwerts, P.V. (1979). The Reaction of CO_2 with Ethanolamines. *Chemical Engineering Science,*34, 443–446.

Dang, H. and Rochelle. G. T. (2003). CO_2 Absorption Rate and Solubility in Monoethanolamine/Piperazine/Water. *Sep. Sci. Tech*. 38(2): 337-357.

Darde, A., R. Prabhakar, J.-P. Tranier, and N. Perrin, (2009). *Air separation and flue gas compression and purification units for oxy-coal combustion systems.* Energy Procedia, 1, 527-534.

Darde, V., Thomsen, K., van Well, W. J. M., & Stenby, E. H. (2010). Chilled ammonia process for CO_2 capture. *International Journal of Greenhouse Gas Control, 4*(2), 131-136.

Davison, J. (2007). Performance and costs of power plants with capture and storage of CO2. *Energy*, *32*(7), 1163-1176.

Davison, J. and K. Thambimuthu, (2004). *Technologies for capture of carbon dioxide*, in *7th International conference on Greenhouse Gas Control Technologies*: Vancouver, Canada

Davison, J., and Thambimuthu, K. (2005). Technologies for Capture of Carbon Dioxide. In: *Proceedings of the seventh international conference on greenhouse gas control technologies (GHGT-7)*, Vancouver, Canada, 1, 3-13.

Davidson, R.M., (2007). Post-combustion Carbon Capture from Coal Fired Plants – Solvent Scrubbing. IEA Clean Coal Centre, CCC/125.

DeCoursey, W. J. (1974). Absorption with chemical reaction: Development of a new relation for the danckwerts model. *Chemical Engineering Science, 29*(9), 1867-1872.

DeCoursey, W. J. (1982). Enhancement factors for gas absorption with reversible reaction. *Chemical Engineering Science*, *37*(10), 1483-1489.

DeCoursey, W. J. (1992). A simpler approximation for enhancement of mass transfer by second-order reversible reaction. *ICHEME Symposium*, Series no. 128, 2, B269-276.

DeCoursey, W. J., & Thring, R. W. (1989). Effects of unequal diffusivities on enhancement factors for reversible and irreversible reaction. *Chemical Engineering Science, 44*(8), 1715-1721.

Delfort, B., Carrette, P., & Bonnard, L. (2011). MEA 40% with improved oxidative stability for CO2 capture in post-combustion. *Energy Procedia, 4*(0), 9-14.

Deshmukh, R. D., & Mather, A. E. (1981). A mathematical model for equilibrium solubility of hydrogen sulfide and carbon dioxide in aqueous alkanolamine solutions. *Chemical Engineering Science*, *36*(2), 355-362.

Desideri, U., & Paolucci, A. (1999). Performance modelling of a carbon dioxide removal system for power plants. *Energy Conversion and Management, 40*(18), 1899-1915.

Dey, A., & Aroonwilas, A. (2009). CO_2 absorption into MEA-AMP blend: Mass transfer and absorber height index. *Energy Procedia, 1*(1), 211-215.

Diagne, D., Goto, M., Hirose, T. (1995). Parametric studies on CO2 separation and recovery by a dual reflux PSA process consisting of both rectifying and stripping sections. Ind. Eng. *Chem. Res.* 34, 3083–3089.

Donaldson, T. L., & Nguyen, Y. N. (1980). Carbon dioxide reaction kinetics and transport in aqueous amine membranes. *Ind. Eng. Chem. Fundamen., 19*(3), 260-266.

Drage, T. C., Smith, K. M., Pevida, C., Arenillas, A., & Snape, C. E. (2009). Development of adsorbent technologies for post-combustion CO2 capture. *Energy Procedia, 1*(1), 881-884.

Dugas, E. R. (2006). Pilot plant study of carbon dioxide capture by aqueous monoethanolamine. Master Thesis, The University of Texas at Austin.

Dugas, R. E., & Rochelle, G. T. (2011). Modeling CO_2 absorption into concentrated aqueous monoethanolamine and piperazine. *Chemical Engineering Science, 66*(21), 5212-5218.

Delfort, B., Carrette, P-L., Bonnard, L. (2011). MEA 40% with improved oxidative stability for CO_2 capture in post-combustion. Energy Procedia, 4, 9-14.

Edwards, J. E. (2008). Design and rating shell and tube heat exchangers. Teeside, UK. www.pidesign.co.uk.

Elwell, L. C., & Grant, W. S. (2006). Technology options for capturing CO_2-Special Reports. *Power, 150*(8), 60-65.

Escobillana, G. P. Saez, J. A., Perez-Correa J. R. and Neuburg H. J. (1991). Behaviour of Absorption/Stripping Columns for the CO_2-MEA System; Modelling and Experiments. *The Canadian Journal of Chemical Engineering*. 69, 969-977.

Fang, Fan., Li, Z. S. and Cai, N. S. (2009). Continuous CO_2 Capture from Flue Gases Using a Dual Fluidized Bed Reactor with Calcium-Based Sorbent. *Ind. Eng. Chem. Res*., 48, 11140–11147.

Faramarzi, L., Kontogeorgis, G. M., Thomsen, K., & Stenby, E. H. (2009). Extended UNIQUAC model for thermodynamic modeling of CO2 absorption in aqueous alkanolamine solutions. *Fluid Phase Equilibria, 282*(2), 121-132.

Feron, P. H. M., & Hendriks, C. A. (2005). CO_2 capture process principles and costs. *Oil & Gas Science and Technology – Rev. IFP, 60*(3), 451-459.

Freeman, S. A., Dugas, R., Van Wagener, D. H., Nguyen, T., & Rochelle, G. T. (2010). Carbon dioxide capture with concentrated, aqueous piperazine. *International Journal of Greenhouse Gas Control, 4*(2), 119-124.

Freguia, S., & Rochelle, G. T. (2003). Modeling of CO_2 capture by aqueous monoethanolamine. *AICHE Journal, 49*(7), 1676-1686.

Froment, G. F., & Bischoff, K. B. (1990). *Chemical reactor analysis and design* (2nd ed.). New York; Wiley.

Geankoplis, C. J. (2003). *Transport processes and separation process principles : (includes unit operations)* (4th ed.). Upper Saddle River, NJ: Prentice Hall.

Ghaemi, A., Shahhosseini, S., & Maragheh, M. G. (2009). Nonequilibrium dynamic modeling of carbon dioxide absorption by partially carbonated ammonia solutions. *Chemical Engineering Journal, 149*(1-3), 110-117.

Gibson, J., Schallehn, D., Zheng, Q., Chen, J., (2009) "Carbon dioxide capture from coal-fired power plants in China", Summary Report for NZEC Work Package 3, [2010-10-13], http://www.nzec.info/en/assets/Reports/Techno-Economic-Comparison-WP3-Final-English.pdf.

Gomes, V. G., & Yee, K. W. K. (2002). Pressure swing adsorption for carbon dioxide sequestration from exhaust gases. *Separation and Purification Technology, 28*(2), 161-171.

Grande, C. A., Ribeiro, R. P. L., Oliveira, E. L. G., & Rodrigues, A. E. (2009). Electric swing adsorption as emerging CO2 capture technique. *Energy Procedia, 1*(1), 1219-1225.

Grande, C. A., & Rodrigues, A. E. (2008). Electric swing adsorption for CO2 removal from flue gases. *International Journal of Greenhouse Gas Control, 2*(2), 194-202.

Greer, T., Bedelbayev, A., Igreja, J. M., Gomes, J. F., & Lie, B. (2010). A simulation study on the abatement of CO2 emissions by de-absorption with monoethanolamine. *Environmental Technology, 31*(1), 107-115.

Haimour, N., & Sandall, 0. C. (1984). Absorption of carbon dioxide into aqueous methyldiethanolamine. *Chemical Engineering Science, 39*(12), 1791-1796.

Herzog, H., Meldon, J., Hatton, A., "Advanced post-combustion CO2 capture", (2009) [2011-02-05], http://web.mit.edu/mitei/docs/reports/ herzog-meldon-hatton.pdf.

Higbie, R. (1935). The rate of absorption of a pure gas into a still liquid during short periods of exposure. *Trans. Am. Inst. Chem. Engr., 31*, 365-388.

Hikita, H., Asai, S., Ishikawa, H., & Honda, M. (1977). Kinetics of reactions of carbon-dioxide with monoethanolamine, diethanolamine and triethanolamine by a rapid mixing method. *Chemical Engineering Journal and the Biochemical Engineering Journal, 13*(1), 7-12.

Hilliard, M.D. (2008). A Predictive Thermodynamic Model for an Aqueous Blend of Potassium Carbonate, Piperazine, and Monoethanolamine for Carbon Dioxide Capture from Flue Gas. Master Thesis, The University of Texas at Austin.

Hoff, K. A., Juliussen, O., Falk-Pedersen, O., & Svendsen, H. F. (2004). Modeling and experimental study of carbon dioxide absorption in aqueous alkanolamine solutions using a membrane contactor. *Industrial & Engineering Chemistry Research, 43*(16), 4908-4921.

Hsu, C.H and Li, M.H. (1997). Densities of Aqueous Blended Amines. *J. Chem. Eng. Data* , *42*, 502-507.

Hu, W., & Chakma, A. (1990a). Modelling of equilibrium solubility of CO, and H_2S in aqueous diglycolamine (DGA) Solutions. *The Canadian Journal of Chemical Engineering, 68*, 523-525.

Hu, W., & Chakma, A. (1990b). Modelling of equilibrium solubility of CO_2 and H_2S in aqueous amino methylpropanol (AMP) solutions. *Chem. Eng. Comm., 94*, 53-61.

Idem, R., Wilson, M., Tontiwachwuthikul, P., Chakma, A., Veawab, A., Aroonwilas, Adisorn and Gelowitz, D. (2006). Pilot Plant Studies of the CO_2 Capture Performance of Aqueous MEA and Mixed MEA/MDEA Solvents at the University of Regina CO_2 Capture Technology Development Plant and the Boundary Dam CO_2 Capture Demonstration Plant. *Ind. Eng. Chem. Res., 45,* 2414-2420.

IEA (2008a). *Energy Efficiency Indicators for Public Electricity Production from Fossil Fuels.* IEA/OECD, Paris. Available at www.iea.org/papers/2008/En_Efficiency_Indicators.pdf

IEA (2008b). Key world energy statistics. http://www.iea.org/textbase/nppdf/free/2008/key_stats_2008.pdf

IEA (2004*). Prospects for CO_2 capture and storage*. *Energy Technology Analysis*, IEA/OECD, Paris. http://www.iea.org/textbase/nppdf/free/2004/prospects.pdf

IEA GHG (2006a). CO_2 capture in low rank coal power plants. Report 2006/1, Cheltenham, UK, IEA Greenhouse Gas R&D Programme, 617.

IEA GHG (2007). Post combustion carbon capture from coal fired plants-solvent scrubbing. Report 2007/15, IEA Greenhouse Gas R&D Programme.

IEA GHG (2008). Greenhouse Gas Issues, No. 90, June 2008. Pg. 5.

IESO (2011). Generator output capability. http://reports.ieso.ca/public/Genoutputcapability.

IPCC. (2005). *IPCC special report on carbon dioxide capture and storage*. New York, Cambridge University Press.

Ishibashi, M., K. Otake, S. Kanamori, and A. Yasutake. (1999). Study on CO_2 Removal Technology from Flue Gas of Thermal Power Plant by Physical Adsorption Method, Greenhouse Gas Control Technologies. P. Riemer, B. Eliasson, and A. Wokaun (eds.), Elsevier Science, Ltd., United Kingdom, 95-100.

Jarvis, R. B., & Pantelides, C. C. (1992). *DASOLV-A differential-algebraic equation solver*. Imperial College, London: Centre for Process Systems Engineering.

Jens-Uwe Repkea,Marc-Oliver Schacha*, Rüdiger Schneiderb, Henning Schrammb,. 1st Post Combustion Capture Conference, Control structure design for CO2 absorption processes for large operating ranges.

Jou, F. Y., Mather, A. E., & Otto, F. D. (1982). Solubility of hydrogen sulfide and carbon dioxide in aqueous methyldiethanolamine solutions. *Ind. Eng. Chem. Process Des. Dev., 21*(4), 539-544.

Kaewsichan, L., Al-Bofersen, O., Yesavage, V. F., & Selim, M. S. (2001). Predictions of the solubility of acid gases in monoethanolamine (MEA) and methyldiethanolamine (MDEA) solutions using the electrolyte-UNIQUAC model. *Fluid Phase Equilibria, 183-184*, 159-171.

Kanniche, M., Gros-Bonnivard, R., Jaud, P., Valle-Marcos, J., Amann, J., & Bouallou, C. (2010). Pre-combustion, post-combustion and oxy-combustion in thermal power plant for CO2 capture. *Applied Thermal Engineering, 30*(1), 53-62.

Kenig, E. Y., Schneider, R., & Górak, A. (1999). Rigorous dynamic modelling of complex reactive absorption processes. *Chemical Engineering Science, 54*(21), 5195-5203.

Kenig, E. Y., Schneider, R., & Górak, A. (2001). Reactive absorption: Optimal process design via optimal modelling. *Chemical Engineering Science, 56*(2), 343-350.

Kent, R. L., & Eisenberg, B. (1976). Better data for amine treating. *Hydrocarbon Processing, 55*(2), 87-90.

Knudsen, J. N., Vilhelmsen, P.J., Biede, O., and Jensen, J. N. (2006). Castor 1 t/h CO2 absorption pilot plant at the elsam kraft a/sesbjerg power plant – first year operation experience. In 8th International Conference on Greenhouse Gas Control Technologies, Trondheim, Norway, June 2006. Elsevier, Ltd.

Ko, J., Tsai, T., Lin, C., & Li, M. (2001). Diffusivity of nitrous oxide in aqueous alkanolamine solutions. *Journal of Chemical Engineering and Data, 46*, 160-165.

Kohl, A. L., & Nielsen, R. B. (1997). *Gas purification* (5th ed.). Houston, Tex.: Gulf Pub.

Krishnamurthy, R. and Taylor, R. (1985). A Nonequilibrium Stage Model of Multicomponent Separation Processes. Part I: Model Description and Method of Solution. *AlChE Journal*, 31 (3), 449-456.

Kritpiphata, W., & Tontiwachwuthikul, P. (1996). New modified kent-eisenberg model for predicting carbon dioxide solubility in aqueous 2-amino-2-methyl-1-propanol (amp) solutions . *Chemical Engineering Communications, 144*(1), 73-83.

Kucka, L., Müller, I., Kenig, E. Y., & Górak, A. (2003). On the modelling and simulation of sour gas absorption by aqueous amine solutions. *Chemical Engineering Science, 58*(16), 3571-3578.

Kvamsdal, H. M., Jakobsen, J. P., & Hoff, K. A. (2009). Dynamic modeling and simulation of a CO_2 absorber column for post-combustion CO2 capture. *Chemical Engineering and Processing: Process Intensification, 48*(1), 135-144.

Kvamsdal, H. M., & Rochelle, G. T. (2008). Effects of the temperature bulge in CO_2 absorption from flue gas by aqueous monoethanolamine. *Industrial & Engineering Chemistry Research, 47*(3), 867-875.

Lawal, A., Wang, M., Stephenson, P., & Yeung, H. (2009a). Dynamic modelling of CO_2 absorption for post combustion capture in coal-fired power plants. *Fuel, 88*(12), 2455-2462.

Lawal A, Wang M, Stephenson P, Yeung H. (2009b). Dynamic Modeling and simulation of CO_2 chemical absorption process for coal-fired power plants. In: 10th International Symposium on Process Systems Engineering – PSE '09; 16–20 August, Brazil.

Lawal, A., Wang, M., Stephenson, P., Koumpouras, G., & Yeung, H. (2010). Dynamic modelling and analysis of post-combustion CO_2 chemical absorption process for coal-fired power plants. *Fuel, 89*(10), 2791-2801.

Lewis, W. K., and Whitman, W. G. (1924). Principles of Gas Absorption. *Ind. Eng. Chem.*, 16 (12), 1215-1220.

Li, M., & Shen, K. (1993). Calculation of equilibrium solubility of carbon dioxide in aqueous mixtures of monoethanolamine with methyldiethanolamine. *Fluid Phase Equilibria, 85, pp. 129-140,* May.

Li, Z.S., Cai, N.S., Croiset, E., (2008). Process analysis of CO2 capture from flue gas using carbonation/calcination cycles. AIChE J. 54, 1912–1925.

Lin, Y. J., Pan, T. H., Wong, D. S. H., Jang, S. S., Chi, Y. W., & Yeh, C. H. (2011). Plantwide control of CO_2 capture by absorption and stripping using monoethanolamine solution. *Ind. Eng. Chem. Res.*, *50*(3), 1338-1345.

Littel, R.J., Versteeg, G.F., and van Swaaij, W.P.M. (1992). Solubility and diffusivity data for the absorption of carbonyl sulfide, carbon dioxide, and nitrous oxide in amine solutions. *J. Chem. Eng. Data*,37 (1), 49-55.

Liu, G.B., Yu, K.T., Yuan, X.G., Liu, C.J. and Guo, Q.C. (2006). Simulations of chemical absorption in pilot-scale and industrial-scale packed columns by computational mass transfer. *Chemical Engineering Science*, 61, 6511–6529.

Liu, Y., Zhang, L., and Watanasiri, S. (1999). Representing Vapor-Liquid Equilibrium for an Aqueous MEA-CO_2 System Using the Electrolyte Nonrandom-Two-Liquid Model. *Ind. Eng. Chem. Res. 38*, 2080-2090.

Lucquiaud, M., & Gibbins, J. (2011). Effective retrofitting of post-combustion CO_2 capture to coal-fired power plants and insensitivity of CO_2 abatement costs to base plant efficiency. *International Journal of Greenhouse Gas Control, 5*(3), 427-438.

Mahajani, V. V., & Joshi, J. B. (1988). Kinetics of reactions between carbon dioxide and alkanolamines. *Gas Separation & Purification, 2*(2), 50-64.

Moe, H. I., Hauan, S., Lien, K. M., & Hertzberg, T. (June/0). Dynamic model of a system with phase- and reaction equilibrium. *Computers & Chemical Engineering, 19*(Supplement 1), 513-518.

Natural Resources Canada (2006). *Canada CCS technology roadmap*

Natural Resources Canada (2008). Electricity Generation Energy Use and Generation by Energy Source. http://www.oee.nrcan.gc.ca/corporate/statistics/neud/dpa/tableshandbook2/egen_00_1_e_4.cfm?attr=0

OECD/IEA. (2011). Cost and performance of carbon dioxide capture from power generation.

Onda, K., Takeuchi, H., & Okumuto, Y. (1968). Mass transfer coefficients between gas and liquid phases in packed columns. *Journal of Chemical Engineering of Japan, 1*(1), 56-62.

OPG. (2009). *Sustainable development report*.

Oyenekan, B. A., & Rochelle, G. T. (2007). Alternative stripper configurations for CO_2 capture by aqueous amines. *AIChE Journal, 53*(12), 3144-3154.

Oyenekan, B. A., & Rochelle, G. T. (2009). Rate modeling of CO_2 stripping from potassium carbonate promoted by piperazine. *International Journal of Greenhouse Gas Control, 3*(2), 121-132.

Pacheco, M. A., & Rochelle, G. T. (1998). Rate-based modeling of reactive absorption of CO2 and H2S into aqueous methyldiethanolamine. *Industrial & Engineering Chemistry Research, 37*(10), 4107-4117.

Panahi, M.; Karimi, M.; Skogestad, S.; Hillestad, M.; Svendsen, H. F.(2010). Self-Optimizing and Control Structure Design for a CO2 Capture Plant. In *2nd Annual Gas Processing Symposium*, 2010.

Park, S. H., Lee, K. B., & Hyun, J. C. (2002). Correlation and prediction of the solubility of carbon dioxide in aqueous alkanolamine and mixed alkanolamine solutions. *Industrial & Engineering Chemistry Research, 41*(6), 1658-1665.

Pellegrini, G., Strube, R., & Manfrida, G. (2010). Comparative study of chemical absorbents in postcombustion CO2 capture. *Energy, 35*(2), 851-857.

Penny, D. E., & Ritter, T. J. (1983). Kinetic study of the reaction between carbon dioxide and primary amines. *Journal of the Chemical Society, Faraday Transactions 1: Physical Chemistry in Condensed Phases, 79*(9), 2103-2109.

Pintola, T., Tontiwachwuthikul, P., & Meisen, A. (1993). Simulation of pilot plant and industrial CO_2-MEA absorbers. *Gas Separation & Purification, 7*(1), 47-52.

Pires, J. C. M., Martins, F. G., Alvim-Ferraz, M. C. M., & Simões, M. (2011). Recent developments on carbon capture and storage: An overview. *Chemical Engineering Research and Design, 89*(9), 1446-1460.

Posey, M.L. and Rochelle, G. T. (2007). A Thermodynamic Model of Methyldiethanolamine−CO_2−H_2S−Water**.** *Ind. Eng. Chem. Res.*, 1997, 36 (9), pp 3944–3953**.**

Prausnitz, J. M., Lichtenthaler, R. N. and de Azevedo, E. G. (1999). Molecular Thermodynamics of Fluid-Phase Equilibria. Prentice Hall, New Jersey.

Process Systems Enterprise (PSE), Ltd. (2009). *gPROMS introductory user guide*.

PSE. (2009). *Model developer guide*. London, UK:

Rackley, S.A. (2010). Carbon capture and storage. Butterworth-Heinemann, Burlington, USA

Reid, R. C., Prausnitz, J. M., & Poling, B. E. (1987). *Properties of gases and liquids* (4th ed ed.). New York ; Montreal: McGraw-Hill.

Resnik, K.P., Yeh, J.T., and Pennline, H.W. (2004). Aqua ammonia process for simultaneous removal of CO_2, SO_2 and NOx. *International Journal Environment Technology Management*, **4** , 89–104

Romeo, L. M., Bolea, I., & Escosa, J. (2008). Integration of power plant and amine scrubbing to reduce CO2 capture costs. *Applied Thermal Engineering, 28*(8-9), 1039-1046.

Rubin, E. S., Chen, C., & Rao, A. B. (2007). Cost and performance of fossil fuel power plants with CO2 capture and storage. *Energy Policy, 35*(9), 4444-4454.

Sada, E., Kumazawa, H., Butt, M. A., & Hayashi, D. (1976). Simultaneous absorption of carbon dioxide and hydrogen sulfide into aqueous monoethanolamine solutions. *Chemical Engineering Science, 31*(9), 839-841.

Sada, E., Kumazawa, H., and Butt, M.A. (1978). Solubility and Diffusivity of Gases in Aqueous Solutions of Amines. *Journal of Chemical and Engineering Data*, 23(2), 161-163.

Schiesser, W. E. (1991). *The numerical method of lines: Integration of partial differential equations*. London: Academic Press.

Schneider, R. (., Sander, F. (., & Górak, A. (. (2003). Dynamic simulation of industrial reactive absorption processes. *Chemical Engineering and Processing, 42*(12), 955-964.

Schneider, R., Kenig, E. Y., & Gorak, A. (1999). Dynamic modelling of reactive absorption with the maxwell-stefan approach.

Scholes, C. A., Smith, K. H., Kentish, S. E., & Stevens, G. W. (2010). CO_2 capture from pre-combustion processes—Strategies for membrane gas separation. *International Journal of Greenhouse Gas Control, 4*(5), 739-755.

Seborg, D. E.; Edgar, T. F.; Mellichamp, D. A. *Process Dynamics and Control*, 2nd ed.; Wiley: New York, 2003.

Simbeck, D. R., & Mcdonald, M. (2001). Existing coal power plant retrofit CO2 control options analysis. *Proceedings of the Fifth International Conference Greenhouse Gas Control Technologies: GHGT5,* Cairns, Qld., Australia. pp. 103-108.

Singh, D., Croiset, E., Douglas, P. L., & Douglas, M. A. (2003). Techno-economic study of CO2 capture from an existing coal-fired power plant: MEA scrubbing vs. O2/CO2 recycle combustion. *Energy Conversion and Management, 44*(19), 3073-3091.

Smith, J. M., Van Ness, H. C., & Abbott, M. M. (1996). *Introduction to chemical engineering thermodynamics* (3rd ed. ed.). New York: McGraw-Hill.

Snijder, E. D., te Riele, M. J. M., & Versteeg, G. F. (1993). Diffusion coefficients of several aqueous alkanolamine solutions. *Journal of Chemical and Engineering Data, 38*, 475-480.

Song, C. (2006). Global challenges and strategies for control, conversion and utilization of CO2 for sustainable development involving energy, catalysis, adsorption and chemical processing. *Catalysis Today, 115*(1-4), 2-32.

Statistic Canada. (2002). *Electric power generation, transmission, and distribution* No. Technical Report 57-202-XIB) Energy Section, Manufacturing, Construction & Energy Division.

Steeneveldt, R., Berger, B., & Torp, T. A. (2006). CO_2 capture and storage: Closing the Knowing–Doing gap. *Chemical Engineering Research and Design, 84*(9), 739-763.

Suda, T., Fujii, M., Yoshida, K., Iijima, M., Seto, T., & Mitsuoka, S. (1992). Development of flue gas carbon dioxide recovery technology. *Energy Conversion and Management, 33*(5-8), 317-324.

Taylor, R., & Krishna, R. (1993). *Multicomponent mass transfer*. New York: Wiley.

Thomas, P. (1999). Simulation of Industrial Processes for Control Engineers. Elsevier Science & Technology Books.

Tlili, N., Grévillot, G., & Vallières, C. (2009). Carbon dioxide capture and recovery by means of TSA and/or VSA. *International Journal of Greenhouse Gas Control, 3*(5), 519-527.

Tobiesen, F. A., Juliussen, O., & Svendsen, H. F. (2008). Experimental validation of a rigorous desorber model for CO2 post-combustion capture. *Chemical Engineering Science, 63*(10), 2641-2656.

Tontiwachwuthikul, P., Meisen, A., & Lim, C. J. (1992). CO_2 absorption by NaOH, monoethanolamine and 2-amino-2-methyl-1-propanol solutions in a packed column. *Chemical Engineering Science, 47*(2, pp. 381-390).

Tsai, T., Ko, J., Wang, H., Lin, C., and Li, M. (2000). Solubility of nitrous oxide in alkanolamine aqueous solutions. *Journal of Chemical and Engineering Data*. 45, 341–347.

Vaidya, P.D., and Kenig, E.Y. (2007). CO_2-Alkanolamine Reaction Kinetics: A Review of Recent Studies. *Chem. Eng. Technol., 30(*11), 1467–1474.

Van Kravelen, D. W. and Hoftijzer P. J., (1948). *Rec. TMV. Chim. 67, 563.*

Van Wagener, D. H., & Rochelle, G. T. (2011). Stripper configurations for CO_2 capture by aqueous monoethanolamine. *Chemical Engineering Research and Design, 89*(9), 1639-1646.

Veldsink, J.W., van Damme, R.M.J., Versteeg, G.F., and van Swaaij, W.P.M. (1995). The use of the dusty-gas model for the description of mass transport with chemical reaction I porous media. *The Chemical Engineering Journal*, 57, 115-125.

Versteeg, G. F., & van Swaaij, W. P. M. (1988). On the kinetics between CO_2 and alkanolamines both in aqueous and non-aqueous solutions—II. tertiary amines. *Chemical Engineering Science, 43*(3), 587-591.

Versteeg, G. F., Van Dijck, L. A. J., & Van Swaaij, W. P. M. (1996). On the kinetics between CO2 and alkanolamines both in aqueous and non-aqueous solutions. An overview. *Chemical Engineering Communications, 144*, 113-158.

Vrachnos, A., Kontogeorgis, G. and Voutsas, E. (2006). Thermodynamic Modeling of Acidic Gas Solubility in Aqueous Solutions of MEA, MDEA and MEA-MDEA Blends. *Ind. Eng. Chem. Res., 45,* 5148-5154.

Wang, G. Q., Yuan, X. G. and Yu, K. T. (2005). Review of Mass-Transfer Correlations for Packed Columns. *Ind. Eng. Chem. Res, 44,* 8715-8729.

Wang, Y.W., Xu, S., Otto, F.D., and Mather, A.E. (1992). Solubility of N_2O in alkanolamines and in mixed solvents. *The Chemical Engineering Journal,* 48, 31-40.

Weiland, R.H., Dingman, J.C., Cronin, D.B., and Browning, G.J. (1998). Density and viscosity of some partially carbonated aqueous alkanolamine solutions and their blends, *J.Chem. Eng. Data,* 43, 378-382.

Weiland, R. H., Rawal, M., & Rice, R. G. (1982). Stripping of carbon dioxide from monoethanolamine solutions in a packed column. *AICHE Journal, 28*(6), 963-973.

Wellek, R.M., Brunson, , R.J., Law, F.H. (1978). Enhancement factors for gas absorption with second order irreversible chemical reaction. The Canadian Journal of Chemical Engineering, 56,181-186.

Whitman, W.G. (1923). The two-film theory of gas absorption. *Chem. Metall. Eng*, 29, p. 146.

Winnick, J. (1997). *Chemical engineering thermodynamics*. New York: Wiley.

Yamasaki, A. (2003). An overview of CO2 mitigation options for global warming - emphasizing CO2 sequestration options. *J. Chem. Eng. Jpn., 36*(4), 361-375.

Yang, H., Xu, Z., Fan, M., Gupta, R., Slimane, R. B., Bland, A. E., et al. (2008). Progress in carbon dioxide separation and capture: A review. *Journal of Environmental Sciences, 20*(1), 14-27.

Yang H., Fan, S., Lang, X., Wang, Y., Nie, J. (2011). Economic Comparison of Three Gas Separation Technologies for CO_2 Capture from Power Plant Flue Gas. *Chinese Journal of Chemical Engineering*, 19(4), 615-620.

Yagi, Y., MimuraT., Lijima M., Ishida, K., Yoshiyama, R., Kamijo, T. &Yonekawa,T. (2004). Improvements of carbon dioxide capture technology from flue gas. In: 7th International Conference on greenhouse gas control technologies. Canada: Vancouver Convention Center. Pg. E3-4.

Yong, Z., Mata, V., & Rodrigues, A. E. (2002). Adsorption of carbon dioxide at high temperature—a review. *Separation and Purification Technology, 26*(2-3), 195-205.

Yokoyama, T., 2003: Japanese R&D on CO2 Capture. Greenhouse Gas Control Technologies, Proc. of the 6th International Conference on Greenhouse Gas Control Technologies (GHGT-6), 1-4 Oct. 2002, Kyoto, Japan, J. Gale and Y. Kaya (eds.), Elsevier Science Ltd, Oxford, UK. 13-18.

Zarzycki, R., & Chacuk, A. (1993). *Absorption : Fundamentals & applications* (1st ed ed.). Oxford ; New York: Pergamon Press.

Ziaii, S., Rochelle, G. T., & Edgar, T. F. (2009). Dynamic modeling to minimize energy use for CO_2 capture in power plants by aqueous monoethanolamine. *Industrial & Engineering Chemistry Research, 48*(13), 98-101.

Appendix A

Overall mass transfer coefficient derivation

The flux (the rate of mass transfer per unit time and of contact surface) of a gaseous component A absorbed in the gas and liquid phase can be determined by following equations,

$$N_A^L = k_L\left(C_{A,i} - C_{A,L}\right) \quad \text{A.1}$$

$$N_A^G = k_G\left(p_{A,G} - p_{A,i}\right) \quad \text{A.2}$$

At steady state, the fluxes in the gas and liquid phase are equal, $N_A^L = N_A^G$, so that

$$\frac{k_L}{k_G} = \frac{\left(p_{A,G} - p_{A,i}\right)}{\left(C_{A,i} - C_{A,L}\right)} \quad \text{A.3}$$

In order to eliminate the interfacial composition ($p_{A,i}$and $C_{A,i}$), an overall effect in terms of bulk driving force is used. It is assumed that the composition in the gas phase in equilibrium with the liquid bulk concentration and the liquid composition in equilibrium with the composition of the bulk gas phase. The entire two-phase mass transfer effect can then be determined in terms of an overall mass transfer coefficient which includes the resistance to diffusion in both phases.

$$N_A^L = K_L\left(C_A^* - C_{A,L}\right) \quad \text{A.4}$$

$$N_A^G = K_G\left(p_{A,G} - p_A^*\right) \quad \text{A.5}$$

It is assumed that the physical equilibrium exist across the interface and according to the Henry's law,

$$p_{A,i} = HC_{A,i} \quad \text{A.6}$$

The partial pressure in equilibrium with the bulk liquid concentration (p_A^*) is expressed by,

$$p_A^* = HC_{A,L} \quad \text{A.7}$$

The concentration in equilibrium with the bulk gas partial pressure (C_A^*) is given by,

$$C_A^* = \frac{p_{A,G}}{H} \tag{A.8}$$

Substituting Equation (A.6) in (A.3) the following expression is derived,

$$C_{A,i}\left(\frac{k_L}{k_G} + H\right) = p_{A,G} + \frac{k_L}{k_G} C_{A,L} \tag{A.9}$$

Rearrange this equation,

$$\begin{aligned} C_{A,i} \quad &= \frac{p_{A,G} + \frac{k_L}{k_G} C_{A,L}}{\left(\frac{k_L}{k_G} + H\right)} \\ &= \frac{k_G p_{A,G} + k_L C_{A,L}}{k_L + H k_G} \end{aligned} \tag{A.10}$$

Knows that (A.4 = A.1),

$$K_L\left(\frac{p_{A,G}}{H} - C_{A,L}\right) = k_L\left(C_{A,i} - C_{A,L}\right) \tag{A.11}$$

Substitute Equation (A.10) in (A.11) to obtain,

$$K_L\left(\frac{p_{A,G}}{H} - C_{A,L}\right) = k_L\left(\frac{k_G p_{A,G} + k_L C_{A,L}}{k_L + H k_G} - C_{A,L}\right)$$

$$K_L = \frac{k_L\left(\frac{k_G p_{A,G} + k_L C_{A,L}}{k_L + H k_G} - C_{A,L}\right)}{\left(\frac{p_{A,G}}{H} - C_{A,L}\right)}$$

$$\begin{aligned} &= \frac{k_L\left(k_G p_{A,G} + k_L C_{A,L} - k_L C_{A,L} - H k_G C_{A,L}\right)}{\left(\frac{p_{A,G}}{H} - C_{A,L}\right)(k_L + H k_G)} \\ &= \frac{k_L k_G\left(p_{A,G} - H C_{A,L}\right)}{\frac{1}{H}\left(p_{A,G} - H C_{A,L}\right)(k_L + H k_G)} \end{aligned} \tag{A.12}$$

$$= \frac{k_L k_G}{\frac{k_L}{H} + k_G}$$

Therefore overall liquid mass transfer coefficient is,

$$\frac{1}{K_L} = \frac{1}{Hk_G} + \frac{1}{k_L} \qquad \text{A.13}$$

The overall gas mass transfer coefficient can be determined in the same ways result the following equation,

$$\frac{1}{K_G} = \frac{H}{k_L} + \frac{1}{k_G} \qquad \text{A.14}$$

If *H* is very large (solute A relatively insoluble in the liquid), the first term $\frac{1}{Hk_G}$ of Equation (A.13) becomes minor and the major resistance to mass transfer resides within the liquid, which is the said to control the rate. The Equation (A.13) becomes,

$$\frac{1}{K_L} = \frac{1}{k_L} \qquad \text{A.15}$$

Conversely, when *H* is small (solute A is very soluble in the liquid), the term $\frac{H}{k_L}$ in Equation (A.14) becomes minor, the major resistance is represented by $\frac{1}{k_G}$. Then the rate of mass transfer is gas phase-controlled.

$$\frac{1}{K_G} = \frac{1}{k_G} \qquad \text{A.16}$$

The use of overall mass transfer coefficient will eliminate the need to calculate the concentrations at the interface.

Appendix B

Derivation for heat exchanger model

Energy Balance for tube/shell

$$\Delta z \left(\frac{\pi}{4}\right) d^2 \frac{\Delta E}{\Delta t} = Q|_z - Q|_{z+\Delta z} + Q_{flux} \Delta z \pi d \qquad \text{B.1}$$

where $\Delta z \pi d$ represent the surface area for heat transfer within the volume element. Dividing the Equation B.1 with $\Delta z \left(\frac{\pi}{4}\right) d^2$ and taken the limit $\Delta z \rightarrow 0$

$$\frac{dE}{dt} = -\frac{1}{A}\frac{\partial Q}{\partial z} + Q_{flux}\frac{4}{d} \qquad \text{B.2}$$

Knows that $d = 2r$, then Equation B.2

$$\frac{dE}{dt} = -\frac{1}{A}\frac{\partial Q}{\partial z} + Q_{flux}\frac{2}{r} \qquad \text{B.3}$$

If using normalized axial domain,

$$z_{norm} = \frac{z}{L} \quad \text{and} \quad dz_{norm} = \frac{dz}{L} \qquad \text{B.4}$$

Substitute into Equation B.3,

$$\frac{dE}{dt} = -\frac{1}{AL}\frac{\partial Q}{\partial z_{norm}} + Q_{flux}\frac{2}{r} \qquad \text{B.5}$$

where E (J/m^3) is the volumetric specific internal energy; Q (J/s) is the energy flowrate; Q_{flux} (J/m^2/s) is the heat flux; A (m^2) is the cross sectional area; r (m) is the radius; L (m) is the tube length; d (m) is the diameter.

Appendix C

Regression analysis of vapor liquid equilibrium constant (K_{value})

C.1 K_{value} Regression correlation for CO_2

The summary of regression analysis obtained from the *Statistical Package* for the Social Sciences (SPSS) software for the K_{value} correlation of CO_2 component at different temperature range is given in the following tables:

Temperature range: 387-388 K

$$ln\ K_{CO_2} = 490.131 - 82.103lnT + 2.562x_{CO_2} + 1.597x_{mea} + 0.022Tx_{CO_2}x_{mea}$$

Table C.1: Regression analysis for K_{value} correlation of CO_2 for temperature 387-388 K

Model summary

R	R^2	Adjusted R^2	Std. Error of the Estimate
.990	.980	.980	.01002

Analysis of Variance (ANOVA)

	Sum of Squares	df	Mean Square	F	Sig. (p-value)
Regression	.717	4	.179	1.787E3	.000
Residual	.015	145	.000		
Total	.732	149			

Coefficient analysis

	Unstandardized Coefficients		Standardized Coefficients	F test	p-value
	B	Std. Error	Beta		
Constant	490.131	6.592		74.351	.000
lnT	-82.103	1.106	-.871	-74.257	.000
x_{CO_2}	2.562	1.168	.246	2.194	.030
x_{mea}	1.597	.530	.243	3.012	.003
$Tx_{CO_2}x_{mea}$	.022	.032	.102	.683	.496

Temperature range: 388.2-389 K

$$ln\, K_{CO_2} = 531.525 - 89.121 lnT + 10.441 x_{CO_2} + 4.158 x_{mea} - 0.062 T x_{CO_2} x_{mea}$$

Table C.2: Regression analysis for K_{value} correlation of CO_2 for temperature 388.2-389 K

Model summary

R	R^2	Adjusted R^2	Std. Error of the Estimate
.992	.984	.984	.01235

Analysis of Variance (ANOVA)

	Sum of Squares	df	Mean Square	F	Sig. (p-value)
Regression	1.536	4	.384	2.518E3	.000
Residual	.025	162	.000		
Total	1.561	166			

Coefficient analysis

	Unstandardized Coefficients		Standardized Coefficients	F test	p-value
	B	Std. Error	Beta		
Constant	531.525	7.822		67.956	.000
lnT	-89.121	1.311	-.678	-67.979	.000
x_{CO_2}	10.441	1.166	.728	8.955	.000
x_{mea}	4.158	.505	.515	8.241	.000
$Tx_{CO_2}x_{mea}$	-.062	.031	-.210	-1.998	.047

Temperature range: 389-390 K

$$ln\ K_{CO_2} = 505.895 - 84.832lnT + 12.072x_{CO_2} + 0.006Tx_{mea} + 0.046Tx_{CO_2}x_{mea}$$

Table C.3: Regression analysis for K_{value} correlation of CO_2 for temperature 389.2-390 K

Model summary

R	R^2	Adjusted R^2	Std. Error of the Estimate
.991	.983	.982	.01685

Analysis of Variance (ANOVA)

	Sum of Squares	df	Mean Square	F	Sig. (p-value)
Regression	.968	4	.242	852.459	.000
Residual	.017	60	.000		
Total	.985	64			

Coefficient analysis

	Unstandardized Coefficients		Standardized Coefficients	F test	p-value
	B	Std. Error	Beta		
Constant	505.895	15.408		32.833	.000
lnT	-84.832	2.585	-.562	-32.817	.000
x_{CO_2}	12.072	2.624	.701	4.601	.000
Tx_{mea}	.006	.003	.220	2.109	.039
$Tx_{CO_2}x_{mea}$	.046	.069	.122	.667	.507

C.2 K_{value} Regression correlation for MEA

The summary of regression analysis obtained from the *Statistical Package* for the Social Sciences (SPSS) software for the K_{value} correlation of MEA component at different temperature range is given in the following tables:

Temperature range: 385-387 K

$$ln\, K_{MEA} = -315.592 + 52.289lnT - 3.471x_{CO_2} - 0.003Tx_{mea} + 0.112Tx_{CO_2}x_{mea}$$

Table C.4: Regression analysis for K_{value} correlation of MEA for temperature 385-387 K

Model summary					
R	R^2	Adjusted R^2	Std. Error of the Estimate		
.998	.995	.995	.00600		
Analysis of Variance (ANOVA)					
	Sum of Squares	df	Mean Square	F	Sig. (p-value)
Regression	1.087	4	.272	7.552E3	.000
Residual	.005	143	.000		
Total	1.093	147			
Coefficient analysis					
	Unstandardized Coefficients		Standardized Coefficients	F test	p-value
	B	Std. Error	Beta		
Constant	-315.592	1.802		-175.123	.000
lnT	52.289	.303	.996	172.577	.000
x_{CO_2}	-3.471	.689	-.271	-5.036	.000
Tx_{mea}	-.003	.001	-.149	-3.730	.000
$Tx_{CO_2}x_{mea}$	.112	.019	.452	5.850	.000

Temperature range: 387.2-389 K

$$ln\ K_{MEA} = -341.477 + 56.65lnT - 4.008x_{CO_2} - 1.762x_{mea} + 0.098Tx_{CO_2}x_{mea}$$

Table C.5: Regression analysis for K_{value} correlation of MEA for temperature 387.2-389 K

Model summary

R	R^2	Adjusted R^2	Std. Error of the Estimate
.997[a]	.994	.994	.00336

Analysis of Variance (ANOVA)

	Sum of Squares	df	Mean Square	F	Sig. (p-value)
Regression	.269	4	.067	5.972E3	.000
Residual	.002	145	.000		
Total	.271	149			

Coefficient analysis

	Unstandardized Coefficients		Standardized Coefficients	F test	p-value
	B	Std. Error	Beta		
Constant	-341.477	2.209		-154.615	.000
lnT	56.650	.370	.989	152.927	.000
x_{CO_2}	-4.008	.391	-.632	-10.246	.000
x_{mea}	-1.762	.178	-.441	-9.918	.000
$Tx_{CO_2}x_{mea}$	.098	.011	.753	9.163	.000

Temperature range: 389.2-390 K

$$ln\ K_{MEA} = -339.542 + 56.331lnT - 3.901x_{CO_2} - 0.003Tx_{mea} + 0.026Tx_{CO_2}x_{mea}$$

Table C.6: Regression analysis for K_{value} correlation of MEA for temperature 389.2-390 K

Model summary

R	R^2	Adjusted R^2	Std. Error of the Estimate
.996[a]	.991	.991	.00486

Analysis of Variance (ANOVA)

	Sum of Squares	df	Mean Square	F	Sig. (p-value)
Regression	.160	4	.040	1.692E3	.000
Residual	.001	60	.000		
Total	.161	64			

Coefficient analysis

	Unstandardized Coefficients		Standardized Coefficients	F test	p-value
	B	Std. Error	Beta		
Constant	-339.542	4.443		-76.424	.000
lnT	56.331	.745	.922	75.572	.000
x_{CO_2}	-3.901	.757	-.560	-5.156	.000
Tx_{mea}	-.003	.001	-.241	-3.242	.002
$Tx_{CO_2}x_{mea}$	.026	.020	.174	1.329	.189

C.3 K_{value} Regression correlation for H_2O

The summary of regression analysis obtained from the *Statistical Package* for the Social Sciences (SPSS) software for the K_{value} correlation of H_2O component at different temperature range is given in the following tables:

Temperature range: 385-390 K

$$K_{H_2O} = -71.927 + 12.203lnT + 0.34x_{CO_2} + 0.265x_{H_2O}$$

Table C.7: Regression analysis for K_{value} correlation of MEA for temperature 385-390 K

Model summary					
R	R^2	Adjusted R^2	Std. Error of the Estimate		
.998	.997	.996	.01340		
Analysis of Variance (ANOVA)					
	Sum of Squares	df	Mean Square	F	Sig. (p-value)
Regression	3.725	3	1.242	6.914E3	.000
Residual	.013	71	.000		
Total	3.738	74			
Coefficient analysis					
	Unstandardized Coefficients		Standardized Coefficients	F test	p-value
	B	Std. Error	Beta		
Constant	-71.927	.509		-141.262	.000
lnT	12.203	.085	.991	142.820	.000
x_{CO_2}	.340	.110	.022	3.104	.003
x_{H_2O}	.265	.024	.078	11.158	.000

C.4 Regression correlation validation

The correlations obtained from the previous sections were validated using data generated from Aspen Plus® simulation.

Table C.8: K_{value} correlation comparison with Aspen Plus® data of CO_2

T (K)	x_{co2}	x_{mea}	x_{h2o}	K_{value}		% difference
				Aspen Plus® data	Regression correlation	
385	0.035	0.080	0.885	4.8884	4.7965	1.9
385	0.040	0.110	0.850	4.5767	4.7252	-3.2
385	0.045	0.080	0.875	4.7838	4.7462	0.8
385	0.045	0.120	0.835	4.5263	4.7320	-4.5
385	0.050	0.080	0.870	4.7395	4.7213	0.4
385	0.050	0.120	0.830	4.5172	4.7541	-5.2
385.2	0.035	0.080	0.885	4.7290	4.6383	1.9
385.2	0.040	0.080	0.880	4.6791	4.6140	1.4
385.2	0.045	0.110	0.845	4.4485	4.5795	-2.9
385.2	0.045	0.120	0.835	4.4253	4.5761	-3.4
385.2	0.050	0.080	0.870	4.5954	4.5658	0.6
385.2	0.050	0.120	0.830	4.4190	4.5976	-4.0
385.4	0.035	0.080	0.885	4.5692	4.4855	1.8
385.4	0.040	0.080	0.880	4.5244	4.4621	1.4
385.4	0.045	0.110	0.845	4.3386	4.4287	-2.1
385.4	0.045	0.120	0.835	4.3235	4.4254	-2.4
385.4	0.050	0.080	0.870	4.4516	4.4155	0.8
385.4	0.050	0.090	0.860	4.3918	4.4232	-0.7
385.6	0.040	0.080	0.880	4.3692	4.3152	1.2
385.6	0.045	0.080	0.875	4.3362	4.2927	1.0
385.6	0.045	0.120	0.835	4.2209	4.2798	-1.4
385.6	0.050	0.080	0.870	4.3082	4.2703	0.9
385.6	0.050	0.090	0.860	4.2631	4.2777	-0.3
385.6	0.050	0.120	0.830	4.2215	4.3000	-1.9
385.8	0.030	0.080	0.890	4.2848	4.2170	1.6
385.8	0.035	0.100	0.865	4.1464	4.1473	0.0
385.8	0.040	0.110	0.850	4.1183	4.1328	-0.4
385.8	0.045	0.110	0.845	4.1156	4.1421	-0.6

Table C.8: Continues

T (K)	x_{co2}	x_{mea}	x_{h2o}	K_{value}		% difference
				Aspen Plus® data	Regression correlation	
385.8	0.045	0.120	0.835	4.1175	4.1390	-0.5
385.8	0.050	0.110	0.840	4.1153	4.1514	-0.9
386	0.035	0.080	0.885	4.0840	4.0571	0.7
386	0.040	0.120	0.840	4.0075	3.9840	0.6
386	0.045	0.080	0.875	4.0390	4.0150	0.6
386	0.045	0.090	0.865	4.0134	4.0120	0.0
386	0.050	0.120	0.830	4.0219	4.0220	0.0
386.2	0.035	0.080	0.885	3.9215	3.9237	-0.1
386.2	0.040	0.080	0.880	3.9043	3.9033	0.0
386.2	0.040	0.120	0.840	3.8985	3.8530	1.2
386.2	0.045	0.080	0.875	3.8913	3.8831	0.2
386.2	0.045	0.120	0.835	3.9091	3.8714	1.0
386.2	0.050	0.110	0.840	3.8993	3.8831	0.4
386.2	0.050	0.120	0.830	3.9213	3.8899	0.8
386.4	0.035	0.080	0.885	3.7591	3.7947	-0.9
386.4	0.040	0.080	0.880	3.7502	3.7751	-0.7
386.4	0.040	0.120	0.840	3.7884	3.7264	1.6
386.4	0.045	0.080	0.875	3.7453	3.7555	-0.3
386.4	0.045	0.090	0.865	3.7471	3.7527	-0.1
386.4	0.050	0.080	0.870	3.7451	3.7361	0.2
386.4	0.050	0.120	0.830	3.8210	3.7622	1.5
386.6	0.035	0.080	0.885	3.5974	3.6701	-2.0
386.6	0.040	0.110	0.850	3.6470	3.6157	0.9
386.6	0.040	0.120	0.840	3.6782	3.6040	2.0
386.6	0.045	0.080	0.875	3.6016	3.6322	-0.9
386.6	0.045	0.120	0.835	3.6984	3.6213	2.1
386.6	0.050	0.080	0.870	3.6079	3.6135	-0.2
386.6	0.050	0.090	0.860	3.6266	3.6198	0.2
386.8	0.035	0.110	0.855	3.5061	3.4890	0.5
386.8	0.040	0.080	0.880	3.4464	3.5313	-2.5
386.8	0.040	0.120	0.840	3.5671	3.4857	2.3
386.8	0.045	0.110	0.845	3.5511	3.5051	1.3
386.8	0.045	0.120	0.835	3.5924	3.5025	2.5
386.8	0.050	0.110	0.840	3.5754	3.5133	1.7

Table C.8: Continues

T (K)	x_{co2}	x_{mea}	x_{h2o}	K_{value}		% difference
				Aspen Plus® data	Regression correlation	
386.8	0.050	0.120	0.830	3.6190	3.5194	2.8
387	0.030	0.080	0.890	3.2604	3.4509	-5.8
387	0.035	0.100	0.865	3.3404	3.3939	-1.6
387	0.040	0.120	0.840	3.4552	3.3713	2.4
387	0.045	0.110	0.845	3.4380	3.3902	1.4
387	0.045	0.120	0.835	3.4863	3.3876	2.8
387	0.050	0.080	0.870	3.3431	3.3804	-1.1
387	0.050	0.120	0.830	3.5174	3.4040	3.2
387.2	0.030	0.080	0.890	3.0919	3.0316	1.9
387.2	0.035	0.110	0.855	3.2532	3.2615	-0.3
387.2	0.040	0.080	0.880	3.1520	3.1316	0.6
387.2	0.045	0.080	0.875	3.1832	3.1828	0.0
387.2	0.045	0.120	0.835	3.3800	3.4451	-1.9
387.2	0.050	0.110	0.840	3.3614	3.4372	-2.3
387.2	0.050	0.120	0.830	3.4168	3.5074	-2.7
387.4	0.030	0.100	0.870	3.0257	3.0155	0.3
387.4	0.035	0.110	0.855	3.1262	3.1261	0.0
387.4	0.040	0.110	0.850	3.1703	3.1813	-0.3
387.4	0.040	0.120	0.840	3.2304	3.2436	-0.4
387.4	0.045	0.120	0.835	3.2739	3.3022	-0.9
387.4	0.050	0.080	0.870	3.0907	3.1006	-0.3
387.4	0.050	0.120	0.830	3.3165	3.3619	-1.4
387.6	0.030	0.080	0.890	2.7633	2.7853	-0.8
387.6	0.035	0.110	0.855	2.9993	2.9965	0.1
387.6	0.040	0.080	0.880	2.8717	2.8771	-0.2
387.6	0.040	0.120	0.840	3.1178	3.1090	0.3
387.6	0.045	0.120	0.835	3.1682	3.1653	0.1
387.6	0.050	0.110	0.840	3.1511	3.1580	-0.2
387.6	0.050	0.120	0.830	3.2167	3.2225	-0.2
387.8	0.030	0.080	0.890	2.6053	2.6698	-2.5
387.8	0.035	0.080	0.885	2.6745	2.7135	-1.5
387.8	0.040	0.120	0.840	3.0055	2.9802	0.8
387.8	0.045	0.110	0.845	2.9925	2.9746	0.6
387.8	0.045	0.120	0.835	3.0629	3.0341	0.9
387.8	0.050	0.080	0.870	2.8544	2.8488	0.2

Table C.8: Continues

T (K)	x_{co2}	x_{mea}	x_{h2o}	K_{value}		% difference
				Aspen Plus® data	Regression correlation	
387.8	0.050	0.090	0.860	2.9162	2.9070	0.3
388	0.030	0.100	0.870	2.5946	2.6558	-2.4
388	0.035	0.110	0.855	2.7473	2.7533	-0.2
388	0.040	0.080	0.880	2.6102	2.6436	-1.3
388	0.045	0.110	0.845	2.8842	2.8513	1.1
388	0.045	0.120	0.835	2.9585	2.9084	1.7
388	0.050	0.080	0.870	2.7430	2.7308	0.4
388	0.050	0.090	0.860	2.8080	2.7866	0.8
388.2	0.030	0.080	0.890	2.3085	2.2624	2.0
388.2	0.035	0.080	0.885	2.4033	2.3608	1.8
388.2	0.035	0.090	0.875	2.4727	2.4404	1.3
388.2	0.040	0.120	0.840	2.7825	2.7994	-0.6
388.2	0.045	0.120	0.835	2.8551	2.9071	-1.8
388.2	0.050	0.110	0.840	2.8468	2.9311	-3.0
388.2	0.050	0.120	0.830	2.9229	3.0190	-3.3
388.4	0.030	0.080	0.890	2.1717	2.1608	0.5
388.4	0.035	0.080	0.885	2.2779	2.2548	1.0
388.4	0.035	0.120	0.845	2.5845	2.5745	0.4
388.4	0.040	0.120	0.840	2.6727	2.6736	0.0
388.4	0.045	0.080	0.875	2.4572	2.4552	0.1
388.4	0.045	0.120	0.835	2.7532	2.7765	-0.8
388.4	0.050	0.110	0.840	2.7495	2.7994	-1.8
388.6	0.030	0.080	0.890	2.0437	2.0639	-1.0
388.6	0.035	0.120	0.845	2.4663	2.4590	0.3
388.6	0.040	0.080	0.880	2.2625	2.2473	0.7
388.6	0.045	0.080	0.875	2.3547	2.3450	0.4
388.6	0.045	0.120	0.835	2.6529	2.6518	0.0
388.6	0.050	0.090	0.860	2.5070	2.5203	-0.5
388.6	0.050	0.110	0.840	2.6546	2.6737	-0.7
388.8	0.030	0.110	0.860	2.1398	2.1853	-2.1
388.8	0.035	0.110	0.855	2.2658	2.2721	-0.3
388.8	0.040	0.120	0.840	2.4584	2.4390	0.8
388.8	0.045	0.100	0.855	2.3971	2.3818	0.6
388.8	0.050	0.090	0.860	2.4152	2.4072	0.3
388.8	0.050	0.110	0.840	2.5626	2.5537	0.3

Table C.8: Continues

T (K)	x_{co2}	x_{mea}	x_{h2o}	K_{value}		% difference
				Aspen Plus® data	Regression correlation	
				1.8154	1.8829	-3.7
389	0.035	0.110	0.855	2.1543	2.1702	-0.7
389	0.035	0.120	0.845	2.2370	2.2433	-0.3
389	0.040	0.080	0.880	2.0633	2.0502	0.6
389	0.040	0.120	0.840	2.3549	2.3296	1.1
389	0.045	0.080	0.875	2.1675	2.1394	1.3
389	0.045	0.090	0.865	2.2326	2.2061	1.2
389	0.050	0.080	0.870	2.2622	2.2324	1.3
389.2	0.030	0.110	0.860	1.8990	1.8723	1.4
389.2	0.035	0.120	0.845	2.1271	2.0688	2.7
389.2	0.040	0.110	0.850	2.1747	2.1545	0.9
389.2	0.040	0.120	0.840	2.2545	2.2213	1.5
389.2	0.045	0.080	0.875	2.0824	2.1034	-1.0
389.2	0.045	0.090	0.865	2.1448	2.1705	-1.2
389.2	0.050	0.080	0.870	2.1811	2.2503	-3.2
389.2	0.050	0.120	0.830	2.4666	2.5607	-3.8
389.4	0.030	0.080	0.890	1.6241	1.6446	-1.3
389.4	0.035	0.080	0.885	1.7657	1.7595	0.4
389.4	0.035	0.120	0.845	2.0215	1.9809	2.0
389.4	0.040	0.110	0.850	2.0807	2.0630	0.9
389.4	0.040	0.120	0.840	2.1577	2.1269	1.4
389.4	0.045	0.080	0.875	2.0031	2.0139	-0.5
389.4	0.045	0.090	0.865	2.0626	2.0782	-0.8
389.4	0.050	0.110	0.840	2.3053	2.3740	-3.0
389.4	0.050	0.120	0.830	2.3828	2.4520	-2.9
389.6	0.030	0.080	0.890	1.5414	1.5747	-2.2
389.6	0.030	0.090	0.880	1.5825	1.6206	-2.4
389.6	0.030	0.100	0.870	1.6301	1.6679	-2.3
389.6	0.030	0.110	0.860	1.6855	1.7166	-1.8
389.6	0.030	0.120	0.850	1.7501	1.7666	-0.9
389.6	0.035	0.080	0.885	1.6857	1.6847	0.1
389.6	0.035	0.090	0.875	1.7337	1.7354	-0.1
389.6	0.035	0.100	0.865	1.7883	1.7876	0.0
389.6	0.035	0.110	0.855	1.8502	1.8414	0.5
389.6	0.035	0.120	0.845	1.9206	1.8968	1.2

Table C.8: Continues

T (K)	x_{co2}	x_{mea}	x_{h2o}	K_{value}		% difference
				Aspen Plus® data	Regression correlation	
389.6	0.040			1.8137	1.8024	0.6
389.6	0.040	0.090	0.870	1.8665	1.8583	0.4
389.6	0.040	0.100	0.860	1.9256	1.9160	0.5
389.6	0.040	0.110	0.850	1.9914	1.9754	0.8
389.6	0.040	0.120	0.840	2.0647	2.0367	1.4
389.6	0.045	0.080	0.875	1.9289	1.9283	0.0
389.6	0.045	0.090	0.865	1.9852	1.9899	-0.2
389.6	0.045	0.100	0.855	2.0471	2.0535	-0.3
389.6	0.045	0.110	0.845	2.1154	2.1191	-0.2
389.6	0.045	0.120	0.835	2.1902	2.1868	0.2
389.6	0.050	0.080	0.870	2.0342	2.0631	-1.4
389.6	0.050	0.090	0.860	2.0927	2.1309	-1.8
389.6	0.050	0.100	0.850	2.1567	2.2009	-2.0
389.6	0.050	0.110	0.840	2.2263	2.2732	-2.1
389.6	0.050	0.120	0.830	2.3018	2.3479	-2.0
389.8	0.030	0.080	0.890	1.4666	1.5078	-2.8
389.8	0.030	0.120	0.850	1.6468	1.6917	-2.7
389.8	0.035	0.110	0.855	1.7607	1.7633	-0.1
389.8	0.035	0.120	0.845	1.8252	1.8164	0.5
389.8	0.040	0.080	0.880	1.7424	1.7258	1.0
389.8	0.040	0.090	0.870	1.7911	1.7794	0.7
389.8	0.045	0.110	0.845	2.0358	2.0292	0.3
389.8	0.045	0.120	0.835	2.1074	2.0940	0.6
389.8	0.050	0.120	0.830	2.2240	2.2483	-1.1
390	0.030	0.080	0.890	1.3986	1.4438	-3.2
390	0.030	0.120	0.850	1.5515	1.6199	-4.4
390	0.035	0.110	0.855	1.6774	1.6885	-0.7
390	0.035	0.120	0.845	1.7356	1.7393	-0.2
390	0.040	0.090	0.870	1.7210	1.7039	1.0
390	0.045	0.080	0.875	1.7958	1.7680	1.5
390	0.045	0.120	0.835	2.0284	2.0052	1.1
390	0.050	0.120	0.830	2.1494	2.1530	-0.2

Table C.9: K_{value} correlation comparison with Aspen Plus® data of MEA

T (K)	x_{co2}	x_{mea}	x_{h2o}	K_{value}		% difference
				Aspen Plus® data	Regression correlation	
385	0.035	0.080	0.885	0.01215	0.01233	-1.4
385	0.040	0.110	0.850	0.01263	0.01254	0.8
385	0.045	0.080	0.875	0.01223	0.01232	-0.7
385	0.045	0.120	0.835	0.01292	0.01272	1.6
385	0.050	0.080	0.870	0.01228	0.01232	-0.3
385	0.050	0.120	0.830	0.01301	0.01283	1.4
385.2	0.035	0.080	0.885	0.01249	0.01267	-1.4
385.2	0.040	0.080	0.880	0.01253	0.01266	-1.1
385.2	0.045	0.110	0.845	0.01302	0.01297	0.4
385.2	0.045	0.120	0.835	0.01322	0.01307	1.1
385.2	0.050	0.080	0.870	0.01262	0.01266	-0.4
385.2	0.050	0.120	0.830	0.01331	0.01318	1.0
385.4	0.035	0.080	0.885	0.01284	0.01301	-1.3
385.4	0.040	0.080	0.880	0.01288	0.01301	-1.1
385.4	0.045	0.110	0.845	0.01334	0.01332	0.1
385.4	0.045	0.120	0.835	0.01353	0.01343	0.7
385.4	0.050	0.080	0.870	0.01296	0.01301	-0.4
385.4	0.050	0.090	0.860	0.01309	0.01314	-0.4
385.6	0.040	0.080	0.880	0.01324	0.01337	-1.0
385.6	0.045	0.080	0.875	0.01328	0.01337	-0.7
385.6	0.045	0.120	0.835	0.01385	0.01380	0.4
385.6	0.050	0.080	0.870	0.01332	0.01337	-0.4
385.6	0.050	0.090	0.860	0.01343	0.01350	-0.5
385.6	0.050	0.120	0.830	0.01394	0.01392	0.2
385.8	0.030	0.080	0.890	0.01358	0.01374	-1.2
385.8	0.035	0.100	0.865	0.01374	0.01384	-0.7
385.8	0.040	0.110	0.850	0.01393	0.01398	-0.3
385.8	0.045	0.110	0.845	0.01401	0.01407	-0.4
385.8	0.045	0.120	0.835	0.01418	0.01418	0.0
385.8	0.050	0.110	0.840	0.01408	0.01416	-0.5
386	0.035	0.080	0.885	0.01400	0.01412	-0.9
386	0.040	0.120	0.840	0.01444	0.01444	-0.1
386	0.045	0.080	0.875	0.01404	0.01412	-0.5
386	0.045	0.090	0.865	0.01412	0.01423	-0.8

Table C.9: Continues

T (K)	x_{co2}	x_{mea}	x_{h2o}	K_{value}		% difference
				Aspen Plus® data	Regression correlation	
386	0.050	0.120	0.830	0.01461	0.01469	-0.6
386.2	0.035	0.080	0.885	0.01442	0.01451	-0.6
386.2	0.040	0.080	0.880	0.01442	0.01451	-0.6
386.2	0.040	0.120	0.840	0.01479	0.01484	-0.3
386.2	0.045	0.080	0.875	0.01445	0.01450	-0.4
386.2	0.045	0.120	0.835	0.01487	0.01497	-0.6
386.2	0.050	0.110	0.840	0.01480	0.01495	-1.0
386.2	0.050	0.120	0.830	0.01496	0.01510	-0.9
386.4	0.035	0.080	0.885	0.01485	0.01490	-0.3
386.4	0.040	0.080	0.880	0.01485	0.01490	-0.3
386.4	0.040	0.120	0.840	0.01516	0.01525	-0.6
386.4	0.045	0.080	0.875	0.01487	0.01490	-0.3
386.4	0.045	0.090	0.865	0.01491	0.01502	-0.7
386.4	0.050	0.080	0.870	0.01489	0.01490	-0.1
386.4	0.050	0.120	0.830	0.01532	0.01551	-1.2
386.6	0.035	0.080	0.885	0.01531	0.01531	0.0
386.6	0.040	0.110	0.850	0.01543	0.01558	-0.9
386.6	0.040	0.120	0.840	0.01554	0.01567	-0.8
386.6	0.045	0.080	0.875	0.01530	0.01531	-0.1
386.6	0.045	0.120	0.835	0.01562	0.01580	-1.2
386.6	0.050	0.080	0.870	0.01532	0.01531	0.0
386.6	0.050	0.090	0.860	0.01537	0.01547	-0.6
386.8	0.035	0.110	0.855	0.01580	0.01590	-0.6
386.8	0.040	0.080	0.880	0.01576	0.01573	0.2
386.8	0.040	0.120	0.840	0.01594	0.01610	-1.0
386.8	0.045	0.110	0.845	0.01590	0.01611	-1.3
386.8	0.045	0.120	0.835	0.01601	0.01624	-1.4
386.8	0.050	0.110	0.840	0.01596	0.01621	-1.6
386.8	0.050	0.120	0.830	0.01609	0.01638	-1.8
387	0.030	0.080	0.890	0.01636	0.01616	1.2
387	0.035	0.100	0.865	0.01622	0.01628	-0.4
387	0.040	0.120	0.840	0.01635	0.01654	-1.1
387	0.045	0.110	0.845	0.01632	0.01655	-1.4
387	0.045	0.120	0.835	0.01642	0.01668	-1.6
387	0.050	0.080	0.870	0.01622	0.01616	0.4

Table C.9: Continues

T (K)	x_{co2}	x_{mea}	x_{h2o}	K_{value}		% difference
				Aspen Plus® data	Regression correlation	
387	0.050	0.120	0.830	0.01649	0.01683	-2.1
387.2	0.030	0.080	0.890	0.01690	0.01702	-0.7
387.2	0.035	0.110	0.855	0.01670	0.01672	-0.1
387.2	0.040	0.080	0.880	0.01675	0.01686	-0.7
387.2	0.045	0.080	0.875	0.01671	0.01678	-0.4
387.2	0.045	0.120	0.835	0.01684	0.01674	0.6
387.2	0.050	0.110	0.840	0.01681	0.01676	0.3
387.2	0.050	0.120	0.830	0.01690	0.01679	0.7
387.4	0.030	0.100	0.870	0.01725	0.01731	-0.4
387.4	0.035	0.110	0.855	0.01718	0.01722	-0.2
387.4	0.040	0.110	0.850	0.01719	0.01724	-0.3
387.4	0.040	0.120	0.840	0.01723	0.01719	0.2
387.4	0.045	0.120	0.835	0.01727	0.01724	0.2
387.4	0.050	0.080	0.870	0.01719	0.01719	0.0
387.4	0.050	0.120	0.830	0.01733	0.01729	0.3
387.6	0.030	0.080	0.890	0.01807	0.01805	0.1
387.6	0.035	0.110	0.855	0.01768	0.01773	-0.3
387.6	0.040	0.080	0.880	0.01781	0.01788	-0.4
387.6	0.040	0.120	0.840	0.01769	0.01770	-0.1
387.6	0.045	0.120	0.835	0.01773	0.01775	-0.1
387.6	0.050	0.110	0.840	0.01771	0.01778	-0.4
387.6	0.050	0.120	0.830	0.01778	0.01780	-0.1
387.8	0.030	0.080	0.890	0.01869	0.01859	0.5
387.8	0.035	0.080	0.885	0.01850	0.01850	0.0
387.8	0.040	0.120	0.840	0.01817	0.01823	-0.3
387.8	0.045	0.110	0.845	0.01817	0.01829	-0.7
387.8	0.045	0.120	0.835	0.01820	0.01828	-0.5
387.8	0.050	0.080	0.870	0.01822	0.01823	-0.1
387.8	0.050	0.090	0.860	0.01818	0.01826	-0.4
388	0.030	0.100	0.870	0.01897	0.01890	0.4
388	0.035	0.110	0.855	0.01875	0.01880	-0.3
388	0.040	0.080	0.880	0.01894	0.01896	-0.1
388	0.045	0.110	0.845	0.01868	0.01884	-0.9
388	0.045	0.120	0.835	0.01868	0.01883	-0.8
388	0.050	0.080	0.870	0.01875	0.01877	-0.1

Table C.9: Continues

T (K)	x_{co2}	x_{mea}	x_{h2o}	K_{value}		% difference
				Aspen Plus® data	Regression correlation	
388	0.050	0.090	0.860	0.01870	0.01880	-0.5
388.2	0.030	0.080	0.890	0.02000	0.01971	1.5
388.2	0.035	0.080	0.885	0.01973	0.01961	0.6
388.2	0.035	0.090	0.875	0.01957	0.01953	0.2
388.2	0.040	0.120	0.840	0.01920	0.01933	-0.7
388.2	0.045	0.120	0.835	0.01919	0.01939	-1.0
388.2	0.050	0.110	0.840	0.01919	0.01941	-1.2
388.2	0.050	0.120	0.830	0.01921	0.01944	-1.2
388.4	0.030	0.080	0.890	0.02069	0.02029	1.9
388.4	0.035	0.080	0.885	0.02037	0.02019	0.9
388.4	0.035	0.120	0.845	0.01981	0.01985	-0.2
388.4	0.040	0.120	0.840	0.01974	0.01991	-0.8
388.4	0.045	0.080	0.875	0.01998	0.02000	-0.1
388.4	0.045	0.120	0.835	0.01971	0.01996	-1.3
388.4	0.050	0.110	0.840	0.01971	0.01999	-1.4
388.6	0.030	0.080	0.890	0.02139	0.02089	2.3
388.6	0.035	0.120	0.845	0.02041	0.02044	-0.2
388.6	0.040	0.080	0.880	0.02077	0.02069	0.4
388.6	0.045	0.080	0.875	0.02058	0.02059	-0.1
388.6	0.045	0.120	0.835	0.02026	0.02055	-1.5
388.6	0.050	0.090	0.860	0.02036	0.02052	-0.8
388.6	0.050	0.110	0.840	0.02025	0.02058	-1.6
388.8	0.030	0.110	0.860	0.02145	0.02112	1.6
388.8	0.035	0.110	0.855	0.02117	0.02114	0.2
388.8	0.040	0.120	0.840	0.02089	0.02111	-1.0
388.8	0.045	0.100	0.855	0.02096	0.02118	-1.1
388.8	0.050	0.090	0.860	0.02094	0.02113	-0.9
388.8	0.050	0.110	0.840	0.02081	0.02119	-1.8
389	0.030	0.080	0.890	0.02283	0.02215	3.0
389	0.035	0.110	0.855	0.02184	0.02176	0.3
389	0.035	0.120	0.845	0.02168	0.02167	0.0
389	0.040	0.080	0.880	0.02205	0.02194	0.5
389	0.040	0.120	0.840	0.02150	0.02173	-1.1
389	0.045	0.080	0.875	0.02181	0.02183	-0.1
389	0.045	0.090	0.865	0.02168	0.02182	-0.6

Table C.9: Continues

T (K)	x_{co2}	x_{mea}	x_{h2o}	K_{value}		% difference
				Aspen Plus® data	Regression correlation	
389	0.050	0.080	0.870	0.02163	0.02173	-0.4
389.2	0.030	0.110	0.860	0.02293	0.02258	1.5
389.2	0.035	0.120	0.845	0.02235	0.02209	1.2
389.2	0.040	0.110	0.850	0.02226	0.02196	1.3
389.2	0.040	0.120	0.840	0.02213	0.02179	1.5
389.2	0.045	0.080	0.875	0.02244	0.02212	1.4
389.2	0.045	0.090	0.865	0.02231	0.02197	1.6
389.2	0.050	0.080	0.870	0.02225	0.02178	2.1
389.2	0.050	0.120	0.830	0.02191	0.02121	3.2
389.4	0.030	0.080	0.890	0.02431	0.02385	1.9
389.4	0.035	0.080	0.885	0.02378	0.02349	1.2
389.4	0.035	0.120	0.845	0.02304	0.02273	1.4
389.4	0.040	0.110	0.850	0.02292	0.02260	1.4
389.4	0.040	0.120	0.840	0.02278	0.02243	1.5
389.4	0.045	0.080	0.875	0.02309	0.02277	1.4
389.4	0.045	0.090	0.865	0.02296	0.02261	1.5
389.4	0.050	0.110	0.840	0.02257	0.02198	2.6
389.4	0.050	0.120	0.830	0.02250	0.02184	2.9
389.6	0.030	0.080	0.890	0.02506	0.02455	2.0
389.6	0.030	0.090	0.880	0.02489	0.02434	2.2
389.6	0.030	0.100	0.870	0.02470	0.02413	2.3
389.6	0.030	0.110	0.860	0.02449	0.02392	2.3
389.6	0.030	0.120	0.850	0.02426	0.02372	2.2
389.6	0.035	0.080	0.885	0.02449	0.02417	1.3
389.6	0.035	0.090	0.875	0.02432	0.02398	1.4
389.6	0.035	0.100	0.865	0.02414	0.02378	1.5
389.6	0.035	0.110	0.855	0.02395	0.02359	1.5
389.6	0.035	0.120	0.845	0.02376	0.02340	1.5
389.6	0.040	0.080	0.880	0.02406	0.02380	1.1
389.6	0.040	0.090	0.870	0.02391	0.02362	1.2
389.6	0.040	0.100	0.860	0.02375	0.02344	1.3
389.6	0.040	0.110	0.850	0.02359	0.02326	1.4
389.6	0.040	0.120	0.840	0.02344	0.02309	1.5
389.6	0.045	0.080	0.875	0.02374	0.02344	1.3
389.6	0.045	0.090	0.865	0.02361	0.02327	1.4

Table C.9: Continues

T (K)	x_{co2}	x_{mea}	x_{h2o}	K_{value}		% difference
				Aspen Plus® data	Regression correlation	
389.6	0.045	0.100	0.855	0.02348	0.02311	1.6
389.6	0.045	0.110	0.845	0.02335	0.02294	1.7
389.6	0.045	0.120	0.835	0.02323	0.02278	2.0
389.6	0.050	0.080	0.870	0.02350	0.02308	1.8
389.6	0.050	0.090	0.860	0.02339	0.02293	2.0
389.6	0.050	0.100	0.850	0.02328	0.02278	2.2
389.6	0.050	0.110	0.840	0.02319	0.02263	2.4
389.6	0.050	0.120	0.830	0.02310	0.02248	2.7
389.8	0.030	0.080	0.890	0.02582	0.02527	2.1
389.8	0.030	0.120	0.850	0.02507	0.02441	2.6
389.8	0.035	0.110	0.855	0.02469	0.02428	1.6
389.8	0.035	0.120	0.845	0.02450	0.02408	1.7
389.8	0.040	0.080	0.880	0.02475	0.02450	1.0
389.8	0.040	0.090	0.870	0.02460	0.02431	1.1
389.8	0.045	0.110	0.845	0.02401	0.02361	1.6
389.8	0.045	0.120	0.835	0.02388	0.02345	1.8
389.8	0.050	0.120	0.830	0.02372	0.02313	2.5
390	0.030	0.080	0.890	0.02657	0.02601	2.1
390	0.030	0.120	0.850	0.02590	0.02512	3.0
390	0.035	0.110	0.855	0.02544	0.02499	1.7
390	0.035	0.120	0.845	0.02525	0.02479	1.8
390	0.040	0.090	0.870	0.02530	0.02503	1.1
390	0.045	0.080	0.875	0.02507	0.02483	1.0
390	0.045	0.120	0.835	0.02454	0.02413	1.7
390	0.050	0.120	0.830	0.02436	0.02381	2.2

Table C.10: K_{value} correlation comparison with Aspen Plus® data of H_2O

T (K)	x_{co2}	x_{mea}	x_{h2o}	K_{value}		% difference
				Aspen Plus® data	Regression correlation	
385	0.035	0.080	0.885	0.9712	0.9669	0.4
385	0.040	0.110	0.850	0.9692	0.9593	1.0
385	0.045	0.080	0.875	0.9712	0.9676	0.4
385	0.045	0.120	0.835	0.9666	0.9570	1.0
385	0.050	0.080	0.870	0.9711	0.9680	0.3
385	0.050	0.120	0.830	0.9657	0.9574	0.9
385.2	0.035	0.080	0.885	0.9773	0.9732	0.4
385.2	0.040	0.080	0.880	0.9774	0.9736	0.4
385.2	0.045	0.110	0.845	0.9747	0.9660	0.9
385.2	0.045	0.120	0.835	0.9728	0.9633	1.0
385.2	0.050	0.080	0.870	0.9773	0.9743	0.3
385.2	0.050	0.120	0.830	0.9719	0.9637	0.8
385.4	0.035	0.080	0.885	0.9835	0.9795	0.4
385.4	0.040	0.080	0.880	0.9836	0.9799	0.4
385.4	0.045	0.110	0.845	0.9809	0.9723	0.9
385.4	0.045	0.120	0.835	0.9791	0.9697	1.0
385.4	0.050	0.080	0.870	0.9834	0.9807	0.3
385.4	0.050	0.090	0.860	0.9828	0.9780	0.5
385.6	0.040	0.080	0.880	0.9897	0.9862	0.4
385.6	0.045	0.080	0.875	0.9897	0.9866	0.3
385.6	0.045	0.120	0.835	0.9853	0.9760	0.9
385.6	0.050	0.080	0.870	0.9896	0.9870	0.3
385.6	0.050	0.090	0.860	0.9890	0.9843	0.5
385.6	0.050	0.120	0.830	0.9843	0.9764	0.8
385.8	0.030	0.080	0.890	0.9957	0.9918	0.4
385.8	0.035	0.100	0.865	0.9955	0.9869	0.9
385.8	0.040	0.110	0.850	0.9941	0.9846	1.0
385.8	0.045	0.110	0.845	0.9934	0.9850	0.8
385.8	0.045	0.120	0.835	0.9916	0.9823	0.9
385.8	0.050	0.110	0.840	0.9926	0.9854	0.7
386	0.035	0.080	0.885	1.0021	0.9985	0.4
386	0.040	0.120	0.840	0.9988	0.9883	1.1
386	0.045	0.080	0.875	1.0021	0.9993	0.3
386	0.045	0.090	0.865	1.0018	0.9966	0.5

Table C.10: Continues

T (K)	x_{co2}	x_{mea}	x_{h2o}	K_{value}		% difference
				Aspen Plus® data	Regression correlation	
386	0.050	0.120	0.830	0.9968	0.9890	0.8
386.2	0.035	0.080	0.885	1.0083	1.0048	0.3
386.2	0.040	0.080	0.880	1.0084	1.0052	0.3
386.2	0.040	0.120	0.840	1.0051	0.9946	1.0
386.2	0.045	0.080	0.875	1.0084	1.0056	0.3
386.2	0.045	0.120	0.835	1.0042	0.9950	0.9
386.2	0.050	0.110	0.840	1.0051	0.9980	0.7
386.2	0.050	0.120	0.830	1.0031	0.9954	0.8
386.4	0.035	0.080	0.885	1.0146	1.0111	0.3
386.4	0.040	0.080	0.880	1.0147	1.0115	0.3
386.4	0.040	0.120	0.840	1.0115	1.0009	1.0
386.4	0.045	0.080	0.875	1.0146	1.0119	0.3
386.4	0.045	0.090	0.865	1.0142	1.0092	0.5
386.4	0.050	0.080	0.870	1.0144	1.0123	0.2
386.4	0.050	0.120	0.830	1.0094	1.0017	0.8
386.6	0.035	0.080	0.885	1.0208	1.0175	0.3
386.6	0.040	0.110	0.850	1.0192	1.0099	0.9
386.6	0.040	0.120	0.840	1.0178	1.0072	1.0
386.6	0.045	0.080	0.875	1.0209	1.0182	0.3
386.6	0.045	0.120	0.835	1.0168	1.0076	0.9
386.6	0.050	0.080	0.870	1.0207	1.0186	0.2
386.6	0.050	0.090	0.860	1.0201	1.0159	0.4
386.8	0.035	0.110	0.855	1.0262	1.0158	1.0
386.8	0.040	0.080	0.880	1.0272	1.0241	0.3
386.8	0.040	0.120	0.840	1.0242	1.0135	1.0
386.8	0.045	0.110	0.845	1.0248	1.0166	0.8
386.8	0.045	0.120	0.835	1.0231	1.0139	0.9
386.8	0.050	0.110	0.840	1.0238	1.0169	0.7
386.8	0.050	0.120	0.830	1.0220	1.0143	0.8
387	0.030	0.080	0.890	1.0331	1.0297	0.3
387	0.035	0.100	0.865	1.0332	1.0248	0.8
387	0.040	0.120	0.840	1.0305	1.0199	1.0
387	0.045	0.110	0.845	1.0311	1.0229	0.8
387	0.045	0.120	0.835	1.0295	1.0202	0.9
387	0.050	0.080	0.870	1.0332	1.0312	0.2

Table C.10: Continues

T (K)	x_{co2}	x_{mea}	x_{h2o}	K_{value}		% difference
				Aspen Plus® data	Regression correlation	
387	0.050	0.120	0.830	1.0283	1.0206	0.7
387.2	0.030	0.080	0.890	1.0394	1.0360	0.3
387.2	0.035	0.110	0.855	1.0389	1.0284	1.0
387.2	0.040	0.080	0.880	1.0397	1.0368	0.3
387.2	0.045	0.080	0.875	1.0397	1.0371	0.2
387.2	0.045	0.120	0.835	1.0358	1.0265	0.9
387.2	0.050	0.110	0.840	1.0364	1.0296	0.7
387.2	0.050	0.120	0.830	1.0346	1.0269	0.7
387.4	0.030	0.100	0.870	1.0460	1.0370	0.9
387.4	0.035	0.110	0.855	1.0452	1.0347	1.0
387.4	0.040	0.110	0.850	1.0446	1.0351	0.9
387.4	0.040	0.120	0.840	1.0433	1.0325	1.0
387.4	0.045	0.120	0.835	1.0422	1.0328	0.9
387.4	0.050	0.080	0.870	1.0456	1.0438	0.2
387.4	0.050	0.120	0.830	1.0409	1.0332	0.7
387.6	0.030	0.080	0.890	1.0519	1.0486	0.3
387.6	0.035	0.110	0.855	1.0516	1.0410	1.0
387.6	0.040	0.080	0.880	1.0523	1.0494	0.3
387.6	0.040	0.120	0.840	1.0497	1.0388	1.0
387.6	0.045	0.120	0.835	1.0486	1.0391	0.9
387.6	0.050	0.110	0.840	1.0490	1.0422	0.7
387.6	0.050	0.120	0.830	1.0473	1.0395	0.7
387.8	0.030	0.080	0.890	1.0581	1.0549	0.3
387.8	0.035	0.080	0.885	1.0585	1.0553	0.3
387.8	0.040	0.120	0.840	1.0561	1.0451	1.0
387.8	0.045	0.110	0.845	1.0563	1.0481	0.8
387.8	0.045	0.120	0.835	1.0549	1.0454	0.9
387.8	0.050	0.080	0.870	1.0581	1.0564	0.2
387.8	0.050	0.090	0.860	1.0575	1.0538	0.3
388	0.030	0.100	0.870	1.0648	1.0559	0.8
388	0.035	0.110	0.855	1.0643	1.0536	1.0
388	0.040	0.080	0.880	1.0648	1.0619	0.3
388	0.045	0.110	0.845	1.0626	1.0544	0.8
388	0.045	0.120	0.835	1.0613	1.0517	0.9
388	0.050	0.080	0.870	1.0643	1.0627	0.1

Table C.10: Continues

T (K)	x_{co2}	x_{mea}	x_{h2o}	K_{value}		% difference
				Aspen Plus® data	Regression correlation	
388	0.050	0.090	0.860	1.0637	1.0600	0.3
388.2	0.030	0.080	0.890	1.0706	1.0675	0.3
388.2	0.035	0.080	0.885	1.0710	1.0679	0.3
388.2	0.035	0.090	0.875	1.0711	1.0652	0.5
388.2	0.040	0.120	0.840	1.0689	1.0576	1.1
388.2	0.045	0.120	0.835	1.0677	1.0580	0.9
388.2	0.050	0.110	0.840	1.0678	1.0610	0.6
388.2	0.050	0.120	0.830	1.0663	1.0584	0.7
388.4	0.030	0.080	0.890	1.0769	1.0738	0.3
388.4	0.035	0.080	0.885	1.0773	1.0741	0.3
388.4	0.035	0.120	0.845	1.0762	1.0635	1.2
388.4	0.040	0.120	0.840	1.0752	1.0639	1.1
388.4	0.045	0.080	0.875	1.0771	1.0749	0.2
388.4	0.045	0.120	0.835	1.0740	1.0643	0.9
388.4	0.050	0.110	0.840	1.0741	1.0673	0.6
388.6	0.030	0.080	0.890	1.0831	1.0801	0.3
388.6	0.035	0.120	0.845	1.0826	1.0698	1.2
388.6	0.040	0.080	0.880	1.0835	1.0808	0.3
388.6	0.045	0.080	0.875	1.0833	1.0812	0.2
388.6	0.045	0.120	0.835	1.0803	1.0706	0.9
388.6	0.050	0.090	0.860	1.0822	1.0789	0.3
388.6	0.050	0.110	0.840	1.0803	1.0736	0.6
388.8	0.030	0.110	0.860	1.0898	1.0784	1.0
388.8	0.035	0.110	0.855	1.0894	1.0788	1.0
388.8	0.040	0.120	0.840	1.0879	1.0765	1.1
388.8	0.045	0.100	0.855	1.0886	1.0822	0.6
388.8	0.050	0.090	0.860	1.0884	1.0852	0.3
388.8	0.050	0.110	0.840	1.0865	1.0799	0.6
389	0.030	0.080	0.890	1.0955	1.0926	0.3
389	0.035	0.110	0.855	1.0957	1.0850	1.0
389	0.035	0.120	0.845	1.0953	1.0824	1.2
389	0.040	0.080	0.880	1.0959	1.0934	0.2
389	0.040	0.120	0.840	1.0943	1.0828	1.1
389	0.045	0.080	0.875	1.0956	1.0937	0.2
389	0.045	0.090	0.865	1.0953	1.0911	0.4

Table C.10: Continues

T (K)	x_{co2}	x_{mea}	x_{h2o}	K_{value}		% difference
				Aspen Plus® data	Regression correlation	
389	0.050	0.080	0.870	1.0951	1.0941	0.1
389.2	0.030	0.110	0.860	1.1021	1.0909	1.0
389.2	0.035	0.120	0.845	1.1015	1.0887	1.2
389.2	0.040	0.110	0.850	1.1012	1.0917	0.9
389.2	0.040	0.120	0.840	1.1006	1.0890	1.0
389.2	0.045	0.080	0.875	1.1018	1.1000	0.2
389.2	0.045	0.090	0.865	1.1014	1.0974	0.4
389.2	0.050	0.080	0.870	1.1012	1.1004	0.1
389.2	0.050	0.120	0.830	1.0977	1.0898	0.7
389.4	0.030	0.080	0.890	1.1078	1.1052	0.2
389.4	0.035	0.080	0.885	1.1082	1.1055	0.2
389.4	0.035	0.120	0.845	1.1078	1.0949	1.2
389.4	0.040	0.110	0.850	1.1074	1.0980	0.9
389.4	0.040	0.120	0.840	1.1068	1.0953	1.0
389.4	0.045	0.080	0.875	1.1079	1.1063	0.1
389.4	0.045	0.090	0.865	1.1076	1.1036	0.4
389.4	0.050	0.110	0.840	1.1051	1.0987	0.6
389.4	0.050	0.120	0.830	1.1039	1.0961	0.7
389.6	0.030	0.080	0.890	1.1139	1.1114	0.2
389.6	0.030	0.090	0.880	1.1141	1.1088	0.5
389.6	0.030	0.100	0.870	1.1143	1.1061	0.7
389.6	0.030	0.110	0.860	1.1144	1.1035	1.0
389.6	0.030	0.120	0.850	1.1144	1.1008	1.2
389.6	0.035	0.080	0.885	1.1144	1.1118	0.2
389.6	0.035	0.090	0.875	1.1144	1.1091	0.5
389.6	0.035	0.100	0.865	1.1144	1.1065	0.7
389.6	0.035	0.110	0.855	1.1143	1.1038	0.9
389.6	0.035	0.120	0.845	1.1140	1.1012	1.2
389.6	0.040	0.080	0.880	1.1143	1.1122	0.2
389.6	0.040	0.090	0.870	1.1142	1.1095	0.4
389.6	0.040	0.100	0.860	1.1140	1.1069	0.6
389.6	0.040	0.110	0.850	1.1136	1.1042	0.8
389.6	0.040	0.120	0.840	1.1131	1.1016	1.0
389.6	0.045	0.080	0.875	1.1140	1.1125	0.1
389.6	0.045	0.090	0.865	1.1137	1.1099	0.3

Table C.10: Continues

T (K)	x_{co2}	x_{mea}	x_{h2o}	K_{value}		% difference
				Aspen Plus® data	Regression correlation	
389.6	0.045	0.100	0.855	1.1132	1.1072	0.5
389.6	0.045	0.110	0.845	1.1126	1.1046	0.7
389.6	0.045	0.120	0.835	1.1118	1.1019	0.9
389.6	0.050	0.080	0.870	1.1133	1.1129	0.0
389.6	0.050	0.090	0.860	1.1128	1.1103	0.2
389.6	0.050	0.100	0.850	1.1122	1.1076	0.4
389.6	0.050	0.110	0.840	1.1113	1.1050	0.6
389.6	0.050	0.120	0.830	1.1102	1.1023	0.7
389.8	0.030	0.080	0.890	1.1201	1.1177	0.2
389.8	0.030	0.120	0.850	1.1205	1.1071	1.2
389.8	0.035	0.110	0.855	1.1204	1.1101	0.9
389.8	0.035	0.120	0.845	1.1202	1.1075	1.1
389.8	0.040	0.080	0.880	1.1204	1.1184	0.2
389.8	0.040	0.090	0.870	1.1203	1.1158	0.4
389.8	0.045	0.110	0.845	1.1187	1.1109	0.7
389.8	0.045	0.120	0.835	1.1180	1.1082	0.9
389.8	0.050	0.120	0.830	1.1163	1.1086	0.7
390	0.030	0.080	0.890	1.1262	1.1239	0.2
390	0.030	0.120	0.850	1.1266	1.1133	1.2
390	0.035	0.110	0.855	1.1265	1.1164	0.9
390	0.035	0.120	0.845	1.1263	1.1137	1.1
390	0.040	0.090	0.870	1.1264	1.1220	0.4
390	0.045	0.080	0.875	1.1261	1.1251	0.1
390	0.045	0.120	0.835	1.1241	1.1145	0.9
390	0.050	0.120	0.830	1.1225	1.1148	0.7